



**HAL**  
open science

# Novel design concepts of efficient electrolytes and new organic materials for Magnesium batteries

Ngoc Anh Tran

► **To cite this version:**

Ngoc Anh Tran. Novel design concepts of efficient electrolytes and new organic materials for Magnesium batteries. Chemical and Process Engineering. Université Grenoble Alpes [2020-..], 2020. English. NNT : 2020GRALI073 . tel-03172306

**HAL Id: tel-03172306**

**<https://theses.hal.science/tel-03172306>**

Submitted on 17 Mar 2021

**HAL** is a multi-disciplinary open access archive for the deposit and dissemination of scientific research documents, whether they are published or not. The documents may come from teaching and research institutions in France or abroad, or from public or private research centers.

L'archive ouverte pluridisciplinaire **HAL**, est destinée au dépôt et à la diffusion de documents scientifiques de niveau recherche, publiés ou non, émanant des établissements d'enseignement et de recherche français ou étrangers, des laboratoires publics ou privés.

## THÈSE

Pour obtenir le grade de

### DOCTEUR DE L'UNIVERSITE GRENOBLE ALPES

Spécialité : **2MGE : Matériaux, Mécanique, Génie civil, Electrochimie**

Arrêté ministériel : 25 mai 2016

Présentée par

**Ngoc Anh TRAN**

Thèse dirigée par **Jean-Claude LEPRÊTRE**, Professeur, Université Grenoble Alpes, et codirigée par **Fannie ALLOIN**, Directeur de recherche, CNRS

préparée au sein du **Laboratoire d'Electrochimie et de Physico-Chimie des Matériaux et des Interfaces**,  
dans l'**École Doctorale I-MEP2 – Ingénierie – Matériaux, Mécanique, Environnement, Energétique, Procédés, Production**

## **Nouveaux électrolytes et cathodes organiques pour les batteries au Magnésium**

## **Novel design concepts of efficient electrolytes and new organic materials for Magnesium batteries**

Thèse soutenue publiquement le **8 décembre 2020**,  
devant le jury composé de :

**Madame Fannie ALLOIN**

Directeur de recherche, CNRS, Directrice de thèse

**Madame Cristina IOJOIU**

Directeur de recherche, CNRS, Présidente

**Monsieur François TRAN VAN**

Professeur des Universités, Université de Tours, Rapporteur

**Monsieur Philippe POIZOT**

Professeur des Universités, Université de Nantes, Examineur

**Monsieur Romain BERTHELOT**

Chargé de Recherche, CNRS, Rapporteur





## Acknowledgements

Childhood, student, or adolescent, middle-aged, etc. are the short and long journeys of each person's life. In the early stages, people have changed the most, both physically and mentally. In the next stages, the change occurs more slowly but contributes to deepening our sense of life. And, PhDs: the tortuous passage that I have been in for three years. Three-unforgettable-year help a person become more individual, confident, and especially more human. And I have to sincerely thank some people for what they brought me:

First of all, I want to thank my supervisors: Prof. Jean-Claude Lepretre and Dr. Fannie Alloin. Most likely, I'm not their easiest case they've supervised to explain things more complicated than they are, particularly regarding my habit. I am nevertheless pleased with their input and assistance in clarifying my thoughts and words whenever appropriate. During my first year at LEPMI in particular, their inspiring words were extremely helpful when times were tough. Fannie has always been there, she's paid a lot of attention to my job every time and during these three years she's taken the right choice every time. To be more accurate, I have learned a considerable amount of skills in all the fields: how to address a new subject, the working technique, the analysis of data not limited to the outcome that can be obtained at first glance, the ability to carry on having the most from the job. And there may be more to the chart. Thank you above everything, and all the work you poured into my study, with all its facets.

I would like to express my deepest appreciation to the Jury that accepted to examine and referee for my thesis. Thank you for all the interesting questions and fruitful comments on this work.

I'd also like to extend my gratitude to my erstwhile supervisor: Prof. Le Ngoc Thach and Ass. Prof. Le My Loan Phung that have been belonged to me and gave me helpful and sincere advice since I was a student up to now.

I am also grateful to all MIEL team even if they did not directly supervise my thesis from Dr. Cristina Iojoiu, Prof. Renaud Bouchet, Dr. Laure Lavernot, Dr. Didier Devaux, Dr. Laureline Lecarme, Mr. Vincent Martin to all of my colleagues, Ph.D. students, post-doctorates for their helpfulness and effective discussion.

I gratefully acknowledge the assistance that I received from Mme. Claire Girardi, Mme. Yasmine Bouhadjar, Mme. Claire Benoit and all secretary team.

Many thanks to the closest people in the laboratory, started by Dr. Nguyen Thi Khanh Ly and Dr. Doan Thi Huong, who are my sharing sisters and help me many things from the beginning.

Thanks also to my friend: Misgina Tilahun Tsehay, Regis Porhiel, Sajad Rahimi, Ibrahim Shalayel, and Andriana Capozzi. Thank you for the talking, the laughter, the ski, the beer, the diner at my flat, and the helpfulness in every moment.

An enormous thanks should be deserved to the potes de Grenoble, M. Edmond Prunier, Mme. Tran Huynh Lan, Mme. Nguyen Kieu Vinh, Prof. Nguyen Khac Nhan, Dr. Phan Hai Trieu. Thank you for your time and your unwavering support when I got into trouble here.

I am also grateful to Vietnamese association in Grenoble: Kim Nguyễn, Phương Uyên, Uyên Phương, Đăng Khoa, Minh Công, Anh Tuấn, Hạ Uyên, Hương Quỳnh, Ass. Prof. Mai Thai Son, Dr. Diep Phan, thank you to bring the Vietnamese way of life to me: eating Vietnamese foods, talking Vietnamese topics, play Vietnamese games and hiking Vietnamese way.

Thanks should also go to my friends in Vietnam, Canada, the UK who always care about me and my family. I hope that we will have at least one more back-pack trip together.

I must also thank my family including paternal and maternal parents, brothers who support me all the time help me to take care of Su Hào during my last year of work here.

Minh Quân, my son, you are always in my heart every single day. Our lives will never be complete without you. You've always been the source of my joy and truly an amazing gift from above. I am so sorry that I could not keep you beside me for a year. That has been the toughest time for us in life surely. I love you!

Finally, I would like to say thank you to my love, also my wife. Thanks for your sacrifice during this time. Each moment of being together eating, having fun, traveling, made me a lot less troublesome and anxious. Not only that, you are always smiling and considerate even when you behave strangely or unreasonably. Once again, thank you very much. Love you.

Grenoble, 08/12/2020

Ngoc Anh TRAN



# Table of Contents

<b>Chapter 1: Introduction.....</b>	<b>1</b>
1.1. General context .....	2
1.2. Rechargeable batteries overview.....	4
1.3. Li-ion technology .....	6
1.3.1. Introduction .....	6
1.3.2. Active materials for the positive electrode .....	7
1.4. Forecasts, consumption, and resources for post-lithium ion.....	9
1.5. Multivalent rechargeable batteries .....	11
1.5.1. Calcium.....	11
1.5.2. Aluminum.....	13
1.6. Magnesium.....	14
1.6.1. Plating/stripping on Mg metal .....	15
1.6.2. Electrolyte.....	16
1.6.2.1. Electrolyte involves halide ion .....	16
1.6.2.2. Electrolyte involves non-chloride ion.....	20
1.6.3. Negative electrodes .....	23
1.6.3.1. Insertion-type anode .....	24
1.6.3.2. Alloying-type anode .....	25
1.6.4. Positive electrodes .....	28
1.6.4.1. Layered intercalation positive material.....	28
1.6.4.2. Materials based on conversion and displacement reactions .....	29
1.6.4.3. Spinel structure .....	30
1.6.4.4. Organic materials.....	31
1.7. Conclusion and aim of the work .....	48
<b>Chapter 2: Electrolyte design for Mg batteries.....</b>	<b>49</b>
2.1. Borohydride based salt .....	51
2.1.1. Effect of solvent on the $\text{Mg}[\text{B}(\text{OPh})_3\text{H}]_2$ solubility.....	52
2.1.2. Phenolate borohydride derivatives.....	53
2.1.3. Thiophenolate borohydride study .....	59
2.1.3.1. Cyclic voltammetry investigation .....	59
2.1.3.2. NMR spectroscopy characterization .....	64
2.1.3.3. Mg/electrolyte interface .....	68
2.1.3.4. Galvanostatic test .....	71

2.1.3.5. Mg/Chevrel phase investigation.....	73
2.2. $\pi$ -rich compounds .....	74
2.2.1. Non-anthracene based compounds .....	76
2.2.2. Derivative anthracenes .....	78
2.2.2.1. Alkylanthracene in 9,10 positions .....	78
2.2.2.2. Alkylanthracene in position 2 .....	85
2.2.2.3. Alkoxyanthracene .....	88
2.3. Conclusion .....	90
<b>Chapter 3: PBQDS as organic positive electrode for Mg and Li batteries .91</b>	
3.1. Introduction.....	92
3.2. Results and discussion .....	93
3.2.1. Synthesis and active material characterization .....	93
3.2.2. Electrolyte properties .....	97
3.2.3. Electrochemical performance in Li batteries .....	98
3.2.4. Electrochemical performance in Mg batteries .....	101
3.2.5. GITT investigation for Li and Mg batteries.....	103
3.2.6. The impact of crown-ether as an additive.....	108
3.2.7. Forward to calcium batteries.....	111
3.3. Conclusion .....	113
<b>Chapter 4: Organic cathode materials based on salts of 2,5-dihydroxyterephthalic acid.....</b>	<b>114</b>
4.1. Overview .....	115
4.2. Galvanostatic test in lithium battery .....	116
4.3. Electrochemical performance in magnesium system .....	118
4.4. Conclusion .....	123
<b>Chapter 5: Experimental: Synthesis and Characterizations .....</b>	<b>124</b>
5.1. Synthesis .....	125
5.1.1. Solvent and chemicals preparation .....	125
5.1.2. Borohydride compounds .....	125
5.1.3. Alkoxyanthracene.....	126
5.1.4. Poly(benzonylquinonyldisulfide) .....	127
5.2. Characterizations.....	128
5.2.1. Spectroscopy.....	128
5.2.1.1. Nuclear magnetic resonance (NMR) .....	128
5.2.1.2. Infrared spectroscopy.....	128



5.2.1.3. Scanning Electron Microscopy (SEM) and elemental mapping with energy-dispersive X-ray spectroscopy (EDX).....	128
5.2.1.4. Atomic absorption spectroscopy (AAS).....	129
5.2.2. Physical properties.....	129
5.2.2.1. Thermogravimetric analysis (TGA).....	129
5.2.2.2. Brunauer-Emmett-Teller (BET) .....	129
5.2.2.3. Granulometry .....	129
5.2.3. Mechanical milling.....	130
5.2.4. Electrochemical characterization.....	130
5.2.4.1. Cyclic voltammetry.....	130
5.2.4.2. Galvanostatic Cycling with Potential Limitation.....	131
5.2.4.3. Galvanostatic Intermittent Titration Technique.....	131
5.3. Battery preparation.....	132
5.3.1. Electrolytes preparation.....	132
5.3.1.1. Electrolyte containing hydroborate compound.....	132
5.3.1.2. Electrolyte containing $\pi$ -rich compounds .....	132
5.3.2. CV on microcavity electrode .....	132
5.3.3. Ink and cathode preparation .....	133
5.3.4. Cell assembling .....	133
<b>General Conclusion and Perspectives .....</b>	<b>135</b>
<b>Reference .....</b>	<b>139</b>
<b>Annex .....</b>	<b>164</b>

# **Chapter 1:**

## **Introduction**

## 1.1. General context

Human evolution, from its appearance on Earth to the present day, has always been based upon the ability to harness and handle energy for various applications. Primarily, for survival and leadership on other species, and then for the technical and scientific advancement that accounts for the inherent evolutionary and auto-preserving instincts.

Looking at humankind's history, it's easy to understand that it has been marked by tremendous energetic revolutions. From the fire-control period, through up to the production of fossil fuels, energy management innovations have always opened up new horizons of assets, population expansion (**Figure 1.1a**), and overall growth. However, conserving these conditions was sometimes reliant on the urgent need for alternative resources and/or vectors of energy. Recently, this scenario threatens to occur, as Western societies' relative prosperity has a tremendous impact on emerging countries' outstanding inflation rates that need to feed their growing population and drive their industrial expansion.<sup>1,2</sup>

Nonetheless, important issues inevitably arise about the energetic durability of this scenario, bearing in mind the complex geopolitical situation in most oil-producing countries. While crude oil consumption (**Figure 1.1b**) has been improved over the past few years, with consequent price reductions and more realistic reserve estimates, excessive dependence on fossil fuels puts non-producing countries in an unfavorable position and, could, therefore, affect their strategies to expand.<sup>3</sup>

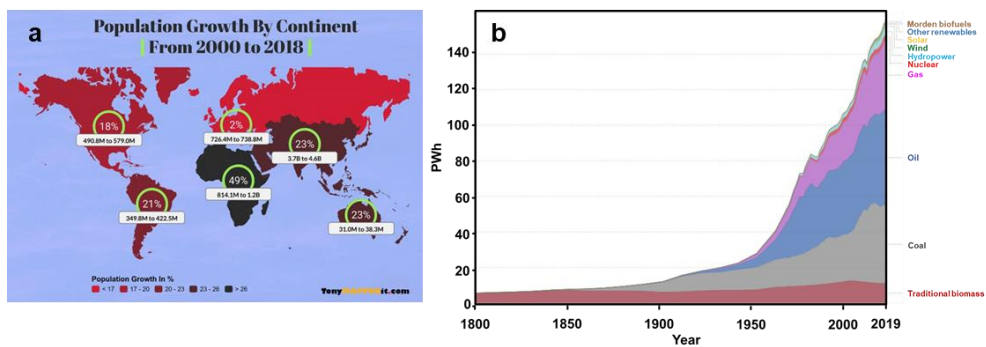


**Figure 1.1.** (a) Population growth by continent and (b) global energy using.<sup>4,5</sup>

Global warming entails drastic environmental changes, with significant implications for most living organisms. While the rise in the greenhouse effect is not universally recognized as the main culprit of the elevated average temperature, many countries have implemented policies aimed at gradually reducing CO<sub>2</sub> emissions (**Figure 1.2**). This involves not only rationalizing production processes but also producing energy with limited CO<sub>2</sub> emissions, reducing the

amount of electricity generated from fossil sources. On the other hand, the majority of developing countries are more hesitant and focus on feeding their “industrial revolution” with relatively cheap and easily accessible fuels.<sup>6,7</sup>

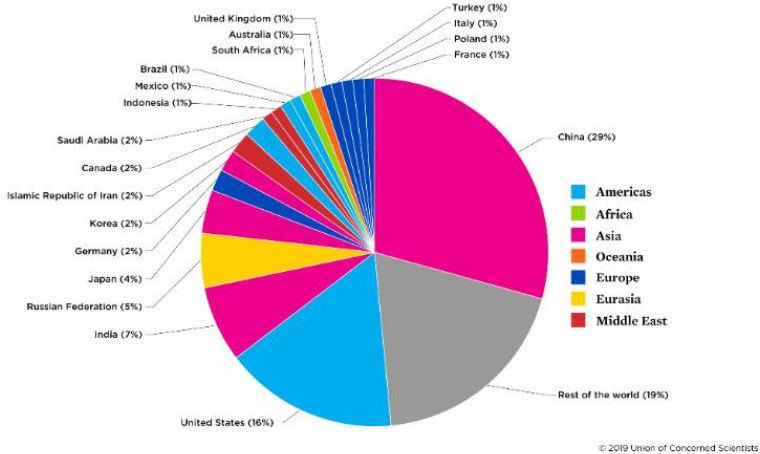


**Figure 1.2.** Carbon dioxide emission by countries.<sup>8</sup>

European countries offset for the reduced energy supply from fossil fuels by concentrating on alternative energy sources, allowing the conversion of energy from potentially permanent sources, such as solar radiation, wind, water, etc., to electricity. The processing of such sources has a limited impact on the environment, as it is not followed by the creation of hazardous/polluting by-products, is usually flexible, allows local development, and thus provides power in regions or areas not connected to major power grids.<sup>9</sup>

The major drawback of renewable sources of energy production, however, is represented by their intermittent nature. This state is not compatible with current electricity usage, which can be required in a very oscillating fashion at any time. To overcome this problem, it is necessary to combine a renewable energy source with an energy storage system capable of storing the possible surplus of energy when production exceeds demand and eventually releasing it when the needs arise. One of the main methods used to store this energy is to pump a mass of water from a low reservoir to a high reservoir, increasing its potential energy, and transform it. This approach is relatively expensive and involves installation that can be complicated to realize, especially where water is scarce. The use of batteries represents a more efficient storage system, which allows the storage of electrical energy produced by renewable sources, transforms it into chemical energy, and converts it back into electricity when necessary. Enhancing the efficiency and cost reduction of energy storage systems is a crucial point for sustainable energy production to grow further and enter the market.<sup>9,10</sup> Hydrogen was targeted also as a promising alternative

energy vector for automotive applications, but several drawbacks have to be overcome as safety issues related to gaseous or liquid H<sub>2</sub> tanking, cost and energy efficiency.

At present, hybrid, plug-in hybrid, and fully-electric vehicles could not be treated as a completely compatible alternative to combustion engine cars, as there is still a difference in cost, efficiency and power supply. Nonetheless, electric mobility is competitive under specific conditions such as urban mobility, where driving range is not a major issue and emissions reduction is mandatory. In addition to these specific applications, the power supply of partially/full electric cars is now becoming a credible alternative for common automotive purposes.<sup>11</sup>

In conclusion, in a dramatic energy-consuming scenario, the future development of modern society has to face several challenging issues, such as the sustainability of energy supply for many purposes (automotive transport, electricity production, etc.), which can be achieved by shifting from polluting fossil fuels to renewable energy sources. Another key to success in this conversion is the possibility to store energy at reduced costs with enhanced protection of the environment. One potential solution is using electrochemical storage devices, which are targeted as credible candidates, indeed their costs are critical targets for promoting this energy storage solution.<sup>6,10</sup>

## **1.2. Rechargeable batteries overview**

An electrochemical cell permits the reversible storage of electricity into chemical energy. There are three main components in a cell including an anode (negative electrode), a cathode (positive electrode), and an electrolyte. Rechargeable batteries are made from one or many cells with various shapes and sizes, ranging from coin cells to wired megawatt systems. Different combinations of electrode and electrolyte materials are applied, such as lead-acid, nickel-cadmium (Ni-Cd), nickel-metal hydride (Ni-MH), Lithium-ion (Li-ion), and Lithium-ion polymer (Li-ion polymer).<sup>12,13</sup>

Rechargeable batteries are used in various devices, for consumer and industrial applications including portable electronics, power tools, battery electric vehicles, emergency power backup, and storage power stations.<sup>14</sup> As presented in a Research and Markets study, the analysts predicted that the global rechargeable battery market will grow at an annual growth rate of 8.32% over the period 2018-2022. Small rechargeable batteries can be used in portable electronic devices, power tools, appliances, etc (**Figure 1.3**). Bulky batteries are used in various

devices from scooters to locomotives, aircraft, and fuel electric vehicles. These are also used for the production of distributed electricity and in stand-alone power systems.<sup>15</sup>

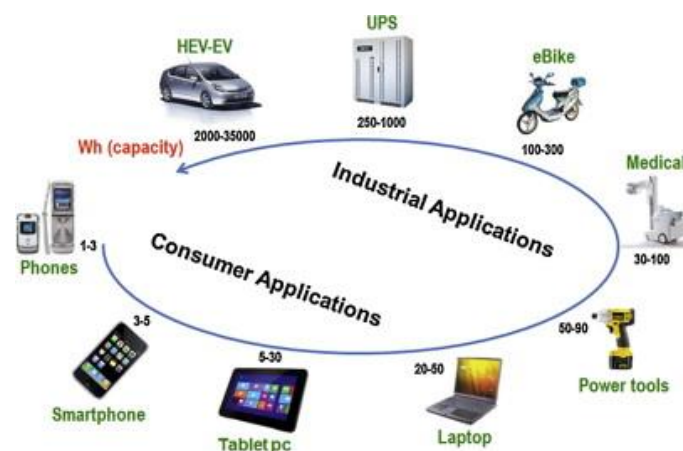


**Figure 1.3.** The application of rechargeable batteries.<sup>16</sup>

In charge and discharge terms, the positive active material is oxidized during charging, creating electrons, and the negative material consumes electrons and is reduced. Those electrons constitute the current in the external circuit. As in Li-ion and Ni-Cd cells, the electrolyte permits the ion movement between the electrodes and avoids short-circuit, or is an active participant in the electrochemical reaction, as in lead-acid cells<sup>14,17</sup> and Li/S batteries.<sup>18,19</sup>

When batteries are used regularly even without mistreatment, they lose energy as the number of charging cycles increases, until finally, they reached the end of their useful life. For example, many reactive lithium metals can be formed on charging in Li-ion forms, particularly on deep discharge, which is no longer available to participate in the next discharge cycle.<sup>20</sup>

Rechargeable batteries are combining various cell types, such as lead-acid, Ni-Cd, Ni-MH, and Lithium-ion batteries (LIBs). While lead-acid batteries and Ni-Cd batteries have been used for a long time, relatively young are Ni-MH and LIBs. Ni-MH and LIBs have played critical roles in the market of rechargeable batteries, particularly LIBs. **Table 1.1** compares the main characteristics of those four battery types.<sup>21,22</sup>

**Table 1.1.** Characteristics of rechargeable batteries.<sup>22</sup>

Characteristics	Lead-acid battery	Ni-Cd battery	Ni-MH battery	Li-ion battery
Gravimetric energy density (Wh/kg)	30 – 50	40 – 60	60 – 120	170 – 250
Volumetric energy density (Wh/L)	60 – 110	150 – 190	140 – 300	350 – 700
Battery voltage (V)	2.0	1.2	1.2	3.7
Cycle life (to 80% of the initial capacity)	300	1500	1000	500 – 2000
Self-discharge per month (%)	5	20	30	< 10

Fast charging time (hours)	8 – 16	1	1 – 4	1 or less
In use since	Late 1800s	1950	1990	1991
Toxicity	High	High	Low	Low
Overcharge tolerance	High	Moderate	Low	Low
Operating temperature range (°C)	-20 to 60	-40 to 60	-20 to 60	-20 to 60

Over the past two decades, the challenge of rising battery energy density has powered all the battery technology advancement. Up to now, battery energy density remains the primary criteria in choosing a battery system, which is particularly critical for rechargeable batteries. The advances in increasing battery energy density, however, continue to keep pace with growing demands from rechargeable batteries. Even though LIBs exhibit the highest energy density among different rechargeable batteries, their energy density, ranging from 170 to 250 Wh/kg or 350 to 700 Wh/L, is still not able to cope with the growing energy storage demands of emerging rechargeable batteries (**Figure 1.4**). Therefore, it is a global and urgent desire to further increase the energy density of rechargeable batteries.<sup>23,24</sup>

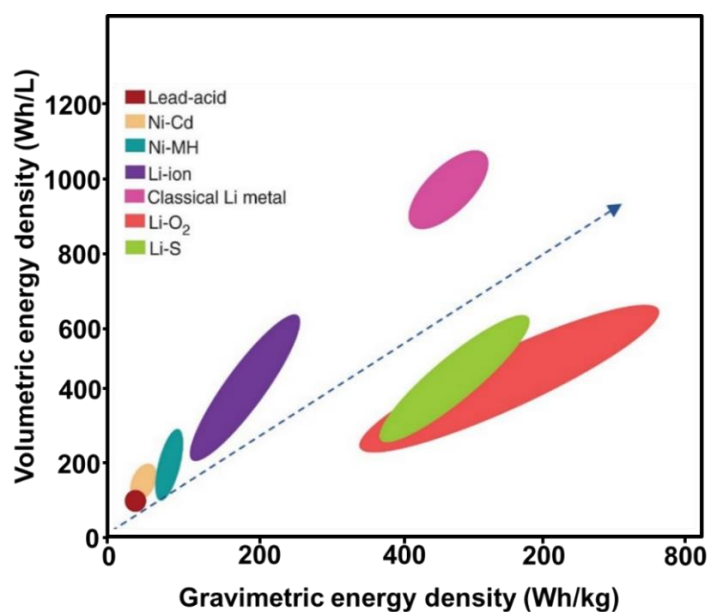


**Figure 1.4.** The plot of different types of rechargeable batteries with gravimetric energy density vs. volumetric energy density.<sup>25</sup>

### 1.3. Li-ion technology

#### 1.3.1. Introduction

LIBs have become the primary means of energy storage for off-grid solar products due to their high performance, low cost, high capacity, lack of memory, and long-life cycle. Li-ion is an advanced technology, first commercialized in the early 1990s, and research and development

try to improve security, enhance performance and widen lifetime. For some Li-ion chemistries, charging efficiency is excellent, up to 99% (**Figure 1.5**).

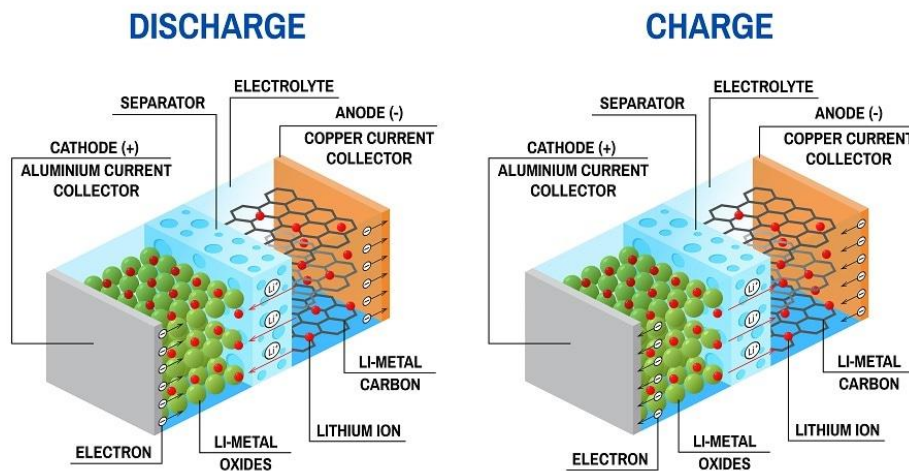


**Figure 1.5.** Charge/discharge in a Li-ion battery.<sup>26</sup>

Li-ion systems must be designed accurately to achieve good performance and to avoid serious safety hazards that may result from the mistreatment of battery cells and unauthorized operation. Overcharging, overheating, short-circuiting, or damaging the charged Li-ion battery can lead to fire or explosion.<sup>27</sup>

### 1.3.2. Active materials for the positive electrode

LIBs use a concept known as intercalation that incorporates lithium ions into the electrode materials structure. Within the cell, lithium ions move during charging from the positive to the negative electrode, and from the negative to the positive electrode as the battery is discharged. When the battery is discharged, electrons pass through an external circuit in the same direction as the lithium ions.<sup>27,28</sup>

The Li-ion battery refers to various battery chemistries. All Li-ion battery cells have three functional layers: the positive electrode, the negative electrode, and the separator. The separator is generally a polymeric membrane swelled with a liquid electrolyte that allows for the transport of Li-ion but prevents shorts-circuits.<sup>28</sup>

LIBs are frequently categorized by the composition of their positive electrodes. **Table 1.2** addresses the major types of commercially produced positive electrode materials on the market.<sup>29,30</sup>



**Table 1.2.** Common positive electrode materials.<sup>27</sup>

Material	Pr. Cap. (mAh/g)	Density (g/cc)	Vol. En. Den. (mAh/cc)	Shape of Dis. Curve	Safety	Cost	Comment
LiCoO <sub>2</sub>	160	5.05	808	Flat	Fair	High	Small-size
LiNiO <sub>2</sub>	220	4.80	1056	Sloping	Poor	Fair	Impossible
Li Ni <sub>0.8</sub> Co <sub>0.2</sub> O <sub>2</sub>	180	4.85	873	Sloping	Fair	Fair	LIP-small scale
LiNi <sub>0.8</sub> Co <sub>0.15</sub> Al <sub>0.05</sub> O <sub>2</sub>	200	4.80	960	Sloping	Fair	Fair	LIP-small scale
LiMn <sub>0.5</sub> Ni <sub>0.5</sub> O <sub>2</sub>	160	4.70	752	Sloping	Good	Low	
LiMn <sub>1/3</sub> Ni <sub>1/3</sub> Co <sub>1/3</sub> O <sub>2</sub>	200	4.70		Sloping	Good	Low	
LiMn <sub>0.4</sub> Ni <sub>0.4</sub> Co <sub>0.2</sub> O <sub>2</sub>	200	4.70					
LiMn <sub>2</sub> O <sub>4</sub>	110	4.20	462	Flat	Good	Low	HEV-EV
Li <sub>1.06</sub> Mg <sub>0.06</sub> Mn <sub>1.88</sub> O <sub>4</sub>	100	4.20	420	Flat	Good	Low	HEV-EV
LiFePO <sub>4</sub>	160	3.70	592	Flat	Good	Low	Low cond.

The most effective positive electrodes are LiNi<sub>1-x</sub>M<sub>x</sub>O<sub>2</sub> (M = Co, Mn, and Al with (1 - x) > 0.5) nickel-rich layered materials. In the field of sample composition, morphology, and microstructure with optimum capacity, cyclability, and thermal stability, ongoing efforts are mostly focused on. One strategy is to reduce the amount of cobalt in LiNi<sub>1-x-y</sub>Co<sub>x</sub>Mn<sub>y</sub>O<sub>2</sub> (NMC) to reduce the price. For this purpose, NMC 811,<sup>31</sup> NMC 532,<sup>32</sup> and NMC 442<sup>33</sup> are being developed and applied for commercial usage (particularly for automotive applications). On the other hand, for high-power Li-ion applications with decent safety, spinel LiNi<sub>0.5</sub>Mn<sub>1.5</sub>O<sub>4</sub> is promising, awaiting advances in electrolyte capable of withstanding its high operating voltage (4.7 V vs. Li/Li<sup>+</sup>). High-voltage Li-rich layered Li<sub>1+x</sub>M<sub>1-x</sub>O<sub>2</sub> and polyanion-based compounds have the potential to increase battery energy densities more significantly over the long term. Particularly, manganese-based Li<sub>1+x</sub>M<sub>1-x</sub>O<sub>2</sub> offers the highest volumetric energy densities coupled with graphite-silicon blends as negative electrodes among all secondary Li-based chemistries produced.<sup>34</sup> Recent developments in the literature have shown that redox processes incorporating reversible oxygen and 4d/5d metal (Ru, Nb, Ir) could be a viable path to potentially eradicate voltage decay.<sup>35,36</sup> Despite good structural and thermal stability, the high-voltage polyanion-based materials are still severely penalized by a greater formula weight, a poor kinetic response resulting in low volumetric energy densities and a reactivity versus the electrolyte. Besides inorganic materials, a vast number of new generation organic cathodes are also investigated for lithium batteries. Metal-organic frameworks (MOFs) such as nanoconfined poly(anthraquinonyl sulfide)@3D-C show a high reversible specific capacity at low and high-rates.<sup>37</sup> Recently, poly(naphthalene diimide-alt-benzoquinone) (NDI-BQ) delivers a practical capacity of 168 mAh/g which is higher than common inorganic materials (LiFePO<sub>4</sub> or LiCoO<sub>2</sub>).<sup>38</sup>

## **Anode materials**

At present, the four most commonly used anode materials are those based on graphite, alloyed graphite, silicon, and lithium metals. Unlike the case of Li and K batteries, graphite cannot be used as a negative electrode material for Na and Mg batteries because of the too weak thermodynamic interaction between  $\text{Na}^+$  and  $\text{Mg}^{2+}$  ion and graphite. However, the reversible cointercalation of  $\text{Mg}^{2+}$  ions with solvent molecule into graphite for magnesium-ion batteries was introduced as preliminary work in this field.<sup>39</sup> Besides, oxide spinel  $\text{Li}_4\text{Ti}_5\text{O}_{12}$  is one of the commercialized alloyed lithium metals.<sup>40</sup> Its higher potential prevents cycling and safety issues associated with dendrite formation on lithium anodes. The downside is expressed in the form of performance loss due to a decrease in cell voltage, which further decreases the energy density and power.<sup>41</sup>

Therefore, most researchers have concentrated on the successful development and marketing of high-capacity conversion negative electrode for electric vehicles and portable electronic applications by achieving high conversion efficiency and good Solid Electrolyte Interphase (SEI) stability compared to traditional graphite with low-cost materials. Electrode materials could include a series of different chemical and physical phenomena during the charge/discharge process at the electrode/electrolyte interface.<sup>42-44</sup>

The main studied one is the silicon-based anode which provides significantly higher energy density than graphite<sup>45,46</sup> using carbon-coated nano Si dispersed oxide/graphite composite. It showed impressive performance on improving cycling stability and reducing the irreversible capacity of the LIBs. However, the conversion electrode materials face various difficulties during the electrochemical process, such as volume expansion, poor conductivity, and poor stability. The decomposition of the electrolytes on the continuously renewed results in the formation of SEI which induces the irreversible consumption of  $\text{Li}^+$  and the weak cyclability of the system. Eventually, novel conversion anode materials are believed to potentially explore the field of Li-ion rechargeable batteries by increasing capacity, stability, and performance.<sup>47</sup>

### **1.4. Forecasts, consumption, and resources for post-lithium ion**

LIBs (LIBs) have developed evolutionarily in terms of their common energy (Wh/kg) and energy densities (Wh/L) since their market launch in 1991. Including LIBs, there is a variety of different technologically promising battery concepts that might also be ideal for different applications, depending on the respective technology. Such “next generation” devices, the so-called post-lithium ion batteries (PLIBs), such as metal/sulfur, metal/air or metal/oxygen, or

“post-lithium technologies” (systems without Li), based on an alternative single ( $\text{Na}^+$ ,  $\text{K}^+$ ) or multivalent ( $\text{Mg}^{2+}$ ,  $\text{Ca}^{2+}$ ) ions, are presently under intensive study. In today’s perspective, it seems quite clear that not only a single technology will be the answer for all the applications, but different battery systems, which can be especially suited or adapted for a particular application (technology diversity).<sup>48-51</sup>

To ensure sustainable long-term energy generation, conversion, and storage, the creation of new technologies is of utmost importance. Such enormous progress has been challenged recently because of the Li ability issues. Li is a relatively uncommon metal and is not distributed uniformly over the crust of Earth. It is usually extracted from brines, and Li-rich minerals’. The largest natural reservoirs are located in South America, and more precisely in a desert region shared by Chile, Bolivia, and Argentina. Other large reservoirs are located in Australia, which has increased Li production in recent years. Smaller grades can be found in the USA, China, and Zimbabwe.<sup>46-52</sup>

The problem of cheap and efficient energy storage in conjunction with renewable energy generators will not be overcome with “mobile” applications but will face the urgent need for large-scale deployment. Several companies have produced MWh scale LIBs, the likelihood that current Li-based technologies satisfy the growing demand for such installations are being questioned and the scientific community is pursuing alternative systems based on cheaper, more abundant, and more effective ion vectors.

In addition to the aforementioned lithium batteries, several novel battery ideas and technologies have been approached and developed in recent years, making the situation for concepts of electrochemical energy storage much more complicated since the commercial launch of LIBs in the 1990s (**Figure 1.6**). These innovative or alternative post-lithium ion developments include, for example, sodium-ion batteries, all-solid-state batteries (ASSB), dual-ion or dual-carbon batteries, redox flow batteries, magnesium batteries, potassium-ion batteries, and calcium batteries.<sup>52-58</sup> Since all of these technologies are fairly “young” and can not be considered mature, significant research and development efforts are needed to improve these new storage concepts to be able to compete with state-of-the-art Li-ion technology for some applications.<sup>25</sup>

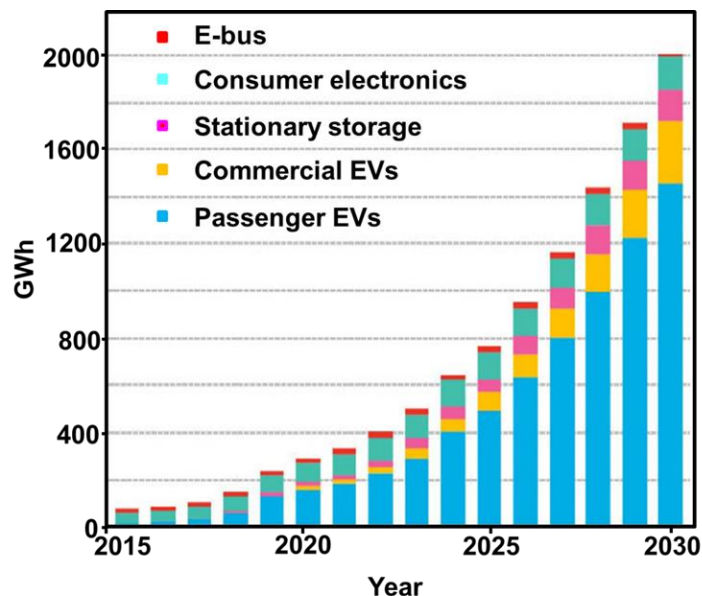


**Figure 1.6.** Annual Li-ion battery demand.<sup>59</sup>

### 1.5. Multivalent rechargeable batteries

Using the very simple measure of Earth’s crust abundance, it is considered Mg to be 7<sup>th</sup>, Ca 5<sup>th</sup>, and Al 3<sup>rd</sup>, and this can be compared with Li’s rate (33<sup>rd</sup>) at 18 ppm. This section will briefly discuss the properties of several promising elements for multivalent-based energy storage systems (**Figure 1.7**).

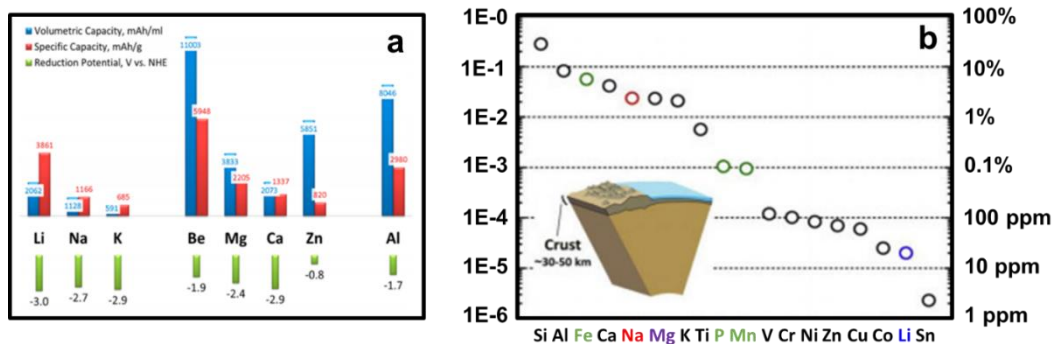


**Figure 1.7.** (a) Capacities and reductive potentials for various metal anodes (b) The abundance of different elements on earth.<sup>53,60</sup>

#### 1.5.1. Calcium

Calcium is the fifth most abundant element in the Earth, it is non-toxic and its standard reduction potential is -2.87 vs. NHE, resulting in a theoretical energy density of 2.06 Ah/cm<sup>3</sup>. Due to its less polarizing character (charge/radius ratio), the Ca<sup>2+</sup> ion should be more mobile in liquid

electrolytes than both  $\text{Mg}^{2+}$  and  $\text{Al}^{3+}$  ions, which are used in much more intensively researched battery concepts.

The first calcium study as the electroactive element occurred in 1964 and relates to primary thermal batteries, a technology mostly used in military and aviation technologies.<sup>61,62</sup> Staniewicz *et al.* became the first to report the electrochemistry of  $\text{CaSOCl}_2$  used for military applications, and addressed the impossibility of calcium plating, due to the formation of a passivation layer consisting mainly of  $\text{CaCl}_2$  impermeable to the  $\text{Ca}^{2+}$  ions.<sup>63,64</sup> Interest in intercalation cathodes, like those used in LIB technology, also re-emerged, but the bottlenecks related to the discrepancies between  $\text{Li}^+$  and  $\text{Ca}^{2+}$  as charging carriers were soon clearly realized and hence the need for the specific design of materials.<sup>65</sup>

The feasibility of reversible calcium metal plating and stripping using traditional alkyl-carbonate organic-solvent-based electrolytes was assessed at moderate temperatures by the end of 2015.<sup>66</sup> It opened up for a more thorough screening of electrode products, considering problems associated with these electrolytes. With Ca metal anodes being the most attractive choice, research focused on electrolyte formulations that enable better coulombic efficiency and, if possible, make room-temperature operation feasible, while at the same time using them to unravel suitable cathode materials.

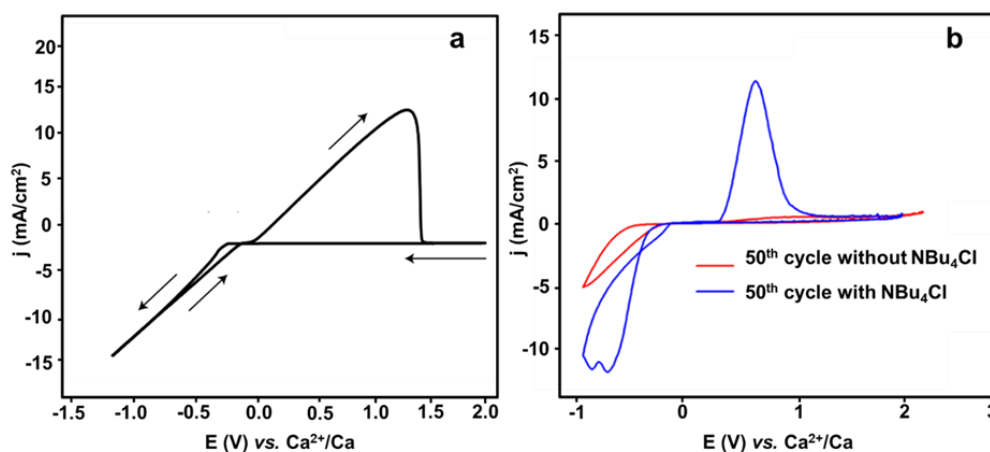


**Figure 1.8.** Cyclic voltammograms of some studies on calcium plating/stripping (a) using 1.5 M  $\text{Ca}(\text{BH}_4)_2$  in THF as an electrolyte and Au, Ca, Pt as the working, reference, and counter electrodes, respectively at 25 mV/s (b) for the 50<sup>th</sup> CV cycles in two electrolytes: with a 500 mM  $\text{Ca}(\text{B}(\text{Ohfip})_4)_2$  electrolyte and a 500 mM  $\text{Ca}(\text{B}(\text{Ohfip})_4)_2$  + 100 mM  $\text{Bu}_4\text{NCl}$  electrolyte (Ohfip = hexafluoroisopropoxy and Bu = butyl).<sup>67,68</sup>

Ca batteries are strongly dependent on the electrolyte/electrode interface properties and efficiency. Important research by Aurbach *et al.*<sup>62</sup> investigated the method of calcium anode plating from an organic electrolyte using  $\text{Ca}(\text{BF}_4)_2$  and  $\text{Ca}(\text{ClO}_4)_2$  as salts and PC,  $\gamma$ -BL, THF, and ACN as solvents. Plating was observed by infrared spectroscopy to be limited by electrolyte decomposition to form a passivation layer on top of the Ca metal somewhat similar to the SEI developed on graphite and lithium electrode. None of the various electrolytes studied allowed reversible calcium plating/stripping, as the passivation films, mainly composed of  $\text{CaCO}_3$  and  $\text{Ca}(\text{OH})_2$ , did not conduct  $\text{Ca}^{2+}$  ions. Even though these findings seriously halted the production of Ca metal-anode-based batteries, two recent studies have indeed reported efficient calcium plating and stripping using organic electrolytes in the presence of passivation layers: 1.5 M  $\text{Ca}(\text{BH}_4)_2$  in THF and 0.45 M  $\text{Ca}(\text{BF}_4)_2$  in EC:PC. The former electrolyte allows reversible cell output at room temperature, with an electrochemical stability window of about 3 V (**Figure 1.8**), while the latter provides more than 4 V but requires high temperature (100 °C).<sup>54,67,68</sup>

In a brief conclusion, this stressed that the actual study of electrochemical behavior in Ca study is in progress with two main approaches. The first strategy is electrolyte development to prevent resistive SEI formation while the second attempt is to optimize the performance of Ca anode and to design new cathode material.

### 1.5.2. Aluminum

One of the differences between Al and Ca is the triple-charged  $\text{Al}^{3+}$  ion to be transported and activated at the electrodes. However, the biggest difference is that, until now, nearly all practical Al batteries have used an electrolyte with an anionic  $[\text{AlCl}_4]^-$  transfer complex, the formation of such a complex resulted in low energy densities, Cl corrosion, and the need for specific intercalation electrodes.<sup>69</sup> To date, there are only a few reviews,<sup>70,71</sup> and a proof of concept for an Al/ $\text{V}_2\text{O}_5$  cell.<sup>72</sup> In this study, the use of an electrolyte based on an ionic liquid ( $\text{AlCl}_3$ -EMICl) was the key to creating the  $[\text{AlCl}_4]^-$ -complex. In contrast, traditional organic electrolytes display no electrochemical activity.<sup>73</sup> The Al-battery cell achieved 20 stable cycles that ended at 273 mAh/g and about 240 Kg/Wh. In later studies, however, these findings have been questioned, challenging the electrochemical reaction and indicating that corrosion of the stainless steel current collector is rather the cause.<sup>73</sup>

In reality, Al-based research into rechargeable batteries is not new, but over the past 30 years or more they have been laden with massive problems. This was noted in 2015, Lin *et al.* introduced a new Al-battery with significantly better performance and surprisingly long cycle life (> 7000 cycles).<sup>74</sup> One of the key drawbacks, however, was the consumption of electrolyte

during cycling, the reason why for each gram of carbon between 2 and 6 g of electrolyte (EMIMCl:AlCl<sub>3</sub>) was required and therefore the battery has very limited energy capacity.<sup>75</sup>

A rather more recent route of research for Al battery cathodes has been the use of organic active species grafted on polymers, like those originally developed for Mg batteries. Specifically, a proof-of-concept was presented for an Al metal-organic battery that provides 5000 stable cycles and a reversible capacity of 110 mAh/g, a battery in which the organic component is mixed with graphite particles.<sup>76,77</sup>

## 1.6. Magnesium

At 20 °C, the density of Mg is 1.74 g/cm<sup>3</sup>, about two-thirds that of aluminum (Al). Magnesium is an abundant element, being the 8<sup>th</sup> most abundant element in the crust of the earth and the 3<sup>rd</sup> most abundant ion in seawater<sup>78</sup>. According to the U.S. Geological Survey, the estimated economically viable reserves is 8.5 million tons, equivalent to a lifespan of 306 years, given the constant global annual production of 27 700 tons. When most of the world's resources are found in Russia (27%) and China (25%) and two-thirds of the currently produced Mg comes from China, led by Turkey (10%), Russia (5%), and Austria (3%). Even if the abundance of Mg is very important, China's current dominant market power explains the classification of Mg as a vital raw material. One other advantage is that magnesium can be quickly recycled without any loss in quality.<sup>79</sup> Mg<sup>2+</sup> is light but heavier than Li (1.74 g/cm<sup>3</sup> and 0.53 g/cm<sup>3</sup>), however, its divalent character induces high volumetric energy density (3837 mAh/cm<sup>3</sup>), which is approximately twice that of Li metal and ten times that of Li graphite. It should be remembered that the potential of the couple Mg<sup>2+</sup>/Mg is only -2.36 V vs. SHE, higher than Li<sup>+</sup>/Li or Ca<sup>2+</sup>/Ca.<sup>80</sup> Mg batteries can be regarded as a credible alternative for storage systems.<sup>81,82</sup> **Table 1.3** compares the main physical and electrochemical properties of alkaline and alkaline-earth metals for energy storage applications.

**Table 1.3** Summary of availability, cost, physical and electrochemical properties of different elements used for energy storage device.<sup>80</sup>

Ion	Li <sup>+</sup>	Na <sup>+</sup>	Mg <sup>2+</sup>	Ca <sup>2+</sup>	Zn <sup>2+</sup>	Al <sup>3+</sup>
<b>Abundance on Earth's crust (ppm)</b>	2	23600	23300	41500	70	80000
<b>Price (US/tonne)</b>	6400	250	1990	160	2280	1635
<b>Mp (°C)</b>	180	98	650	851	420	660
<b>E<sub>0</sub> (V vs. SHE)</b>	-3.04	-2.71	-2.37	-2.87	-0.76	-1.67
<b>g/mol e<sup>-</sup></b>	6.941	22.99	12.15	20.04	32.69	8.99
<b>Shannon Ionic radius (Å)</b>	0.76	1.02	0.72	1	0.74	0.53
<b>Gravimetric capacities (mAh/g)</b>	3800	1160	2000	1340	820	2980
<b>Volumetric capacities (mAh/cm<sup>3</sup>)</b>	2060	1140	3800	2060	5851	8046

### 1.6.1. Plating/stripping on Mg metal

The creation of dendrites in batteries with a metal electrode and liquid electrolyte presents a major safety threat as the thin metal needles can expand through the separator and induce short circuits inside the battery, which can trigger the exposure of harmful substances, flame, and explosions. Nevertheless, magnesium metal seems to be less affected by dendrite formation during plating even if some dendrite can be obtained in some conditions.<sup>83</sup>

The SEI was subsequently recognized as a key factor in the magnesium deposit morphology, reversibility, and battery life.<sup>84</sup> Li has been shown to react quickly with both electrolyte solvents (mostly carbonates) and dissolved salt anions, such as ClO<sub>4</sub><sup>-</sup>, PF<sub>6</sub><sup>-</sup>, BF<sub>4</sub><sup>-</sup>, etc. Such reactions form insoluble Li salts that require Li-ion diffusion, such as Li<sub>2</sub>CO<sub>3</sub>, Li<sub>2</sub>O, LiF, etc. Analogous electrolyte formulations on the surface of Mg metal result in the same reactions but, sadly, Mg<sup>2+</sup> could not move through this layer. Therefore, the Mg electrode is passivated and no more reversible Mg cycling is hindered. Such evidence limits electrolyte solvent selection and Mg-based salts; electrolyte engineering is still considered one of the most challenging problems for magnesium batteries.<sup>55,85</sup>

Also, multivalent ions face a specific challenge for electrodes to intercalate, while their mobility in host materials is generally low. Thus, to maximize both ion packing density and mobility, techniques need to be established to build an “ideal” geometrical and chemical environment for the mobile ion.



## 1.6.2. Electrolyte

Electrolytes for magnesium batteries are a specific challenge from the outset. The anions of the salts being tested either reacted with the magnesium electrode or a passivation layer covered the negative electrode. The electrochemical reaction stops in both cases.

Such as, the creation of Mg electrolytes is strongly linked to Mg metal-compatible salts and solvents, which for many years have limited electrolyte designs to a variety of highly reactive and/or heavily-reduced reagents further as halide-based reagents. There are significant developments within the field of electrolytes over the past decade which have displayed new avenues to supply innovative designs beyond those previously known.

### 1.6.2.1. Electrolyte involves halide ion

Halide anions, especially chloride, have historically been strongly embedded within the production of Mg electrolytes mainly because Grignard reagents were readily available precursors. The majority of known Mg electrolytes still contain chloride anions. It could be separated into two classes based on the structure of magnesium salt  $\text{RMgX}$  and  $\text{MgR}_2$  or  $\text{MgX}_2$  ( $\text{R}$  = alkyl and  $\text{X}$  = Br or Cl) compounds (**Figure 1.9**).

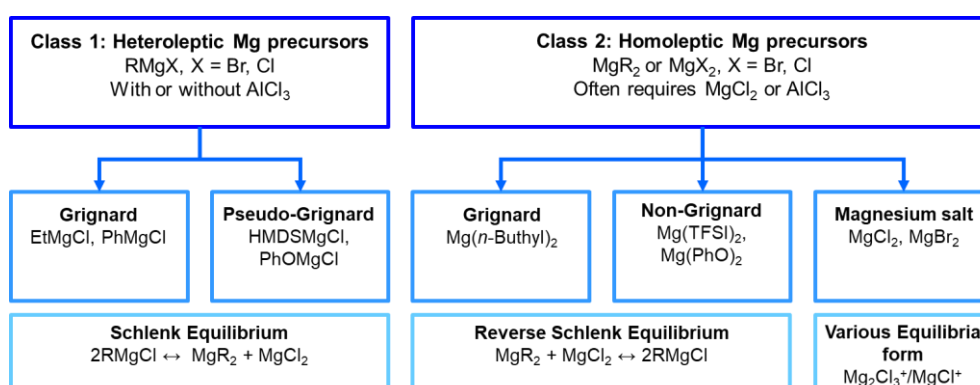


**Figure 1.9.** Classify of halide-ion containing in Mg electrolyte.

Any use of chloride-containing Mg electrolytes provides many benefits: (1) assistance in activating the native MgO passivating layer on the Mg surface; (2) improvement of electrolyte performance in terms of cycling efficiency (approximately 100%) and low over-potential for both deposition and stripping processes; (3) reduces precursor costs, especially in the case of chloride-containing Mg electrolytes. However, there are a lot of obstacles that have demonstrated to be hard to overcome till now: (1) limited anodic stability due to chloride oxidation at 3.3 V vs.  $\text{Mg}^{2+}/\text{Mg}$ ; (2) corrosiveness to non-noble metal parts typically at voltages above 2.5 V vs.  $\text{Mg}^{2+}/\text{Mg}$ ; (3) the existence of tight Mg-Cl bonds, challenging to sever at the

positive electrode interface, leading to lower energy-density  $[\text{MgCl}]^+$ -storage chemistry and; (4) low cationic transference of relatively large  $[\text{Mg}_x\text{Cl}_y]^{(2x-y)+}$  cations.<sup>86</sup>

#### a. Magnesium chloride-based anions

Although the number of studies on Grignard reagents on magnesium system is steadily decreasing because of unstable anodic stability, it is still the most interesting precursors for preparing electrolyte for Mg batteries.<sup>87-89</sup> The most recent work involving Grignard reagent precursors is based on aromatic structures, such as phenyl and carboranyl anions, associated with their improved oxidative stability compared to their alkyl congenerous.

In the report of Nelson *et al.*<sup>90</sup>  $\text{PhMgCl}/\text{AlCl}_3$  was used as an electrolyte to minimize the corrosion to non-noble current collectors. Although the electrolyte displayed remarkable anodic stability of 5 V vs.  $\text{Mg}^{2+}/\text{Mg}$  on stainless steel his impact was attributable to the adsorption of electron-insulating aromatic species resulting from the oxidation of anionic phenyl constituents.<sup>90</sup>

In 2014, Carter *et al.*<sup>88</sup> prepared 1-(1,7-carboranyl) magnesium chloride. The compound in THF showed high coulombic efficiency ( $> 98\%$ ) and relatively high oxidative stability (3.2 V vs.  $\text{Mg}^{2+}/\text{Mg}$  on Pt). Curiously, the same anodic stability was measured on 316-stainless steel and aluminum, indicating lower corrosivity compared to other chloride-containing electrolytes, although a similar adsorption process<sup>88</sup>.

#### b. Magnesium nitrogen-based anions

Since the 90s, Gregory and his team investigated a range of amido-magnesium chloride which helps to arise the oxidation stability potential even if it shows lower conductivity than Grignard compounds.<sup>91</sup> A few years later, Liebenow presented an anion of hexamethyldisilylazide (HMDS) and demonstrated that it exhibits superior oxidative stability compared with other highly basic amides.<sup>92</sup>

Further works relied on the non-nucleophilic character of the  $\text{HMDS}^-$  to prepare a series of electrolytes compatible with sulfur cathode and allowed the Mg-S battery system to be further developed.<sup>93-95</sup> These new HMDS-based systems were obtained by adding precursors  $\text{AlCl}_3$  or  $\text{MgCl}_2$  to either  $(\text{HMDS})\text{MgCl}$  or  $\text{Mg}(\text{HMDS})_2$  (**Figure 1.10**), increased anodic stability (3.3 V vs.  $\text{Mg}^{2+}/\text{Mg}$ ) and high coulombic efficiency (98 – 99%) were obtained.<sup>96,97</sup> Electrolytes with a high ratio of  $\text{MgCl}_2/\text{Mg}(\text{HMDS})_2$  show a broader electrochemical window and higher coulombic efficiency. Crystal structure data suggested that  $[\text{Mg}_2\text{Cl}_3]^+$  dimer was the dominant cationic species in solution, but recent mass spectrometry experiments support the presence of

$[\text{MgCl}]^+$  cation as one of the predominant species.<sup>98,99</sup> In the presence of  $\text{Mg}(\text{TFSI})_2$  as a solubility enhancer, other amidomagnesium chloride salts have been recently studied at 100 °C in triglyme. Its oxidative stability was consistent with previous reports.<sup>100</sup>

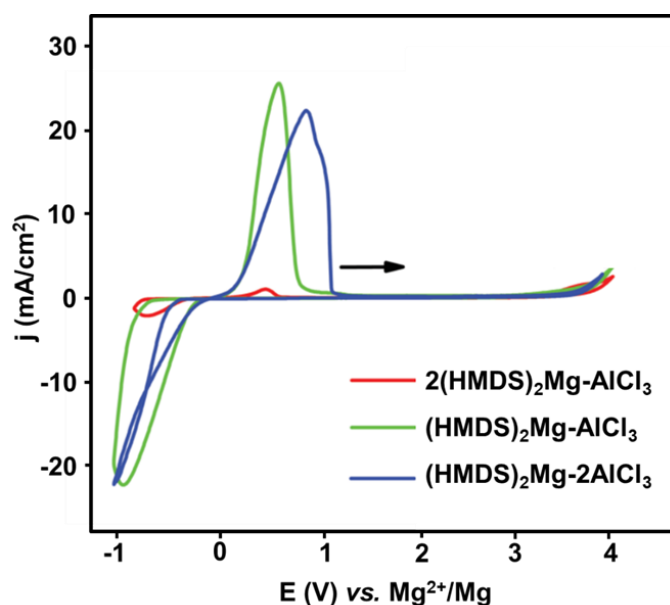


**Figure 1.10.** Cyclic voltammograms of Pt electrodes in THF solutions of selected HMDS-containing electrolytes.<sup>96</sup>

### c. Magnesium oxygen-based anions

Recently, alkoxide- and phenolate-based magnesium electrolytes have obtained much attention due to the less nucleophilic nature of oxygen-based anions compared to amides, as well as being able to provide higher oxidative stability due to higher oxygen-based electronegativity.

In 2012, Wang *et al.* has first introduced oxygen-based anions as magnesium electrolytes, where reversible Mg plating/stripping, anodic stability up to 2.6 V vs.  $\text{Mg}^{2+}/\text{Mg}$ , and a maximum conductivity of 2.5 mS/cm at 0.5 M were shown to support a variety of phenolate-based  $(\text{ArO})\text{MgCl}/\text{AlCl}_3$  systems in THF.<sup>101</sup>

Alkoxide systems based on several short-chain alcohols were studied in mixture with  $\text{MgBr}_2$ , the maximum ionic conductivity of 4.1 mS/cm was achieved for 1.0 M  $\text{Mg}(\text{OEt})_2/\text{MgBr}_2$  in THF with a coulombic efficiency at 90% for Mg plating/stripping.<sup>102</sup>  $\text{Mg}(\text{TFSI})_2$  (TFSI= bis(trifluoromethanesulfonyl)imide) was also added to prepare concentrated solutions of 2.5 M.<sup>102-104</sup>

For alkoxide anions, such as  $(\text{Ph}_3\text{CO})\text{MgCl}$  or  $(\text{Ph}_3\text{SiO})\text{MgCl}$ , the enhancement offered by adding  $\text{MgCl}_2$  or  $\text{AlCl}_3$  was lower compared to smaller anions, while the strong Lewis acid

AlCl<sub>3</sub> offering a better option (**Figure 1.11**). Like MgCl<sub>2</sub>, using 0.5 equivalents of AlCl<sub>3</sub> enhances all electrochemical properties, including oxidative stability (up to 3.0 V vs. Mg<sup>2+</sup>/Mg); moreover, adding one equivalent of both AlCl<sub>3</sub> and MgCl<sub>2</sub> improves even more than using AlCl<sub>3</sub> alone (**Figure 1.11**).<sup>105</sup>

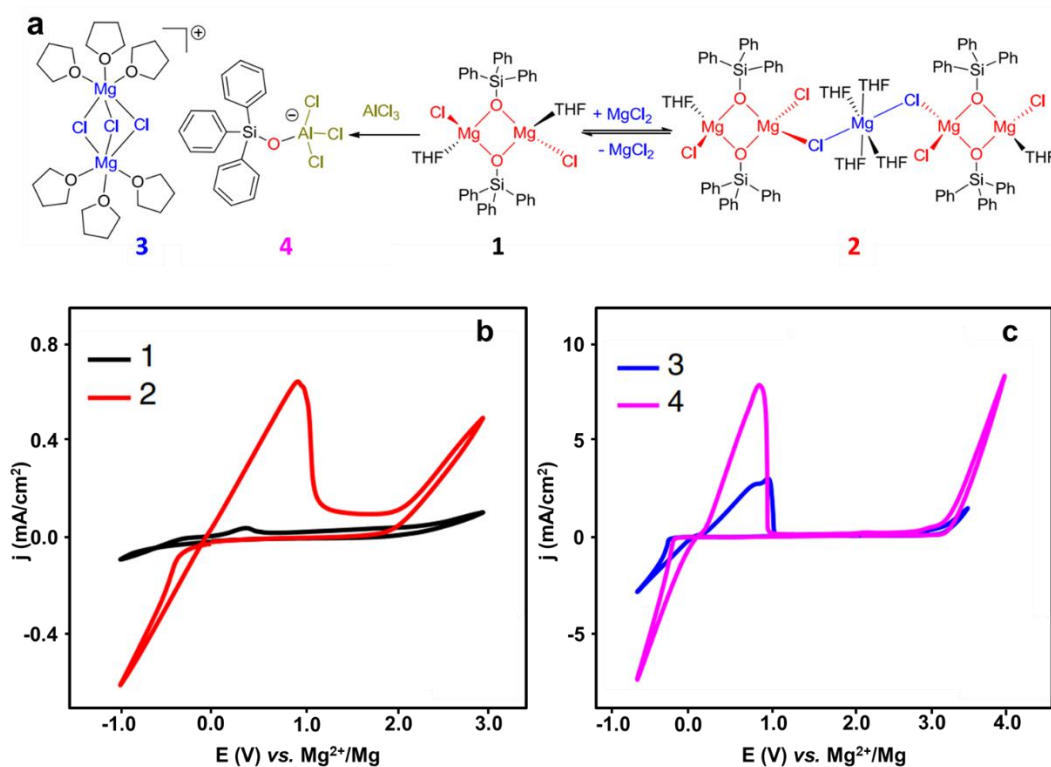


**Figure 1.11.** (a) Equilibria of Ph<sub>3</sub>SiOMg with MgCl<sub>2</sub> and AlCl<sub>3</sub>. The CV of Pt electrodes at a scan rate of 100 mV/s in THF solutions (b) 0.25 M (Ph<sub>3</sub>SiO)MgCl (black) and 0.25 M (Ph<sub>3</sub>SiO)MgCl/MgCl<sub>2</sub> (1:1); (c) 0.25 M (Ph<sub>3</sub>SiO)MgCl/MgCl<sub>2</sub>/AlCl<sub>3</sub> (1:1:0.5) (blue) and 0.25 M (Ph<sub>3</sub>SiO)MgCl/MgCl<sub>2</sub>/AlCl<sub>3</sub> (1:1:1).<sup>105</sup>

#### d. Magnesium halides

In the 20s, THF solution of MgCl<sub>2</sub>/AlCl<sub>3</sub> was studied but the electrolyte showed poor efficiency, with a high overpotential for Mg deposition (> 900 mV) and low stripping efficiency (34%).<sup>106</sup> The magnesium-aluminum chloride complex (MACC) obtained by mixing MgCl<sub>2</sub> and AlCl<sub>3</sub> in THF or glyme presents higher properties to many of the existing electrolytes based on organic Mg<sup>2+</sup> precursors associated with AlCl<sub>3</sub>. It exhibits excellent reversibility of deposition and dissolution of Mg, high anodic stability, and low nucleophilicity.<sup>107,108</sup> One of the most important drawbacks of MACC (and other halide-ion-containing) electrolytes, is their incompatibility with conventional current collectors due to the very high Cl<sup>-</sup> content, low anodic

stability in stainless steel (2.2 V vs.  $\text{Mg}^{2+}/\text{Mg}$ ) and aluminum (1.1 V vs.  $\text{Mg}^{2+}/\text{Mg}$ ) can be noticed with MACC.<sup>109</sup>

Many Lewis acids besides  $\text{AlCl}_3$  have recently been studied in conjunction with  $\text{MgCl}_2$  and many have yielded effective electrolyte systems. For example,  $\text{AlPh}_3$  and  $\text{AlEtCl}_2$  were also shown to provide 100% Coulombic efficiency for Mg deposition/dissolution. A series of 29 inorganic chlorides and  $[\text{NBu}_4]\text{Cl}$  were investigated in combination with  $\text{MgCl}_2$  in DME, where only  $\text{BCl}_3$ ,  $\text{InCl}_3$ ,  $\text{SnCl}_2$ ,  $\text{SbCl}_3$ , and  $\text{BiCl}_3$  supported reversible Mg deposition, although in all cases with low anodic stability ( $< 2$  V vs.  $\text{Mg}^{2+}/\text{Mg}$ ) and insufficient coulombic efficiency.<sup>110,111</sup>

Certain magnesium halide salts have also been used as precursors to Mg. For example, electrolyte solutions obtained by mixing  $\text{MgF}_2$  and the highly fluorinated Lewis acid tris(2H-hexafluoroisopropyl) borate showed high coulombic efficiency (95%) in different electrolytes based on DME. This electrolyte showed good anodic stability in stainless steel and aluminum ( $> 3.5$  V vs.  $\text{Mg}^{2+}/\text{Mg}$ ).

#### e. Weakly coordinating anions

Magnesium salts of many common low-coordinating anions usually used in lithium batteries, such as  $\text{BF}_4^-$ ,  $\text{PF}_6^-$  or  $\text{ClO}_4^-$ , show minimal reversibility of Mg plating/stripping due to the formation of  $\text{Mg}^{2+}$  insulating films that inhibit further electrochemical activity. Recent work has shown, however, that in some cases, such as  $\text{PF}_6^-$  and  $\text{TFSI}^-$ , coulombic efficiency may be highly effective. Early work at Pellion Technologies revealed that the addition of  $\text{MgCl}_2$  to  $\text{Mg}(\text{TFSI})_2$  in ethereal solvents provides electrolytes capable of displaying high Mg plating/stripping coulombic performance.<sup>112,113</sup>

The allowing effect of chloride to otherwise Mg-passivating solutions was also shown for the  $\text{PF}_6^-$  anion, adding  $\text{MgCl}_2$  to a 0.25 molar ratio resulted in reversible Mg deposition/dissolution solutions with an average coulombic efficiency of 94%, following galvanostatic conditioning.<sup>114</sup>

#### 1.6.2.2. Electrolyte involves non-chloride ion

Indeed, all Mg organic cathodes cycled in electrolytes containing  $\text{MgCl}^+$  species have recently been revealed to interact with  $\text{MgCl}^+$ , not  $\text{Mg}^{2+}$ . Another obvious obstacle is the corrosive properties of  $\text{Cl}^-$  which cause parasitic side reactions whose effects are pronounced at voltages greater than 2.5 V vs.  $\text{Mg}^{2+}/\text{Mg}$ . New classes of electrolytes that are free from  $\text{Cl}^-$  based salts and reagents have been identified in the last few years.<sup>115</sup> In 2012, Mohtadi *et al* used  $\text{Mg}(\text{BH}_4)_2$  as salt for Mg electrolyte and shown a highly efficient magnesium plating/stripping with high

coulombic efficiency (94%), high current densities (25 mA/cm<sup>2</sup> stripping peak current), and low deposition overpotentials (-0.3 V) and stripping (0 V).<sup>116</sup>

Another idea is the use of boron clusters which is highly stable and non-corrosive. In 2014, Carter *et al.* developed closoborane magnesium dodecahydrododecaborate (MgB<sub>12</sub>H<sub>12</sub>) with good anodic stability up to 4 V vs. Mg<sup>2+</sup>/Mg.<sup>88</sup> To improve the solubility of the salt, Tutusaus *et al.* proposed an efficient and stable electrolyte based on Mg(CB<sub>11</sub>H<sub>12</sub>)<sub>2</sub> salt using tetraglyme as solvent.<sup>117</sup> In 2017, Zhang *et al.* introduced a salt with B-centered anions with large size and CF<sub>3</sub> function in response to the complicated synthesis of the previous product.<sup>118</sup> However, the low Mg<sup>2+</sup> salt concentration in this electrolyte is a limit for this strategy.

One of the most frequently studied salts for Mg batteries is magnesium bis(trifluoromethanesulfonyl)imide known as Mg(TFSI)<sub>2</sub>. This anion presents high anodic stability, as well as reasonable solubility in ethers or ethereal solvents<sup>104,119,120</sup> and is commercially available. One common strategy to improve the compatibility of Mg(TFSI)<sub>2</sub> with Mg metal was to combine it with Mg(BH<sub>4</sub>)<sub>2</sub>. A new approach to modifying Mg(TFSI)<sub>2</sub> solutions with BH<sub>4</sub><sup>-</sup> was the use of a BH<sub>4</sub><sup>-</sup> anion hydride groups partially replaced with phenol. This strategy enables to improve the stability in the oxidation part. 0.5 M Mg(TFSI)<sub>2</sub> combined with 0.15 M Mg[B(OPh)<sub>3</sub>H]<sub>2</sub> electrolyte displays a reversible Mg plating/stripping with high coulombic efficiency. By the addition of a slight amount of MgCl<sub>2</sub> to this electrolyte, a coulombic efficiency of 90 % in SS/Mg cell, a stable cycling performance, no dendrite formation, and wide anodic potential of 3.4 V vs. Mg<sup>2+</sup>/Mg on Al current collector can be reached. Moreover, this electrolyte ables to support reversible and efficient Mg insertion/de-insertion with a high capacity of 94 mAh/g and 96% of coulombic efficiency in Mo<sub>6</sub>S<sub>8</sub> Chevrel cathode phase.<sup>121</sup> Another strategy used, to ensure better performance of Mg(TFSI)<sub>2</sub>/diglyme, was the incorporation of an anthracene-Mg coordinating agent.<sup>122</sup> The Mg(TFSI)<sub>2</sub>/anthracene electrolyte permits a good plating/stripping reversibility and has a large electrochemical stability window greater than 3 V. Due presumably to the low anthracene concentration used, a non-uniform reactivity of the Mg electrode is noticed and the addition of 0.1 M MgCl<sub>2</sub> overcomes this drawback and permits to obtain a high cyclability of a Mg/Mo<sub>6</sub>S<sub>8</sub> cell.

In terms of solvent, electrolytes based on conventional aprotic solvents such as carbonates and nitriles are incompatible with Mg metal chemistry due to their instability at Mg deposition potential. Their instability, and decomposition induced passivation that blocks Mg<sup>2+</sup> transport.<sup>123,124</sup> Some recent reports about sulfone solvents as the main solvent or combined with THF have been reported,<sup>98</sup> however, this was only possible in the presence of reducing

agents or chloride-based systems such as  $\text{MgCl}_2$ , and showed high plating/stripping potential.<sup>125</sup> Considering the undesirable flammability of most popular aprotic solvents, the use of ionic liquids due to their very low volatility, non-flammability, and high thermal stability in addition to a large electrochemical window would be an attractive choice to remove the safety hazards. In most of the above-mentioned tests, the oxidative stability of these solutions was poor ( $< 2.5$  V) and those based on strong reducing agents are supposed to be incompatible with a nucleophilic attack-prone positive electrode such as sulfur. To avoid the challenges associated with the use of chlorides and strong reducing agents, a new, recent alternative approach was used in the design of ionic liquids (ILs) that are compatible with Mg.<sup>126</sup> However, they were usually used as co-solvents in electrolytes, 1-butylmethylpyrrolidinium trifluoromethanesulfonate,<sup>127</sup> diethylmethyl(2-methoxyethyl)ammonium bis(trifluoromethylsulfonyl)imide<sup>128</sup> mixed with THF or glyme solvents permit reversible Mg plating/stripping processes. Another electrolyte was prepared from a mixture of  $\text{Mg}(\text{TFSI})_2$ , ILs, and tetraglyme which shown high thermal and electrochemical stability.<sup>129</sup>

### ***Polymer-based electrolytes for magnesium batteries***

One strategy would be trapped the electrolyte within polymeric matrices (polyethylene oxide, PEO) or porous hosts to reduce the risks associated with using volatile solvents. Though, the applicability of this approach remains questionable, as the magnesium salts applied were known to be incompatible with the magnesium metal in most of these electrolytes.<sup>130</sup>

Another approach presented in electrolyte development for magnesium batteries is the use of polymer electrolytes including PEO,<sup>131,132</sup> PVA,<sup>133</sup> PEC,<sup>134</sup> PVdF,<sup>135</sup> or even biopolymer<sup>133,136</sup>. It is divided into two main groups: solid polymer electrolytes (SPEs) and gel polymer electrolytes (GPEs).<sup>137</sup> Due to current awareness of the efficiency in Mg plating/stripping from different liquid magnesium electrolytes, obtaining good results with magnesium GPEs is potentially much simpler than with magnesium SPEs. Polymer electrolyte researchers have a tremendous opportunity to create new rechargeable polymer-metal batteries, either by developing new magnesium-conductive polymer matrices with Mg metal plating/stripping stability and supported or by engineering artificial SEIs on Mg metal that enables stability and reversibility with a wider range of magnesium-conducting polymer electrolyte chemistries.<sup>137</sup>

In assumption, stable, safe and Mg-compatible electrolytes with also high electrochemical performance is a huge challenge, as metallic Mg is not compatible with conventional Mg salts. Additionally, electrolytes compatible with Mg-metal endure from weak electrochemical stability or react irreversibly with many positive electrodes, thereby limiting the choice of

materials that may be used. A better understanding of the anode/electrolyte/cathode interface reactions and the search for new active Mg-species could help for new electrolyte development. To follow this strategy, some derivatives of  $\text{BH}_4^-$  compounds and  $\pi$ -rich molecules for magnesium battery will be synthesized, characterized, and presented in the following chapter.

### 1.6.3. Negative electrodes

Metallic Mg is reported to create a strong passive layer in electrolytes other than ethers, close to the SEI (SEI) layer in LIBs. The Mg surface film does not conduct  $\text{Mg}^{2+}$  ions, unlike LIBs, where the SEI layer bears  $\text{Li}^+$ . The formation of the passivation layer of Mg, therefore, makes the process of plating/stripping irreversible.<sup>113</sup>

One method to enhance elemental Mg's electrochemical properties is by creating nano- and meso-structures in Mg.<sup>138–140</sup> Recently, Son *et al.* reported coating the Mg surface (**Figure 1.12**) with an artificial  $\text{Mg}^{2+}$  conducting polymer interphase to allow reversible stripping and deposition of Mg in a high-voltage electrolyte composed of  $\text{Mg}(\text{TFSI})_2$  dissolved in a carbonate solvent.<sup>141</sup>

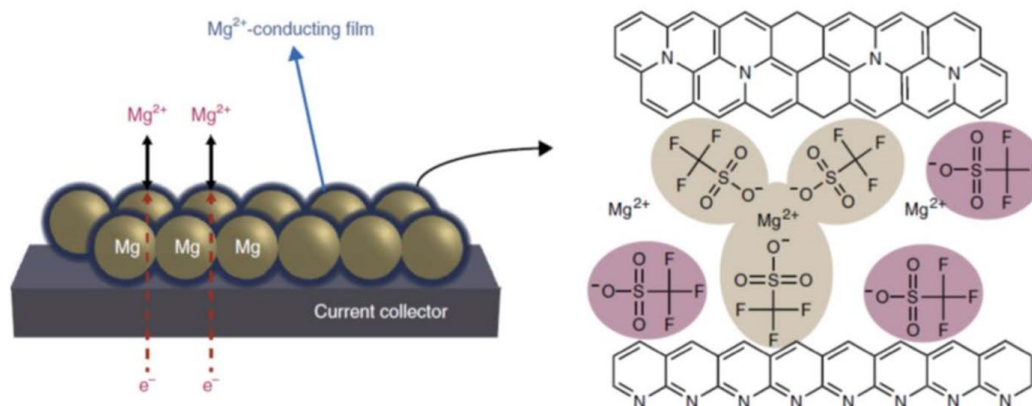


**Figure 1.12.** Mg powder electrode coated with an artificial  $\text{Mg}^{2+}$  conducting interphase and the structure of the artificial magnesium ion.<sup>141</sup>

Similar to LIBs, negative electrode materials for MBs could be categorized as insertion-type materials or alloy-type materials based on the mechanisms involved in the electrochemical reaction. For the first aspect,  $\text{Mg}^{2+}$  ions are inserted and removed from the structure during cycling, while in alloy-type materials, electrochemical conversion occurs with magnesium ions. This section describes the electrochemical behavior of these components and addresses the latest trends in guiding the short-term design of better negative materials.



### 1.6.3.1. Insertion-type anode

For the first sight in insertion-type negative materials part, graphite, graphene are the exciting anode materials that can reversibly intercalate  $\text{Li}^+$  and  $\text{K}^+$  ions. However, several studies pointed out that these were not suitable for its application into the magnesium system. The low capacity for  $\text{Mg}^{2+}$  was attributed to the host substrates, such as graphite and its derivatives, due to the weak chemical binding nature of the  $\text{Mg}^{2+}$ .<sup>142-145</sup>

In 2013, Pontiroli *et al.* first applied fullerene  $\text{C}_{60}$  as the negative material for MBs.<sup>146</sup> In his study,  $\text{Mg}^{2+}$  ion can reversibly intercalate into  $\text{Mg}_2\text{C}_{60}$ . This research prompted further research studies on the possibility of creating an  $\text{Mg}^{2+}$ -intercalated graphite compound (IGC) similar to the way  $\text{Li}^+$  forms  $\text{LiC}_6$  with graphite.<sup>147</sup> A report by Lee *et al.* discovered that afterward,  $\text{Mg}^{2+}$  ions were reversibly intercalated into graphite in ether solvents such as diethylene glycol dimethylether (DEGDME) and 1,2-dimethoxyethane (DME) with the same phenomenon that was also reported when incorporating  $\text{Li}^+$  and  $\text{Na}^+$  ions into graphite layers.<sup>39,148,149</sup> The diffusivity of the  $\text{Mg}^{2+}$ -DEGDME complex into graphite layers is estimated at room temperature at  $1.5 \cdot 10^{-8} \text{ cm}^2/\text{s}$  with the redox potential of graphite was about 1 V vs.  $\text{Mg}^{2+}/\text{Mg}$  comparable to that of  $\text{Li}^+$  in graphite ( $1.8 \cdot 10^{-9} \text{ cm}^2/\text{s}$ ).<sup>39</sup> This suggests that the kinetics engaged in the co-intercalation of the  $\text{Mg}^{2+}$ -DEGDME complex are as fast as the intercalation of  $\text{Li}^+$  ions into graphite. The mechanistic report analyzed by ex-situ X-ray diffraction patterns of the electrodes at different charge/discharge states shows that  $\text{Mg}^{2+}$ -DEGDME co-intercalation displays a well-known graphite staging behavior, meaning that  $\text{Mg}^{2+}$  ions intercalate each  $n^{\text{th}}$  space between the graphene layers.<sup>39,150</sup>

However, the  $\text{Mg}^{2+}$  intercalation performing a staging molecule was not identified with DMF as a co-intercalated solvent. This is important to note that in many cases, the co-intercalation of solvent molecules with metal cations is susceptible to induce irreversible graphite exfoliation, which will progressively deteriorate the electrochemical performance. This aspect of  $\text{Mg}^{2+}$ -solvent pair co-intercalation needs to be somehow studied.<sup>151</sup>

In addition to the non-metallic elements as mentioned above, inorganic compounds have also been deepened and studied to make negative electrode materials for magnesium batteries from recent years.<sup>152,153</sup> **Table 1.4** introduces the main materials that were applied for insertion-type anode studies in the Mg system.

### 1.6.3.2. Alloying-type anode

Alloying-type electrodes operate by a different electrochemical process compared with the insertion-type material. Rather than intercalation for which the crystallographic structure is not significantly altered, electrochemical alloy produces compounds with a different atomic organization. The pristine material is created once again during the dealloying process. Compared with typical insertion-type electrodes in which only the cation is transferred, more than one ion may react electrochemically here. Hence, an electrode of an alloy type usually exhibits high specific and/or volumetric capacities. Nonetheless, during electrochemical cycling, major volume changes occur and may result in the loss of electrical contacts at the electrode level. The drastic volume expansion at the particle scale will locally cause the process of destroying and reforming SEI layers, thus impacting on the cycling performance.<sup>154</sup>

Antimony and bismuth were the first alloy anode elements researched by the Toyota Research Institute of North America. Metallic Sb and Bi, and also the  $Sb_{1-x}Bi_x$  intermediate alloy compositions developed by Berthelot group,<sup>155</sup> were then electrodeposited on titanium/platinum-coated copper substrates and tested with EtMgCl-Et<sub>2</sub>AlCl/THF solution in a half-cell configuration. Anodes using a bismuth/reduced graphene oxide nanocomposite has achieved a high-rate efficiency and cycle life. Various characterization methods have been used to study Bi-based electrodes to understand the mechanisms of reversible alloy and phase transitions.<sup>156-158</sup> The formation of crystalline Mg<sub>2</sub>Sn or Mg<sub>2</sub>Sb has been verified by diffraction with an *ex-situ* X-ray. The corresponding high capacity approximating 900 mAh/g is not maintained during cycling.<sup>159,160</sup> Obrovac *et al.* studied the alloying activity of a lead with the classical Grignard-based electrolyte (EtMgCl:AlCl<sub>3</sub> in THF) on both sputtered and composite electrodes. All the electrochemical work was carried out at 60 °C. Due to the high lead density, this two-phase reaction theoretically provides a very high volumetric capacity of 2300 Ah/L.<sup>157,161,162</sup> Following the above mention methods, the electrochemical alloying of magnesium to indium was also studied. Electrochemical reduction contributes to the formation of crystalline MgIn with 467 mAh/g obtained at low C-rate.<sup>163</sup>

All of the above examples show that tin, antimony, indium, bismuth, and lead can undergo electrochemical magnesium alloy. The extraction of magnesium from the as-formed alloys was also shown. From a practical point of view, it might sometimes be easier to work with alloy powder than with soft and sticky metal particles (such as tin or indium). Alternatively, alloy powders allow for the simple slurry-casted shaping of electrodes. They are compatible with

more traditional magnesium electrolytes and thus open the door to investigating a positive electrode material with high-voltage and free of Mg.<sup>164</sup>

Another interesting approach is Mg<sup>2+</sup> capacitive storage on the surface of the negative electrode with high surface area.<sup>165</sup>

**Table 1.4.** Several insertion-type anode materials for magnesium batteries and their properties.

Anode materials	Theoretical capacity ( mAh/g)	Advantages	Disadvantages	References
Na <sub>2</sub> Ti <sub>3</sub> O <sub>7</sub> nanoribbons	200	Easy synthesis, low redox potentials of Ti <sup>4+</sup> /Ti <sup>3+</sup> , non-toxic, low cost. The lower solubility of Mg <sup>2+</sup> in Ti-based Compounds.	The low reversible capacity of 78 mAh/g. The first process is the irreversible Na <sup>+</sup> de-insertion instead of Mg <sup>2+</sup> insertion.	152
Li <sub>3</sub> VO <sub>4</sub>	592	Low-cost. Electrode materials with high chemical stability, theoretical capacity, and safety.	Poor rate capability, low electronic conductivity, low coulombic efficiency of about 76% in the first cycle, entrapment of inserted Mg <sup>2+</sup> in the host material.	166
Li <sub>4</sub> Ti <sub>5</sub> O <sub>12</sub>	175	High cycle life (only 5% capacity decrease after 500 cycles). Excellent safety characteristics, negligible volume change over cycling, low cost.	Sluggish kinetics of Mg diffusion into the structure. Capacity lower than 70 mAh/g after stability and only 35 mAh/g for the first cycle.	153

#### 1.6.4. Positive electrodes

Nonetheless, one of the main obstacles in developing positive electrodes for Mg-based systems is the slow solid-state diffusion of  $\text{Mg}^{2+}$ , primarily due to its high load/radius ratio, and the consequent difficulty in redistributing the divalent load to the hosting device. During the last 25 years, a wide variety of intercalation products such as oxides, sulfides, and phosphates have been studied. However, most of them had poor electrochemical activity characterized by reduced intercalation and/or elevated polarizations. Furthermore, some of these results should be reviewed as poor activity can also be attributed to less efficient or corrosive electrolytes. However, many types of cathode materials have been studied and get some promising results such as inorganic materials (layered intercalation hosts, materials based on conversion and displacement reactions, spinel structure) and organic materials.<sup>89,167,168</sup>

##### 1.6.4.1. Layered intercalation positive material

###### a. Sulfide and selenide layers

Based on the theory of hard-soft acid-base (HSAB)),  $\text{Mg}^{2+}$  which is hard acid ion interacts weakly with soft base anions such as  $\text{S}^{2-}$  or  $\text{Se}^{2-}$ . This weak interaction may promote the ionic specie displacement inside the active material structure.<sup>169,170</sup> However, full cells using sulfide or selenide-based electrodes exhibit lower theoretical voltage and power than oxide-based cells.

Layered  $\text{TiS}_2$  is a typical intercalation host recorded by Whittingham *et al.*<sup>171</sup> However, due to the large migration energy barrier, the intercalation of  $\text{Mg}^{2+}$  into  $\text{TiS}_2$  layers has been considerably challenging.<sup>172</sup>  $\text{MoS}_2$  is also a typical layered sulfide known to intercalate lithium ions in a reversible manner.<sup>173–175</sup>  $\text{MoS}_2$  was the first positive material to demonstrate compatibility with a broad range of Mg electrolytes.<sup>176</sup> This product has a three-dimensional open structure, consisting of  $\text{Mo}_6\text{S}_8$  blocks, each containing an octahedral  $\text{Mo}_6$  cluster inside an  $\text{S}_8$  cube. Hence  $\text{Mg}^{2+}$  cations could insert easily and delocalized between channels in the active sites.<sup>168,177</sup> The  $\text{Mo}_6$  cluster's variable valence can easily compensate for the charge-unbalance induced by the introduction of divalent ions to preserve electroneutrality during insertion. Given that electronic charges can be readily dispersed on each element (Mo or S), poor interaction with the guest cation is anticipated. Moreover, this material's application for practical rechargeable Mg batteries is limited by its low theoretical capacity (122 mAh/g) and low output voltage (< 1.5 V). Given this,  $\text{Mo}_6\text{S}_8$  has become the traditional material for use in laboratory studies of Mg electrolytes, because it can maintain a stable structure.<sup>119</sup> Although the intercalation of  $\text{Mg}^{2+}$  is slow because of the strong electrostatic forces between the divalent  $\text{Mg}^{2+}$  ions and the sulfur anions. On the other hand, the  $\text{TiSe}_2$  and  $\text{VSe}_2$  selenides offer

capacities of approx. 110 mAh/g at room temperature, with no special treatment, following the general tendency of chalcogenides.<sup>174</sup>

Recently, VS<sub>4</sub> was reported as positive material for rechargeable magnesium batteries by Meng group.<sup>178</sup> Thank to the specific structure, this compound demonstrated high electrochemical performance by over 400 cycles and capacity obtained about 80 mAh/g at 50 mA/g with 90% of capacity retention. The unique linear-chain structure of VS<sub>4</sub> besides the large specific surface area, and more flower-like structure are contributed to the excellent electrochemical efficiency.

### **b. Oxide layers**

MoO<sub>3</sub>, V<sub>2</sub>O<sub>5</sub>, MnO<sub>2</sub>, and TiO<sub>2</sub> were prepared using various methods.<sup>179–181</sup> All of these transition metal compounds are nanosized to provide more active cation intercalation sites with a high surface area and short ion-transport pathways to allow cation diffusion. However, the presence of water has a large impact on the electrode performances. Indeed, the co-intercalation of water molecules with Mg<sup>2+</sup> decreases the strong interaction between oxide and Mg<sup>2+</sup> and largely improve the Mg<sup>2+</sup> diffusion. Amatucci *et al.* argued that the nanosized V<sub>2</sub>O<sub>5</sub> can intercalate Mg<sup>2+</sup> based on electrochemical testing.<sup>182</sup> However, H<sub>2</sub>O is not compatible with the negative electrode and will result in a passivation layer being formed. Based on the initial tests, a few companies were pursuing the production of full battery cells with a cathode of V<sub>2</sub>O<sub>5</sub> and anode of Mg. Pellion technologies have developed a process believed to promote Mg<sup>2+</sup> solid-state diffusion by extending the interlayer gap with the intercalation of bigger organic cations within the interlayer.<sup>183</sup> The electrochemical and spectroscopic tests revealed, however, that the actual content of Mg in V<sub>2</sub>O<sub>5</sub> was minuscule, and proton intercalation prevailed.<sup>184</sup> Such results have contributed to the serious question of whether or not  $\alpha$ -V<sub>2</sub>O<sub>5</sub> is capable of intercalating Mg<sup>2+</sup>.

#### **1.6.4.2. Materials based on conversion and displacement reactions**

One of the biggest roadblocks of layered materials is that it causes a strong Coulombic interaction with the host material framework, resulting in poor kinetics of the reaction.<sup>82,185</sup> Conversion-type reactions may provide an alternative path of reaction to get around this situation. As said previously, S<sup>2-</sup> or Se<sup>2-</sup> exhibit weak interaction with Mg<sup>2+</sup>. For the possibility of using these substances as conversion-type positive materials for rechargeable Mg batteries, copper chalcogenides with a variety of crystal structures have been extensively studied. Series of copper chalcogenides, Cu <sub>$\alpha$</sub> X (1 <  $\alpha$  < 2, X = S, Se), such as CuS, Cu<sub>2</sub>S, and Cu<sub>2</sub>Se were proposed.<sup>186,187</sup> In rechargeable Mg batteries, these are known to undergo conversion reactions

producing Cu metal and MgS or MgSe as discharge products. Such materials have gained attention because at room temperature they display a relatively small overpotential, comparable to that of other effective cathode materials based on intercalation chemistry. The voltage from these conversion reactions varies from 1.0 to 1.5 V vs.  $\text{Mg}^{2+}/\text{Mg}$ . Nazar *et al.* was the first to announce that CuS was able to store Mg ions at 150 °C with a capacity equal to 200 mAh/g.<sup>186</sup> XRD and XPS experiments confirmed that this electrode works based on a conversion mechanism.<sup>187</sup>

Miyasaka *et al.* reported  $\beta\text{-Cu}_2\text{Se}$  (**Figure 1.13**) as a positive-type conversion material for batteries with Mg. Se atoms were arranged in  $\beta\text{-Cu}_2\text{Se}$  in a facially centered cubic structure.  $\text{Cu}^+$  ions are known to be highly mobile in this structure so that  $\beta\text{-Cu}_2\text{Se}$  is treated as a superionic conductor. Nanocrystallites (almost 100 nm) of  $\beta\text{-Cu}_2\text{Se}$  were prepared, providing a reversible discharge capacity of around 230 mAh/g. MgSe and Cu were found primarily in the fully discharged electrode from the XRD measurements, though several other phases, such as  $\alpha\text{-Cu}_2\text{Se}$  and  $\text{Cu}_3\text{Se}_2$  have also been discovered.<sup>188–190</sup>

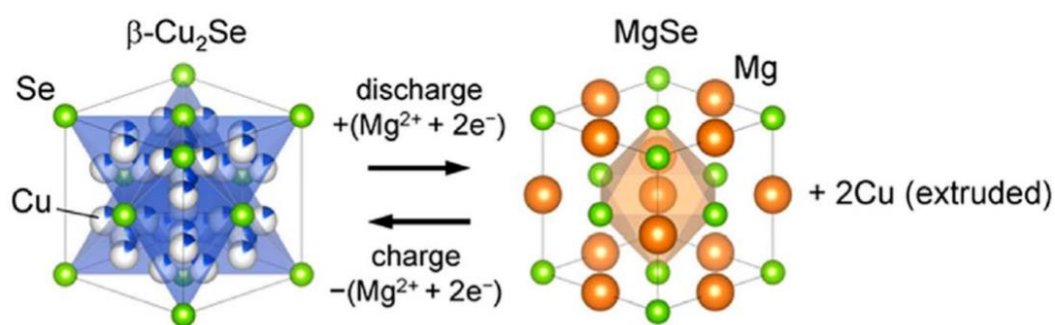


**Figure 1.13.** Crystal structure of  $\beta\text{-Cu}_2\text{Se}$  and a schematic for the displacement reaction with  $\text{Mg}^{2+}$  ions.<sup>190</sup>

#### 1.6.4.3. Spinel structure

With the particular formula  $\text{AB}_2\text{X}_4$  ( $\text{X}$  = chalcogenide, oxygen) the spinel structure has demonstrated to be a hopeful host lattice for magnesium insertion positive electrode. The structure owns cubic symmetry with oxygen ions in a face-centered cubic close packing configuration. The A and B cations complete an eighth of the tetrahedral and half of the octahedral sites in the oxygen sublattice interstices in different configurations, depending on their stabilizing energies in the crystal field. Covering these interstitial sites was proposed for the reversible insertion of Mg resulting in  $\text{Mg}_{1+x}\text{M}_2\text{O}_4$  ( $x < 1$  and  $\text{M} = \text{Co}, \text{Cr}, \text{Fe}, \text{or Mn}$ ). High

oxygen density close packing coupled with interconnected disfavored 4-fold concerted Mg sites is an advantage for high energy density material with potentially high Mg-cation mobility.<sup>191,192</sup>

The first evaluation of an oxo-spinel material for an Mg-ion insertion material confirms its average voltage, high capacity, and stability. Based on these results, spinel-type compounds are promising as electrochemically Mg-ion material. However, high voltage stable electrolytes were problematic, inducing more studies to be performed.<sup>193</sup>

DFT calculations established  $\lambda$ - $\text{Mn}_2\text{O}_4$  as a significant polymorph for high energy density Mg insertion material vs. conversion, and it has obtained a considerable interest.<sup>194,195</sup> The spinel based on chromite,  $\text{Mg}_{1-x}\text{Cr}_2\text{O}_4$  seems to exhibit also interesting properties. Some property improvements can be performed through material engineering and the inclusion of tailored structural, composition, or morphological complexity.<sup>194,196,197</sup>

#### 1.6.4.4. Organic materials

Although inorganic positive materials exhibit several good properties including insolubility, stable during cycling or easy to synthesize, they are still limit by many obstacles: low theoretical capacity, heavy metal containing, and low redox potential. The fact that redox-active organic materials could be used with different counterions allows them became an interesting target for operation in post-LIBs where so many potential inorganic materials suffer from the poor insertion of cations, particularly considering the insertion of multivalent ions, such as  $\text{Mg}^{2+}$ ,  $\text{Ca}^{2+}$ , and  $\text{Al}^{3+}$ . One of the key drawbacks of redox-active organic materials is their poor volumetric power, but this can be effectively compensated by the high volumetric density of the Mg electrode. Because of the difference in the redox potential of Li and Mg metal, the voltage of a Mg metal-organic battery should be about 0.7 V lower than its Li metal equivalent.<sup>198,199</sup> The main drawback of redox-active organic materials in different types of batteries containing organic solvents for electrolytes is the process of dissolution, which can significantly reduce the cycle life of these materials. To mitigate this issue, various research groups proposed either grafting redox-active organics on solid support, insoluble redox-active salts, preparing insoluble polymers, or using selective separators.<sup>198,200</sup> Organic materials frequently comprise electrophilic center which makes them inconsistent with Mg electrolytes containing nucleophilic species, generally those synthesized from Grignard reagents. Thereby, the growth of non-nucleophilic electrolytes has become fundamentally important to allow electrochemical examinations of all organic materials in Mg metal battery systems, particularly those containing conjugated carbonyl groups and various sulfides.<sup>201</sup>



### a. Carbonyl-based materials

Recently, quinone-based materials have become a promising candidate to become cathode for magnesium batteries. In this section, only the materials which were used in magnesium batteries were mentioned. An extensive account of carbonyl materials in batteries was already reviewed.<sup>202</sup>

#### 1,4-benzoquinone (BQ), 1,4-naphthoquinone, anthraquinone

1,4-benzoquinone (BQ), 1,4-naphthoquinone, anthraquinone are commercially available or obtained after oxidizing the corresponding phenols.<sup>203</sup> Besides some recent advances in quinone chemistry were reviewed elsewhere.<sup>204</sup>

In 2020, Bitenc *et al.* investigated three quinone-based materials namely anthraquinone (AQ), 1,4-naphthoquinone (NQ), and 1,4-benzoquinone (BQ) to compare their electrochemical performance and redox potential.<sup>205</sup> They were used as positive electrode in two different electrolytes for magnesium batteries: 0.6 M Mg(TFSI)<sub>2</sub>-2MgCl<sub>2</sub> (MTC) and 0.6 M MgCl<sub>2</sub>-AlCl<sub>3</sub> (MAC) in DME. Using MTC electrolyte, the initial capacities are high with 152 mAh/g, 138 mAh/g, and 130 mAh/g for AQ, BQ, and NQ respectively, at the first cycle. (Figure 1.14a)

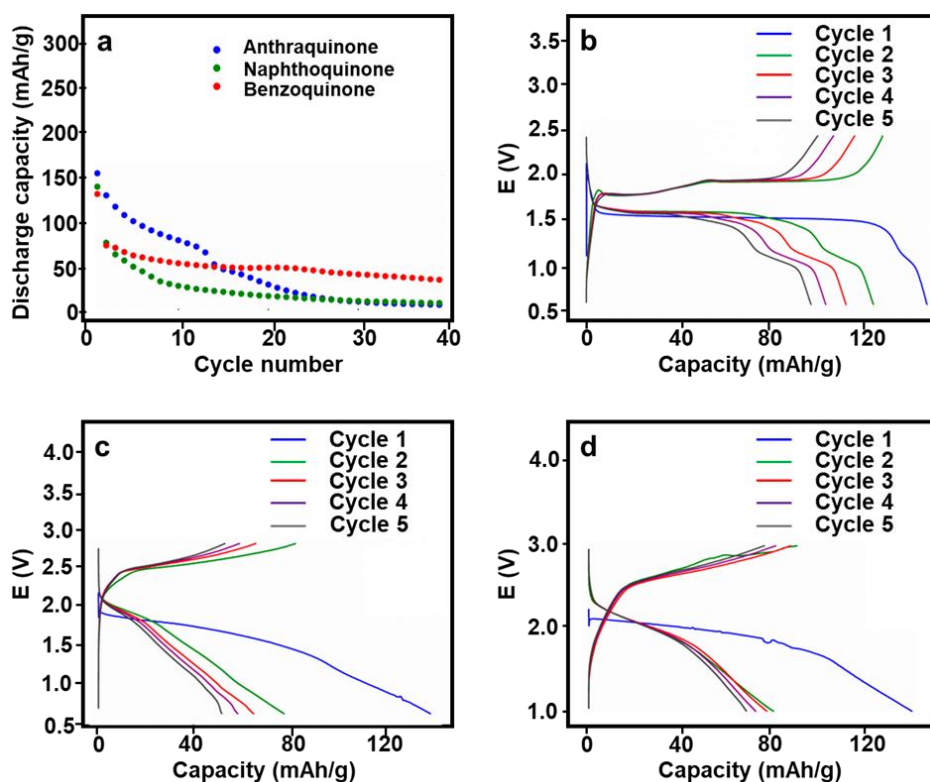


**Figure 1.14.** (a) Discharge capacity of AQ, NQ, BQ in 0.6 M Mg(TFSI)<sub>2</sub>-2MgCl<sub>2</sub> electrolyte with Mg foil as anode after 40 cycles at 100 mA/g. First five charge/discharge curves of (b)

AQ, (c) NQ, (d) BQ at 100 mA/g in MTC electrolyte. AQ, NQ, BQ were cycled in different potential windows 0.5 – 2.5 V, 0.75 – 2.75 V and 1.0 – 3.0 V, respectively.<sup>205</sup>

However, the discharge capacity dramatically decreases for anthraquinone from 150 mAh/g to 10 mAh/g after 40 cycles while the capacity was above 60% of the initial capacity in the case of BQ (**Figure 1.14b,c,d**). The main reason for that was the solubility of active material into the organic solvent used. Thus, for the long-term application in Mg systems, the solubility of positive materials needs to be solved.

### 2,5-dimethoxybenzoquinone

2,5-dimethoxybenzoquinone (DMBQ) was first introduced as a promising cathode for magnesium battery by Yao and coworkers in 2012.<sup>206</sup> To investigate the electrochemical of DMBQ, Kiyobayashi group<sup>206</sup> took different approaches. They tested 2,5-dimethoxybenzoquinone (DMBQ) in two different electrolytes: Mg(ClO<sub>4</sub>)<sub>2</sub> in  $\gamma$ -butyrolactone ( $\gamma$ -GBL)<sup>206</sup> and Mg(TFSI)<sub>2</sub> in sulfone based solvent<sup>207</sup>. As reversible Mg plating/stripping in these electrolytes was not possible, the reversible cycling of the organic cathode was demonstrated using a three-electrode cell. The maximum discharge capacity at DMBQ was 260 mAh/g at the second cycle (theoretical value at 319 mAh/g) and retained 85% of the initial capacity after 5 cycles.

The charge/discharge of DMBQ is shown in **Figure 1.15a** with two plateaus at 0.8 and 1.1 V vs. Mg quasi-reference electrode. This value is significantly lower than 0.7 V the analogy potential of Mg<sup>2+</sup>/Mg versus NHE. One explanation could be the formation of a passive layer on the Mg reference electrode which induces a shift on its potential. EDX and XRD spectroscopies were applied to investigate the reversibility of the insertion/de-insertion Mg<sup>2+</sup> process (**Figure 1.15b**). In sulfolane + 0.5 M magnesium bis(trifluoromethanesulfonyl)imide (Mg(TFSI)<sub>2</sub>), charge/discharge process can be observed over 50 cycles in a two-cell configuration. The discharge capacity of Mg|Mg(TFSI)<sub>2</sub>/sulfolane|DMBQ was obtained at 100 mAh/g at the 10<sup>th</sup> cycle (**Figure 1.15c**) and reduced to 20 mAh/g at the 50<sup>th</sup> cycle (**Figure 1.15d**) with large overpotential for charge and discharge processes. In DME and diglyme solutions, the discharge capacity reached 200 mAh/g, however, the capacity decreased a lot during cycling and stopped at the 20<sup>th</sup> scan with high voltage hysteresis.

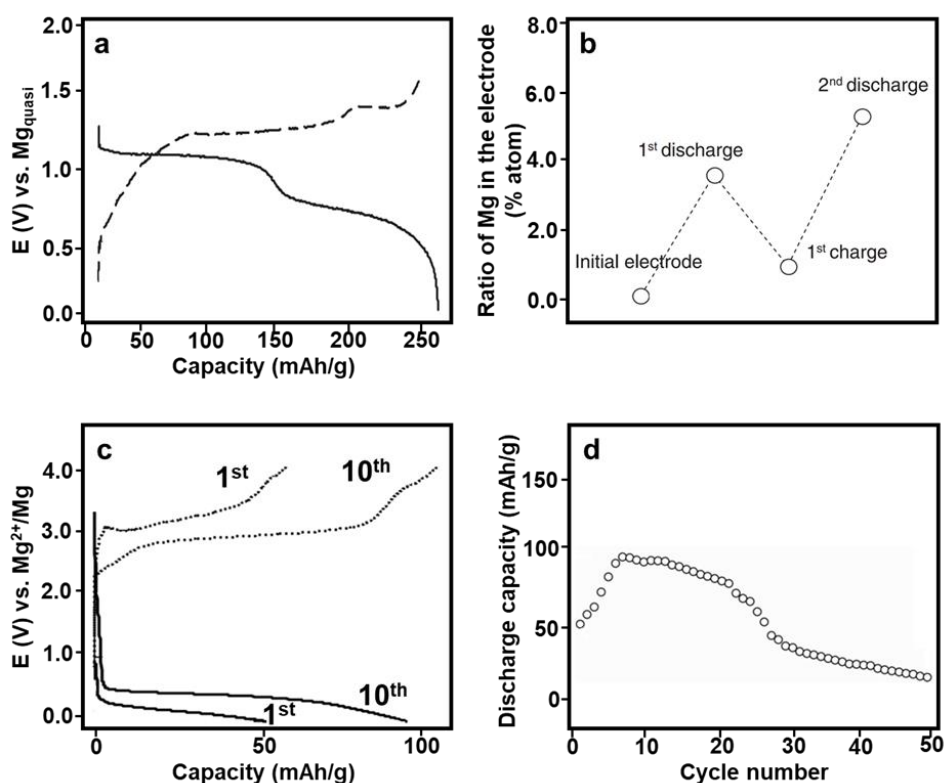


**Figure 1.15.** (a) Typical charge/discharge curve of DMBQ. (b) EDX measurement of cathode after first and second cycle. (c). Charge/discharge of Mg|Mg(TFSI)<sub>2</sub>/sulfolane|DMBQ at 30 °C in potential window 0 – 4 V. (d). Discharge capacity of Mg|Mg(TFSI)<sub>2</sub>/sulfolane|DMBQ with cell voltage from 0 V to 4 V with discharge current at 10 mA/g at 30 °C.<sup>206</sup>

### Rhodizonate salt

A renewable rhodizonate compound was introduced with Mg-Li dual salt electrolyte.<sup>208</sup> Three types of structures were reported based on the crystal structure and cation: as-precipitated Na<sub>2</sub>C<sub>6</sub>O<sub>6</sub>, bulk phase, Li<sub>2</sub>C<sub>6</sub>O<sub>6</sub> renamed as n-SR, b-SR, and LR respectively. All experiments were operated with Mg foil as anode and a hybrid electrolyte containing 1 M LiCl and 0.25 M phenyl complex (ACP) in two potential windows 0.1 – 2.0 V and 0.1 – 2.75 V vs. Mg<sup>2+</sup>/Mg (Figure 1.16). With adapted potential conditions, a long life cyclability up to 600 cycles was reached with high coulombic efficiency and without Mg dendrite formation. However, in that configuration, Li<sup>+</sup> could be the only cation involved in the insertion process.

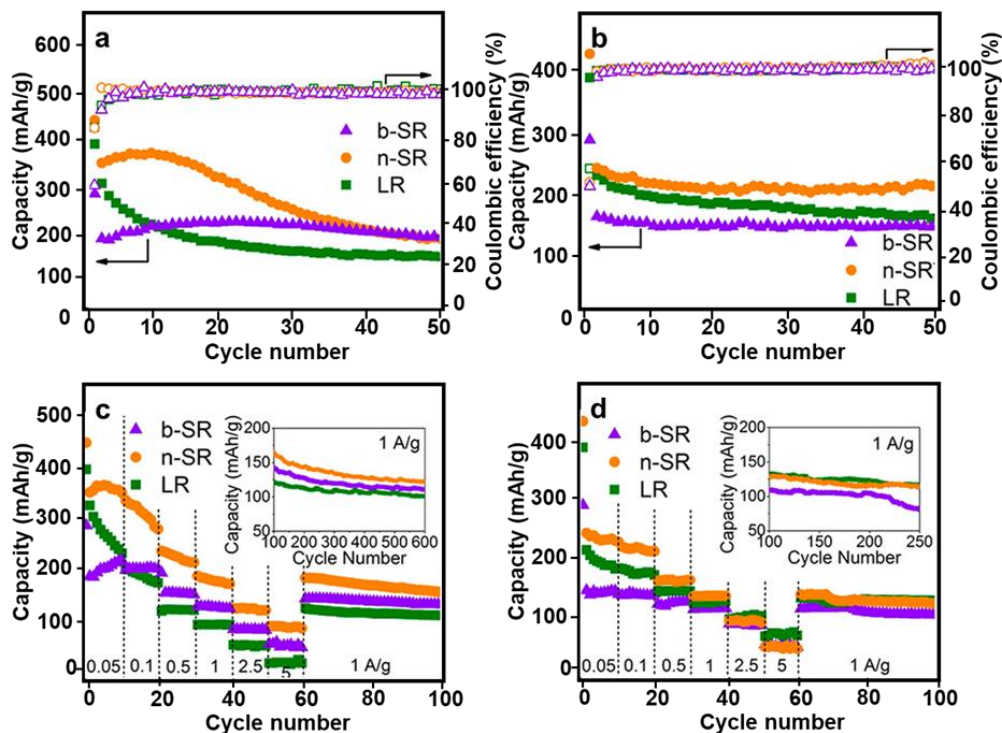


**Figure 1.16.** Discharge capacity and coulombic efficiency of MLBs based on b-SR, n-SR, and LR cathodes as a function of cycle number in a voltage range of (a) 0.1 – 2.75 V and (b) 0.1 – 2.0 V at 50 mA/g. Rate performance of b-SR, n-SR, and LR from 0.05 to 5 A/g at (c) 0.1 – 2.75 V and (d) 0.1 – 2.0 V. Insets: Discharge capacity of corresponding electrodes as a function of cycle number at 1 A/g after 100 cycles.<sup>208</sup>

### Anthraquinone derivatives

Using the electrolyte developed by Kim *et al.*,<sup>209</sup>  $\text{Mg}_2\text{Cl}_3\text{-HMDSAICl}_3$  (HMDS = hexamethyldisilazane), Dominko *et al.* studied poly(anthraquinoyl sulfide) (PAQS) as a positive electrode in a two-cells configuration using Mg as the negative electrode.<sup>210</sup> In order to limit the polarization effect during cycling, associated with the Mg passivation, Mg powder was used instead of Mg foil.

The Mg-PAQS battery showed an initial capacity of 98 mAh/g which subsequently enhanced to 105 mAh/g and gradually faded to 60 mAh/g after 80 cycles. Different electrolytes were used (**Figure 1.17**).  $\text{Mg}(\text{TFSI})_2\text{-MgCl}_2$  in THF:DME (2/3 %vol) (MTCC) exhibited the best performances in terms of capacity and power (**Figure 1.17b**) with over 220 mAh/g at C/5 at the 5<sup>th</sup> cycle and remained at 50 mAh/g after 100 cycles (**Figure 1.17b**) while the pristine capacity in MACC electrolyte was limited at 120 mAh/g at C/5 and decreased to 40 mAh/g at the 100<sup>th</sup> scan (**Figure 1.17a**). At the highest rate (500 mA/g), the discharge capacity of PAQS was

observed at 100 mAh/g in MTTC but it was near zero for the MACC electrolyte and 70 mAh/g in MHCC (Figure 1.17c,d).

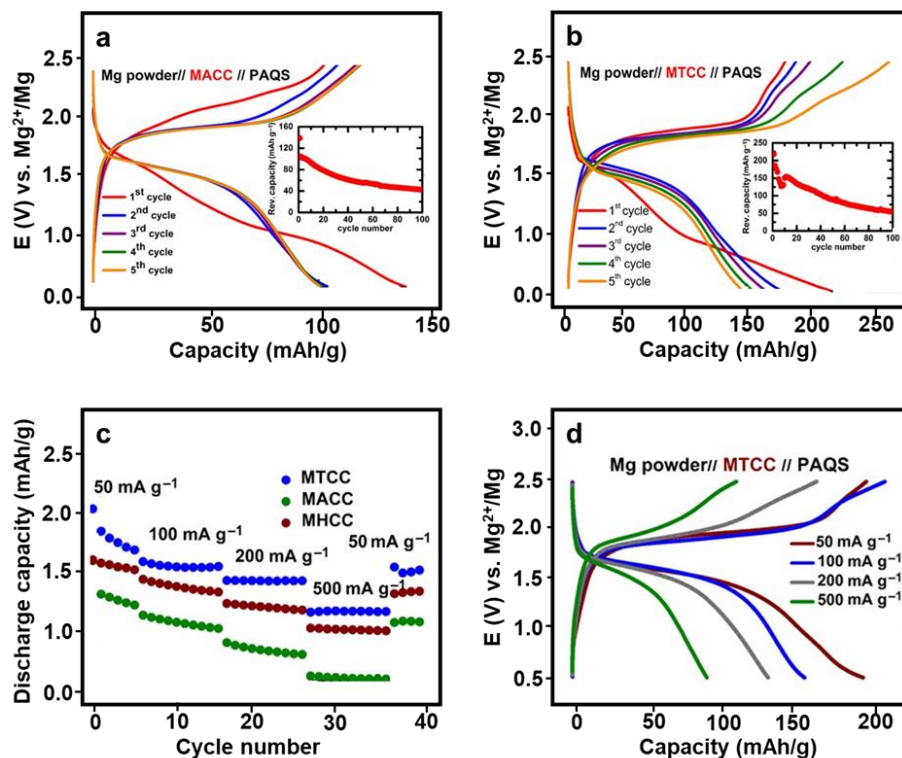


**Figure 1.17.** (a) Charge/discharge curves for cycling of PAQS in a. MACC, (b) MTCC. (c) Rate capacity test of PAQS in MTCC, MACC, MHCC. (d) Charge/discharge cycles in MTCC at different C-rate.<sup>210</sup>

Electrochemical monitoring in another Mg electrolyte,  $\text{Mg}(\text{TFSI})_2\text{-MgCl}_2$  TEG:DOL (1/1 % vol), demonstrates expanded retention capacity with the highest capacity obtained at 135 mAh/g at C/10 and 72 mAh/g at C which was lower than in prior study on MTCC electrolyte.<sup>211</sup> The electrochemical mechanism of the PAQS cathode was subsequently investigated by applying operando infrared (IR) spectroscopy as shown in Figure 1.18.<sup>211</sup> Based on the ATR-IR spectra, changes inside the cathode caused by electrochemical cycling were noticed such as the decrease in the intensity of C=O and C=C bands and the increase of the strong band at 1370  $\text{cm}^{-1}$  related to  $\text{C-O}^- \text{Mg}^{2+}$  during the charge process.

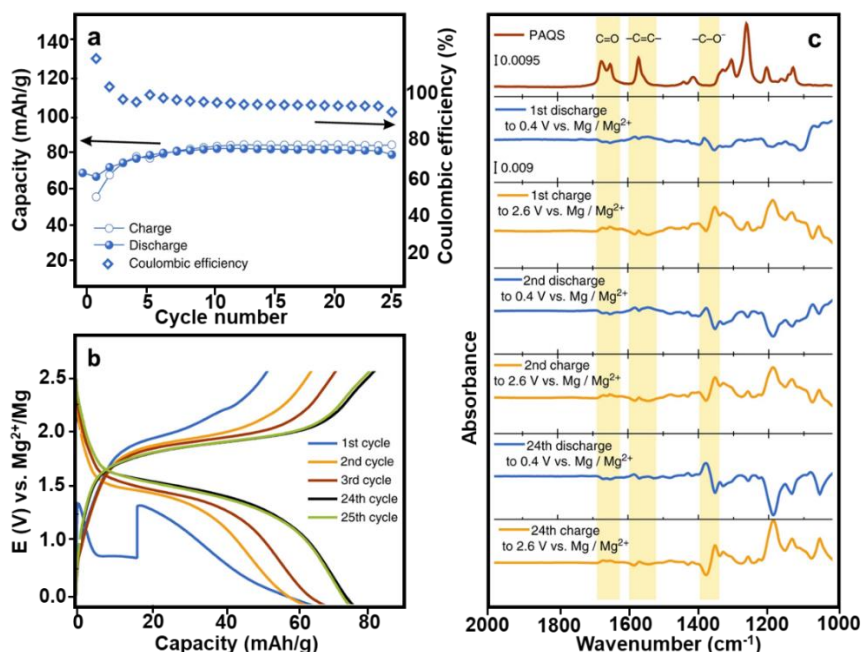


**Figure 1.18.** (a) Capacity and coulombic efficiency of a Mg-PAQS battery cell at 50 mA/g in Mg(TFSI)<sub>2</sub>-MgCl<sub>2</sub> in TEG:DOL (1/1 vol%) and (b) selected galvanostatic cycles. (c) ATR-IR difference spectra for the PAQS cathode during cycling.<sup>211</sup>

Another polyanthraquinone derivatives, 2,6-polyanthraquinone (26PAQ) and 1,4-polyanthraquinone (14PAQ) were tested as cathodes in magnesium batteries.<sup>212</sup> Following the PAQS study, Song *et al.*<sup>213</sup> selected polyanthraquinone (PAQ) (theoretical capacity at 260 mAh/g) as a positive electrode in the Mg system with Mg(HMDS)<sub>2</sub>-4MgCl<sub>2</sub> in THF as an electrolyte. This system showed impressive performance in Li-battery with only 1% capacity reduces after a thousand cycles at 1C.<sup>23</sup> However, the capacity from the first scan in Mg batteries was at 140 mAh/g and retained at 110 mAh/g after 100 cycles at C/2 using 14PAQ (Figure 1.19a,b) and 100 mAh/g for 26PAQ in the same condition.

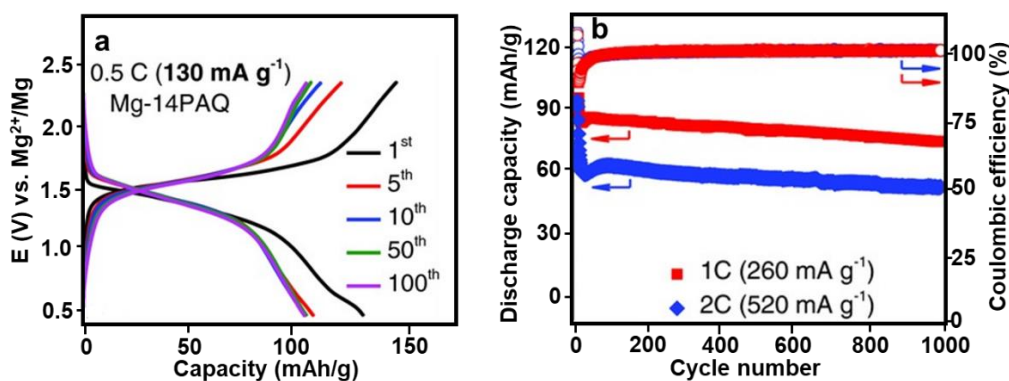


**Figure 1.19.** (a) Charge/discharge curves at 0.5C from in different scans: first, 5<sup>th</sup>, 10<sup>th</sup>, 50<sup>th</sup> and 100<sup>th</sup> cycle. (b) Discharge capacity and Coulombic efficiency of 14PAQ at 1C and 2C.<sup>213</sup>

Recently, a new solution for cathode material in magnesium rechargeable batteries was introduced by Cui *et al.*<sup>214</sup> based on the red pigment naming 3,4,9,10-perylenetetracarboxylic dianhydride (PTCDA). In this study, all phenyl complex (APC) electrolyte with or without LiCl was used because the introduction of dissolvable salt (1 M LiCl) could help to optimize the utilization of the active material. The system showed an attractive cyclability for over hundred scans with a discharge capacity of 126 mAh/g (Figure 1.20a,c) and maintain over 100 mAh/g after 150 cycles.

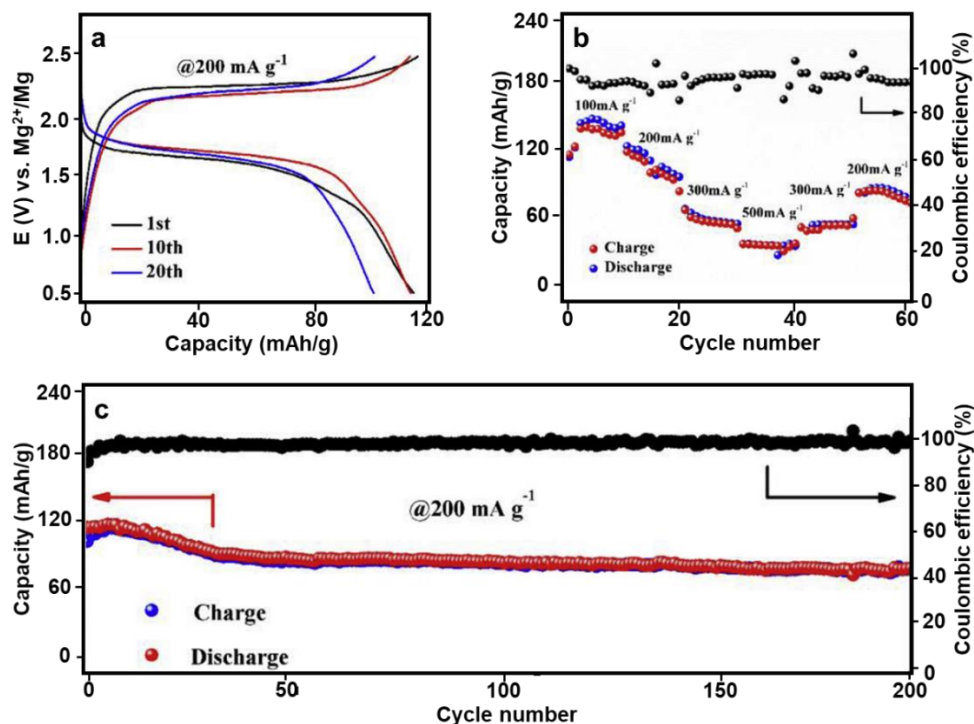


**Figure 1.20.** (a) Charge/discharge of PTCDA in APC electrolyte at 200 mA/g. (b) Rate performance of the PTCDA electrode at current densities of 100, 200, 300, 500 mA/g. (c) Cyclability of PTCDA positive electrode and coulombic efficiency at 200 mA/g after 200 cycles.<sup>214</sup>

## b. Nitrogen-based materials

### Diimide and polyimide derivatives

The polyimide were another group of conjugated carbonyl compounds that had been evaluated as positive materials for Mg battery electrodes. Generally, these materials are synthesized by the polycondensation of various dianhydrides and diamines.<sup>215</sup> Dominko and coworkers<sup>216</sup> used naphthalene-hydrazine diimide as a cathode for magnesium batteries. The discharge voltage

was approximately 1.7 V with a capacity of around 80 mAh/g in TEGDME/DOL and 60 mAh/g after 100 cycles in pure TEGDME involving 0.4 M Mg(TFSI)<sub>2</sub> and 0.4 M MgCl<sub>2</sub> as salt.

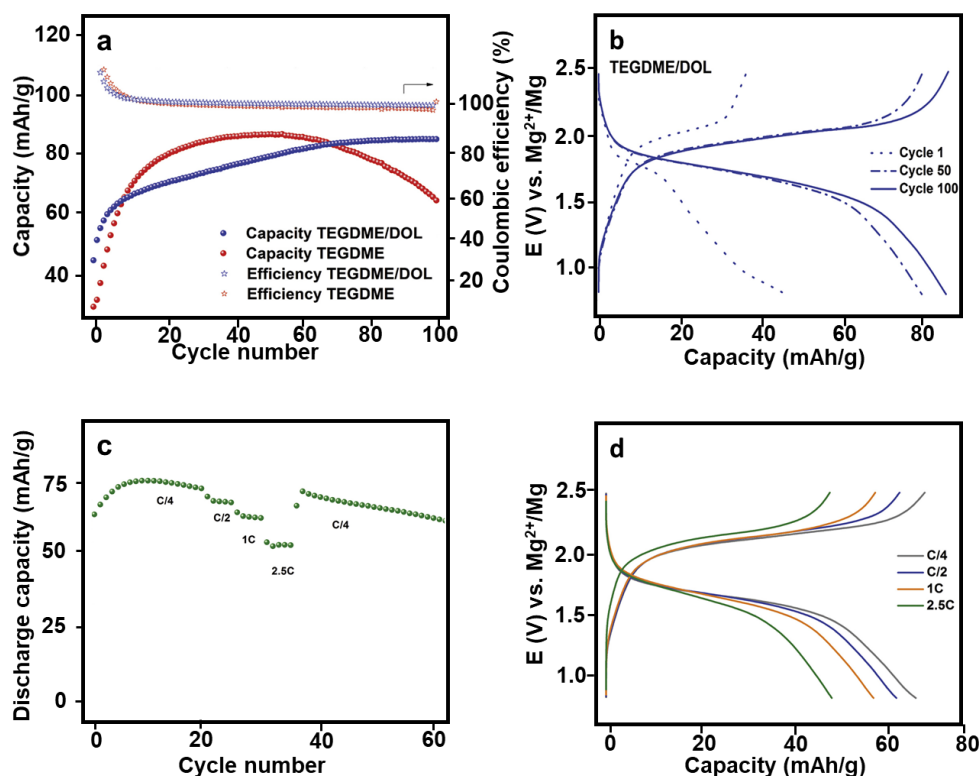


**Figure 1.21.** (a) Cyclability of NP in two electrolytes : TGEDME/DOL and TEGDME at C/4. (b) Charge/discharge of the first, 50, and 100<sup>th</sup> cycles in TEGDME/DOL based electrolyte at C/4. (c) Discharge capacities from C/4 to 2.5C. (d) Charge/discharge curves in different rates: C/4, C/2, 1C and 2.5C with voltage window from 0.8 – 2.5 V vs. Mg<sup>2+</sup>/Mg.<sup>216</sup>

An organic material showing a fast and stable cyclability in rechargeable Li-ion named poly{[N,N'-bis(2-octyldodecyl)-1,4,5,8-naphthalenedicarboximide-2,6-diyl]-alt-5,5'-(2,2'-bithiophene)} (P(NDI2OD-T2)) was introduced for magnesium batteries by Yao and coworkers.<sup>115</sup> This bulky molecule possessed a theoretical capacity of 54 mAh/g. The charge/discharge curve in **Figure 1.22** shown two plateaux corresponding to a specific capacity of 53 mAh/g (97% of theoretical one) in 0.25 M Mg(TFSI)<sub>2</sub> + 0.5 MgCl<sub>2</sub> in DME. EDX measurement was carried during charge/discharge processes and indicated the ratio of Mg:S:Cl at 1:1.97:0.97 corresponding to one-electron transfer to one MgCl<sup>+</sup> insertion. The MgCl<sup>+</sup> insertion instead of Mg<sup>2+</sup> was previously introduced in several reports<sup>217–220</sup>. At the end of the charge, the pristine compound was obtained. MgCl<sup>+</sup> plays a significant role in all the solvent involving chloride ion in organic magnesium batteries. In this specific material, with non-chloride electrolytes, the same capacity is obtained whereas EDX spectrum shown no anion co-



insertion with  $\text{Mg}^{2+}$  (**Figure 1.22**). Moreover, excellent coulombic efficiency and 87% of its initial capacity after 2500 cycles were achieved. In short conclusion, P(NDI2OD-T2) is one of the best organic cathode material until now even though its theoretical capacity is not very high comparing to others.<sup>115</sup>

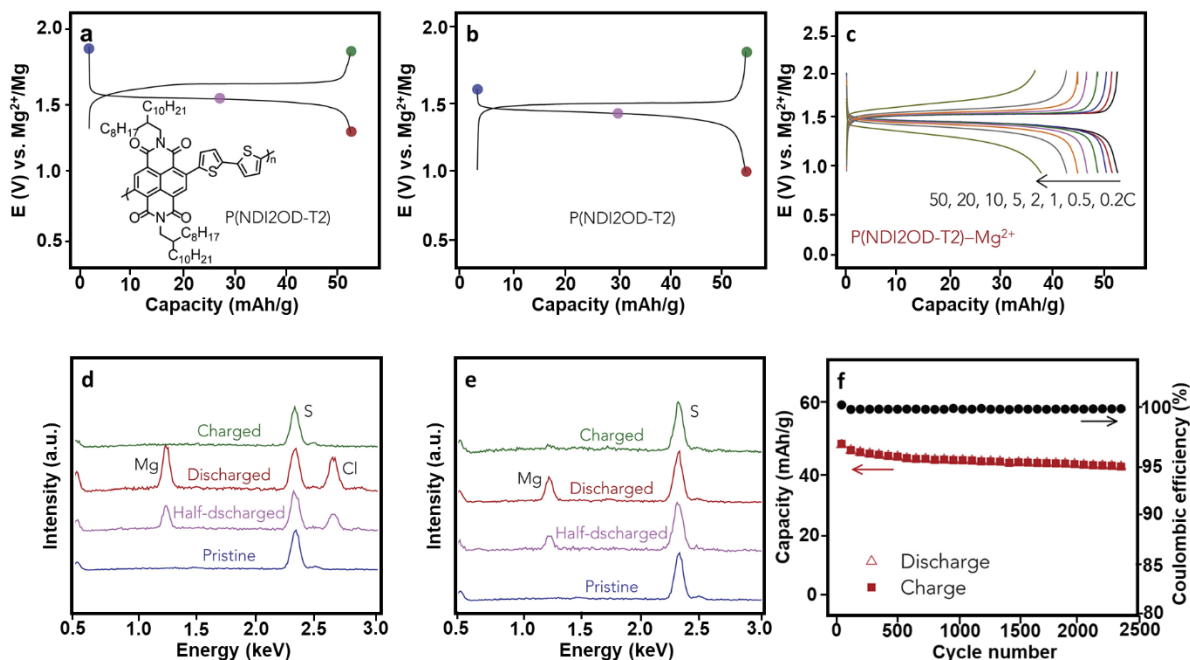
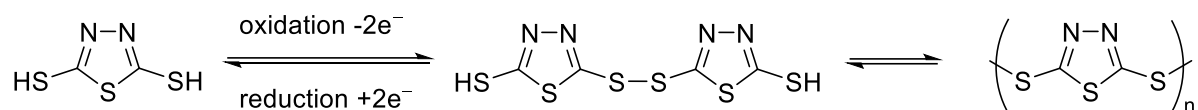


**Figure 1.22.** First charge/discharge curve of P(NDI2OD-T2) in (a) 0.5 M  $\text{MgCl}_2$  and 0.25 M  $\text{Mg}(\text{TFSI})_2$  in DME. (b) 0.2 M  $\text{Mg}(\text{TFSI})_2$  in diglyme at 11 mA/g. (c) Voltage profile in different C-rates. EDX spectra at different states of charge in (d) 0.5 M  $\text{MgCl}_2$  and 0.25 M  $\text{Mg}(\text{TFSI})_2$  in DME. (e) 0.2 M  $\text{Mg}(\text{TFSI})_2$ . (f) Cycling stability and coulombic efficiency of P(NDI2OD-T2) at 300 mA/g.<sup>115</sup>

Recently, Wang and coworkers<sup>221</sup> introduced polyimide-carbon nanotubes as a universal cathode for magnesium-ion batteries, which possessed excellent cyclability performance and strong power density. In their study, 1,2,4,5-benzenetetracarboxylic anhydride-ethylene diamine (PMDA-EDA) and 1,4,5,8-naphthalenetetracarboxylic dianhydride-ethylene diamine (NTCDA-EDA) copolymer were synthesized by the reaction between pyromellitic acid and 1,4,5,8-naphthalenetetracarboxylic dianhydride with ethylenediamine in the presence of carbon nanotube and polyimides@CNT (PI@CNT).<sup>221</sup> The structure of these two polymers was shown in **Figure 1.23**.



the oxidation or reduction processes between thiol and disulfide which included 2 electrons transfer led to the formation of 2,5-dimercapto-1,3,4-thiadiazole (DMcT), and this polymer was easily depolymerization (**Scheme 1.1**). The broken or creation S-S bond during charge/discharge was reversible at a high temperature of 100 – 150 °C.



**Scheme 1.1.** Electrochemical redox process of DMcT.<sup>223</sup>

For the magnesium batteries study, polyaniline (PAn) could be used to make a composite with DMcT to increase the redox potentials. The results showed only 17 mAh/g capacity for the first scan and rise to 29 mAh/g after 10 cycles (**Figure 1.25**). Two plateaus at 0.9 and 1.4 V in the discharge curve indicated two reaction processes of PAn and DMcT with  $Mg^{2+}$ , respectively. After 25 cycles, discharge capacity was increased near double to initial value. It was explained by the incompleted using at the first scan from organic positive material. While the theoretical capacity was about 224 mAh/g, the low capacity reported was due to the high polarization effect associated with the divalent character of magnesium ion.

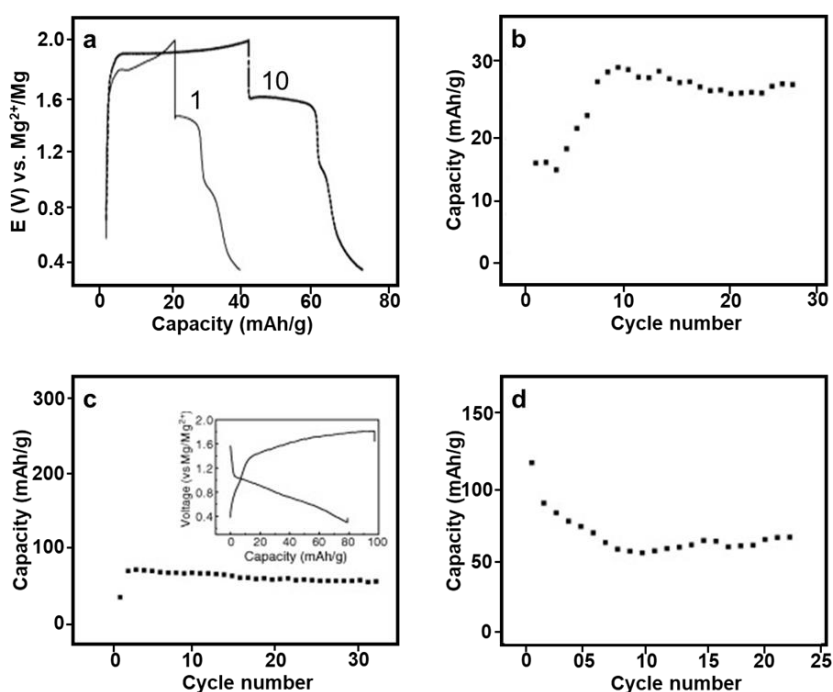
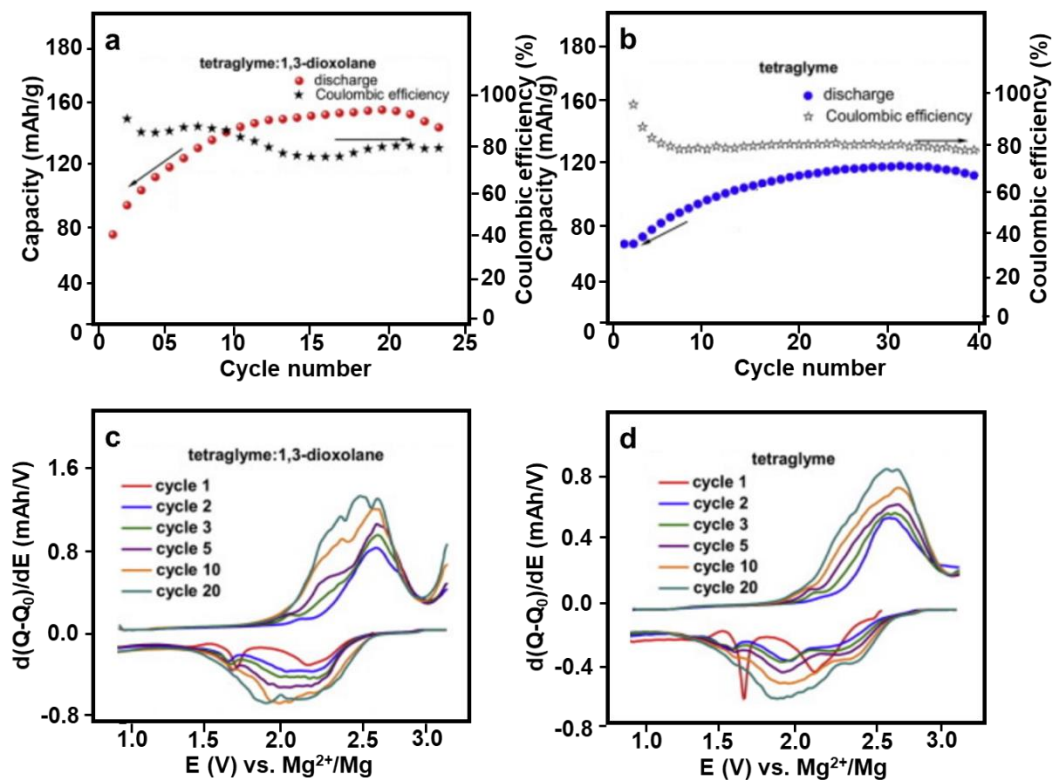


**Figure 1.25.** (a) The charge/discharge results on DMcT-PAN/Mg test for the first and 10<sup>th</sup> cycles. (b) Discharge capacity of DMcT-PAN/Mg test. (c) Discharge capacity of PDTDA/Mg test. (d) Discharge capacity of CSM-PAN/Mg test.<sup>223</sup>

The second compound in NuLi and Guo studies, poly-2,2'-dithiodianiline (PDTDA), which was known as a new class of a conducting polymer with a disulfide bond. PDTDA reached 78 mAh/g (**Figure 1.25c**) after 30 cycles with weak charge/discharge efficiency reaching 80% in 0.25 M MgAlCl<sub>3</sub>Bu<sub>2</sub>/THF electrolyte. The improvement in battery performance could be due to the better S-S creation which led to the increasing electrocatalytic effect on the cell.

In contrast to those molecules, CSM-PAn complex which contains a  $\pi$ -conjugation and C-S-S-C covalent bond showed a higher discharge capacity with 117 mAh/g at the first scan and remained at 78% up to 22 cycles. The disulfide bonds in this polymer help to keep stable polymer chains. While pristine CSM material did not work well with only 51 mAh/g at the first discharge curve which was reduced rapidly after several cycles due to Mg<sup>2+</sup> trapping. The report indicated 3 steps to improve the performance in magnesium batteries with organosulfide as cathode material: i) suitable catalyst, ii) increasing number of S-S function on the polymer, and iii) improve the conductivity of the material. These approaches could help to enhance the specific capacity and cyclability in the study with this kind of material as a positive electrode in the Mg system. Although up to now, only one report from NuLi and Guo<sup>223</sup> introduced this conductive sulfur-containing material as potential material for magnesium batteries cathode.

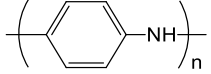
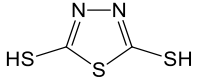
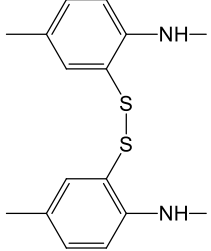
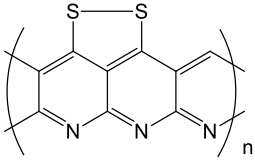
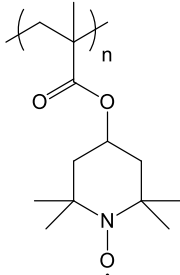
To increase the insolubility of quinone based materials in organic solvent, a sulfur-bridged polymer poly(hydroquinoyl-benzoquinoyl)sulfide (PHBQS)<sup>224</sup> including both hydroquinone and benzoquinone species was formed via solvothermal reaction. This PHBQS was investigated in both Li and Mg battery configurations.<sup>224,225</sup> This polymer in the Mg system exhibits a discharge voltage of about 2 V vs. Mg<sup>2+</sup>/Mg with high capacity at 158 mAh/g (**Figure 1.26**). This study was performed in 0.48 M Mg(TFSI)<sub>2</sub> + 0.32 M MgCl<sub>2</sub> in tetraglyme:1,3-dioxolane solvent. The weak coulombic efficiency (80%) due to the reactive electrolyte system needs to be studied.<sup>224</sup>

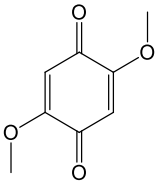
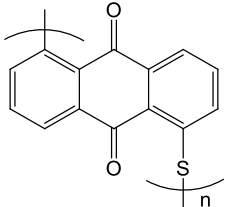
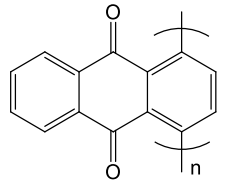
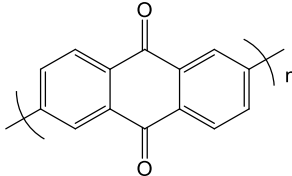
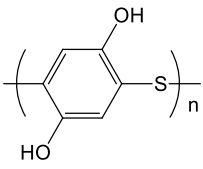
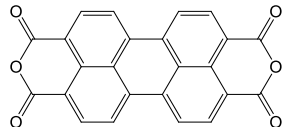


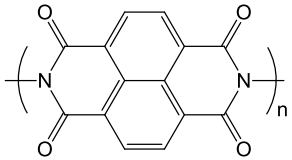
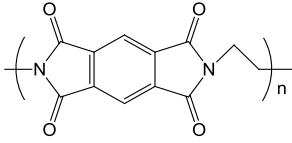
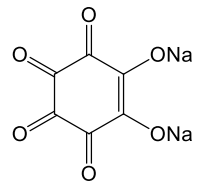
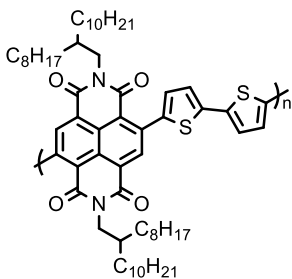
**Figure 1.26.** (a) Discharge capacity and coulombic efficiency in the Mg system at 50 mA/g in tetraglyme: dioxolane electrolyte. (b) discharge capacity and coulombic efficiency in the Mg system at 50 mA/g in tetraglyme electrolyte. (c) derivatives of selected galvanostatic cycles at 50 mA/g in tetraglyme: 1,3-dioxolane electrolyte and (d) derivatives of selected galvanostatic cycles at 50 mA/g in tetraglyme electrolyte.<sup>224</sup>

**Table 1.5** below summarizes all of the organic cathodes using in magnesium batteries.

**Table 1.5.** Organic cathode using in magnesium batteries.

Materials <sup>ref.</sup>	Structure	Anode	Electrolyte	Voltage window (V)	Initial reversible capacity (mAh/g) at current density (mA/g)	Cyclability (mAh/g), current density (mA/g)
Polyaniline (PAn) <sup>226</sup>		Mg foil	2 M MgCl <sub>2</sub> ; MgBr <sub>2</sub> ; Mg(ClO <sub>4</sub> ) <sub>2</sub> (aqueous)	1.0 – 1.6	-	-
2,5-dimercapto-1,3,4-thiadiazole (DMCT) <sup>223</sup>		Mg foil	0.25 M Mg(AlCl <sub>2</sub> BuEt) <sub>2</sub> /THF	0.3 – 2.0	16.8 at 25	27.2 after 26 cycles, 25
Poly-2,20 dithiodianiline (PDTDA) <sup>223</sup>		Mg foil	0.25 M MgAlCl <sub>3</sub> Bu <sub>2</sub> /THF	0.3 – 1.8	50 at 25	65 after 33 cycles, 25
Conductive sulfur-containing material (CSM) <sup>223</sup>		Mg foil	0.25 M Mg(AlCl <sub>2</sub> BuEt) <sub>2</sub> /THF	0.3 – 2.0	117.3 at 25	73 after 22 cycles, 25
Poly(2,2,6,6-tetramethylpiperidinyloxy-4-yl methacrylate) (PTMA) <sup>222</sup>		Mg foil	0.25 M Mg(AlCl <sub>2</sub> BuEt) <sub>2</sub> /THF	0.3 – 1.8	81.2 at 22.8	23 after 21 cycles, 22.8

Dimethoxybenzoquinone (DMBQ) <sup>227</sup>		Mg foil	0.5 M Mg(ClO <sub>4</sub> ) <sub>2</sub> /butyrolactone	0.2 – 1.6	260 at 20	221 after 5 cycles, 20
Poly(antraquinoyl) sulfide (PAQS) <sup>76</sup>		Mg powder	0.37 M MgCl <sub>2</sub> and 0.15 M Mg(TFSI) <sub>2</sub> in THF/glyme	0.5 – 2.5	225 at 50	60 after 100 cycles, 50
1,4-Polyanthraquinone (1,4-PAQ) <sup>228</sup>		Mg foil	0.3 M Mg(HMDS) <sub>2</sub> -4MgCl <sub>2</sub> /THF	0.5 – 2.5	122 at 130	100 after 100 cycles, 130
2,6-Polyanthraquinone (2,6-PAQ) <sup>228</sup>		Mg foil	0.3 M Mg(HMDS) <sub>2</sub> -4MgCl <sub>2</sub> /THF	0.5 – 2.5	132.7 at 130	104.9 after 100 cycles, 130
Polyhydroxybenzoquinonylsulfide (PHBQS) <sup>229</sup>		Mg powder	0.48 M MgCl <sub>2</sub> and 0.32 M Mg(TFSI) <sub>2</sub> in tetraglyme and 1,3-dioxolane 4:5	0.8 – 3.0	75 at 50	140 after 25 cycles, 50
PTCDA <sup>230</sup>		Activated carbon	4.8 M Mg(NO <sub>3</sub> ) <sub>2</sub> (aqueous)	-0.8 – 0.2	136 at 500	80 after 37 cycles, 500

NP <sup>216</sup>		Mg powder + 5 wt.% MgCl <sub>2</sub>	0.4 M Mg(TFSI) <sub>2</sub> and 0.4 M MgCl <sub>2</sub> in tetraglyme/DME/1,3-dioxolane	0.8 – 2.5	45 at 50	85 after 100 cycles, 50
PPMDA <sup>221</sup>		Mg foil	4 M Mg(TFSI) <sub>2</sub> (aqueous)	1.7 – 2.5	110 at 100	96 after 500 cycles, 100
Na <sub>2</sub> C <sub>6</sub> O <sub>6</sub> <sup>208</sup>		Mg foil	0.25 M APC and 1 M LiCl/THF	0.1 – 2.75	350 at 50	200 after 50 cycles, 50
P(NDI2OD-T2) <sup>115</sup>		Mg foil	0.2 M Mg(TFSI) <sub>2</sub> in diglyme	0.8 – 2.0	49 at 300	43 after 2500 cycles, 300



## 1.7. Conclusion and aim of the work

Recently many groups have begun investigating organic materials for their application in Mg batteries and significant progress has been made. Comparing the growth of the state of the art of Mg batteries in recent years, it may conclude that organic materials have swept up rapidly and in some cases even exceeded the performances of inorganic materials. In parallel, the introduction of new non-nucleophilic electrolytes opens up new avenues of study capable of proposing relevant solutions.

As demonstrated by the analysis provided in the previous sections, the interest in this area is actually increasing with drawbacks to be overcome. At the same time, it is also essential to emphasize that most of these studies are only preliminary, presenting generally complex synthetic pathways that could barely match a massive-scale production. Based on these considerations, the following aims can be drawn for this thesis, with two main objectives:

- Development of new non-hazardous magnesium salts and the use of  $\pi$ -electron rich molecules in order to develop relevant electrolytes.
- Development of organic positive electrodes with high energy density and cyclability. For that several targets will be investigated on the basis of enolate/carbonyl-based compounds for which affordable and green chemical approaches can be more easily undertaken. Polymers and polyanionic structures (organic salts) will be investigated in order to obtain insoluble materials.

The manuscript is composed of five chapters, where extensive description of obtained results is presented. Chapter 2 is devoted to the synthesized and characterized of salts and additives for Mg electrolytes. The electrochemical experiments are discussed based on cyclic voltammograms study (CV) with a first section dedicated to borohydride modified salt and the following one associated with the addition of  $\pi$ -molecules.

Chapter 3 is dedicated to the synthesis and the characterisation of poly(benzoquinonyldisulfide) (PBQDS) as organic positive material for both Li and Mg batteries. The comparison of the two systems is performed.

Chapter 4 is devoted to the preliminary study of carboxyphenolate salt as insoluble active material for Mg battery with CV method.

Chapter 5 will present the method and experiment part with all of the synthesizing and characterizing (physical and chemical) schemes. Moreover, the technique to prepare, store, dry electrolyte/electrode are also discussed.

## **Chapter 2:**

# **Electrolyte design for Mg batteries**

As previously discussed in the bibliographic chapter, the use of electrolyte additives and the development of new magnesium salts are effective ways for improving the performance of the Mg battery.<sup>231,232</sup> Most current anions applied in LIBs such as  $\text{PF}_6^-$ ,  $\text{AsF}_6^-$ ,  $\text{ClO}_4^-$ , present high anodic stability.<sup>233,234</sup> However, they cannot be used in the Mg system due to several reasons: formation of a resistive passive layer, incompatible with reversible Mg plating/stripping process associated with the decomposition of the electrolyte on the negative electrode surface. The introduction of  $\text{Mg}(\text{TFSI})_2$  and  $\text{MgCl}_2$  as salts for Mg-based electrolyte was developed, these electrolytes present an anodic stability voltage near 3 V vs.  $\text{Mg}^{2+}/\text{Mg}$ ,<sup>235,236</sup> however the corrosion of Al current collector can be observed in the presence of a large amount of  $\text{MgCl}_2$ . Besides, the solubility of  $\text{MgCl}_2$  is limited in ethereal solution which seems to be the most suitable solvents for magnesium battery. On the other side,  $\text{Mg}(\text{TFSI})_2$  alone is unable to permit the Mg plating/stripping reversibility. A number of magnesium boron salts were developed including:  $\text{Mg}(\text{BF}_4)_2$ ,<sup>116</sup>  $\text{Mg}(\text{C}_2\text{H}_{11}\text{B}_{10})\text{Cl}$ ,<sup>237</sup>  $\text{Mg}[\text{B}(\text{O}_2\text{C}_2(\text{CF}_3)_4)_2]_2$ ,<sup>117</sup> and  $\text{MgB}[(\text{hfip})_4]_2$  (hfip = hexafluoroisopropoxy)<sup>238</sup> as presented in detail in the chapter 1. However, their presences reduce the electrochemical window and limit the positive electrode material usable or, for some of them, there are difficult to synthesize. Latterly,  $\text{Mg}[\text{B}(\text{OPh})_3\text{H}]_2$ <sup>121</sup> besides  $\text{Mg}(\text{TFSI})_2$  was proposed and presented interesting properties (easy synthesis route, high anodic stability, high Mg plating/stripping reversibility).

In line with the work carried out on the  $\text{Mg}[\text{B}(\text{OPh})_3\text{H}]_2$ , this chapter will present our investigations in magnesium electrolytes including new borohydride-based salts relied on thiophenol or phenol derivatives.

Another strategy, using additives to improve the performance for Mg cell is also concerned. Typically, the quantity of additive in the electrolyte is no more than 5% by weight or volume, while its addition significantly improves Mg battery capacity and cycle life.<sup>176,239</sup> In a general point of view, for better battery efficiency, the additives can (1) promote the creation of efficient SEI on the negative electrode surface; (2) improve the Mg plating/stripping reversibility, (3) minimize the irreversible formation of gas during the SEI formation and long-term cycling; (4) protect positive electrode material from dissolution and overload, and (5) boost the physical properties of the electrolyte such as ionic conductivity, viscosity, polyolefin separator wettability, and so on. For better battery safety, the additives should exhibit: (1) lower flammability of organic electrolytes, (2) overload protection or increase overload tolerance, and (3) terminate battery operation under conditions of assault.<sup>240-242</sup> In this context, anthracene<sup>122</sup> was used as an additive to improve the Mg plating/stripping process reversibility. To go deeper

into the electrochemical mechanism understanding, in particular on the formation or not of a  $\pi$ -rich molecule Mg complex, the second part of this chapter will introduce several electrolytes containing  $\pi$ -rich molecules based on anthracene and non-anthracene structures, as additive.

### 2.1. Borohydride based salt

In 2018, Seydou *et al.*<sup>11</sup> designed and synthesized a new electrolyte based on diglyme as a solvent, and Mg(TFSI)<sub>2</sub> and magnesium triphenolateborohydride, Mg[B(OPh)<sub>3</sub>H]<sub>2</sub>, as Mg salts. The Mg[B(OPh)<sub>3</sub>H]<sub>2</sub> was obtained by the reaction of Mg(BH<sub>4</sub>)<sub>2</sub> with phenol in a one-step reaction. The combination of these two salts in diglyme permits to exhibit an electrolyte with high conductivity (5.5 mS/cm at 25 °C) and high Mg plating/stripping reversibility. By the addition of a slight amount of MgCl<sub>2</sub>, a coulombic efficiency of 90% in SS/Mg cell, a stable cycling performance, no dendrite formation, and a wide anodic potential of 3.4 V *vs.* Mg<sup>2+</sup>/Mg on Al current collector can be reached. The addition of a small amount of MgCl<sub>2</sub> enables the homogenous electrochemical reaction on the entire Mg electrode surface during cycling. Moreover, this electrolyte can support reversible and efficient Mg insertion/de-insertion with a high capacity of 94 mAh/g and 96% of coulombic efficiency in the Mo<sub>6</sub>S<sub>8</sub> Chevrel phase.

Although Mg[B(OPh)<sub>3</sub>H]<sub>2</sub> achieves high performances, some adjustments need to be accomplished. Synthesizing more soluble B-centered salts, modulating the degree of hydride substitution, and enhancing oxidative stability, have to be performed. Indeed, the Mg[B(OPh)<sub>3</sub>H]<sub>2</sub> was the only substance obtained with phenol, whatever the stoichiometry phenol/BH<sub>4</sub><sup>-</sup> used.

To these ends, the chemical modification of Mg(BH<sub>4</sub>)<sub>2</sub> with different phenol derivatives was investigated. The substitution of phenol with alkyl or steric hindrance substituents were studied, regarding the reactivity *vs.* the compound and the salt solubility.

Even if very high performances were obtained with Mg[B(OPh)<sub>3</sub>H]<sub>2</sub>, one drawback is the weak solubility of Mg[B(OPh)<sub>3</sub>H]<sub>2</sub>, with a solubility limit of 0.15 M in diglyme. To increase its solubility, phenol used as reactive will be modified by the introduction of ether groups, which will increase the polarity of the salt and the affinity with ether-based solvents. For this purpose, numerous commercial phenol substances are identified as 2-methoxyphenol, 3-methoxyphenol, 4-methoxyphenol, or sesamol ones.

In addition to phenol compounds, we will also investigate thiophenol substituent. Indeed, literature previously showed the formation of [H<sub>(4-n)</sub>B(SPh)<sub>n</sub>]<sup>-</sup> with n = 1, 2, and 3,<sup>243,244</sup> which was not reported for phenol compounds. Thus, to investigate the effect of the hydride

substitution degree on the salt properties, specific thiophenol/Mg(BH<sub>4</sub>)<sub>2</sub> ratios will be investigated.

The resulting salts will be thoroughly characterized by NMR and electrochemistry. The impact of chemical functionalization on the solubility of the borohydride salts will be evaluated. The electrochemical properties of these new salts, especially on the Mg plating/stripping, will be investigated, as it's the overriding criterion to have.

### 2.1.1. Effect of solvent on the Mg[B(OPh)<sub>3</sub>H]<sub>2</sub> solubility

The limit of triphenolateborohydrate magnesium solubility in diglyme leads to low conductivity when using this salt alone.<sup>11</sup> Also, the improvement noticed on the Mg plating/stripping could be increased if the concentration can be improved. To increase the salt concentration, polyethylene glycol dimethyl ether (PEGDME Mw = 250 g/mol) is used instead of diglyme. Although the viscosity of PEGDME is seven times higher than diglyme, it's an oligomer with a higher ether function number per unit, which enhances the donor number of the solvent (DN<sub>diglyme</sub> ≈ 19.2,<sup>245</sup> DN<sub>PEGDME</sub> ≈ 24<sup>246</sup>) and strengthen the cation solvation and at the end, the salt solubility is improved.<sup>246,247</sup>

In this study, a solution of 0.50 M Mg[B(OPh)<sub>3</sub>H]<sub>2</sub> in PEGDME 250 is reached, thus a large increase of the Mg[B(OPh)<sub>3</sub>H]<sub>2</sub> salt concentration can be obtained by increasing the donor number of the solvent used. Then, this new electrolyte is applied to investigate electrochemical properties.

The electrochemical tests are performed by cyclic voltammetry. In the case of diglyme based electrolyte (**Figure 2.1a**), whereas the oxidation of Mg occurs at 2.5 V vs. Mg<sup>2+</sup>/Mg without Mg[B(OPh)<sub>3</sub>H]<sub>2</sub>, then with a large overpotential, there is a reversible magnesium plating/stripping with the addition of 0.15 M Mg[B(OPh)<sub>3</sub>H]<sub>2</sub>, following by the oxidation of Mg at 0 V vs. Mg<sup>2+</sup>/Mg as expected. The same phenomenon is not observed (**Figure 2.1b**) with the electrolyte 0.5 M Mg(TFSI)<sub>2</sub> + 0.5 M Mg[B(OPh)<sub>3</sub>H]<sub>2</sub> in PEGDME. No reversible Mg plating/stripping is obtained with a current density 10 times lower in reduction than the one obtained with diglyme. Different scan rates from 10 to 100 mV/s were investigated, but no improvement was observed and large irreversibility occurred with a high overpotential. This issue could be explained by the larger amount of water presented in the electrolyte (a few tens of ppm) even after the addition of dried molecular sieves using the protocol described in the experimental part. Indeed, several studies emphasized that the amount of water in Mg electrolytes needs to be reduced under a few ppm.<sup>248</sup> For example, in diglyme based electrolyte,

at 34 ppm of water, the magnesium is deposited only at -1.2 V vs.  $\text{Mg}^{2+}/\text{Mg}$  whereas very weak coulombic efficiency is obtained. The reduction of the water content up to 4 ppm is the only way to obtain a high coulombic efficiency. The presence of a small amount of water (more than 10 ppm) is very detrimental for the magnesium plating/stripping as water traces can react with Mg to form  $\text{MgO}$  or  $\text{Mg}(\text{OH})_2$  which passivates the electrode.

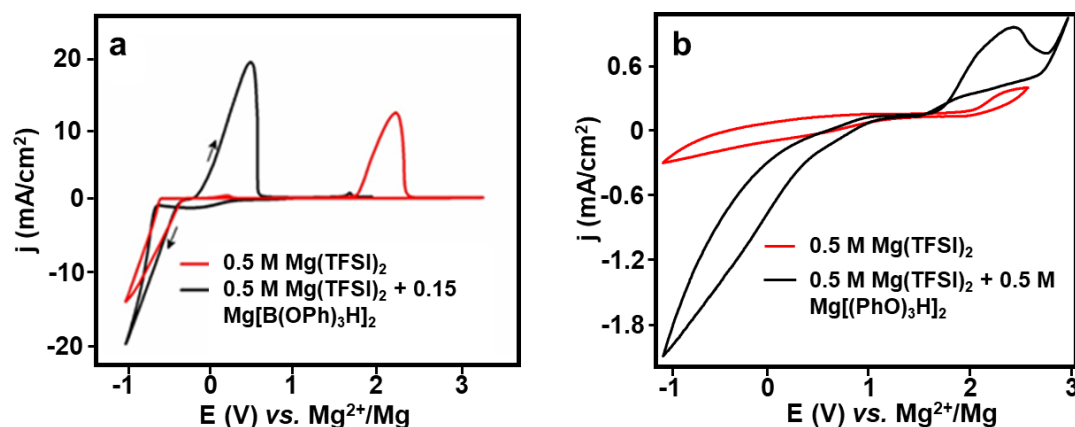


**Figure 2.1.** Cyclic voltammetry on Pt electrode of (a) diglyme solution containing 0.5 M  $\text{Mg}(\text{TFSI})_2$  or 0.5 M  $\text{Mg}(\text{TFSI})_2 + 0.15$  M  $\text{Mg}[\text{B}(\text{OPh})_3\text{H}]_2$  at 50 mV/s. (b) PEGDME solution containing 0.5 M  $\text{Mg}(\text{TFSI})_2$  or 0.5 M  $\text{Mg}(\text{TFSI})_2 + 0.5$  M  $\text{Mg}[\text{B}(\text{OPh})_3\text{H}]_2$  at 50 mV/s. RE and CE electrodes are Mg foil, WE is Pt 2 mm.

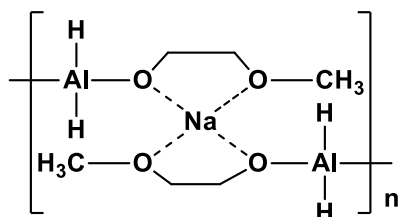
The high viscosity of the electrolyte may be one explanation for the difficulty to remove water to such drastic conditions. These problems and the fact that the electrolyte obtained is very viscous, we have focused our study on other borohydride compounds.

### 2.1.2. Phenolate borohydride derivatives

The limit of solubility is one of the main reasons for investigating new borohydride compounds which can be more soluble in the ether-based solvent. Structures, name, and solubility in ether solvents of several salts obtained by the reaction of phenol derivatives with  $\text{BH}_4^-$  are introduced in **Table 2.1**. The reaction between  $\text{LiBH}_4$  and those substituents is performed *in situ* under Ar flow at room temperature for 30 minutes before identifying by  $^1\text{H-NMR}$ . In those experiments,  $\text{LiBH}_4$  is used instead of  $\text{Mg}(\text{BH}_4)_2$  because of its lower price while chemical behavior is quite similar.<sup>11</sup> If the reaction succeed,  $\text{Mg}(\text{BH}_4)_2$  is applied as salt in electrolyte for electrochemical investigations. The general reaction and mechanism are shown below (**Figure 2.2**).

Three ether solvents from short to long-chain including DME, diglyme, PEGDME are applied with 4 phenol-based compounds. It is believed that the presence of oxygen function in both sesamol and methoxyphenol, could help to raise the solubility of salt. Indeed for example

$\text{Na}[\text{AlH}_2(\text{OC}_2\text{H}_4\text{OMe})_2]$  is more soluble than  $\text{Na}[\text{AlH}_4]$  reactant in ethers due to the solvation of the sodium cations by the oxygen atoms from the alkoxy-groups (**Scheme 2.1**).<sup>121</sup>



**Scheme 2.1.** Structure of  $\text{Na}[\text{AlH}_2(\text{OC}_2\text{H}_4\text{OMe})_2]$ .

**Table 2.1.** Solubility properties of the product(s) formed by the reaction of several phenol derivatives with  $\text{LiBH}_4$  at 25 °C.

Name	Structure	pKa	Diglyme	DME	PEGDME
Phenol		9.98	≈ 0.15 M 1 product	Precipitation	≈ 0.50 M 1 product
2-Methoxyphenol		9.98	Precipitation	Precipitation	Precipitation
3-Methoxyphenol		9.65	≈ 0.50 M 2 products Long time reaction	-	-
4-Methoxyphenol		10.21	Precipitation	Precipitation	Precipitation
Sesamol		9.79	≈ 0.50 M Small precipitation	Precipitation	≈ 0.50 M 1 Product
Thiophenol		6.62	≈ 0.15 M 2 products	Precipitation	-

However, even at low salt concentrations, clear precipitation of products formed by the reaction from both 2-methoxyphenol and 4-methoxyphenol with  $\text{BH}_4^-$  in diglyme is observed. The solubility limit is higher with the use of sesamol. The investigation performed with other solvents (DME, PEGDME, ACN) does not show any significant improvement in terms of solubility. The only case where no precipitation occurred is in PEGDME using sesamol as reagent with  $\text{LiBH}_4$  at 0.5 M.

As shown in **Table 2.1**, several derivative phenols and thiophenol were applied to the investigation with tetrahydroborate salt. The pKa value of these compounds was also introduced on this table.

To propose an explanation of the kinetics of the reaction and on the precipitation observed, the mechanism of the reaction could be useful. The mechanism between  $\text{BH}_4^-$  and alcohol group is investigated by I. E. Golub *et al.*<sup>249</sup> The main points are:

- the dihydrogen bond formation is considered as the first step of proton transfer to hydrides, indeed the combined spectroscopic and computational investigations provided the evidence for dihydrogen bonding of  $\text{BH}_4^-$  with various HX proton donors.<sup>249</sup>
- the first proton transfer step is rate-limiting for each alcohol, the corresponding activation barriers decrease with the increase of the ROH acidity.

In conclusion, the borohydrides' reactivity toward proton donors, meaning that once the first barrier is passed this reaction would run to the completion unless ligands steric bulk or other effects hamper it.

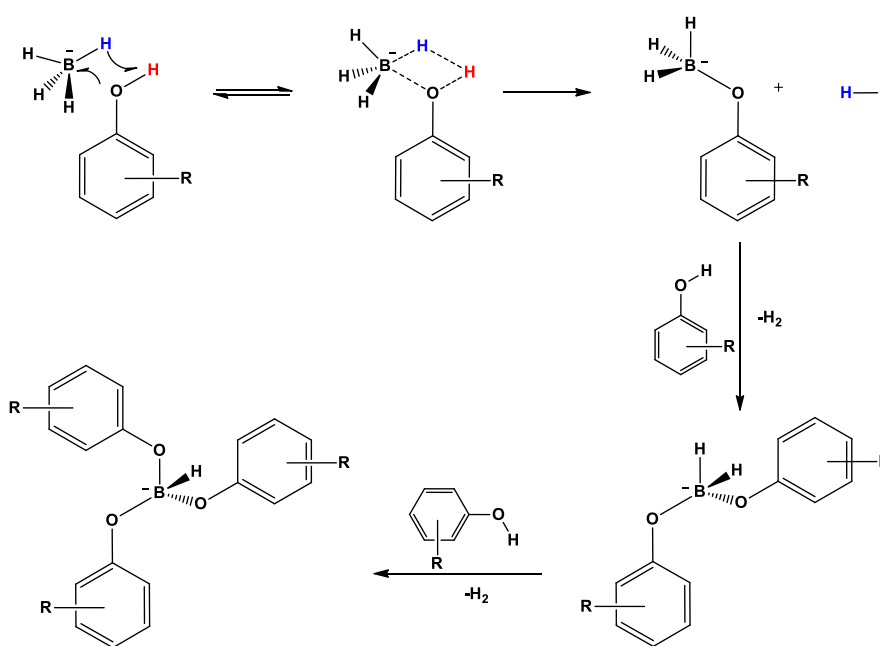


**Figure 2.2.** The mechanism of the reaction between phenol derivatives and  $\text{BH}_4^-$  through four steps.

**Figure 2.2.** shows the reaction between  $\text{BH}_4^-$  and phenol derivatives to give phenolatehydroborate by steps and release  $\text{H}_2$  at the end of each step. Regarding the mechanism proposed, borohydrides with several phenol substituents should be obtained. It was that is



reached with phenol, with three substituents and the formation of the  $\text{Mg}[\text{B}(\text{OPh})_3\text{H}]_2$ , the steric hindrance can avoid the fourth substitution.

The main parameters regarding the different phenol derivatives used are the alcohol acidity (acidity increase induces reactivity increase) and steric hindrance which may limit the number of substituents. However, the 3-methoxyphenol which presents the highest acidity exhibit the lowest kinetic, so in discordance with the expectation. Concerning the weak acidity difference, the steric hindrance and the formation of insoluble species could have a large impact on the reaction kinetics.

The precipitation of the compound appears immediately with methoxyphenol compounds, even in PEGDME which exhibits very high solvation property, as discussed previously this behavior is unexpected. It may be due to the incompatible between solvent and derivative phenol complex, which could be associated with their bulky character. Some specific interactions between  $\text{Li}^+$  and the oxygen groups of the salt cannot be excluded, which, contrarily to improve the solubility as reported in the literature, induces some physical cross-linking between salt molecules favoring their precipitation. The only compound that permits to obtain soluble species is sesamol. Sesamol contains two oxygens at positions 3, 4 with a more rigid structure. Thanks to the presence of those oxygen atoms, the reactivity of sesamol are close to the one with methoxyphenol.

Based on the  $^1\text{H}$ -NMR spectra, there is only one product at any ratio between  $\text{BH}_4^-$  and sesamol from 1:1 to 1:4 respectively, in good accordance with the result obtained with phenol (**Figure 2.3**).

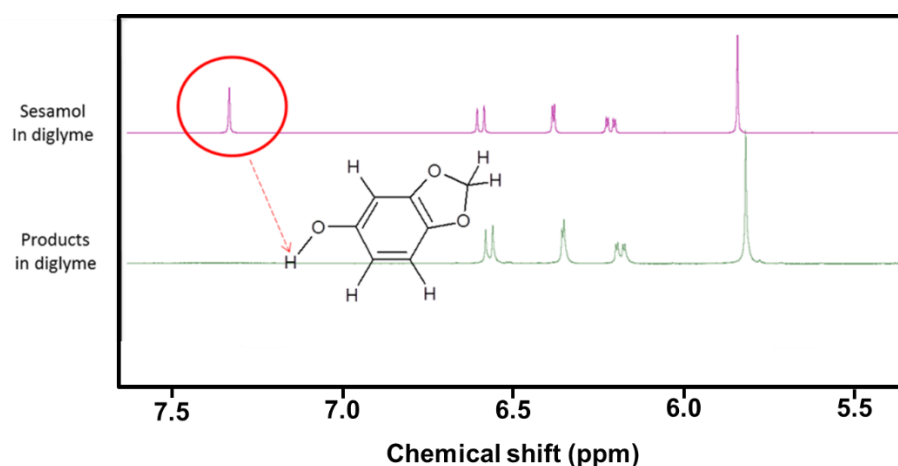


**Figure 2.3.** NMR spectra obtained after the addition of sesamol: $\text{LiBH}_4$  ratio 3:1 in diglyme after 30 minutes.

In the  $^1\text{H-NMR}$  spectrum of the pristine materials, several signals can be noticed and are useful for the reaction study, in particular the  $\text{OH}^-$  function at 7.4 ppm and the proton of  $\text{BH}_4^-$  at -0.545 ppm. After reaction with ratio 3:1 of sesamol: $\text{LiBH}_4$ , there is no protons' peak associated with  $\text{BH}_4^-$ , the consumption of  $\text{BH}_4^-$  is completely done. The signal of OH group is disappeared in the region 7.4 ppm and there is only one product created at any ratio of sesamol and  $\text{BH}_4^-$ . The product proposed in **Figure 2.5b** presents 3 substitutions due to the same reactivity noticed than the one with phenol as mentioned above (detail will be presented in the experimental and method chapter) and in accordance with the mechanism proposed in the literature.<sup>121</sup> The compound obtained should be  $\text{Li}[\text{B}(\text{OC}_7\text{H}_5\text{O}_2)_3\text{H}]$ .

Based on the result obtained with lithium salt,  $\text{Mg}[\text{B}(\text{OC}_7\text{H}_5\text{O}_2)_3\text{H}]_2$  salt is prepared by mixing under Ar  $\text{Mg}(\text{BH}_4)_2$  and dried sesamol using different sesamol/ $\text{BH}_4^-$  ratio in diglyme solvent, after 30 minutes, the solution is applied for the electrochemical investigation.

#### *Electrochemical properties of borohydride magnesium*

Before going into the electrochemical investigation on derivative phenolate borohydride complexes,  $\text{Mg}(\text{BH}_4)_2$  in 0.5 M  $\text{Mg}(\text{TFSI})_2/\text{diglyme}$  is investigated by cyclic voltammetry (**Figure 2.4**).

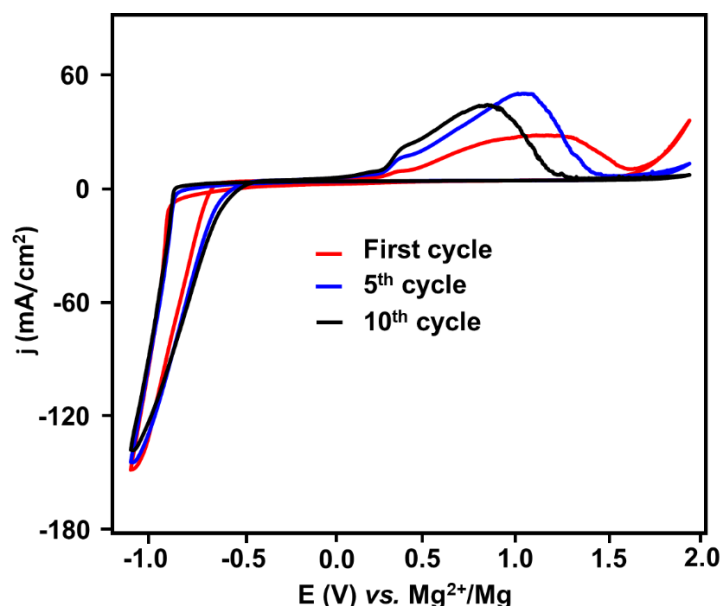


**Figure 2.4.** Cyclic voltammetry on Pt electrode of diglyme solution containing 0.5 M  $\text{Mg}(\text{TFSI})_2$  + 0.15 M  $\text{Mg}(\text{BH}_4)_2$  at 100 mV/s at different cycles.

The Mg deposition is observed at -0.6 V vs.  $\text{Mg}^{2+}/\text{Mg}$  in  $\text{Mg}(\text{TFSI})_2$  + 0.15 M  $\text{Mg}(\text{BH}_4)_2$  in diglyme. The cycle number has a weak effect on both the reduction potential and the peak

intensity. Mg oxidation occurs at 1.2 V vs.  $\text{Mg}^{2+}/\text{Mg}$  with a broad peak at the first scan. This peak shifts toward a lower potential when the cycle number increases. At the 5<sup>th</sup> scan, Mg stripping is observed at 1.1 V vs.  $\text{Mg}^{2+}/\text{Mg}$  with coulombic efficiency associated with Mg plating/stripping equal to 54%. However, the amount of current and the coulombic efficiency (41%) are weakly reduced due to some polarization effect at the 10<sup>th</sup> scan, even if the potential of Mg stripping is reduced to 0.9 V vs.  $\text{Mg}^{2+}/\text{Mg}$ . The results from this investigation are somewhat similar to the study of Wang *et al.*<sup>250</sup> with  $\text{Mg}(\text{BH}_4)_2$  in tetraglyme. Also, the oxidation of  $\text{BH}_4^-$  starts early at 1.8 V vs.  $\text{Mg}^{2+}/\text{Mg}$  in good accordance with the literature.<sup>121</sup>

#### *Electrochemical properties of sesamol based compounds*

The next step is to investigate the electrochemical analysis of magnesium trisesamolathydroborate in diglyme solvent at room temperature. A cyclic voltammetry test was performed on Pt as a working electrode. The CV curves are presented in **Figure 2.5a**.

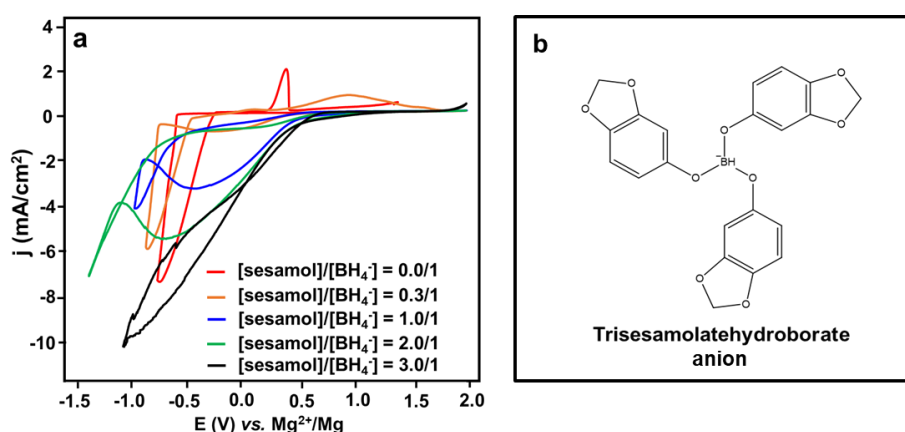


**Figure 2.5.** (a) Cyclic voltammetry on Pt electrode of diglyme solution containing 0.5 M  $\text{Mg}(\text{TFSI})_2$  + 0.15 M  $\text{Mg}(\text{BH}_4)_2$  + sesamol with sesamol/ $\text{BH}_4^-$  from 0 to 3 at 20 mV/s. (b) Structure of trisesamolathydroborate anion.

For this experiment, different amount of sesamol is added to the electrolyte containing  $\text{Mg}(\text{BH}_4)_2$  from very small to large quantity, after each addition the electrochemical measurement is performed at least after 30 minutes to make sure that the reaction is almost finished. With ratio sesamol/ $\text{BH}_4^-$  in 0.3 (orange curve), a weak reduction wave is observed before 0 V vs.  $\text{Mg}^{2+}/\text{Mg}$  following by the magnesium reduction starting at -0.9 V. In the oxidation step, a broad signal between 0.2 V and 1.5 vs.  $\text{Mg}^{2+}/\text{Mg}$  is noticed which can be associated with the Mg oxidation. The reversibility observed is very weak. When the concentration of sesamol increases until the ratio sesamol/ $\text{BH}_4^-$  equal. to 3, the pre-peak starting at 0.5 V vs.  $\text{Mg}^{2+}/\text{Mg}$  increases notably, and the  $\text{Mg}^{2+}$  reduction shifts in more cathodic

potential. Moreover, the oxidation signal disappears. If we compare the curves obtained with  $\text{sesamol}/\text{BH}_4^- = 1$  and  $n = 2$ , the pre-peak increases notably, which seems to indicate that the response observed at  $0.5 \text{ V vs. Mg}^{2+}/\text{Mg}$  may be related to the electrochemical response of the trisesamolateshydroborate or unreacted sesamol. Due to the reactivity in the reduction of the compounds formed, the investigation of sesamol has not been continued. In summary, all of the derivative phenols using in this study could not go further even if the solubility was better in some compounds than in the case of phenol.

Therefore, thiophenol was indicated for the next investigation in this chapter.

### 2.1.3. Thiophenolate borohydride study

#### 2.1.3.1. Cyclic voltammetry investigation

Thiophenol is an organosulfur compound with a sulfur atom instead of the oxygen in the phenol molecule. Due to the bigger diameter, the sulfur electron free-doublet can be easily given to the benzenic ring and stabilizes, after the  $\text{H}^+$  releasing, the formation of thiophenolate. The pKa of thiophenol is 6.62 in water (10.3 in DMSO), while it is 9.95 (18.0 in DMSO) in the case of phenol.<sup>251</sup> Thiophenol is more acid than phenol, therefore the substitution reaction kinetic will be higher in presence of thiophenol.

The addition of 0.3 mol equiv. of thiophenol (**Figure 2.6**) induces a substantial improvement in the Mg plating/stripping process with two close signals in the oxidation scan at  $0.6 \text{ V vs. Mg}^{2+}/\text{Mg}$ , while the Mg plating is observed at  $-0.5 \text{ V vs. Mg}^{2+}/\text{Mg}$  and the coulombic efficiency reaches 79%. The oxidation peak is composed of an important broad signal followed by a narrow peak. This response may be associated with the oxidation of Mg, which is more or less passivated or activated. For the ratio thiophenol/ $\text{BH}_4^-$  at 0.5, an improvement of the plating/stripping process occurs with only one signal in the oxidation step with a shift in the cathodic potential, the peak is observed at  $0.5 \text{ V vs. Mg}^{2+}/\text{Mg}$ , however the coulombic efficiency decreases and reaches 61%. A large modification in the reduction process is shown from the ratio thiophenol/ $\text{BH}_4^- = 2$  (**Figure 2.6**) with a broad peak at  $0.1 \text{ V vs. Mg}^{2+}/\text{Mg}$ , which delays the  $\text{Mg}^{2+}$  reduction. Besides, the oxidation peak decreases dramatically.

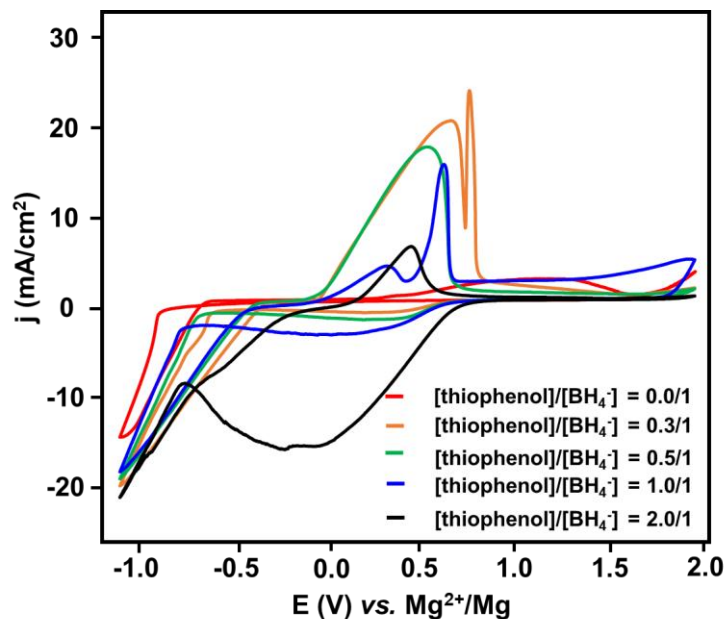


**Figure 2.6.** Cyclic voltammetry on Pt electrode of diglyme solution containing 0.5 M  $\text{Mg}(\text{TFSI})_2 + 0.15 \text{ M Mg}(\text{BH}_4)_2 + \text{thiophenol}$  at 100 mV/s with thiophenol/ $\text{BH}_4^-$  from 0 to 2.

No more magnesium deposition can be observed with ratio thiophenol/ $\text{BH}_4^- = 3$  (**Figure 2.7**). To associate the reduction peak observed at 0.1 vs.  $\text{Mg}^{2+}/\text{Mg}$ , the electrochemical response of the thiophenol in diglyme + 0.5 M  $\text{Mg}(\text{TFSI})_2$  was investigated (**Figure 2.7**).

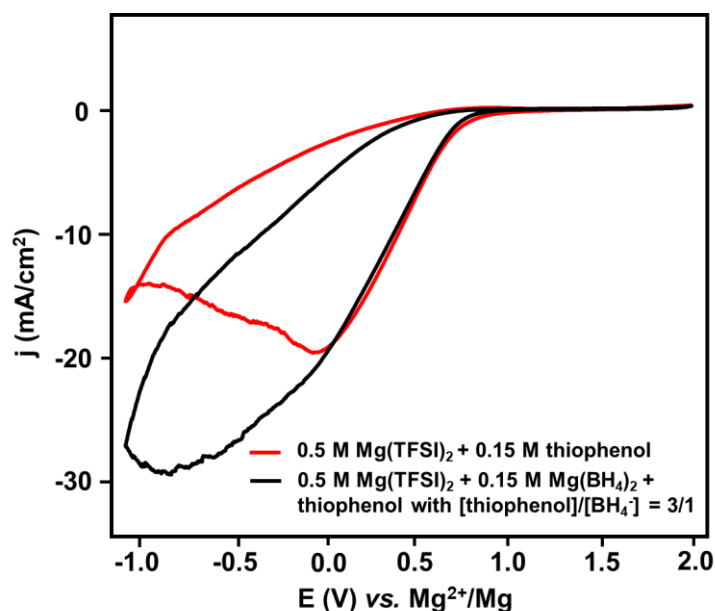


**Figure 2.7.** Cyclic voltammetry on Pt electrode of diglyme solution containing 0.5 M  $\text{Mg}(\text{TFSI})_2 + 0.15 \text{ M Mg}(\text{BH}_4)_2 + \text{thiophenol}$  at 100 mV/s with thiophenol/ $\text{BH}_4^- = 3$  and of diglyme + 0.5 M  $\text{Mg}(\text{TFSI})_2 + 0.15 \text{ M thiophenol}$  in electrolyte.

The reduction of the thiophenol is observed at 1 V vs.  $\text{Mg}^{2+}/\text{Mg}$  with an irreversible process as previously reported for the reduction of  $\text{SH}^-$  group.<sup>252</sup> The reduction behavior is similar to the one observed for the ratio thiophenol/ $\text{BH}_4^-$  at 3, which permits unambiguously to associated this peak with the irreversible response of thiophenol which doesn't react with  $\text{BH}_4^-$  at the time scale of the experiment. In the literature, some improvements in the electrochemical process were noticed with the cycle number, that's why several scans are investigated for the different ratio thiophenol/ $\text{BH}_4^-$ . After 10 cycles (**Figure 2.8**), Mg platings are improving and no more pre-peak is observed at the lowest thiophenol concentration until the ratio thiophenol/ $\text{BH}_4^- = 2$ . This seems to indicate some reactivity of thiophenol with  $\text{BH}_4^-$  with time or thiophenol consumption by reaction with Mg, inducing an improvement of the Mg plating/stripping reversibility. Also, the Mg oxidation peak is more defined after 10 cycles for the different ratios. Especially, there is only one oxidation peak for all the curves at potentially less than 1 V vs.  $\text{Mg}^{2+}/\text{Mg}$ .

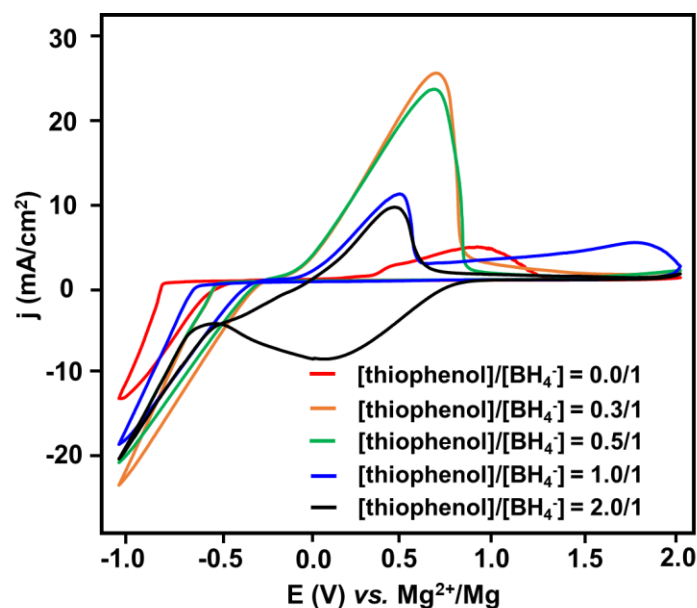


**Figure 2.8.** Cyclic voltammetry on Pt electrode of diglyme solution containing 0.5 M  $\text{Mg}(\text{TFSI})_2 + 0.15 \text{ M Mg}(\text{BH}_4)_2 + \text{thiophenol}$  at 100 mV/s with thiophenol/ $\text{BH}_4^- = 0.0 - 2.0$  at the 10<sup>th</sup> scan.

For a long CV test, the best result is obtained with the ratio 0.5. Contrary to what was observed with phenol, thiophenol seems not to totally react up to the ratio 3. Regarding the coulombic efficiency vs. the cycle number, the same evolution versus the cycle number can be observed whatever the ratio with an increase of the coulombic efficiency up to the 4<sup>th</sup> cycle, and then stabilization.

As an example, **Figure 2.9** shows the effect of cycle number on the curve shape and the coulombic efficiency for the ratio thiophenol/ $\text{BH}_4^- = 0.5$ . At the first scan, Mg plating is observed near  $-0.7 \text{ V vs. Mg}^{2+}/\text{Mg}$  while on the reverse scan, Mg starts its oxidation at  $0 \text{ V}$  with a peak at  $0.7 \text{ V vs. Mg}^{2+}/\text{Mg}$ , however cathodic current is observed from  $0.6 \text{ V vs. Mg}^{2+}/\text{Mg}$ , which can be associated with the reduction of residual thiophenol, as previously discussed. This process disappears completely in the 5<sup>th</sup> cycle. The coulombic efficiency is calculated and gets 60%. This value is improving scan by scan until 90.5% from the 8<sup>th</sup> scan which exhibits the highest efficiency obtained in borohydride complex study.<sup>121</sup>

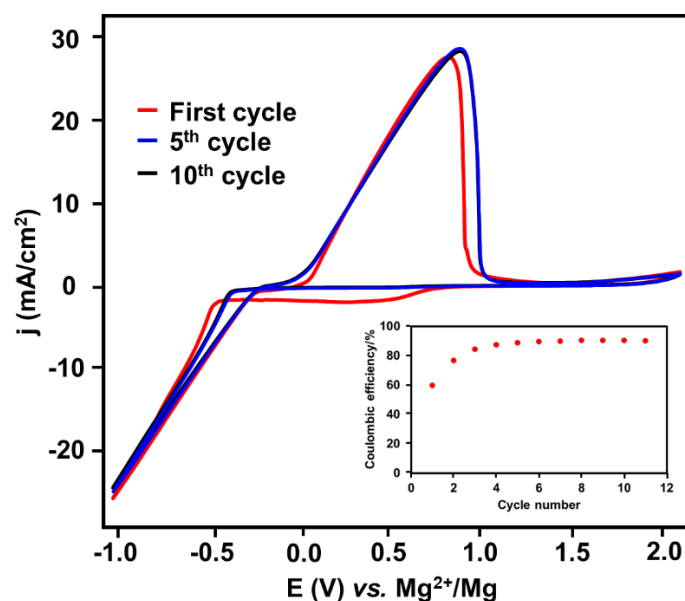


**Figure 2.9.** Cyclic voltammetry on Pt electrode of diglyme solution containing  $0.5 \text{ M Mg}(\text{TFSI})_2 + 0.15 \text{ M Mg}(\text{BH}_4)_2 + \text{thiophenol}$  in  $100 \text{ mV/s}$  ( $\text{thiophenol}/\text{BH}_4^- = 0.5$ ) at different cycles with the plot of coulombic efficiency vs. cycle number.

Following this study, the potential window is investigated up to  $3.4 \text{ V vs. Mg}^{2+}/\text{Mg}$  to see the signal of thiophenolatehydroborate in the oxidation region. As shown in **Figure 2.10**, the  $\text{BH}_4^-$  is oxidized at approximately  $2.6 \text{ V vs. Mg}^{2+}/\text{Mg}$  in accordance with the literature.<sup>11</sup> However, the addition of thiophenol seems to reduce the stability in oxidation with a peak at  $2.5 \text{ V vs. Mg}^{2+}/\text{Mg}$ , lower than the one of triphenolatehydroborate with an oxidation peak at  $3.1 \text{ V vs. Mg}^{2+}/\text{Mg}$ .<sup>121</sup> It could be due to the facile oxidation of the sulfur atom in accordance with the literature.<sup>252</sup>

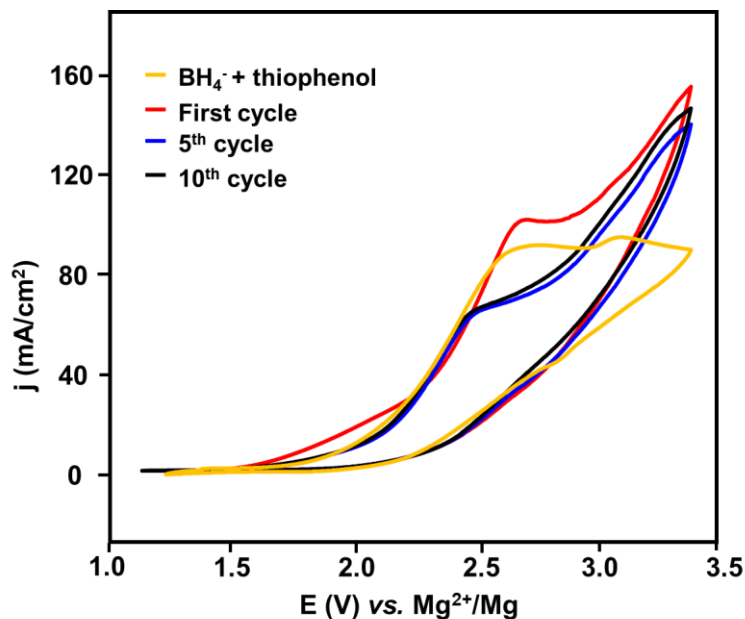


**Figure 2.10.** Cyclic voltammetry on Pt electrode of diglyme solution containing 0.5 M  $\text{Mg}(\text{TFSI})_2$  + 0.15 M  $\text{Mg}(\text{BH}_4)_2$  + thiophenol in 100 mV/s (thiophenol/ $\text{BH}_4^- = 0.5$ ) at different cycles in oxidation area and compare to the first cycle with the electrolyte containing non-thiophenol.

Besides, we evaluated the influence of the scan rate on the electrochemical response of the Mg plating/stripping using the ratio thiophenol/ $\text{BH}_4^- = 0.5$  which presents the more relevant results (**Figure 2.11**).

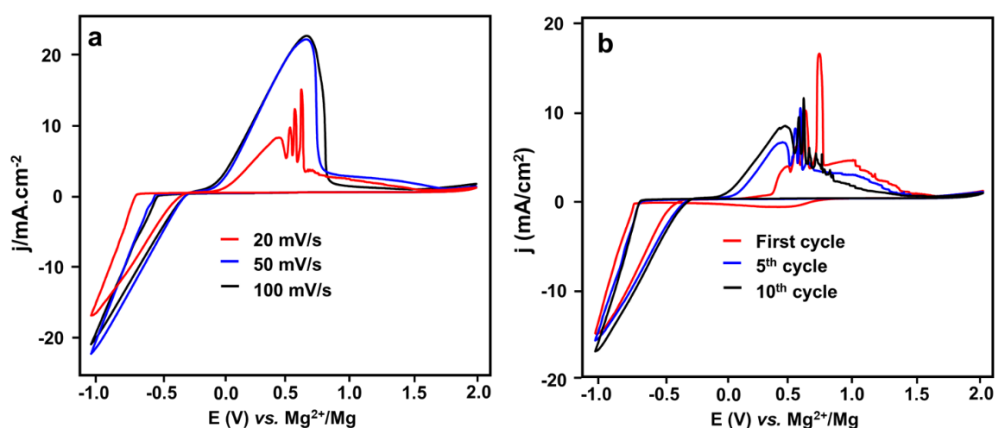


**Figure 2.11.** Cyclic voltammetry on Pt electrode of diglyme solution containing 0.5 M  $\text{Mg}(\text{TFSI})_2$  + 0.15 M  $\text{Mg}(\text{BH}_4)_2$  + thiophenol with thiophenol/ $\text{BH}_4^- = 0.5$  at **(a)** different scan rate at 8<sup>th</sup> cycle. **(b)** at 20 mV/s for different cycles.

Examination of the voltammogram profile recorded at the 8<sup>th</sup> cycle at different scan rates shows the evolution of the Mg plating/stripping curve shape (**Figure 2.11a**). At a low scan rate of 20



mV/s, there are at least four oxidation peaks in Mg stripping process. Also, the behavior noticed during the different cycles from the first to 10<sup>th</sup> cycles (**Figure 2.11b**) shows the complexity of the electrochemical process. The coulombic efficiency decreases with the scan rate with 90.5% at 100 mV/s, 90% at 50 mV/s, and a dramatic drop to 51% at 20 mV/s.

Even if good results are obtained, the electrochemical response is not easy to interpret, the influence of the cycle number and the scan rate on the electrochemical response could be associated with the kinetics of the reaction between BH<sub>4</sub><sup>-</sup> and thiophenol, which seems to be more complex than the one reached with phenol compounds. To go deeper into this investigation, the chemical reaction was investigated by NMR.

### 2.1.3.2. NMR spectroscopy characterization

The NMR spectroscopy of this reaction was performed at room temperature in the same conditions that the ones used for the electrochemical investigations. The concentration of the different peaks obtained by <sup>1</sup>H-NMR spectra after the addition from 0.3 up to 2 molar equiv. of thiophenol into 0.1 M LiBH<sub>4</sub> in diglyme (LiBH<sub>4</sub> is used instead of Mg(BH<sub>4</sub>)<sub>2</sub> to limit the cost of the study) were given in **Table 2.2** after 45 minutes of reaction (which corresponds approximatively to the time before the first CV cycle). The concentration of these compounds was deduced from area peaks based on the <sup>1</sup>H-NMR (show in the **annex 1-8**).

**Table 2.2.** Evolution of <sup>1</sup>H-NMR peak concentration associated with BH<sub>4</sub><sup>-</sup>, thiophenol, and the two formed products obtained for different ratios from 0.0:1.0 to 2.0:1.0 at room temperature under glovebox after 45 minutes (the <sup>1</sup>H-NMR spectra show in annex 1-8).

LiBH <sub>4</sub> : Thiophenol	Concentration after 45 minutes reaction of (mmol/L)			
	BH <sub>4</sub> <sup>-</sup>	Product 1 *	Product 2 **	Thiophenol
0:1	-	-	-	33.3
1:0	33.3	-	-	-
1:0.3	23.0	7.4	0.4	2.0
1:0.5	16.9	14.6	0.9	2.5
1:0.8	3.5	16.0	2.3	6.3
1:1.0	0.7	17.9	3.2	7.9
1:1.5	0	20.3	4.4	18.8
1:2.0	0	22.2	3.6	35.9

\*: could be (C<sub>6</sub>H<sub>5</sub>S)BH<sub>3</sub><sup>-</sup>; \*\*: could be (C<sub>6</sub>H<sub>5</sub>)<sub>2</sub>BH<sub>2</sub><sup>-</sup> and be explained in the following paragraph.

Although the addition of thiophenol, we observe a continuous decrease of the area of the  $\text{BH}_4^-$  signal up to the 1.5 thiophenol/ $\text{BH}_4^-$  molar ratio as illustrated by **Figure 2.12**. However, regarding the amount of remaining thiophenol, as expected the amount is equal to zero for 0.3 and 0.5. However, for the ratio 0.8, surprisingly its area value is quite far from zero whereas the  $\text{BH}_4^-$  quantity is close to zero, and two products, whose ratio depends on the amount of added thiophenol, are obtained, showing that some side reactions are likely to occur.

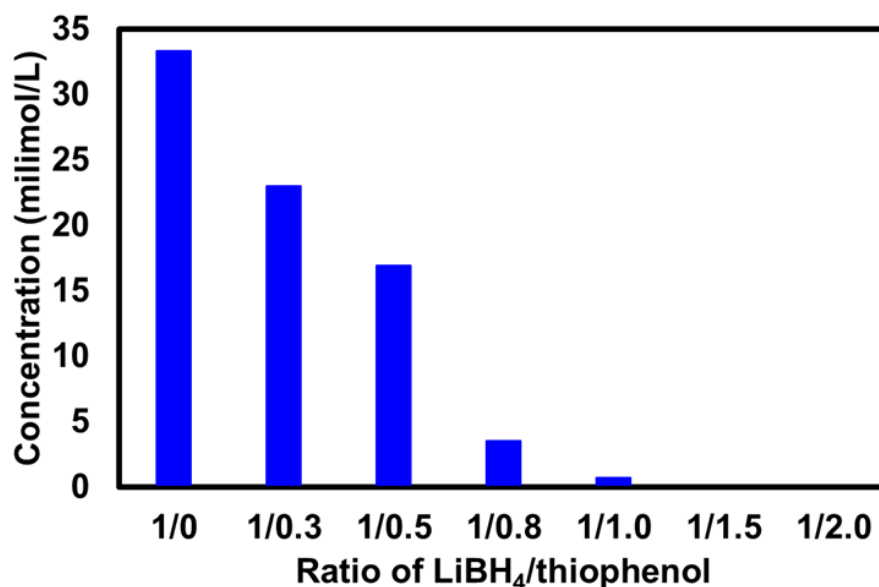


**Figure 2.12.** Correlation of  $\text{BH}_4^-$  concentration remained after 45 mins versus the ratio of thiophenol/ $\text{BH}_4^-$ .

It's clear that the reaction is more complicated than the one obtained with the addition of phenol where the reaction (**Figure 2.13**) is:

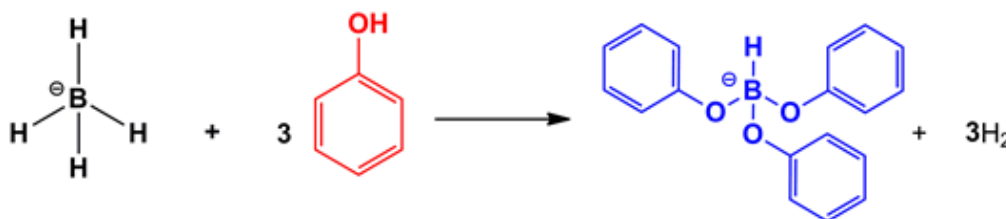


**Figure 2.13.** The reaction between tetrahydroborate and phenol in ratio 1:3.

To deeper understand the reaction, the evolution of the solution composition *vs.* time was investigated using NMR, for the ratio 1 (thiophenol/ $\text{BH}_4^-$ ) in a glovebox to avoid water contamination. The  $^1\text{H}$ -NMR spectra and the evolution of the ratio between the two products formed *vs.* time were shown in **Figure 2.14**.

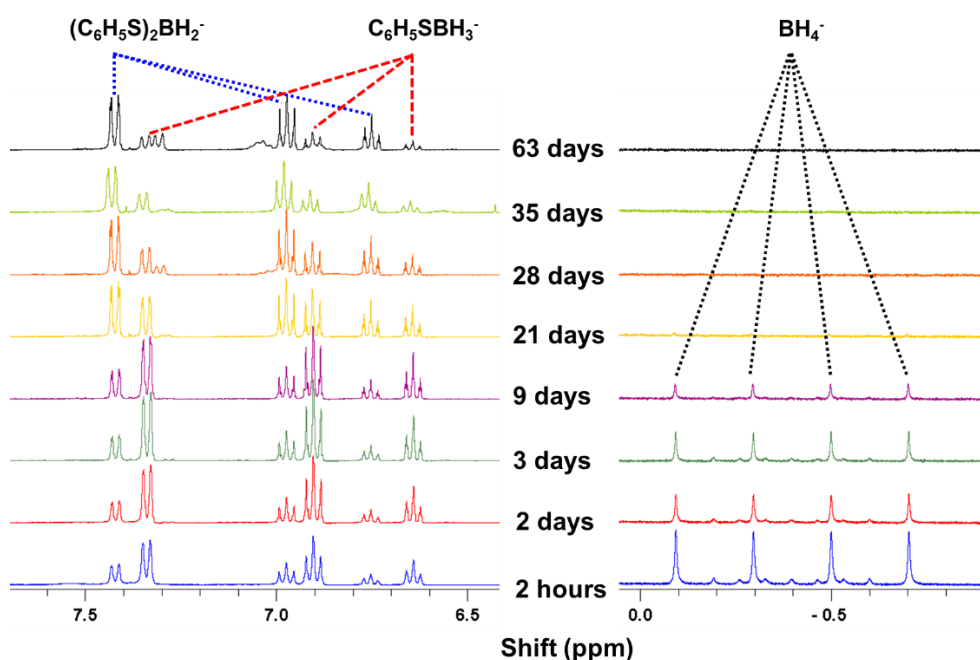


**Figure 2.14.** The  $^1\text{H}$ -NMR spectra of  $\text{BH}_4^-$  and thiophenol (1:1) vs. time in the area of aromatic and  $\text{BH}_4^-$  protons.

Based on the NMR spectrum in the region of aromatic protons, after two hours of reaction, there are two products obtained with a ratio around 2.5. Product 1 with a higher amount could be one substitution of thiophenolate,  $(\text{C}_6\text{H}_5\text{S})\text{BH}_3^-$ , with no more thiophenol. Three signals were indicated at 7.35, 6.91, and 6.65 ppm while the second product with 3 peaks at 7.43, 6.98, 6.76 ppm could be the substance containing two thiophenolate ( $(\text{C}_6\text{H}_5\text{S})_2\text{BH}_2^-$ ), the thiophenol was completely consumed. Interestingly, before 9 days, the ratio is not changed but this ratio is changed to near 0.9 after 21 days besides the appearance of a third product at 28 days of reaction. The investigation is to keep running to 63 days and stopped with 3 products recorded.

In parallel, the lower  $^1\text{H}$  chemical shift from 0 to 0.8 ppm is observed to check the evolution of the proton signals of  $\text{BH}_4^-$ . After 2 hours of reaction (**Figure 2.14**), about 20% of the initial  $\text{BH}_4^-$  is still present which is coherent with the formation of  $(\text{C}_6\text{H}_5\text{S})\text{BH}_3^-$  as the ratio 1/1. The  $\text{BH}_4^-$  amount reduced by time and almost disappeared after 21 days of reaction indicating that there is no more  $\text{LiBH}_4$  in the solution. All the integrates of these peaks are presented in annex 9. Keeping longtime in solution may cause the side reaction of  $\text{BH}_4^-$  with humidity inside the glovebox or, as reported in the literature,<sup>251</sup> with itself inducing the formation of dimers with a B-B link.

In a brief conclusion for NMR study, a stabilization of the ratio product 2/product 1 seems to occur during the first week, with a ratio of 2.5, before decreasing to above 2 after 9 days. Then

it drops dramatically to 0.3 after 3 weeks (**annex 10**). The ratio between the two compounds never becomes stable even after several weeks. The decrease of the ratio product 1/product 2 occurs when the  $\text{BH}_4^-$  was completely consumed, this evolution can be related to the instability of the formed compounds, especially  $((\text{C}_6\text{H}_5\text{S})\text{BH}_3^-)$ , as  $\text{BH}_4^-$  can be reacted with time with the formation of dimers, which can be insoluble or the third product observed, during this reaction  $\text{C}_6\text{H}_5\text{S}^-$  may be produced and react with another molecule of  $(\text{C}_6\text{H}_5\text{S})\text{BH}_3^-$  to form  $(\text{C}_6\text{H}_5\text{S})_2\text{BH}_2^-$ , explaining the decrease of the NMR signal of  $(\text{C}_6\text{H}_5\text{S})\text{BH}_3^-$  and the increase of the one of  $(\text{C}_6\text{H}_5\text{S})_2\text{BH}_2^-$ . The third product detected by NMR was not identified but could be due to some dimer formation.

This study proved that the reaction kinetic is much lower than the one expected due to the higher acidity of thiophenol and the products obtained are not stable.

To try to identify the products and also understand the difference between phenolateborohydride and thiophenolateborohydride, the MM2 method in Chem3D was applied to calculate the steric energy which is usually used to predict the detailed structure through the stretch, bend, Van de Waals force.<sup>237,253,254</sup> All the data from **Table 2.3** are collected after running the MM2 program in Chemoffice 3D software. Each molecule is built up and optimized during this process, the energy values are then shown up under the calculation.

**Table 2.3.** Energy from MM2/Chem3D calculation for substitution borates.

	Total Energy (kcal/mol)
Phenolatetrihydroborate	0.20
Diphenolatedihydroborate	4.84
Triphenolatehydroborate	-1.51
Tetraphenolateborate	-4.36
Thiophenolatetrihydroborate	-0.93
Dithiophenolatetrihydroborate	-3.94
Trithiophenolatehydroborate	-6.66
Tetrathiophenolateborate	-8.65

The evolution of the total energy calculated for the substitution of H by phenol in phenolatehydroborate series is in good accordance with the reaction proposed, as the formation of phenolatetrihydroborate and diphenolatedihydroborate is not favorable, which is not the case for triphenolatehydroborate. With 4 substitutions on boron center, the product seems to be more stable than the one with three substitutes but the steric hindrance effect should be the main reason for its non-existence in solution which was also explained in the publication of the Belkova group.<sup>249</sup>

In the case of thiophenol substituent, the MM2 calculation predicts that the total energy increases follow the rise up of thiophenolate substitutes. All the compounds can be then obtained, with stability increasing with the number of substituents. As experimentally it seems that we can obtain mostly the thiophenolatetrihydroborate and the dithiophenolatedihydroborate, we could suppose a compromising between the stability of the product formed and the steric hindrance due to bulky substituents.

The lower total energy of thiophenol-based products compared to the phenol ones and the higher acidity of thiophenol should increase the kinetics of the reaction, however, in the practical, we observed the contrary with instable formed products in a time range of one week. The steric hindrance, sulfur instead of oxygen could explain the result obtained, even if more investigation is required to explain the unexpected behavior experimentally obtained.

### **2.1.3.3. Mg/electrolyte interface**

Even if the reactivity of thiophenol is complicated, the electrochemical response in CV is very promising, that's why we investigated more properly the electrochemical properties of the thiophenolateborohydride-based electrolyte. We investigated, first, the Mg/electrolyte interface by impedance spectroscopy at OCV using the PEIS technique (potential applied +/-20 mV) and under current using the GEIS technique (sinusoidal current < 10% of the current applied during the chronoamperometry). In this study, 3 electrolytes based on diglyme were investigated using several Mg salts mixture: 0.5 M Mg(TFSI)<sub>2</sub>, 0.5 M Mg(TFSI)<sub>2</sub> + 0.15 M Mg(BH<sub>4</sub>)<sub>2</sub> and 0.5 M Mg(TFSI)<sub>2</sub> + 0.15 M Mg(BH<sub>4</sub>)<sub>2</sub> + 0.15 M of thiophenol (corresponding of a ratio thiophenol/BH<sub>4</sub><sup>-</sup> = 0.5). Based on the NMR and electrochemical investigations, we can believe that in this electrolyte, we will have both BH<sub>4</sub><sup>-</sup> and mainly (C<sub>6</sub>H<sub>5</sub>S)BH<sub>3</sub><sup>-</sup>.

For the first electrolyte diglyme + 0.5 M Mg(TFSI)<sub>2</sub>, the impedance at OCV is very high with a resistance higher than 250 000 Ω and polarization of 2 V even at low current. The addition of Mg(BH<sub>4</sub>)<sub>2</sub> and of the thiophenolateborohydride salt has a positive effect on the magnesium foil/electrolyte interface (**Figure 2.15**), the present paragraph will present the result obtained.

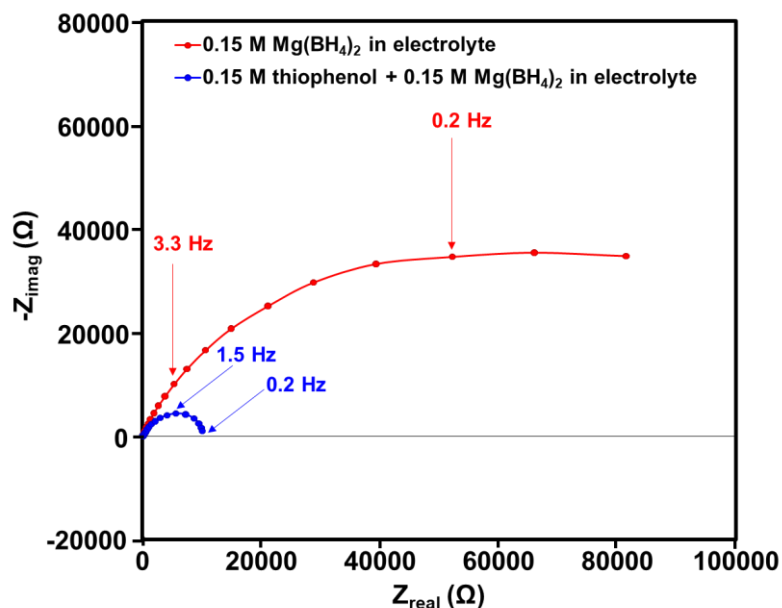


**Figure 2.15.** Nyquist graph of Mg|0.15 M Mg(BH<sub>4</sub>)<sub>2</sub> + 0.5 M Mg(TFSI)<sub>2</sub> in diglyme|Mg and Mg|0.15 M thiophenol + 0.15 M Mg(BH<sub>4</sub>)<sub>2</sub> + 0.5 M Mg(TFSI)<sub>2</sub> in diglyme|Mg at 25 °C.

As the very high resistances obtained are not consistent with the polarization obtained, we investigated some impedance measurements. We performed some chronoamperometry current increase step by step (between 20 μA to 100 μA) for 15 min for each current, with every 5 min GEIS (Galvanostatic Electrochemical Impedance Spectroscopy) measurement was performed (**Figure 2.16**).

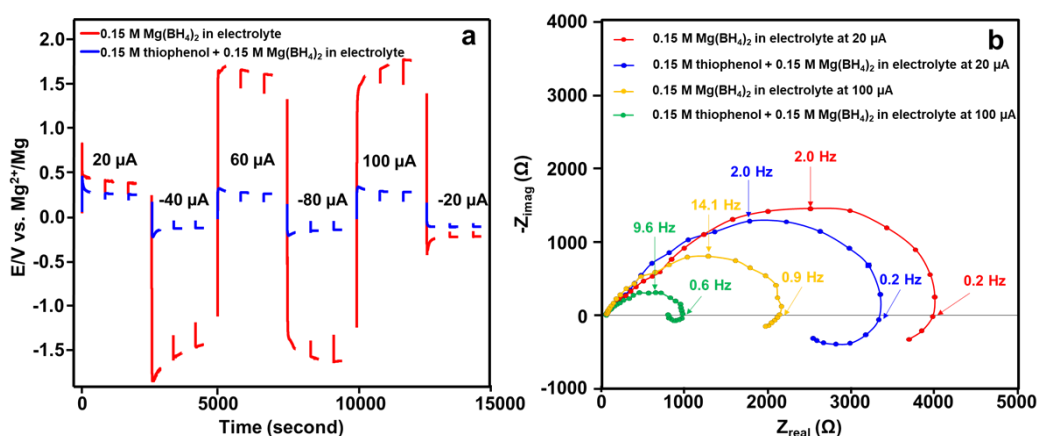


**Figure 2.16.** (a) Chronopotentiometry test in different applied currents (20 μA, -40 μA, 60 μA, -80 μA, 100 μA, and -20 μA) of Mg|0.15 M Mg(BH<sub>4</sub>)<sub>2</sub> + 0.5 M Mg(TFSI)<sub>2</sub> in diglyme|Mg and Mg|0.15 M thiophenol + 0.15 M Mg(BH<sub>4</sub>)<sub>2</sub> + 0.5 M Mg(TFSI)<sub>2</sub> in diglyme|Mg at 25 °C. (b) Nyquist plot of Mg|0.15 M Mg(BH<sub>4</sub>)<sub>2</sub> + 0.5 M Mg(TFSI)<sub>2</sub> in diglyme|Mg and Mg|0.15 M thiophenol + 0.15 M Mg(BH<sub>4</sub>)<sub>2</sub> + 0.5 M Mg(TFSI)<sub>2</sub> in diglyme|Mg at 20 μA and 100 μA.

Whereas the polarization obtained at low current (20  $\mu\text{A}$ ) is weakly lower in presence of thiophenolateborohydride salt, instead of  $\text{BH}_4^-$  with respectively 170 mV and 290 mV. In addition, the increase of current induces a large increase of the polarization in the presence of  $\text{Mg}(\text{BH}_4)_2$  salt up to 1700 mV, whereas the maximum of polarization is lower than 220 mV with thiophenolateborohydride salt. The impedance spectra obtained (**Figure 2.16b**) presents the same shape whatever the electrolytes used, with two semi-circles at high and medium frequencies and an inductive loop at low frequency, with a total impedance which is significantly lower than the ones measured at OCV. The presence of an LF inductive loop is generally attributed to an electrochemical mechanism with two or more stages in the presence of an adsorbed phase, for at least two of them with an electron transfer. This inductive loop was previously reported on the graphite electrode for example, without clear identification.<sup>255,256</sup> An in-depth study of this inductive loop could not be carried out within the framework of this work, but the intervention of magnesium adsorbed species could be considered. The total impedance of the cell decreases with the current increase. The addition of thiophenol enables significantly reduces impedance value especially at high current, for a current of 100  $\mu\text{A}$ , the total resistance is equal to 760  $\Omega$  instead of 2350  $\Omega$  in presence of  $\text{Mg}(\text{BH}_4)_2$ . This reasonable resistance value explains the reversibility of the system, whereas at OCV a resistive passive layer is formed immediately. Regarding the capacitance associated with the bigger semi-circle, it's coherent, as at OCV, with the formation of an SEI with a thickness of about 1 nm (similar to the one obtained at OCV) in presence of the thiophenolateborohydride salt, whereas the thickness seems to be ten times higher with  $\text{Mg}(\text{BH}_4)_2$  i.e. 13 nm considering the same surface area and dielectric properties of the layer.

The plot of the reverse of the total resistance vs. the current value is given in **Figure 2.17**. Linear behaviors are obtained for the two cells, indicating that the interface is not stable, with a resistance which decreases with the current increase ( $R$  proportional to  $1/i$ ), which can be associated with a modification of the electrode texture undercurrent with some heterogeneity of the surface properties (even if we don't perform some SEM image of the surface, such heterogeneity was previously reported)<sup>121</sup>, more the current is high less the interface is resistive, the proportion of the electrode which is electrochemically active may increase.

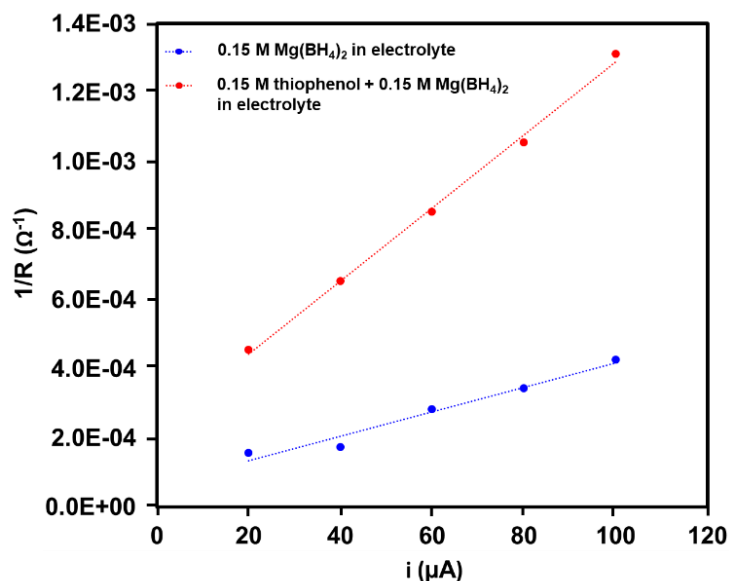


**Figure 2.17.** The plot of the reverse of the total resistance vs. the current values of Mg|0.15 M  $\text{Mg}(\text{BH}_4)_2 + 0.5 \text{ M Mg}(\text{TFSI})_2$  in diglyme|Mg and Mg|0.15 M thiophenol + 0.15 M  $\text{Mg}(\text{BH}_4)_2 + 0.5 \text{ M Mg}(\text{TFSI})_2$  in diglyme|Mg at 25 °C.

The presence of thiophenolateborohydride salt permits to improve notably the Mg/electrolyte interface, even if the interface is not stable and more investigation is required, long cycling tests were then performed.

#### 2.1.3.4. Galvanostatic test

Mg plating/stripping measurements were also performed in Mg/stainless steel (SS). Swagelok-cell with 0.5 M  $\text{Mg}(\text{TFSI})_2 + 0.15 \text{ M Mg}(\text{BH}_4)_2 + 0.15 \text{ M thiophenol} + 0.1 \text{ M MgCl}_2$  in diglyme which was named chloride thiophenolateborohydride-based electrolyte (CTBE) and 0.5 M  $\text{Mg}(\text{TFSI})_2 + 0.15 \text{ M Mg}(\text{BH}_4)_2 + 0.1 \text{ M MgCl}_2$  in diglyme which was named chloride borohydride-based electrolyte (CBE). The addition of a small amount of  $\text{MgCl}_2$  was justified by the previous study performed on phenol-based electrolyte,<sup>121</sup> and shown clearly the need of  $\text{MgCl}_2$  to stabilize the interface for long cycling tests. In the galvanostatic cycling tests, current density was set up at 40  $\mu\text{A}/\text{cm}^2$  for 10 minutes per cycle at 25 °C, the results using CBE and CTBE are shown in **Figures 2.18** and **2.19**, respectively.



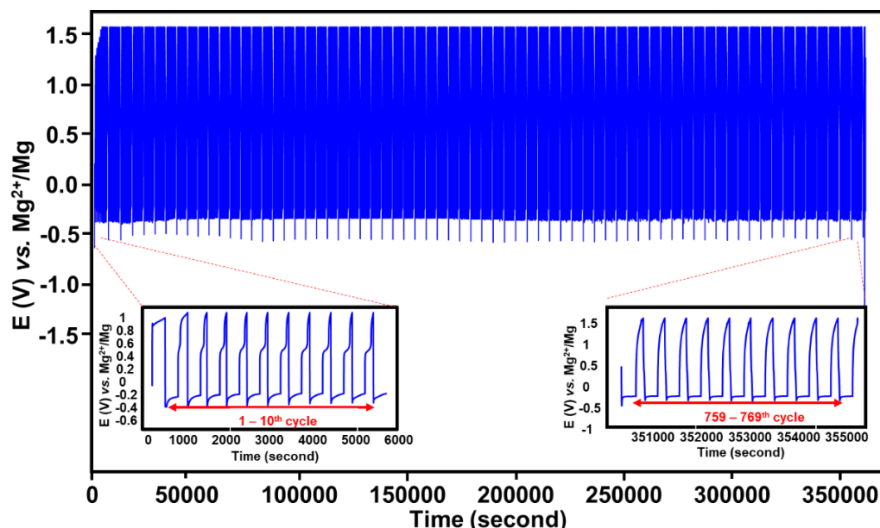


**Figure 2.18.** Full voltage profiles during the galvanostatic Mg plating/stripping processes in SS/Mg Swagelok-cell using CBE with an applied current density of  $\pm 40 \mu\text{A}/\text{cm}^2$  for 10 minutes per cycle at  $25^\circ\text{C}$ .

Galvanostatic experiments in CBE solution show the good shape of Mg plating/stripping after only the 2 first cycles with stable overpotential values  $-0.2$  to  $0.5 \text{ V vs. Mg}^{2+}/\text{Mg}$ . This experiment kept running up to over 760 cycles before short-circuit which is impressive compare to the previous study on this compound. Also, coulombic efficiency reaches near 100% in the few first cycles and is stable until the 30<sup>th</sup> cycle before its decrease, 35% in the last cycle.

With CTBE, the first scans show an irreversible Mg plating/stripping process, 8 cycles are needed to deplete the MgO covered on the Mg foils which can be considered as a preconditioning treating of the interface, as generally recall in the literature. From the eighth cycle, the Mg plating/stripping overpotential is stable at  $-0.24/+0.28 \text{ V vs. Mg}^{2+}/\text{Mg}$  and similar to the one obtained in the study of S. Hebie *et al.*<sup>121</sup>

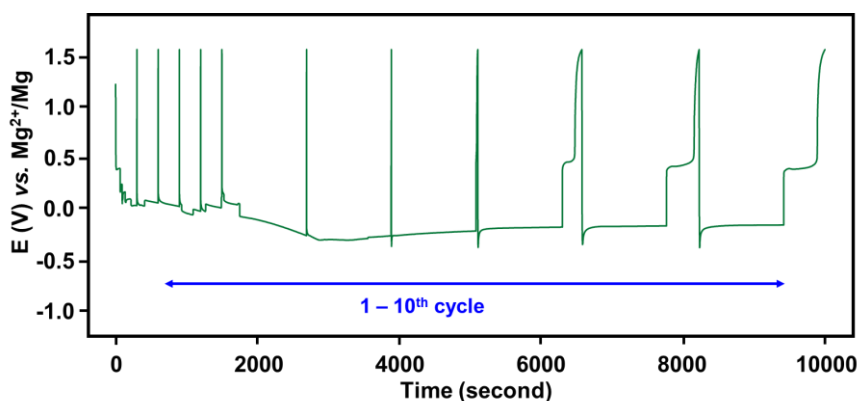


**Figure 2.19.** Galvanostatically cycling of Mg|CTBE|SS Swagelok-cell with  $\pm 40 \mu\text{A}/\text{cm}^2$  for 10 minutes. The voltage profile corresponds to the first ten cycles of this experiment.

The maximum coulombic efficiency of the Mg plating/stripping process reaches 90% after two-hundred cycles (**Figure 2.20**) with an average value of around 80%. This value is similar to the one obtained in phenol-based electrolyte i.e. 90% after 300 cycles in the same conditions.<sup>121</sup> However, instead of 300 cycles with phenol substituent, CTBE performs a promising performance with near 550 cycles before short-circuit.

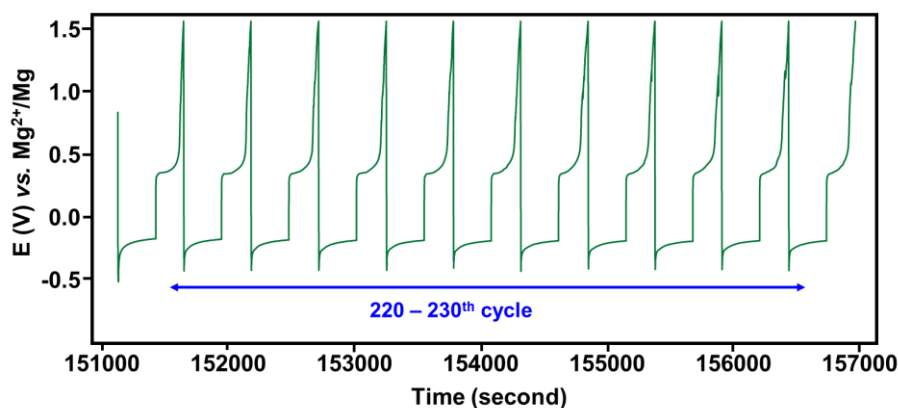


**Figure 2.20.** Galvanostatically cycling of Mg|CTBE|SS Swagelok-cell with  $\pm 40 \mu\text{A}/\text{cm}^2$  for 10 minutes. The voltage profiles correspond to the ten cycles 220 – 230<sup>th</sup> of this experiment.

The presence of both  $\text{MgCl}_2$  and thiophenolborohydrate allows to stabilize the Mg interface and to perform the Mg plating/stripping process with good reversibility and a weak polarisation.

### 2.1.3.5. Mg/Chevrel phase investigation

Full cell measurement was operated by applied CTBE as an electrolyte and  $\text{Mo}_6\text{S}_8$  Chevrel phase as the positive active material. Containing many cavities inside structure, Chevrel phase can received two  $\text{Mg}^{2+}$  during insertion process which related to 2 plateaus observed in charge/discharge curves.<sup>257–260</sup> This inorganic compound was mixed with carbon superP® and PVdF in the ratio 7:2:1. The theoretical capacity of the  $\text{Mo}_6\text{S}_8$  Chevrel phase is equal to 128 mAh/g, and even if its potential is low, this phase is considered as a reference electrode for Mg cell.<sup>257–260</sup> In this experiment, magnesium foil was used as a negative electrode in a two-cell configuration.

During the discharging process, voltage plateaus were obtained at 1.10 and 1.00 V vs.  $\text{Mg}^{2+}/\text{Mg}$  (**Figure 2.21a**). In the oxidation step, two plateaus are located at 1.26 and 1.64 V vs.  $\text{Mg}^{2+}/\text{Mg}$  (**Figure 2.21a**). These plateau values are in good agreement with the ones attained by Hebie's study for the phenol-based electrolyte.<sup>121</sup> Polarization observed from galvanostatic curves, especially for the second insertion/de-insertion process (observed at low potential) is low. This means that the electrolyte of the CTBE is suitable for the use of Mg metal as a negative electrode. Regarding the cell capacity, whereas 70% of the full discharge capacity is obtained

for the first and the second cycles, a high capacity decrease with cycle can be noticed (**Figure 2.21b**), associated with some  $\text{Mg}^{2+}$  trapping in the Chevrel phase. After 25 cycles at C/20, the discharge capacity retained at 50 mAh/g (40% vs. theoretical capacity).

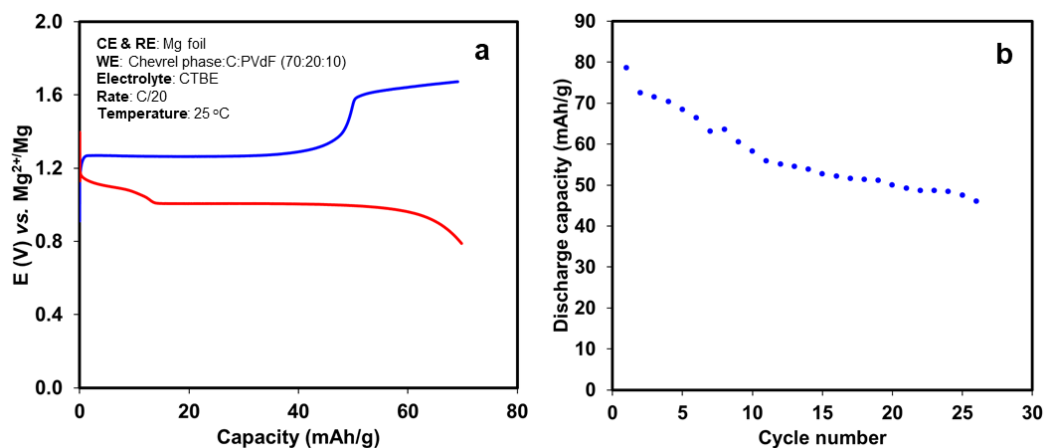


**Figure 2.21.** (a) Charge/discharge profiles of:  $\text{Mg}|\text{CTBE}|\text{Mo}_6\text{S}_8$  at a rate of C/20. (b) Discharge capacity of the cell with 25 cycles in C/20 at 25 °C in CTBE solution.

## 2.2. $\pi$ -rich compounds

An alternative strategy is also developed in the literature, based on the addition of a  $\pi$ -electron-rich molecule (anthracene) in  $\text{Mg}(\text{TFSI})_2/\text{glyme}$  electrolyte,<sup>122</sup> which allows accessing to a reversible Mg plating/stripping with very high current density (**Figure 2.22**), in line with a fast redox reaction.

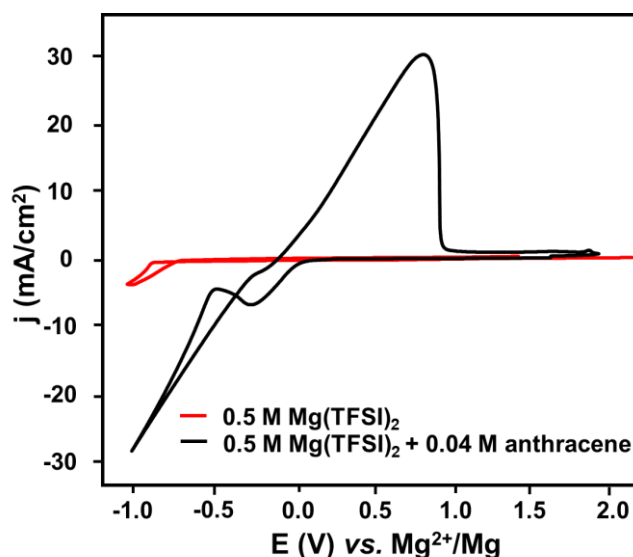
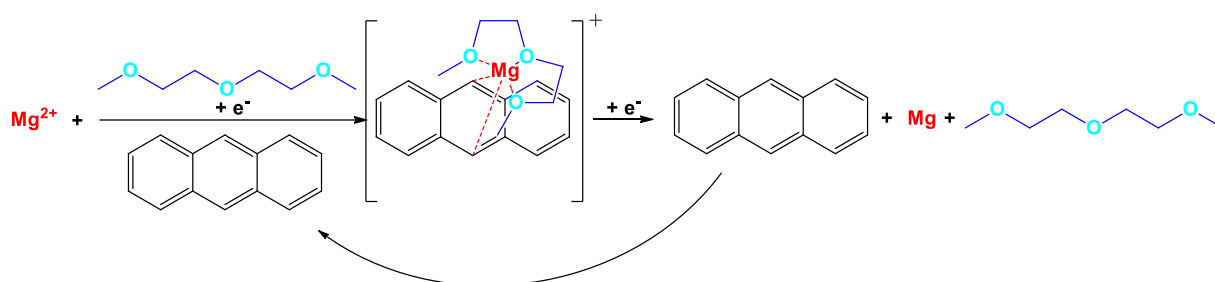


**Figure 2.22.** Cyclic voltammetry on Pt electrode of diglyme solution containing 0.5 M  $\text{Mg}(\text{TFSI})_2$  + 0.04 M anthracene at 100 mV/s.

In addition, this electrolyte exhibits a large electrochemical stability window greater than 3 V. This work was the first example of the use of a  $\pi$ -electron stabilizing agent as an electrolyte additive for Mg battery and opens up a new simple strategy for the development of high-performance electrolytes for Mg batteries. The results obtained seem to indicate that the anthracene is involved in the reduction/oxidation process and can be proposed the formation of the magnesium anthracene complex (named magnesocene complex).

Based on the electrochemical and physical-chemical (UV-visible, NMR) investigations performed, the authors proposed a mechanism for  $\text{Mg}^{2+}$  reduction with two mechanisms, the first one where anthracene ( $\pi$ -stabilizing agent) and diglyme act conjunctly as coordinating ligands to stabilize Mg reduced form in the first step and the second mechanism related to the direct  $\text{Mg}^{2+}$  reduction to form Mg (**Figure 2.23**).

Mechanism 1:



Mechanism 2:

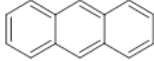
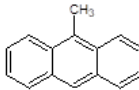
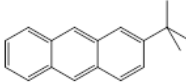
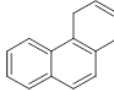
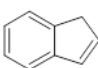
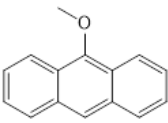
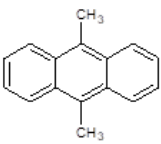
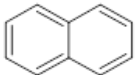
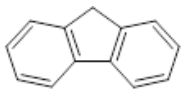
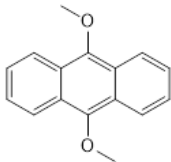


**Figure 2.23.** The mechanism of  $\text{Mg}^{2+}$  reduction with two mechanisms. Mechanism 1: two step mechanism involving magnesocene complex formation as intermediate specy. Mechanism 2:  $\text{Mg}^{2+}$  reduction into Mg

To improve the result obtained and to go deeper in the comprehension of this assisted redox reaction, several  $\pi$ -electron-rich molecules are evaluated in the present study as additives in the Mg-based electrolyte.

The effect of the addition of several  $\pi$  rich molecules on the plating/stripping process of magnesium was evaluated by cyclic voltammety. One of the ideas of this study is to evaluate the impact of the pKa value of the  $\pi$ -protons (**Table 2.4**) on the  $\text{Mg}^{2+}/\text{Mg}$  mechanism assisted by  $\pi$ -rich molecule and the influence of the substituent on the additive solubility and reactivity.

**Table 2.4.** Structure, name, pKa value of several  $\pi$ -rich compounds.

Structure	Name	pKa of $\pi$ -proton
	Anthracene	30
	9-Methylantracene	-
	2-( <i>tert</i> -butyl)anthracene	-
	Phenanthrene	26
	Indene	20
	9-Methoxyanthracene	-
	9,10-Dimethylantracene	-
	Naphthalene	-
	Fluorene	22.6
	9,10-Dimethoxyanthracene	-

The pKa value of  $\pi$ -protons is associated with their electronic density: the lower pKa is, the stronger electronic density is.<sup>261</sup> Also, the electron-donating groups such as alkyl, alkoxy reinforce the electron density on the ring through an inductive donating effect. Therefore, divers non-anthracene-based compounds with smaller pKa including naphthalene, fluorene, phenanthrene, indene, and anthracene derivatives: 9,10-dimethylantracene, 9-methylantracene, 2-(*tert*-butyl)anthracene, 9-methoxyanthracene, and 9,10-dimethoxyanthracene were studied as additives in 0.5 M Mg(TFSI)<sub>2</sub> + glyme electrolyte.

### 2.2.1. Non-anthracene based compounds

The addition of naphthalene, fluorene, or indene induces no improvement of the Mg plating/stripping, a large polarization for the Mg<sup>2+</sup> reduction can be noticed with a very low current at the potential limit (**Figure 2.24a**). In the oxidation part, these compounds are oxidized

at 3.4 V vs.  $\text{Mg}^{2+}/\text{Mg}$ , the same potential as anthracene.<sup>122</sup> The inefficiency of these compounds in the improvement of the Mg plating/stripping process could be explained by the lower charge density of the  $\pi$ -rich carbon for the others compounds as indicated by Bernevo *et al.*<sup>261</sup> To be clearer, the small charge-density may lead to some difficulty for the complex formation between additive, magnesium ion and diglyme as in the anthracene case. The bonds created by those molecules are not strong enough to break the solvation of  $\text{Mg}^{2+}$  by diglyme and so no complex formation can occur. Indeed, no electrochemical signal, which can be related to the formation of such complex, is observed near 0 V vs.  $\text{Mg}^{2+}/\text{Mg}$ , contrary to what was observed with anthracene. In addition, weak reversibility of the Mg plating/stripping is obtained whereas Mg oxidation is obtained close to 2 V vs.  $\text{Mg}^{2+}/\text{Mg}$  with a weak coulombic efficiency. The behavior may be associated with large passivation of the Mg electrode, and the inactive behavior of these additives to form magnesium- $\pi$ -rich molecule complex, contrary to what was observed with anthracene.

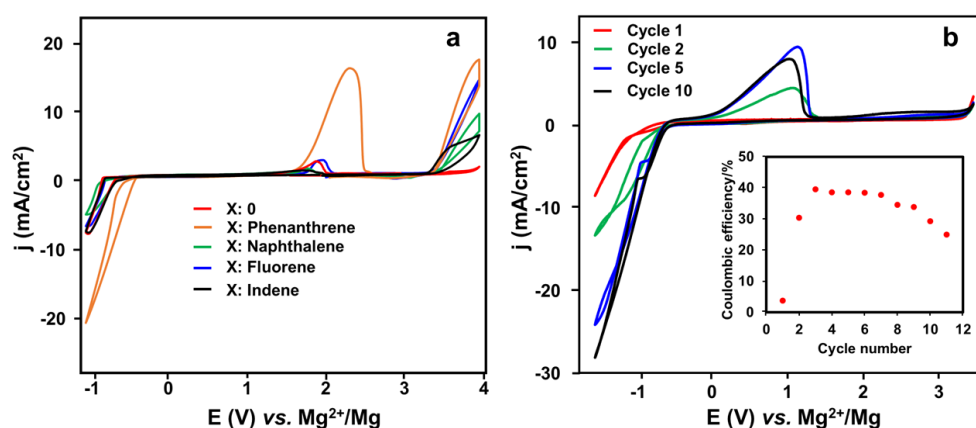


**Figure 2.24.** (a) Cyclic voltammetry on Pt electrode of diglyme solution containing 0.5 M  $\text{Mg}(\text{TFSI})_2$  and 0.04 M of indene, phenanthrene, naphthalene, or fluorene at 100 mV/s. (b) Reversible Mg plating/stripping on 0.5 M  $\text{Mg}(\text{TFSI})_2$  + 0.01 M phenanthrene at 100 mV/s for different cycles and coulombic efficiency versus cycle number.

In presence of phenanthrene, the study was performed several times but without the same results. In some tests, the reduction of  $\text{Mg}^{2+}$  occurs at -500 mV vs.  $\text{Mg}^{2+}/\text{Mg}$  whereas the oxidation process starts at 1.5 V vs.  $\text{Mg}^{2+}/\text{Mg}$  (Figure 2.24a), while for other experiments, the oxidation process starts near 0 V vs.  $\text{Mg}^{2+}/\text{Mg}$  (Figure 2.24b). The addition of phenanthrene enables the reduction of  $\text{Mg}^{2+}$  with a large decrease of the polarization and a kinetic improvement even if a weak coulombic efficiency is obtained at the first cycle, on increases up to 40% at the third cycle. No explanation can be given to date.

Unfortunately, the benefic effect of the addition of anthracene on the Mg oxidation is not observed with the other  $\pi$ -rich molecules.

### 2.2.2. Derivative anthracenes

As anthracene seems to be the best structure for the activation of the Mg plating/stripping process, alkylanthracene and alkoxyanthracene are investigated.

#### 2.2.2.1. Alkylanthracene in 9,10 positions

The effect of the different substituents on the activation of the Mg plating/stripping and the compound solubility were investigated. The presence of methyl groups in position 9 and 10 affect the pKa, the configuration, and the complex formation proposed in the literature (**Figure 2.23**) involving the 9 and 10 positions. The effect of these substituents was then investigated by electrochemistry.

#### *Cyclic voltammetry tests*

To identify the best concentration of 9-methylanthracene in the electrolyte, Mg plating/stripping was investigated from 0.01 M to 0.1 M by CV at 100 mV/s (**Figure 2.25**).

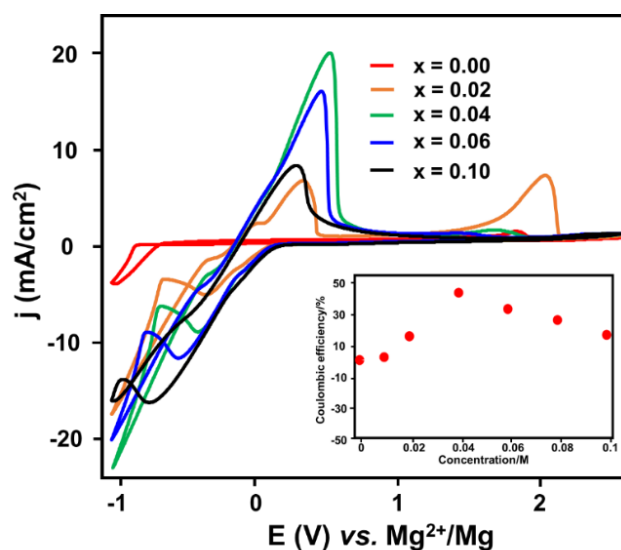


**Figure 2.25.** Cyclic voltammetry on Pt electrode of diglyme solution containing 0.5 M Mg(TFSI)<sub>2</sub> and 9-methylanthracene in different concentration (mol/L) at 100 mV/s and plot of the coulombic efficiency versus the concentration for the first cycle.

Different curve shapes can be observed concerning the 9-methylanthracene amount. Without additive, as previously shown, the plating of Mg occurs with a large polarization without reversibility. However, the addition of a small quantity of 9-methylanthracene activates the Mg plating/stripping by a neat reduction of the overpotential for the plating/stripping process (green

curve). The overpotential for magnesium deposition reduces from 0.6 V to -0.01 V vs.  $\text{Mg}^{2+}/\text{Mg}$  with a two steps process (as observed with anthracene) whereas the oxidation process is divided into 3 steps: one starting at -50 mV associated with the reversible signal of the  $\pi$ -rich molecule complex formed following by the oxidation of part of Mg deposit starting at 0 V vs.  $\text{Mg}^{2+}/\text{Mg}$  while the last oxidation process, associated also with the oxidation of Mg, occurs at 2 V vs.  $\text{Mg}^{2+}/\text{Mg}$  as in diglyme +  $\text{Mg}(\text{TFSI})_2$  electrolyte. However, the coulombic efficiency for the reversible Mg plating/stripping process (considering just the oxidation response near 0 V vs.  $\text{Mg}^{2+}/\text{Mg}$ ) is only 15%. The increase of the 9-methylanthracene amount induces an improvement of the Mg plating/stripping reversibility with the disappearance of the peak at 2 V vs.  $\text{Mg}^{2+}/\text{Mg}$ . The best efficiency of Mg plating/stripping is recorded at 0.04 M with a coulombic efficiency equal to 45% in the first cycle. The increase of the 9-methylanthracene amount induces an increase of the magnesocene complex electrochemical signature (observed at 0 V vs.  $\text{Mg}^{2+}/\text{Mg}$ ), which induces a delay on the  $\text{Mg}^{2+}$  reduction. With the concentration 0.1 M, the main electrochemical response is associated with this complex, and the Mg plating/stripping is no more present. In anodic area (**Figure 2.26**), an irreversible anodic peak occurs at 3.0 V vs.  $\text{Mg}^{2+}/\text{Mg}$  characteristic of 9-methylanthracene oxidation lead to an electrochemical window closed to 3 V.

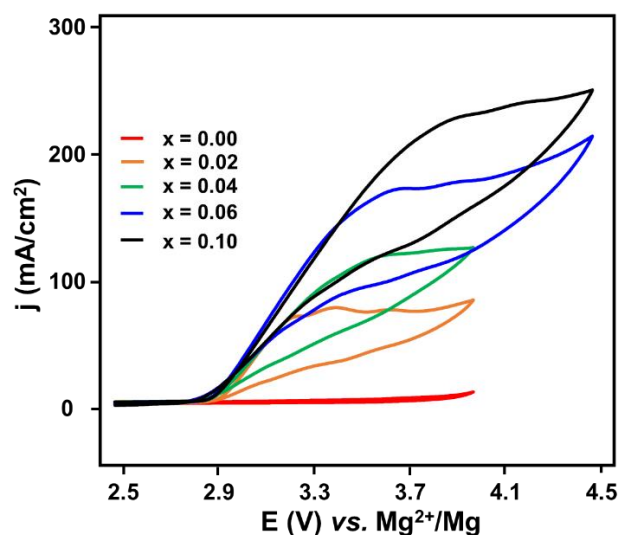


**Figure 2.26.** Cyclic voltammetry on Pt electrode of diglyme solution containing 0.5 M  $\text{Mg}(\text{TFSI})_2$  + 9-methylanthracene in different concentrations (mol/L) in the oxidation area.

The use of 9,10-dimethylanthracene as an additive (**Figure 2.27**) exhibits different behavior. Instead, whereas the  $\text{Mg}^{2+}$  reduction seems to be very similar to the one obtained with 9-methylanthracene, the strong Mg oxidation starting at 0 V vs.  $\text{Mg}^{2+}/\text{Mg}$  is not observed, Mg is



oxidized mainly at 2 V vs.  $\text{Mg}^{2+}/\text{Mg}$  at any concentration of 9,10-dimethylantracene. Only, the use of a large amount of additive (0.07 M) permits to reduce the polarization related to the Mg oxidation and a broad peak is obtained (oxidation between 0.5 and 2 V vs.  $\text{Mg}^{2+}/\text{Mg}$ ). At 3 V vs.  $\text{Mg}^{2+}/\text{Mg}$ , the oxidation of 9,10-dimethylantracene is occurred, as expected the signals increase with the amount of additive.

The comparison of three anthracene derivatives on the Mg plating/stripping is shown in **Figure 2.27**. The behavior of 9-methylantracene and anthracene is similar in both reduction and oxidation parts with the strong reversibility of Mg plating/stripping at 0 V vs.  $\text{Mg}^{2+}/\text{Mg}$  whereas with 9,10-dimethylantracene, even if the reduction part seems to be similar, the oxidation of Mg is less favorable. Regarding the oxidation of these additives, the potential decreases with the addition of the methyl group in accordance with the electron-donating effect of this group, which increases the electronic density then favor the oxidation process. The best stability in oxidation is then obtained with anthracene at around 3 V vs.  $\text{Mg}^{2+}/\text{Mg}$  200 mV higher than the oxidation of 9,10-dimethylantracene.

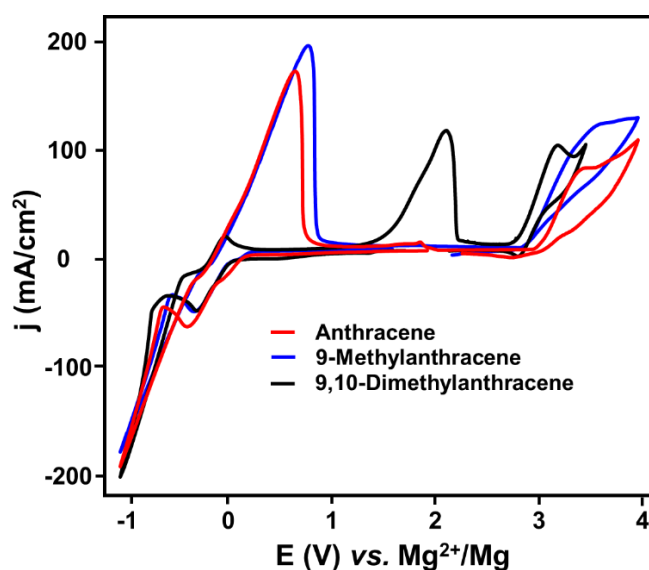


**Figure 2.27.** The comparison of cyclic voltammetry from anthracene, 9-methylantracene, 9,10-dimethylantracene in the same condition at 100 mV/s ( $C = 0.07$  M).

To go deeper into the knowledge of the electrochemical process, the reversible pre-peak associated with the reduction/oxidation of the magnesocene complex is also investigated in the suitable window potential (**Figure 2.28**).

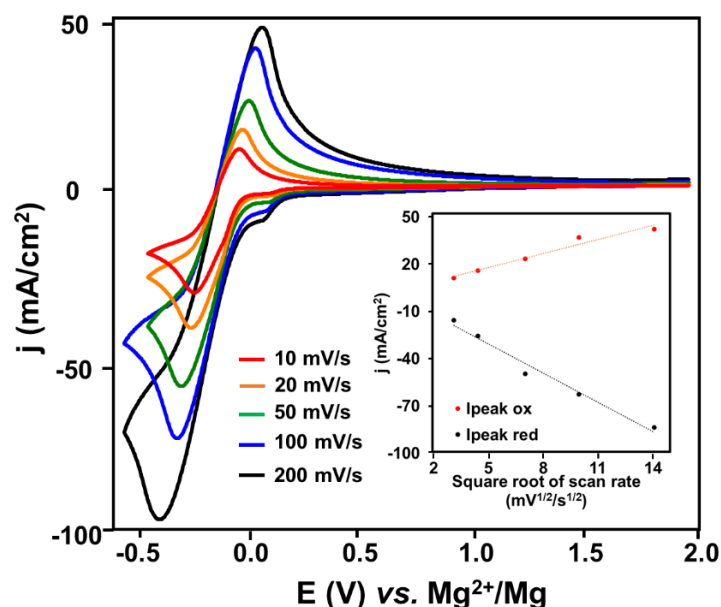


**Figure 2.28.** Cyclic voltammetry on Pt electrode of diglyme solution containing 0.5 M Mg(TFSI)<sub>2</sub> and 9-methylanthracene with the plot of current vs. square root of scan rate.

A reversible oxidation/reduction couple is observed at  $E_{1/2} \approx 20$  mV vs. Mg<sup>2+</sup>/Mg for anthracene and 9-methylanthracene, whereas the potential is lower for 9,10-dimethylanthracene,  $E_{1/2} \approx 160$  mV vs. Mg<sup>2+</sup>/Mg, in the scan rate range investigated, from 10 to 200 mV/s. The shift in potential can be explained, as for the oxidation process, by the electron-donating effect of the methyl groups. Interestingly, the reduction current intensity is linear with the square root of the scan rate (**Figure 2.28**) indicating a process limiting by the diffusion of the soluble active species and not a charge transfer limitation.

Based on the formula (**equ. 1**) which was proposed by Nicholson,<sup>262</sup> the ratio of  $I_{\text{peak ox}}/I_{\text{peak red}}$  and potential peaks are determined for the three compounds including anthracene, 9-methylanthracene, and 9,10-dimethylanthracene at different scan rates (from 10 to 200 mV/s). The extracted values are presented in **Table 2.5**.  $I_{\text{peak ox}}/I_{\text{peak red}}$  increases vs. the scan rate while  $\Delta E_{\text{peak}}$  is also increasing with values far away from  $59/n$  (mV). Thus, the reduction/oxidation of the magnesocene complex could not be considered as a reversible process, some adsorption of the anthracene complex or chemical reaction coupled with electrochemical one may explain such behavior. However, these quasi-reversible systems can be compared regarding the value and the evolution of the  $I_{\text{peak ox}}/I_{\text{peak red}}$  ratio. For all the compounds, the ratio is far from 1 at a low scan rate, whereas at 200 mV/s is close to 1, this large evolution seems to indicate that some parasitic reactions occur in the time of the CV measurement at low C-rate. Indeed, the potential of the redox process is very low, and a reaction with the electrolyte can occur. If we

compare the different systems, the current ratio reaches 0.94 at 100 mV/s for the 9-methylanthracene while the highest value is 0.88 for anthracene, this difference can be observed for all the scan rates, a higher  $I_{\text{peak ox}}/I_{\text{peak red}}$  ratio for the 9-methylanthracene than for anthracene can be associated with the higher reversibility of this system. The result obtained for 9,10-dimethylanthracene is worst with the  $I_{\text{peak ox}}/I_{\text{peak red}}$  lower than 0.7. It could be due to the impact of the two substitutions on 9 and 10 positions which limits the stability of the magnesocene complex. Two explanations can be given the lower potential associated with the complex formation (complex more reactive vs. the electrolyte) or the importance of the acidic protons at the 9 and 10 positions on the complex formation.

$$\frac{I_{\text{peak ox}}}{I_{\text{peak red}}} = \frac{I_{\text{peak ox}}^0}{I_{\text{peak red}}} + \frac{0.485I_{\text{sp}}^0}{I_{\text{peak red}}} + 0.086 \quad (\text{equ. 1})$$

**Table 2.5.** The impact of scan rate into the current ratio and potential of the redox response of anthracene and anthracene derivatives at room temperature.

Scan rate (mV/s)		10	20	50	100	200
<b>Anthracene</b>	$I_{\text{p-ox}}/I_{\text{p-red}}$	0.59	0.65	0.71	0.80	0.88
	$E_{1/2}$ (mV)	-4	-23	-39	-41	-35
	$\Delta E_{\text{peak}}$ (mV)	192	261	353	412	472
<b>9-Methylanthracene</b>	$I_{\text{p-ox}}/I_{\text{p-red}}$	0.74	0.78	0.85	0.94	0.92
	$E_{1/2}$ (mV)	-8	-5	-16	-9	-32
	$\Delta E_{\text{peak}}$ (mV)	192	221	288	331	440
<b>9,10-Dimethylanthracene</b>	$I_{\text{p-ox}}/I_{\text{p-red}}$	0.53	0.56	0.59	0.64	0.69
	$E_{1/2}$ (mV)	-140	-155	-160	-183	-182
	$\Delta E_{\text{peak}}$ (mV)	215	231	271	331	349

Another aspect is the relation between  $I_{\text{peak red}}$  and the square root of sweep rates (**Figure 2.29**). The current peak attained from electrochemically processes limiting by diffusion process increases linearly with the square root of scan rate  $v$  (mV/s) following the Randles-Sevcik equation (**equ. 2**)<sup>263</sup> where  $n$  is the number of electrons transferred,  $S$  (cm<sup>2</sup>) is the surface of the electrode,  $D$  (cm<sup>2</sup>/s) is the diffusion coefficient and  $C$  (mol/L) is the pristine concentration of the chemical identifying.

$$I_{\text{peak}} = 0.446nFSC \left( \frac{nFvD}{RT} \right)^{1/2} \quad (\text{equ. 2})$$

With:  $R$  = constant (8.31 J/mole K);  $T$  = absolute temperature (Kelvin scale);  $F$  = Faraday's constant (96,485 C/mole e<sup>-</sup>)

The  $I_{\text{peak red}}$  value is linear with the square root of the scan rate which indicates that the process is limiting by diffusion, which is coherent with the fast kinetics of the reduction of the magnesocene complex. The diffusion coefficient of anthracene, 9-methylanthracene, 9,10-dimethylanthracene are  $6.3 \cdot 10^{-10} \text{ cm}^2/\text{s}$ ,  $5.3 \cdot 10^{-10} \text{ cm}^2/\text{s}$ , and  $4.1 \cdot 10^{-10} \text{ cm}^2/\text{s}$ , respectively. The evolution of the diffusion coefficient is coherent with the size of the molecule, with the smaller diffusion coefficient in the case of 9,10-dimethylanthracene, the larger molecule, even if the formation of  $\pi$ -stacking complexes can influence the size of the diffusing molecules.

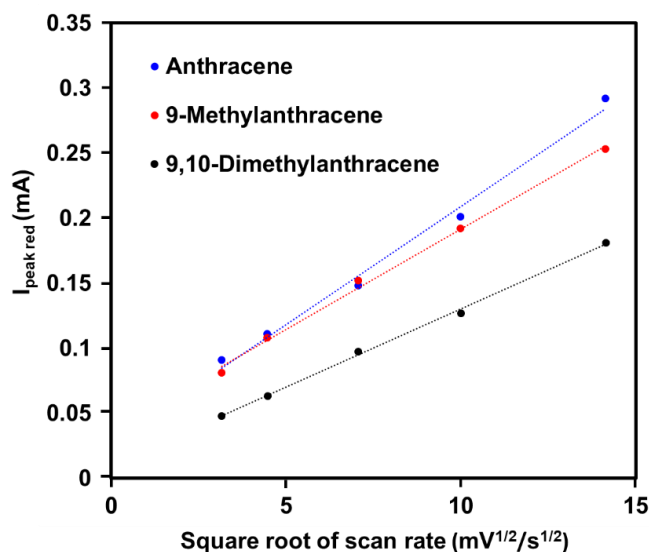


**Figure 2.29.** Evolution of the  $I_{\text{peak ox}}/I_{\text{peak red}}$  of the magnesocene complex vs. the square root of the scan rate.

Regarding now, the global reduction process, the Mg plating/stripping is studied versus the scan rate. Concerning the worst result obtained with 9,10-dimethylanthracene, this study was limited to the comparison of anthracene and 9-methylanthracene additives.

**Figures 2.30a,b** present the CV obtained at the first scan for different scan rates between 10 mV/s and 200 mV/s. The shapes of the curve with the use of anthracene are very similar to whatever the rate applied, with a stable coulombic efficiency between 67 and 70%. With the use of 9-methylanthracene (**Figure 2.30b**), the reversible Mg plating/stripping is also observed but only at a high scan rate from 50 mV/s.

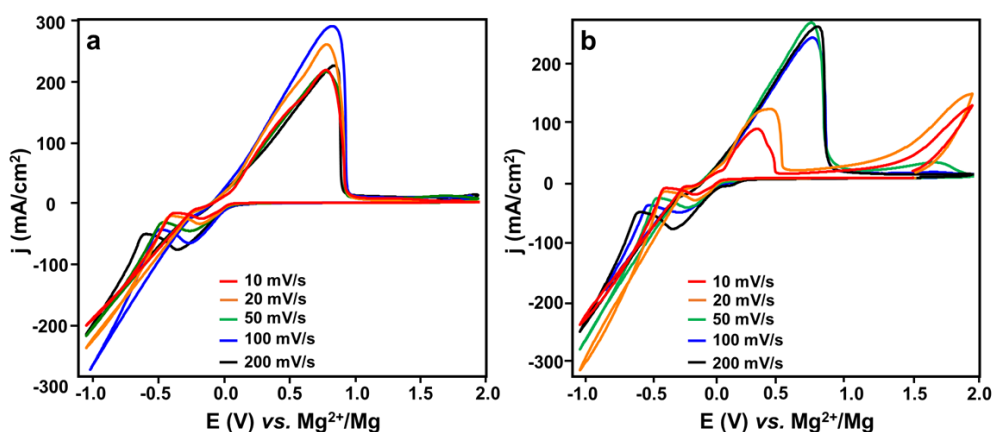


**Figure 2.30.** Cyclic voltammetry on Pt electrode of diglyme solution containing 0.5 M  $\text{Mg}(\text{TFSI})_2$  and (a) 0.04 M anthracene at different scan rates. (b) 0.04 M 9-methylanthracene at different scan rates.

The coulombic efficiency obtained at high scan rates is equal to the one obtained with anthracene, reaching 68% at 100 mV/s. At a low scan rate, 20 mV/s, and 10 mV/s, the Mg oxidation occurs both at 0 V and 1 V vs.  $\text{Mg}^{2+}/\text{Mg}$ . The influence of the scan rate seems to indicate that the magnesocene complex formed with 9-methylanthracene is less effective to help the oxidation of  $\text{Mg}^{2+}$  due to a lack of stability. This weak stability and the fact that no improvement on the Mg plating/stripping was obtained with the addition of 9,10-dimethylanthracene may indicate the importance of the protons on the positions 9 and 10 on the complex formation and that the assisted electrochemical process needs these acidic protons.

The effect of the electrolyte conditioning, performed by several cycles on the Mg plating/stripping was investigated and the results are presented in **Figure 2.31**. With the cycle number increase, a small improvement of the coulombic efficiency is observed for the first three cycles, with a value reaching 50% and then a low decay is obtained with the two additives with the appearance of the oxidation of Mg at 2 V vs.  $\text{Mg}^{2+}/\text{Mg}$ . The coulombic efficiency is worst with 9-methylanthracene. With the cycle number increase, the part of the Mg oxidation occurring at high potential near 2 V vs.  $\text{Mg}^{2+}/\text{Mg}$  increases. It is clear that the conditioning protocol used has no beneficial effect on the electrochemical process efficiency.

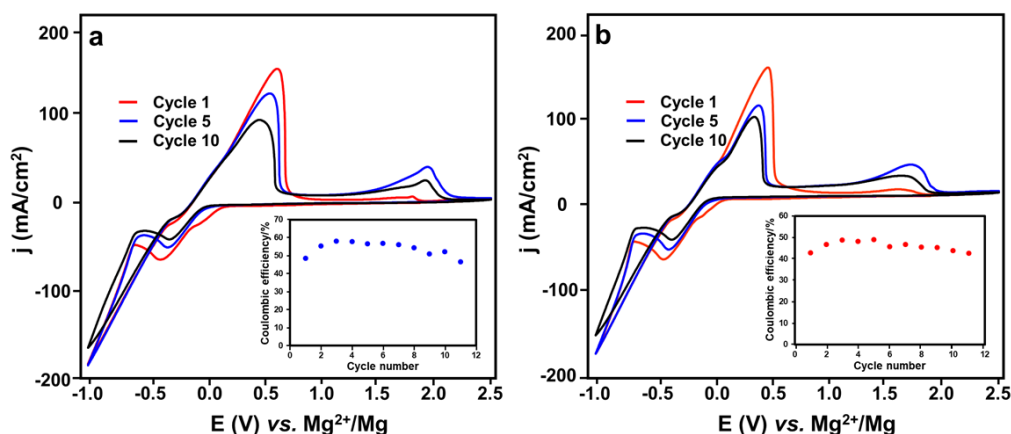


**Figure 2.31.** Cyclic voltammetry on Pt electrode of diglyme solution containing 0.5 M Mg(TFSI)<sub>2</sub> and (a) 0.04 M anthracene in different cycles at 100 mV/s. (b) 0.04 M 9-methylanthracene in different cycle at 100 mV/s.

In a short conclusion, the use of 9-methylanthracene and 9,10-dimethylanthracene is not effective to improve the Mg plating/stripping compare to anthracene one. It could be due to the lack of proton in positions 9 and 10 as previously said and the steric hindrance effect caused by alkyl groups. To evaluate the effect on an alkyl group in another position, the influence of the addition of the 2-(*tert*-butyl)anthracene was investigated.

#### 2.2.2.2. Alkylanthracene in position 2

The impact of the 2-(*tert*-butyl)anthracene concentration on Mg plating/stripping was first investigated at 100 mV/s. **Figure 2.32a** shows the curves from 0.01 to 0.06 M, as with anthracene an improvement is noticed, with the oxidation of Mg occurring at 0 V vs. Mg<sup>2+</sup>/Mg.

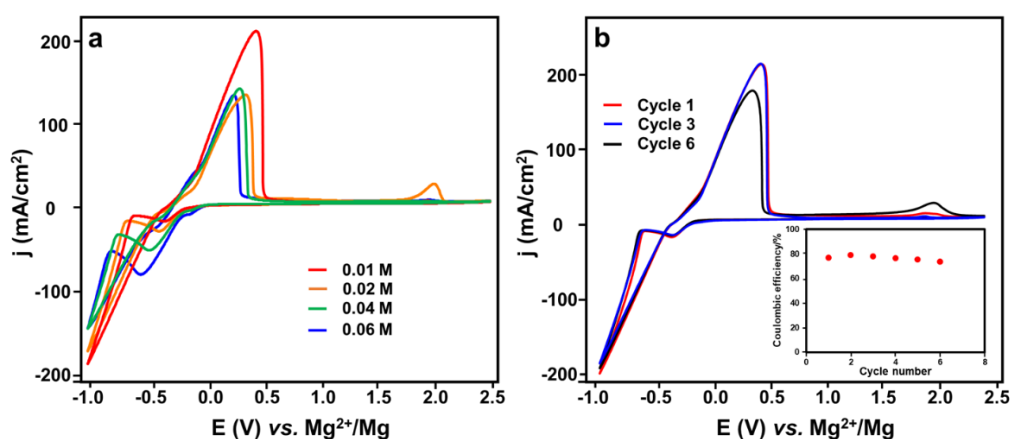


**Figure 2.32.** Cyclic voltammetry on Pt electrode of diglyme solution containing 0.5 M Mg(TFSI)<sub>2</sub> and (a) 2-(*tert*-butyl)anthracene at different concentration. (b) 0.01 M 2-(*tert*-butyl)anthracene at different cycles.

The coulombic efficiency obtained at low additive concentration is very high i.e. 77%, with a significant decrease when the additive concentration increases. As an example, only 28% is obtained at 0.06 M. This phenomenon could be due to the functional group attached to anthracene, its inductive effect may help to stabilize the magnesocene complex. This effect can be counterbalanced by the steric hindrance of the bulky *tert*-butyl substituent at high additive concentration, or some passivation of the electrode by adsorption phenomenon. The electrochemical reduction of the formed complex is observed at 0 V vs.  $\text{Mg}^{2+}/\text{Mg}$ , with an increase of the current proportionally to the anthracene derivative concentration. At high additive concentration, the reduction of  $\text{Mg}^{2+}$  shifts to lower potential, and the current amount associated with the plating of Mg decreases notably. This large improvement on the Mg plating/stripping process reversibility is presented for several cycles (**Figure 2.32b**), with good stability with a high coulombic efficiency, near 80%. It's the best result obtained with the addition of  $\pi$ -rich molecules. To compare with other compounds, 0.04 M 2-(*tert*-butyl)anthracene is applied to measure the impact of scan rate at 10, 20, 50, and 100 mV/s in **Figure 2.33**, even if it's not the best concentration.

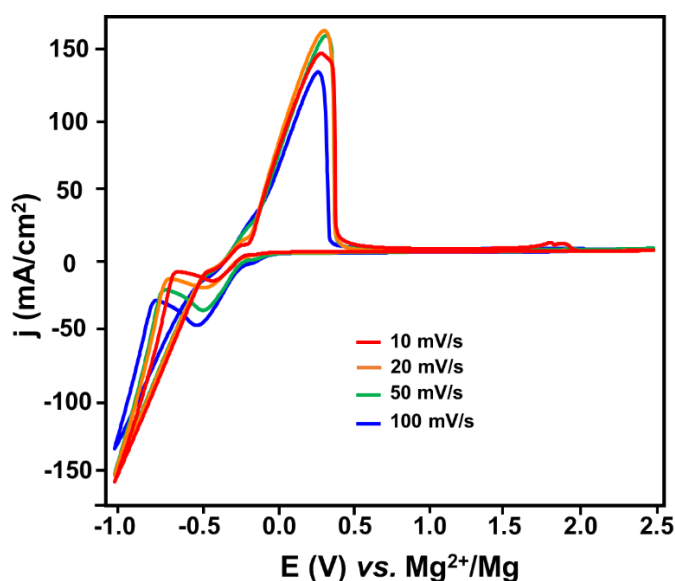


**Figure 2.33.** Cyclic voltammetry on Pt electrode of diglyme solution containing 0.5 M  $\text{Mg}(\text{TFSI})_2$  and 0.04 M of 2-(*tert*-butyl)anthracene at different scan rates.

Whatever the scan rate, only one signal associated with the Mg oxidation is observed, indicating the stability of the complex formed at the time of the experiment (in contrary to what is observed with the addition of 9-methylanthracene). The coulombic efficiency of the reversible Mg plating/stripping is observed at over 50% and increases when the scan rate decrease and reaches

61% at 20 mV/s, which are weakly lower than the results obtained with the addition of anthracene.

### Cycling test

To understand more the electrochemical properties, a galvanostatic cycling test was performed with a constant current applied on 2-electrode Swagelok cell. The result is presented and discussed below.

Galvanostatic measurements were carried out in Mg/Mg Swagelok cell using 0.5 M Mg(TFSI)<sub>2</sub> + 0.01 M 2-(*tert*-butyl)anthracene in diglyme as the electrolyte. From the first cycles, high polarization of 1 V is observed and then increases to near 1.5 V in the 10<sup>th</sup> cycle as shown in **Figure 2.34a**. This high overpotential could be due to the difficulty of the Mg plating/stripping process which is caused by a strong passivating layer forming on the Mg surface, the additive is not effective to consume the passive layer formed on the Mg foils. After long cycling, this overpotential was not improved, even worse with near 2 V of overpotential at the end of cycling before short circuit after 320 scans (**Figure 2.34b**). As just a part of the Mg electrode is involved in the electrochemical process, due to the electrode passivation, the local current density is very high inducing a short-circuit due to the formation of dendrites.

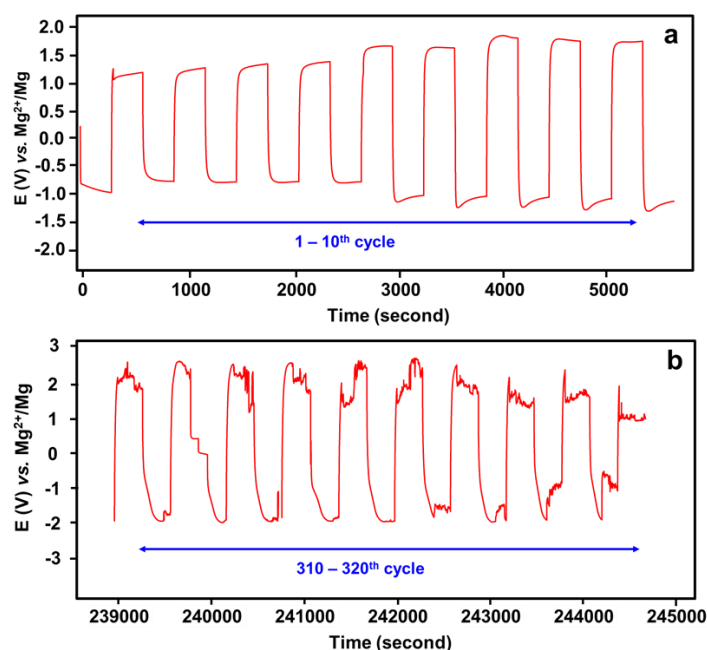


**Figure 2.34.** Galvanostatic cycling test was performed with  $\pm 10 \mu\text{A}/\text{cm}^2$  for 5 minutes on Mg|0.5 M Mg(TFSI)<sub>2</sub> + 0.01 M 2-(*tert*-butyl)anthracene in diglyme|Mg Swagelok-cell. The voltage profiles correspond to (a) the ten first cycles and (b) the ten 310 – 320<sup>th</sup> cycles of this experiment.



Although cycling was run up to over 300 cycles, the high polarization during investigation leads to unsatisfactory results. Therefore, we decide to stop the galvanostatic test here without charge/discharge evaluation, as the high polarization at Mg/electrolyte interface will dramatically reduce the cell energy efficiency.

### 2.2.2.3. Alkoxyanthracene

Another approach to enhance the electron density on anthracene groups, and perhaps to improve the efficiency of the complex formation and stability, is to attach one or two alkoxy group into anthracene. As these two compounds are not commercially available, 9-methoxyanthracene and 9,10-dimethoxyanthracene are synthesized and purified before applying in electrochemical tests. The synthesis of these compounds is started with anthrone/anthraquinone and methyl iodide, the yield for dimethoxyanthracene recorded at over 80% while only 5% of methoxyanthracene is collected. More details about these reactions and purifications are presented in chapter 5.

The study of the additive 9-methoxyanthracene is investigated from 0.01 to 0.06 M (**Figure 2.35a**) at 100 mV/s while the highest concentration for the study of dimethoxyanthracene is 0.04 M due to its limit of solubility. In the case of 9-methoxyanthracene, electrochemical behavior is similar to anthracene and alkylanthracene ones with the complex reduction signal at 50 mV vs.  $\text{Mg}^{2+}/\text{Mg}$  and the following reduction of Mg at -0.5 V vs.  $\text{Mg}^{2+}/\text{Mg}$ . In the reverse scan, the Mg stripping process is reduced by increasing the additive concentration and the highest coulombic efficiency obtained is with 0.01 M 9-methoxyanthracene, i.e. 56%.

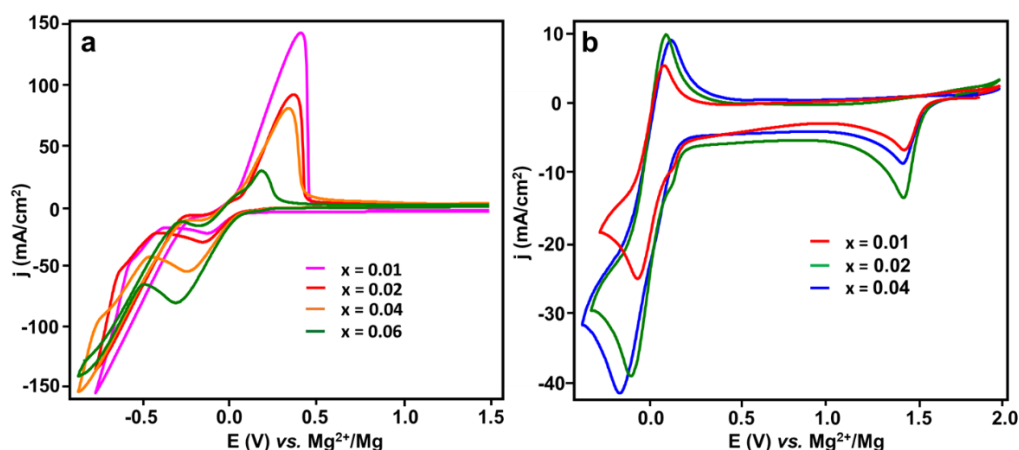


**Figure 2.35.** Cyclic voltammetry on Pt electrode of diglyme solution containing 0.5 M  $\text{Mg}(\text{TFSI})_2$  and (a) 9-methoxyanthracene and (b) 9,10-dimethoxyanthracene in different concentration at 100 mV/s.

For 9,10-dimethoxyanthracene, an additional reduction signal at 1.5 V vs.  $\text{Mg}^{2+}/\text{Mg}$  is obtained and could be due to the reduction of methoxy group. The redox response of the magnesocene complex is observed at 0 V vs.  $\text{Mg}^{2+}/\text{Mg}$  but no Mg plating can be noticed up to -1 V vs.  $\text{Mg}^{2+}/\text{Mg}$ . These results are worse than the ones obtained with anthracene and alkylanthracene. For both alkyl and alkoxy substituents, the di-substitution is worse than the mono substitution, the results obtained with 9-methylanthracene and 9-methoxyanthracene are compared in **Figure 2.36**. The same curve shape is obtained, with a pre-peak associated with the magnesocene complex reduction following with the Mg plating. The complex formed with 9-methoxyanthracene is reduced at a lower potential than the one formed with the 9-methylanthracene i.e. peak observed at -0.5 V vs.  $\text{Mg}^{2+}/\text{Mg}$  instead of 0 V vs.  $\text{Mg}^{2+}/\text{Mg}$  with 9-methylanthracene. The currents associated with the Mg plating/stripping are very similar for the two additives, whereas the coulombic efficiency is slightly higher with the use of 9-methoxyanthracene with 50% instead of 40%. Overall, those two compounds are quite similar with one donor group (methyl and methoxy) at position 9 of anthracene. Even if, the donor effect is not the same, methoxy is stronger than methyl group, the increase of the electron density in the anthracene group seems to have a weak effect on the Mg plating/stripping mechanism whereas the lack of proton in position 9 is detrimental. The lower potential of the magnesocene formed with the 9-methoxyanthracene increases its reactivity with the electrolyte which can explain part of the worst results obtained.

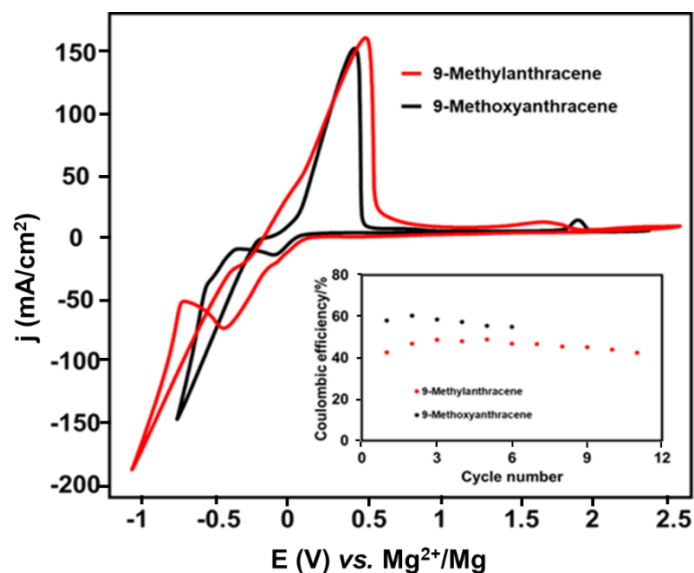


**Figure 2.36.** Cyclic voltammetry at the first cycle on Pt electrode of diglyme solution containing 0.5 M  $\text{Mg}(\text{TFSI})_2$  + 0.01 M 9-methoxyanthracene or 0.04 M 9-methylanthracene at 100 mV/s and plots of coulombic efficiency versus cycle number.

### 2.3. Conclusion

Electrochemistry experiments of borohydrate-based compounds shown the difficulty to manage the reaction, in particular, the drastic dry condition needed. The study on thiophenol reaches some promising results with improved Mg plating/strip reversibility. Whereas some parasitic reactions were observed in the full cell study.

Anthracene's study is obtained with several improvements in the solubility point of view. The best result recorded with the additive  $\pi$ -rich compound is 2-(*tert*-butyl)anthracene with impressive coulombic efficiency at 80%. In presence of 9-methoxyanthracene, good reversibility of the Mg plating/stripping obtained but only for the low additive concentration.

## **Chapter 3:**

# **PBQDS as organic positive electrode for Mg and Li batteries**

### 3.1. Introduction

In addition to the development of new electrolytes adapted for magnesium battery, one of the main aspects is to propose relevant organic material that can be used as active material in the positive electrode, due to their versatility vs. cation nature and sustainability.<sup>264</sup> The insertion of multivalent cations such as  $\text{Mg}^{2+}$ ,  $\text{Ca}^{2+}$ , and  $\text{Al}^{3+}$  in inorganic materials present some drawbacks. Indeed, a large variety of inorganic materials was investigated including  $\text{V}_2\text{O}_5$ ,  $\text{MoS}_2$ , Olivine compounds.<sup>265–269</sup> For such materials, promising capacities were only obtained in the presence of water, which permits to lower the  $\text{Mg}^{2+}$ -oxide electrostatic interaction, but which is incompatible with metallic Mg.<sup>270</sup> Despite intense studies, the performance obtained with inorganic material remains very poor and, to date, reasonable capacity and cyclability have only been obtained with very low potential ( $< 1$  V) cathodes such as the Chevrel phase  $\text{Mo}_6\text{S}_8$  and  $\text{TiO}_2$ .<sup>271,272</sup> Alternative approach that seems to be promising concerns redox-active organic materials in which intermolecular forces are weaker than those in inorganic materials.<sup>273,274</sup> One of the key drawbacks of redox-active organic materials is their poor volumetric power<sup>275</sup> and their solubility which can significantly reduce the cycle life of these materials.<sup>115,185,210,276</sup> To overcome the drawback of dissolution of small organic molecules, many research was focused on redox polymers organic salts or the use of the selective separators.<sup>76,205,212,223,224,277–279</sup> Organic materials generally present electrophilic group, which make them inconsistent with Mg electrolytes containing nucleophilic species, generally those synthesized from Grignard reagents.<sup>207,280,281</sup> The growth of non-nucleophilic electrolytes has become fundamentally important to allow the electrochemical investigation of all organic materials in Mg metal battery systems. The most studied organic electrodes are dimethylbenzoquinone (DMBQ) and polyanthraquinone (PAQ) since they contain conjugated carbonyl groups.<sup>223,282,283</sup> DMBQ<sup>276</sup> was a promising candidate in the Mg system with a capacity of over 200 mAh/g beside P(NDI2OD-T2)<sup>115</sup> and PDI-EDA<sup>221</sup> showed a more impressive performance with high cyclability with more than 2000 cycles with a capacity near the theoretical value 54 mAh/g. Another auspicious material for organic electrode was the PAQ, which exhibits stable performances after one hundred cycles with a capacity of 100 mAh/g with  $\text{MgCl}_2$ -Mg(TFSI)<sub>2</sub> in a mixture of THF and glyme (MTCC) as the electrolyte, between 0.5 and 2.5 V vs.  $\text{Mg}^{2+}/\text{Mg}$ .<sup>284,285</sup>

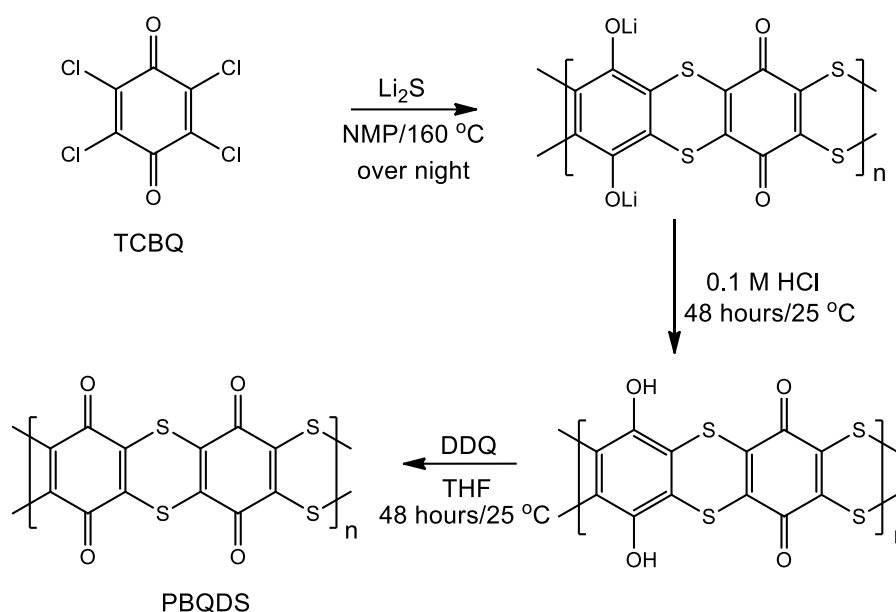
Here we study for the first time poly(benzoquinonyldisulfide) as a positive active material. The material was obtained using a low-cost, 3-steps synthesis. Its electrochemical properties are

presented in both lithium and magnesium batteries which enable the comparison of the two systems, in terms of electrochemical processes.

## 3.2. Results and discussion

### 3.2.1. Synthesis and active material characterization

Linking active organic units with thioether bonds is a simple strategy to synthesize polymer electrode materials, and was previously proposed by Song *et al.*<sup>225</sup> with one thioether link. To increase the insolubility property of polymer, two sulfur bridges were designed on this work. Three steps are required. First of all, a polycondensation reaction permits to obtain the lithiated polymer, whereas two more steps are needed to have the  $Mg^{2+}$ -based product. The detail is presented in the experimental part. After a three steps reaction summarized in **Scheme 3.1**, the PBQDS was obtained in a high yield, more than 95%.



**Scheme 3.1.** PBQDS preparation from TCBQ.

To check the complete oxidation of the PHBQDS hydroquinone groups into quinone ones, during the last reaction step, the products were characterized by FT-IR. In the FT-IR spectra (**Figure 3.1**), the oxidation of hydroquinone was observed with the disappearances of the strong and broad O-H stretching mode (between  $2100$  and  $3600\text{ cm}^{-1}$ ) and of the C-O stretching band at  $1190\text{ cm}^{-1}$  observed in the PHBQDS spectra. Characteristic peaks at  $1623\text{ cm}^{-1}$  for C=O stretching,  $692\text{ cm}^{-1}$  for C-S stretching were obtained in the intermediate and final products.

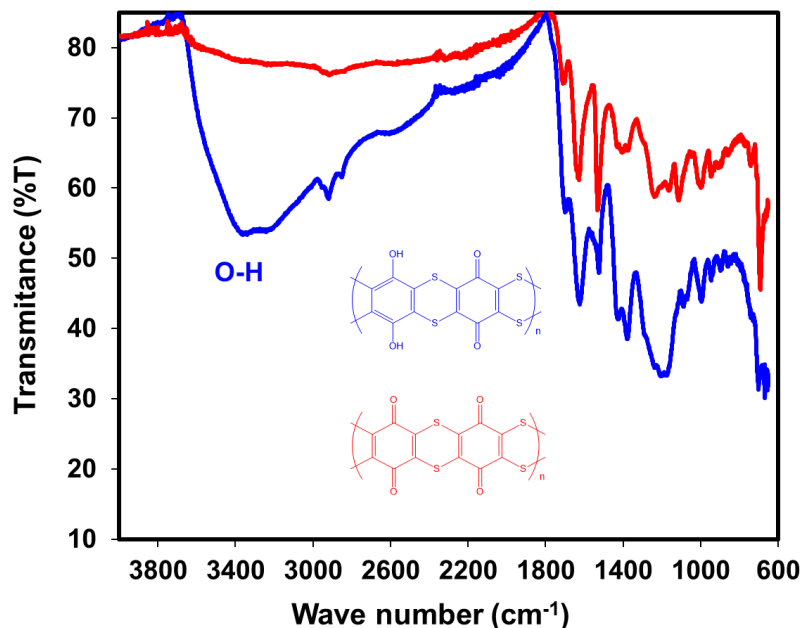


**Figure 3.1.** FT-IR spectra of PBQDS and PHBQDS in the region of 4000 – 600  $\text{cm}^{-1}$ .

Thermogravimetric analysis (TGA) is used to analyze the thermal stability of the obtained polymer. The polymer is stable up to 200 °C, with a small weight loss at 75 °C associated with water removal (**Figure 3.2a**). The derivative weight loss overtime indicates a degradation process in two steps weakly separated in temperature with the first step corresponds to the first sulfide-bridge broken and the second step is the total degradation of the polymer at high temperature.

The elemental analysis of the obtained polymer is shown in **Figure 3.2b**. The presence of H (1.42%) and the excess of O may be associated with some water absorption, as no OH group was noticed in PBQDS compounds by the FTIR investigation. The lack of S may indicate some monosulfide bridges in the polymer.

Energy-dispersive X-ray spectroscopy (EDX) was used to complete the elemental analysis performed in particular to evaluate the presence or not of some chloride atoms (**Figure 3.2c**). The peaks of the different elements such as S, C, O are observed. Only a small amount of Cl is detected at 2.6 keV, this weak amount could be associated with the polymer chain end relating to the moderate molecular weight of the polymer. No other elements are detected.

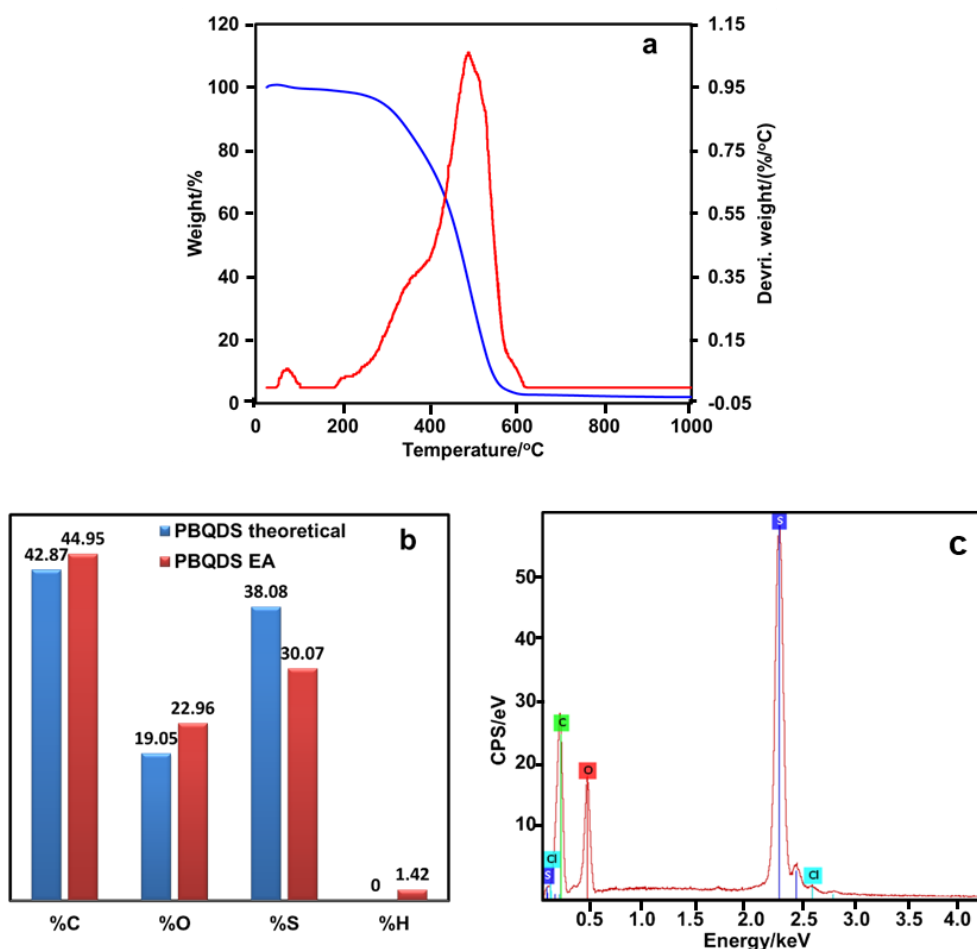


**Figure 3.2.** (a) TGA of PBQDS from room temperature to 1000 °C under airflow. (b) Elemental analysis of PBQDS. (c) EDX analysis of PBQDS under N<sub>2</sub> flow.

Based on literature data<sup>286</sup>, it is clear that the particle size has a large impact on the electrochemical cell capacity as the diffusion process in large solid particles can be the limiting process. Pristine synthesized PBQDS particle sizes are in the range of dozens  $\mu\text{m}$  or even higher. Thus, a manual grinding method (MGM) and ball milling technique (BMT) were used to reduce the pristine particle diameters. Several BMT speeds and experiment time were investigated. More detail of the condition used is presented in chapter 5. The pristine particles are large and not homogeneous with some particles having a diameter of 70  $\mu\text{m}$ . At low BMT speed (220 rpm), the particle size was reduced from over 30  $\mu\text{m}$  to 13  $\mu\text{m}$ . When the polymer was ground at 550 rpm, the size of the polymer particles dropped to around 11  $\mu\text{m}$  after 15 minutes and decreased slightly to 10  $\mu\text{m}$  after 30 minutes (**Figure 3.3**). In addition to SEM characterization, the specific surface area was measured by Brunauer–Emmett–Teller (BET) method, whereas the pristine material exhibits a surface of 3  $\text{m}^2/\text{g}$ , after 30 minutes at 550 rpm MBT, the BET value increases up to 15  $\text{m}^2/\text{g}$ . The low BET surface area of the pristine material



is associated with the aggregation of the polymer during the polymerization and this value is comparable to the one obtained from PAQS.<sup>287</sup> To evaluate if the BMT process can induce some degradation level, Raman spectroscopy was applied after each experiment of time and speed (Figure 3.4).

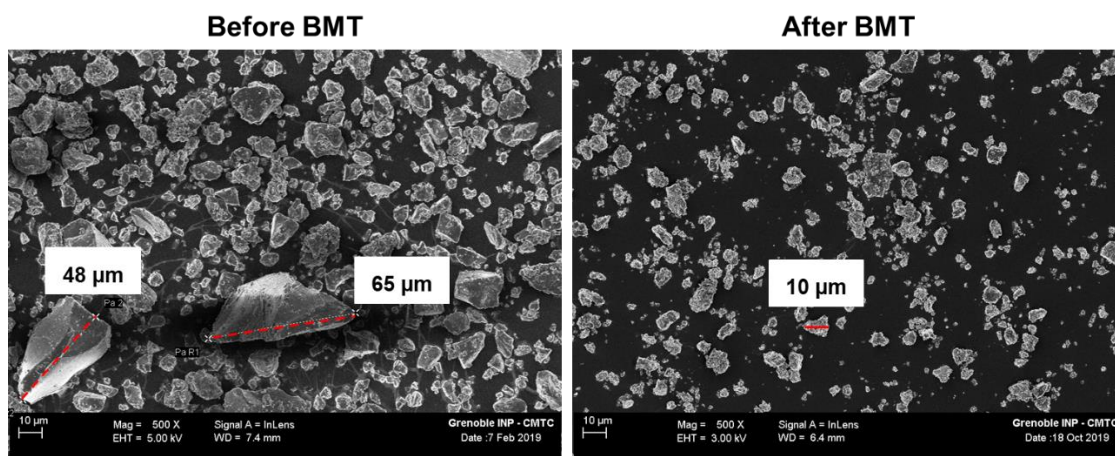


**Figure 3.3.** SEM of PBQDS before and after using BMT.

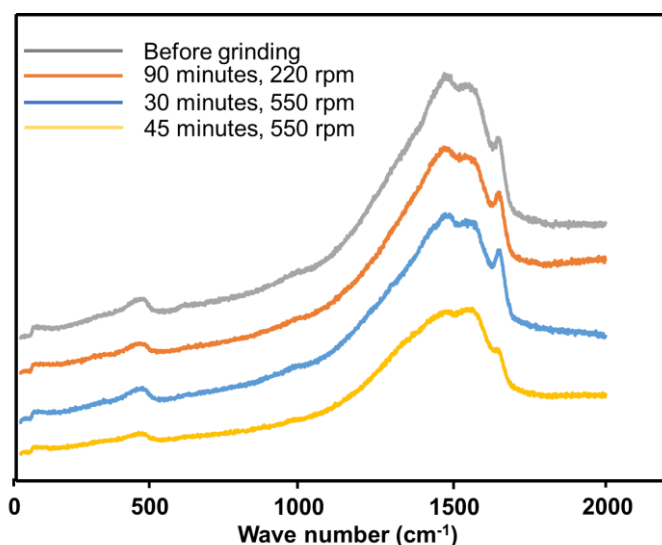


**Figure 3.4.** Raman spectrum of PBQDS after MBT using several experimental conditions.

Based on the Raman spectrum, it could be said that some degradation seems to occur after 45 minutes BMT at 550 rpm with the reduction of the quinone peak intensity at  $1500 - 1600 \text{ cm}^{-1}$ , whereas at low speed no degradation can be noticed even after a long time. Based on the result obtained, the BMT conditions were fixed at 550 rpm for 30 mins, even if some optimization should improve the result obtained.

### 3.2.2. Electrolyte properties

To evaluate the impact of the electrolyte composition on the electrochemical performances, both sulfolane and diglyme were used as solvent. Indeed, the solvent polarity and donor number could have a large impact on the organic material solubility during the cycling test and the ability for solvating  $Mg^{2+}$ . These solvents were selected as they exhibited high stability in reduction *vs.* lithium and were previously used in the lithium battery.<sup>288–300</sup> The properties of the two solvents are given in **Table 3.1**.

**Table 3.1.** Physical and electrochemical properties of solvent and magnesium, lithium electrolytes in diglyme, or sulfolane solvents

	DN [kcal/mol]	AN [kcal/mol]	Permittivity 25 °C	Viscosity mPa s	Conductivity (mS/cm) 25 °C 0.5 M Mg(TFSI) <sub>2</sub>	Conductivity (mS/cm) 25 °C 1 M Li(TFSI) <sub>2</sub>
Sulfolane	14.8	19.2	44	10.3 (30 °C)	1.5	2.4
Diglyme	18	10.5	7.6	1.14 (20 °C)	4.3	8.3

Diglyme exhibits a lower polarity and a higher solvation ability *vs.*  $Mg^{2+}$  than sulfolane (**Table 3.1**), whereas the viscosity of sulfolane is significantly higher. The conductivity for both lithium and magnesium-based electrolytes is plotted *vs.* temperature in **Figure 3.5**.

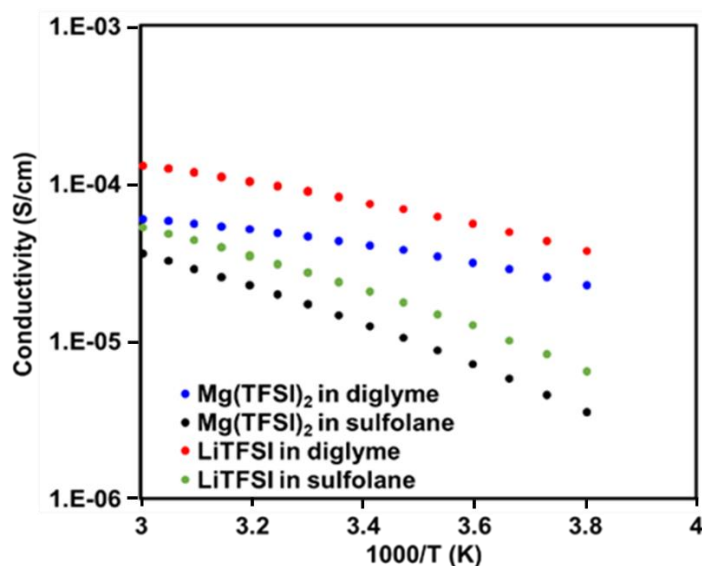


**Figure 3.5.** Conductivity of magnesium and lithium electrolytes in different solvents from -15 °C to 60 °C.

As expected, due to the high viscosity of sulfolane, the conductivities obtained in this solvent for both lithium and magnesium salts are lower, especially at low temperatures. At 60 °C, the values obtained are very closed with  $6 \cdot 10^{-3}$  S/cm and  $3.6 \cdot 10^{-3}$  S/cm for 0.5 M Mg(TFSI)<sub>2</sub> in diglyme and sulfolane while these values recorded for lithium-based solutions are  $13 \cdot 10^{-3}$  S/cm and  $5.3 \cdot 10^{-3}$  S/cm, respectively. In lithium-based electrolyte, a classical VTF law is observed, with a pseudo-activation process, which is not the case for 0.5 M Mg(TFSI)<sub>2</sub> in glyme. The weak activation of the conductivity vs. temperature in glyme can be related to a decrease in Mg<sup>2+</sup> salt dissociation in glyme as observed in Ca<sup>2+</sup> based electrolyte<sup>301</sup>, with a decrease of the salt dissociation with the temperature. Such behavior seems not to occur in the sulfolane solvent, indeed the high dielectric constant of sulfolane may improve the salt dissociation.

### 3.2.3. Electrochemical performance in Li batteries

The polymer is firstly tested by cyclic voltammetry in both diglyme and sulfolane lithium electrolytes. The CV curves show good reversibility of the oxidation/reduction of the carbonyl groups in presence of Li<sup>+</sup>, with  $E^0 = 2.8$  V vs. Li<sup>+</sup>/Li and  $\Delta E = 1.2$  V and 0.8 V in sulfolane and diglyme solution, respectively, and a ratio  $I_{\text{peak ox}}/I_{\text{peak red}} = 1.4$  (**Figure 3.6a**). The kinetics of the reaction seems lower in the sulfolane-based electrolyte, with higher  $\Delta E$  which can be related to the high viscosity of the solvent at room temperature. These values are quite similar to the  $E^0$  and  $\Delta E$  obtained from the study of polybenzoquinonesulfide (PBQS)<sup>225</sup> containing one sulfide bridge instead of two in PBQDS.

The solvent seems to have a weak effect on the electrochemical redox reaction, indeed, the oxidation process seems to occur in one step in both solvents, whereas two steps are observed during the reduction, even if the two signals are more separated in diglyme based electrolyte.

The electrochemical performance of manual grinding PBQDS electrodes was evaluated in the Swagelok cell at C/20 in presence of the different electrolytes (**Figures 3.6b** and **3.6c**). In diglyme, the cell capacity increases during the first cycles and reaches 110 mAh/g at the 3<sup>rd</sup> cycle. The capacity is far from the theoretical one i.e. 319 mAh/g based on a two-electron redox reaction. The capacity obtained in literature with PBQS<sup>225</sup> reached 275 mAh/g (over 70% of the theoretical capacity). The main reason evoked is the presence of water and residual NMP which false the active material amount. In our study, the low capacity obtained may be associated with the high particle size, few microns, which limit the accessibility of part of the active material. Also, during cycling, the capacity decreases notably up to 85 mAh/g after 50 cycles. The capacity decrease may be associated with the solubility of the PBQDS in its

reduction form in diglyme based electrolyte, which can also explain that the maximum of capacity is far from the expected one. The use of sulfolane as solvent permits to avoid the solubility of the PBQDS and increased capacity with the cycle number is obtained. However, the capacity obtained is lower than the ones in diglyme which can be associated with its high viscosity associated with the big PBQDS particle sizes.

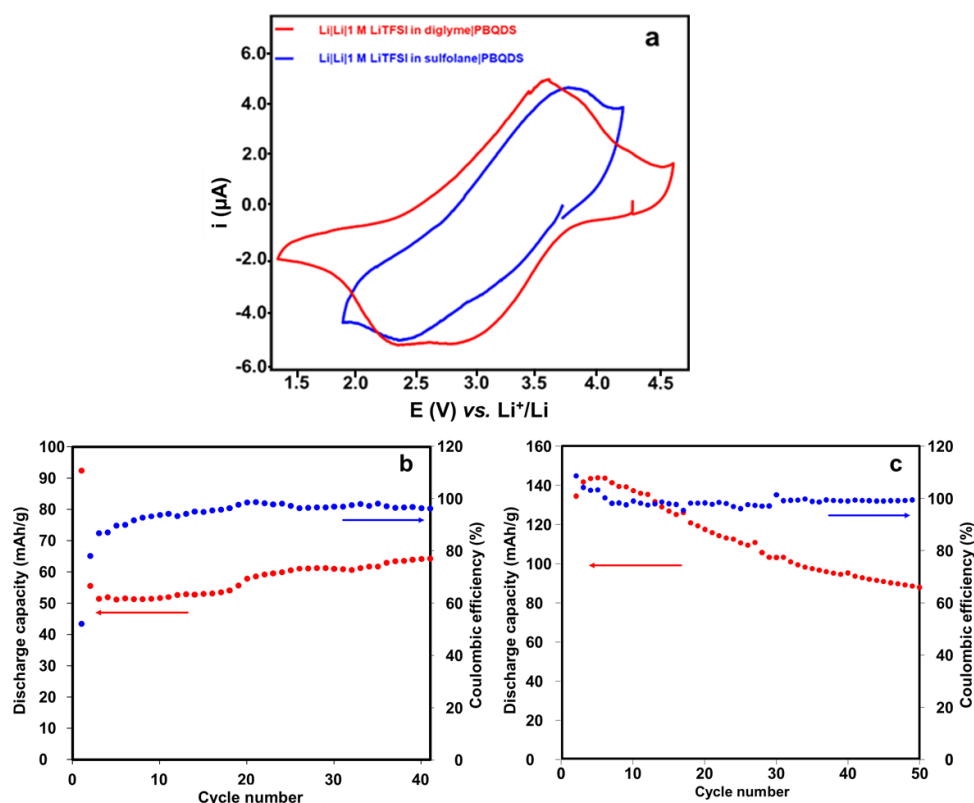


**Figure 3.6.** (a) Cyclic voltammetry of manual grinding PBQDS as active material in two different electrolytes at 1 mV/s and 25 °C. (b) Discharge capacity and coulombic efficiency of Li system with manual grinding PBQDS in sulfolane electrolyte at 40 °C including 3 cycles at C/50 and 40 cycles at C/20. (c) Discharge capacity and coulombic efficiency of Li system with manual grinding PBQDS in diglyme electrolyte at 25 °C including 3 cycles at C/50 and 40 cycles at C/20.

To improve the capacity of this system, active material was ground using ball-milling technique to reduce the particle size, and the electrochemical performances of the new electrodes were investigated in sulfolane based electrolyte at 40 °C.

During the first cycles, the discharge capacity reached 180 mAh/g, with a stable capacity up to 50 cycles around 140 mAh/g (Figure 3.7b), with a coulombic efficiency of around 97%. The maximum capacity is half of the theoretical one, which may be explained by several aspects,

the presence of some particles or aggregates with size of few microns even after ball milling (**Figure 3.3**), which can limit the accessibility of part of the material, or the difficulty to oxidize the two quinone functions in the potential range used. A power test was performed between C/20 to 2 C (**Figure 3.7c**). The capacity values slowly decrease while increasing the current density from C/20 to 2 C, the main decrease is observed at C, with respectively 80 mAh/g at C and 60 mAh/g at 2C. These values are smaller than the one obtained with a polymer containing one sulfide bridge at 198 mAh/g at a high rate 5000 mA/g from the work of Song *et al.*<sup>225</sup> It could be due to the use of sulfolane, the high viscosity of the electrolyte can induce some limitation due to ionic diffusion process and limit the charge/discharge capacity compare to other electrolytes,<sup>302</sup> the particle size or the electronic conductivity of the electrode. Based on the large capacity improvement observed with the decrease of the particle size, some optimization of the BMT protocol should be efficient to increase the capacity obtained. When returning to moderate C-rate C/20, the capacity almost comes back to its initial values. Regarding the coulombic efficiency, it increases with the C-rate, with 98% at C/20, 99% at C/10, and higher than 99.5% for the high C-rate.

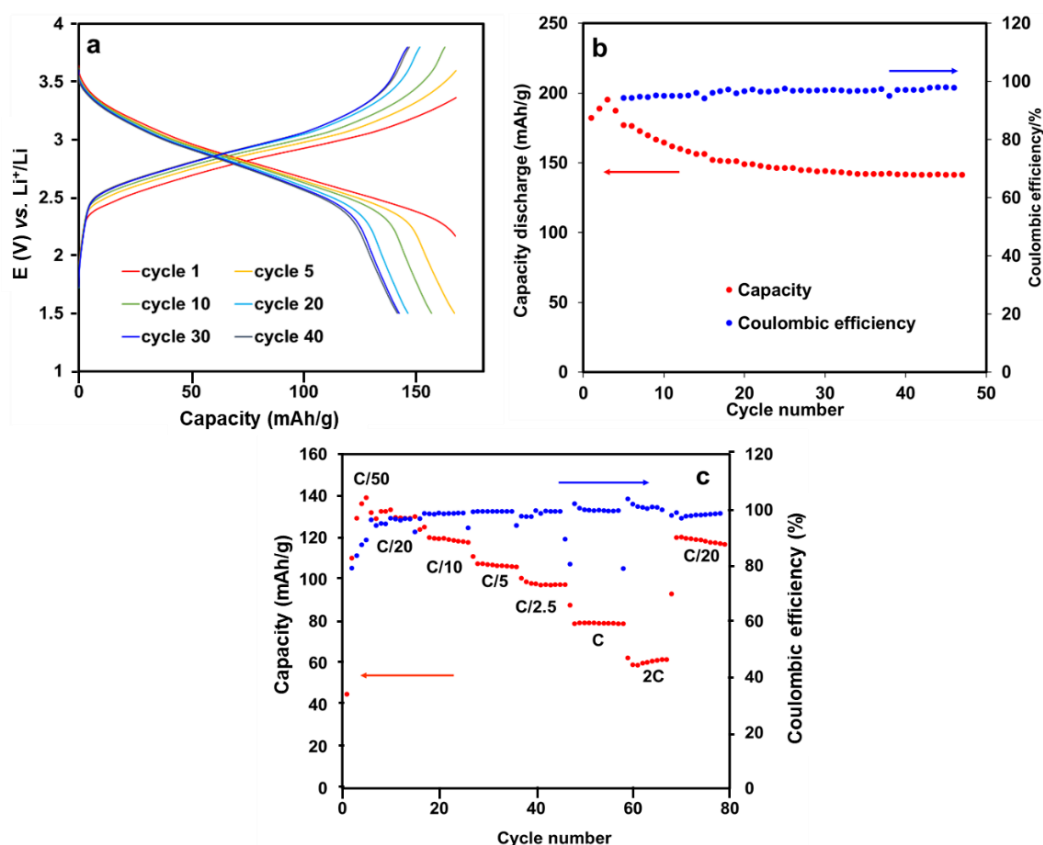


**Figure 3.7.** (a) Galvanostatic charge/discharge curves in sulfolane electrolyte with ground PBQDS at C/20 and 40 °C. (b) Discharge capacity and coulombic efficiency of Li system with

PBQDS ground by the ball-milling technique in sulfolane electrolyte at 40 °C including 3 cycles at C/50 and 40 cycles at C/20. (c) Power test and coulombic efficiency of the Li cell from C/10 to C at 40 °C.

### 3.2.4. Electrochemical performance in Mg batteries

Electrochemical characterization in the Mg batteries was investigated with cyclic voltammetry and Galvanostatic tests with 0.5 M Mg(TFSI)<sub>2</sub> in diglyme or 0.4 M Mg(TFSI)<sub>2</sub> in sulfolane as electrolytes. The CV analysis was performed at 1 mV/s with cavity microelectrode. For the first cycle, the CV curve obtained has the same shape in both diglyme (**Figure 3.8a**) and sulfolane (**Figure 3.8b**) with the reversibility of the magnesium insertion/de-insertion processes in PBQDS. However, whereas stable oxidation and reduction processes occur in sulfolane based electrolyte, with the superposition of the different scans, a significant decrease of the current is obtained in the glyme-based electrolyte, indicating the solubilization of the active material as in lithium form. For galvanostatic test, the only sulfolane-based electrolyte was used.

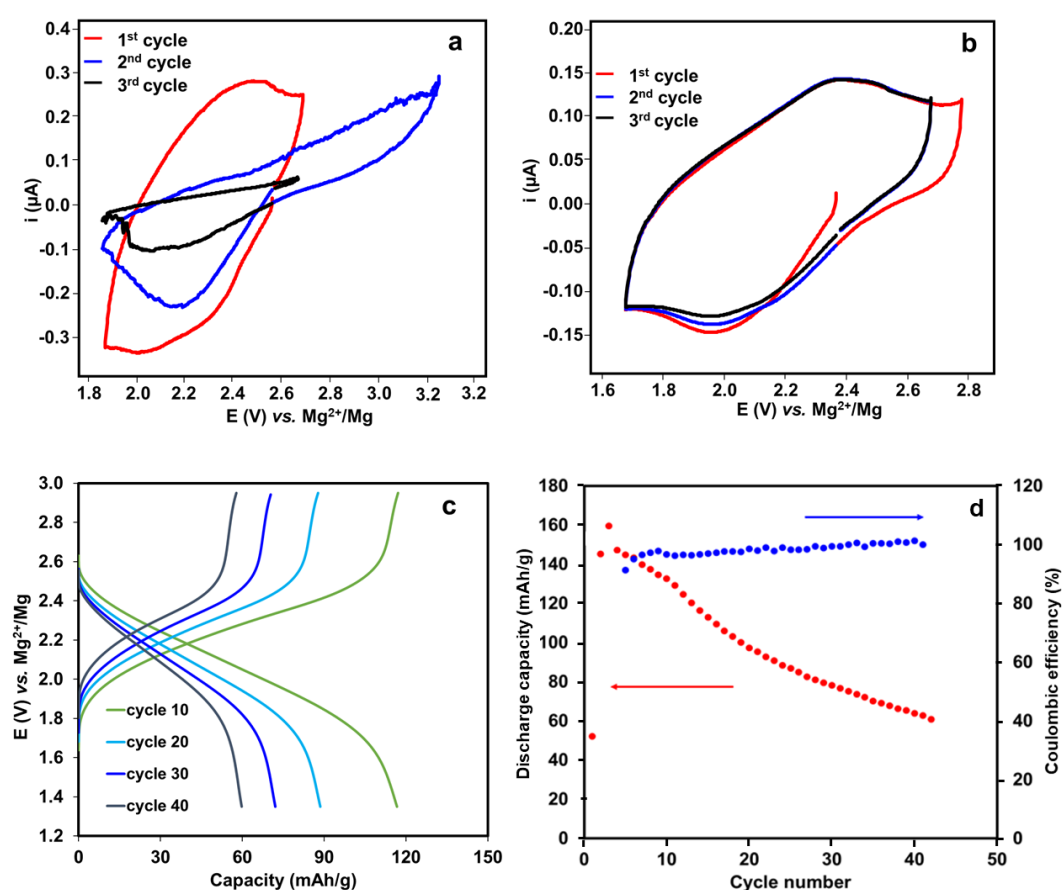


**Figure 3.8.** Cyclic voltammetry of PBQDS ground by ball-milling technique as active material in two different electrolytes: (a) diglyme solvent and (b) sulfolane solvent in Mg battery

systems at 1 mV/s and 25 °C. (c) Galvanostatic charge/discharge curves in sulfolane electrolyte with ground PBQDS at C/20 and 40 °C. (d) Discharge capacity and coulombic efficiency of Mg system with ground PBQDS in sulfolane electrolyte at 40 °C including 3 cycles at C/50 and 40 cycles at C/20.

The shape of the galvanostatic curves obtained in the Mg electrolyte is close to the one obtained in the lithium one (**Figure 3.8c**). The derivative of potential is extracted from the 4<sup>th</sup> cycle (**Figure 3.9**) for both Li and Mg systems, a peak potential shift of 900 mV. The shift is mainly linked to the potential of the negative electrode; the potential of  $\text{Mg}^{2+}/\text{Mg}$  is equal to 668 mV vs.  $\text{Li}^+/\text{Li}$ , the shift is 230 mV higher which can be associated with some polarization. However, whereas fine peaks are obtained for the lithium system, broad ones are obtained for Mg one, which is the sign of a slow electrochemical process in Mg cell. The peak potential in charge of  $\text{Mg}^{2+}$  and discharge can also give information about the polarization phenomenon associated with the ion insertion/de-insertion ( $\text{Li}^+$ ,  $\text{Mg}^{2+}$ ) in the positive electrode. Whereas the same peak potential is obtained in both charge and discharge for Li cell (at 3.45 V vs.  $\text{Li}^+/\text{Li}$ ), in the case of Mg cell 200 mV separates the cathodic peak and the anodic one with respectively 2.7 V and 2.5 V vs.  $\text{Mg}^{2+}/\text{Mg}$ , the  $\text{Mg}^{2+}$  insertion/de-insertion is much more difficult than the  $\text{Li}^+$  one.

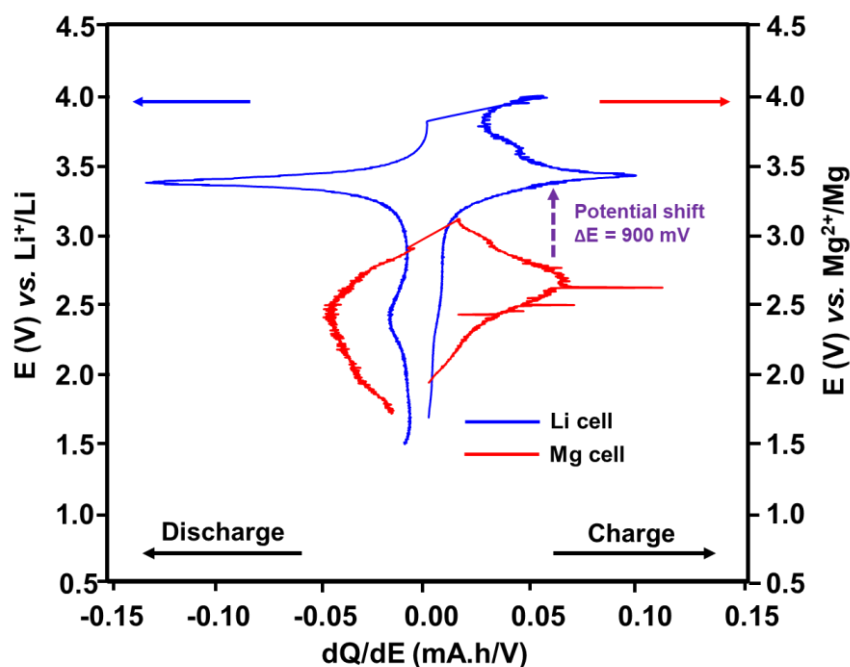


**Figure 3.9.** Superimposition of the potential vs. differential capacity curves (4<sup>th</sup> cycle) for PBQDS in Li and Mg cells in the sulfolane-based electrolyte.

Regarding capacity retention, a large difference can be noticed between Mg and Li systems. In the Mg system, a capacity increase is observed during the first cycles with a maximum at 180 mAh/g then a continuous decrease of the capacity is obtained. The same capacity can be reached in the two systems however whereas in lithium a capacity stabilization is observed, in Mg the capacity decreases cycle per cycle. Regarding the coulombic efficiency (determined by  $D_{n+1}/C_n$ ) values higher than 98% were obtained throughout the cycling test, whereas the ratio  $C_n/D_n$  is close to 95% inducing the capacity decrease. This behavior may be associated with some solubility problem in the reduction step or some diffusion process limitation, to evaluate this point, the cycling tests were performed also at low C-rate i.e. C/50, and at a higher temperature, C/20 and  $T = 60\text{ }^\circ\text{C}$ . However, whatever the experimental conditions, near the same capacity evolution, was obtained with an increase of the capacity during the first cycles and a continuous capacity decrease, no improvement or increase can be obtained. The nature of the anion was also investigated and  $\text{Mg}(\text{ClO}_4)_2$  was used instead of  $\text{Mg}(\text{TFSI})_2$ , the same evolution is noticed at both  $60\text{ }^\circ\text{C}$  and  $40\text{ }^\circ\text{C}$ . Some solubility problem can be eliminated as it will increase the solubility phenomenon. To go further in understanding the difference observed between lithium and magnesium, GITT studies were carried out.

### 3.2.5. GITT investigation for Li and Mg batteries

In Mg battery, one of the key parameters governing the overall reaction rate, and therefore the possibility of quickly charging or discharging the battery, is the diffusion coefficient of the  $\text{Mg}^{2+}$  inside the active material. Indeed, this phenomenon is often the one that is limiting concerning diffusion in the electrolyte and the charge transfer at the interface electrode/electrolyte or electronic conduction within the electrode. The galvanostatic intermittent titration technique (GITT) is widely used to study cation diffusion in both anode and cathode materials.<sup>303,304</sup> While the transport properties of electrode materials are largely available on the inorganic positive electrode,<sup>305,306</sup> the study using GITT on organic electrodes is less reported in the literature.

GITT tests were observed on the PBQDS electrode at  $40\text{ }^\circ\text{C}$  in both lithium and magnesium-based battery to explain the different electrochemical behavior obtained during galvanostatic tests. The cells are cycled in the voltage window of 1.0 – 2.1 V vs.  $\text{Mg}^{2+}/\text{Mg}$  and 1.6 – 3.4 V vs.  $\text{Li}^+/\text{Li}$  for Mg and Li tests, respectively. GITT was applied with a pulse duration of 20 minutes with a current  $3.83\text{ }\mu\text{A}$  (corresponding to C/20). Then, the cells were relaxed for one or two hours for Li and Mg respectively and this progress was repeated until the cut-off potential was reached.



The relation to extracting the diffusion coefficient from the GITT measurements was proposed by Weppner and Huggins<sup>307</sup> and give in **equ. 3** The initial stoichiometry is known ( $\delta = 0$  in  $\text{Li}_\delta\text{PBQDS}$  or  $\text{Mg}_\delta\text{PBQDS}$ ) and the electrochemical cell is in thermodynamic equilibrium (homogeneous concentration of the species inside the electrode), corresponding to the cell voltage  $E_0$ . When a current  $i$  is applied, a concentration gradient is formed inside the electrode at the phase boundary with the electrolyte.

$$D = \frac{4}{\pi} \left( \frac{iV_m}{FSz_A} \right)^2 \left[ \frac{\left( \frac{dE}{d\delta} \right)}{\left( \frac{dE}{d\sqrt{t}} \right)} \right]^2 \quad (\text{equ. 3})$$

With  $i$  the current in ampere;  $V_m$  the molar volume of the active material ( $\text{cm}^3/\text{mol}$ );  $F$  the Faraday's constant (96,485);  $z_A$  the charge number;  $dE/d\sqrt{t}$  the slope of the linear plot of the potential ( $E$ ) during the current pulse of duration  $t$  (s) which was removed of the Ohmic drop ( $IR$  drop);  $S$  is the surface area ( $\text{cm}^2$ ) of the active material in the electrode which was calculated from BET value;  $dE/d\delta$  is obtained from the slope of the plot of the steady-state voltage  $E_1$  (which is defined as  $\Delta E_s$ ) collected after each titration step  $\delta$  as shown in **Figure 3.10**.

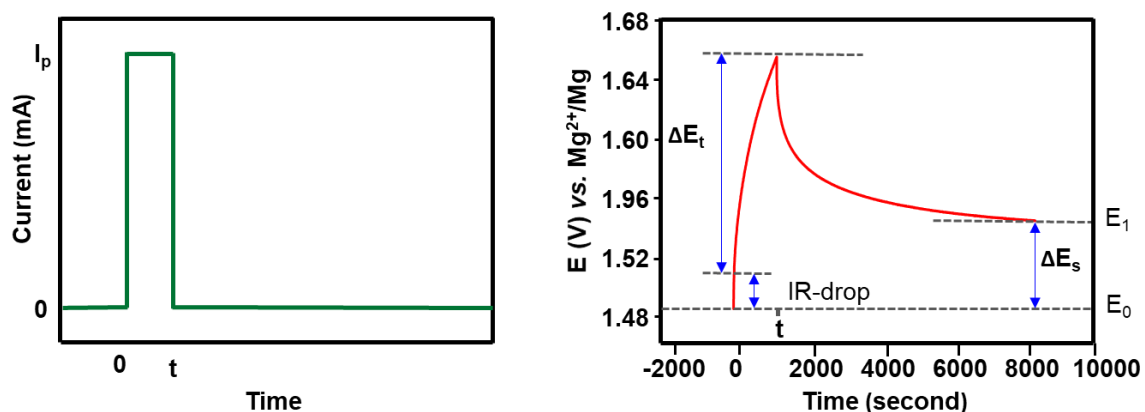


**Figure 3.10.** Single-step of a GITT measurement (a) the constant current pulse (b) potential response with  $t$  the current pulse time,  $\Delta E_t$  the cell voltage modification, and  $\Delta E_s$  the steady state voltage modification.

### Lithium investigation

The GITT in both discharge/charge of PBQDS vs. Li is presented in **Figure 3.11**, the discharge and charge capacity reach 181 mAh/g and 179 mAh/g, respectively (in good accordance with the cycling test). Even if all the capacity is not reached, good reversibility is obtained.

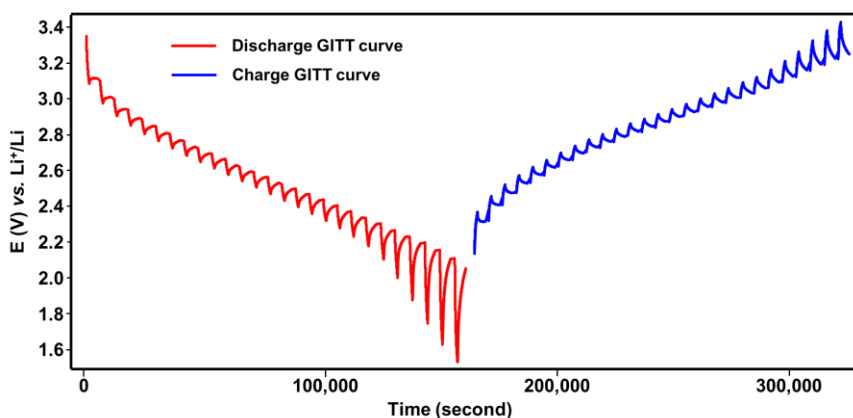


**Figure 3.11.** The GITT curve in both discharge/charge of PBQDS at  $3.83 \mu\text{A}$  (C/20) and  $40^\circ\text{C}$  during 26 pulses.

The apparent diffusion coefficient evolution in discharge is shown in **Figure 3.12**. The apparent diffusion coefficient decreases with the insertion of  $\text{Li}^+$  from  $4.1 \cdot 10^{-12} \text{ cm}^2/\text{s}$  for  $\text{Li}_{0.04}\text{PBQDS}$  to  $4.2 \cdot 10^{-14} \text{ cm}^2/\text{s}$  for  $\text{Li}_{0.9}\text{PBQDS}$  ( $\delta = 1$  corresponds to half of the state of charge if we suppose that all the active material is accessible, maximum capacity obtained for  $\delta = 2$ ) and the diffusion average value is near  $10^{-12} \text{ cm}^2/\text{s}$  while the molar volume of active material used is  $1200 \text{ cm}^3/\text{mol}$  (the D value obtained can be sur-estimated if the molar volume is lower). These values are in the same order of magnitude as the ones obtained with benzoquinone (between  $7.9 \cdot 10^{-14} \text{ cm}^2/\text{s}$  and  $6.8 \cdot 10^{-16} \text{ cm}^2/\text{s}$ ).<sup>307</sup>

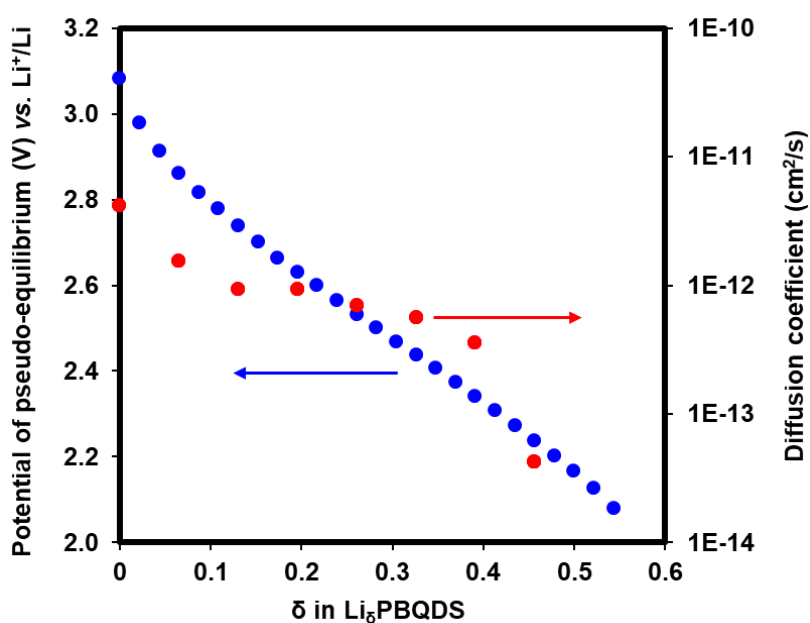


**Figure 3.12.** Evolution of the apparent diffusion coefficient D in different apparent  $\delta$  values recorded from the discharge curve in Li GITT measurement.

## Magnesium investigation

The capacities obtained during the GITT measurement on Mg cell are 130 mAh/g and 80 mAh/g on discharge and charge process, respectively (**Figure 3.13**). The values obtained are lower than that have been obtained from galvanostatic measurements, indeed in the Mg system the maximum capacity is not obtained at the first cycle but after few cycles (between 3 and 10 cycles generally).

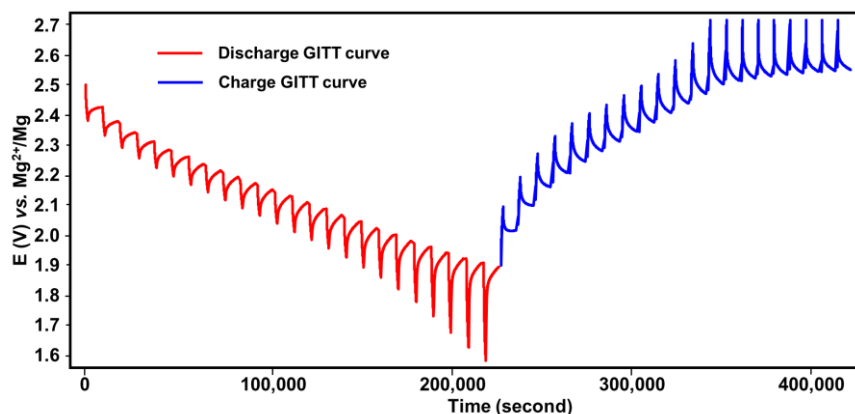


**Figure 3.13.** The GITT in both charge/discharge of PBQDS in magnesium form at C/20 at 40 °C.

First of all, the overpotential obtained vs. the state of charge in both Li and Mg cells were compared. The overpotential calculated as shown in **Figure 3.14** for both Li and Mg after the ohmic-drop removal.

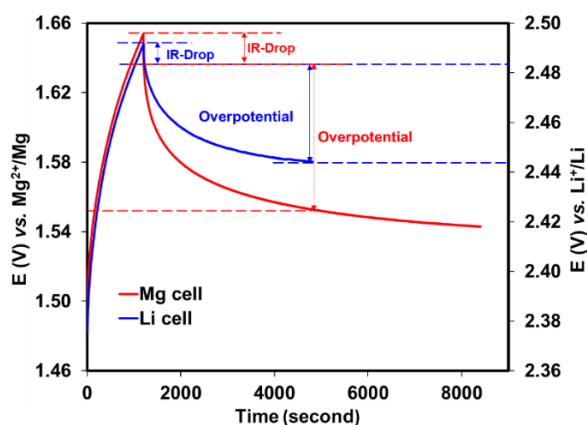


**Figure 3.14.** Overpotential determination based on one pulse (5<sup>th</sup> pulse) in Li and Mg GITT.

The ohmic drop is higher for the Mg system than the Li one in accordance with higher impedance measurement with a relaxation process up to the stationary state which is longer in Mg cell. In the charge and discharge processes, the overpotential in the Mg system is higher

than the ones obtained in lithium one (**Figure 3.15**). The highest overpotentials are obtained in charge of the two systems, indicating a more diffusion limiting process associated with the de-insertion of the cationic charge than the insertion one.

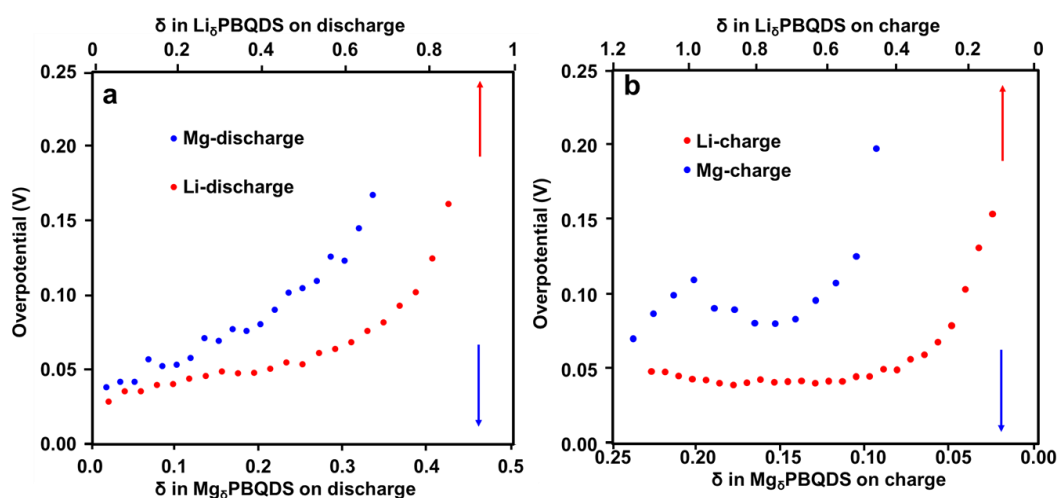


**Figure 3.15.** Overpotential on charge/discharge curves in the GITT test for Mg and Li system.

The evolution of the apparent diffusion coefficient of Mg ion vs. the discharge and charge processes is presented in **Figure 3.16**. The same shape than the one obtained in lithium form is obtained with  $D$  equal to  $4.2 \cdot 10^{-12} \text{ cm}^2/\text{s}$  and  $4.4 \cdot 10^{-14} \text{ cm}^2/\text{s}$  for  $\delta = 0.016$  and  $0.4$  respectively. As in lithium form, a quasi-constant value is obtained near  $\delta = 0.25$  with a value equal to  $10^{-12} \text{ cm}^2/\text{s}$ . The diffusion coefficients are similar to the ones obtained in Li study.

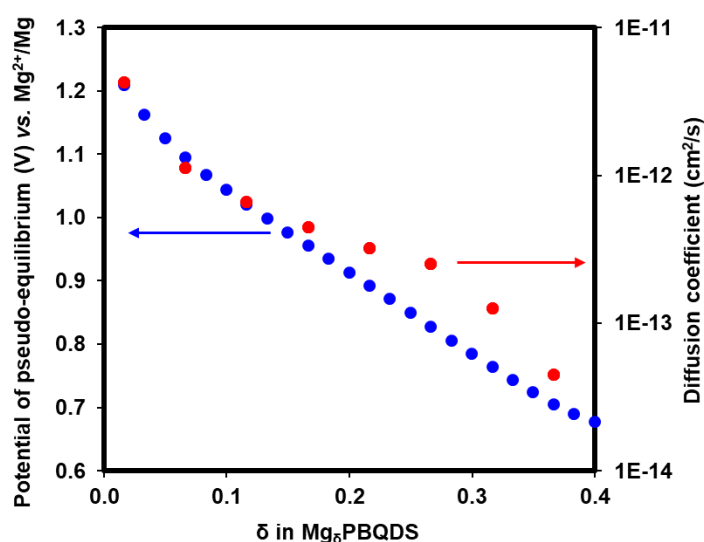


**Figure 3.16.** Evolution of potential of the pseudo-equilibrium potential and the diffusion coefficient  $D$  at different  $\delta$  values recorded from the discharge curve in Mg GITT measurement.

However, the practical capacity fading during cycling is still a question. This behavior could be due to the high  $\text{Mg}^{2+}/\text{O}$  interaction, which limits the diffusion process, and then the capacity obtained in charge, some  $\text{Mg}^{2+}$  ions may be trapped inside the material. To evaluate this hypothesis, the amount of  $\text{Mg}^{2+}$  trapped in PBQDS at the end of the charge, after a long cycling test is determined, the amount of  $\text{Mg}^{2+}$  in the electrode was characterized using the inductively coupled plasma mass spectrometry (ICP-MS). The magnesium amount is equal to 95 ppm which corresponds to 51 at% (count 3% error) of  $\text{Mg}^{2+}$  in the electrode (0.51 Mg per quinone after the end of the charge). In theory, after charging or de-insertion process, there is no more  $\text{Mg}^{2+}$  inside the positive electrode, the large amount of  $\text{Mg}^{2+}$  detected proves the trapping phenomenon as supposed. The capacity reached at the last cycle is equal to only 14 mAh/g, far from the starting capacity.

In a brief summarize, GITT investigation clearly shows that the  $\text{Mg}^{2+}$  diffusion is similar to the one of  $\text{Li}^+$  in the discharging process. The ionic radius of  $\text{Li}^+$  (0.76 Å) and  $\text{Mg}^{2+}$  (0.72 Å)<sup>308</sup> are closed. Although,  $\text{Mg}^{2+}$  needs more solvent molecules to surround for the stabilization of the charge density during the solvation step.<sup>309</sup> This leads to high desolvation energy which limits the electrochemical process kinetic. Moreover, the high charge density of  $\text{Mg}^{2+}$  creates high  $\text{Mg}^{2+}/\text{O}$  interaction which may limiting the diffusion of part of the  $\text{Mg}^{2+}$  in the oxidation step lead to the decrease of capacity in electrochemical operation and the presence of  $\text{Mg}^{2+}$  in the end of charge.

### 3.2.6. The impact of crown-ether as an additive

Recently, crown ether has been used as an additive for Li rechargeable batteries.<sup>310-312</sup> It helps to prevent the dendrite's growth of lithium by forming an efficient protective layer on Li metal. However, there is no much research applying crown ether in magnesium batteries. Following the studies of the K. Kanamura group in 2018<sup>310</sup> and 2016<sup>311</sup> on the effect of crown ether on Mg plating/stripping, in this work, we investigated the impact of the addition of crown ether in the  $\text{Mg}^{2+}$  de-insertion process from the PBQDS positive electrode. Indeed, crown ether presents high solvation property vs. cation<sup>313</sup> due to the presence of chelating oxygen (**Figure 3.17**). This solvation property can improve the extraction of  $\text{Mg}^{2+}$  by balancing the interaction quinone  $\text{O}/\text{Mg}^{2+}$ . As the complex formed between  $\text{Mg}^{2+}$  and 18-crown-6 (18C6) is a 1/1 complex based on Raman investigation,<sup>314</sup> an equimolar ratio  $\text{Mg}^{2+}/18\text{C6}$  was performed in sulfolane based electrolyte.

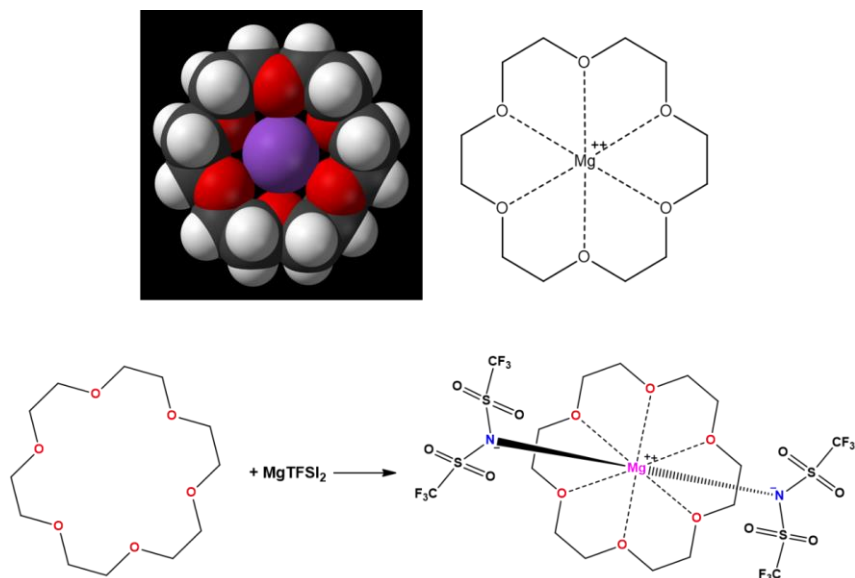


**Figure 3.17.** Structure in 3D and 2D of complex (optimized by MM2 software from ChemBio3D Ultra) of 18-crown-6 and Mg<sup>2+</sup> in the ratio 1:1 and the reaction between 18-crown-6 and Mg(TFSI)<sub>2</sub>.

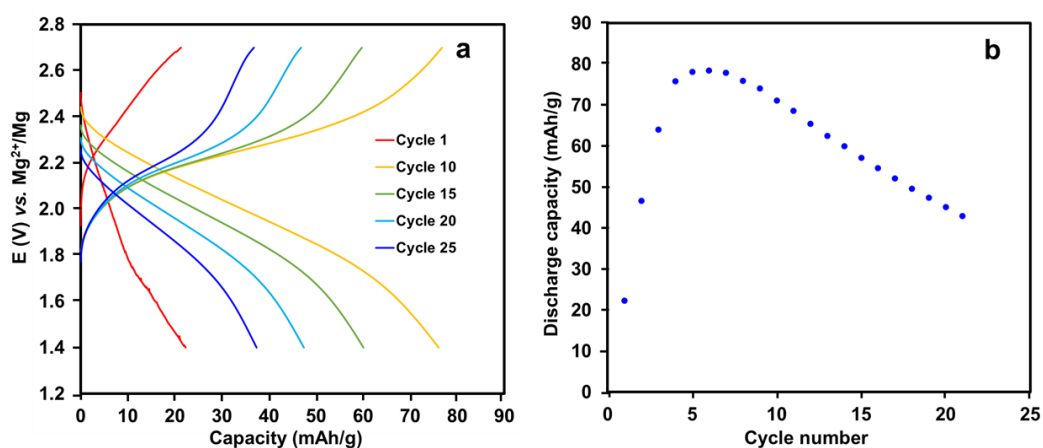


**Figure 3.18.** a) Charge/discharge profile of PBQDS in 0.4 M Mg(TFSI)<sub>2</sub> + 0.4 M 18C6 sulfolane electrolyte at C/20 and 40 °C. b) Discharge capacity vs. cycle number of PBQDS in 0.4 M Mg(TFSI)<sub>2</sub> + 0.4 M 18C6 in sulfolane) at 40 °C.

The presence of 18C6 has not a large effect on the shape of the galvanostatic curves (**Figure 3.18a**), regarding capacity retention (**Figure 3.18b**), near the same evolution can be noticed with, first, a capacity increase and then a continuous decrease of it. However, regarding the coulombic efficiency, some differences can be reached. The ratios  $D_{n+1}/C_n$  and  $C_n/D_n$  obtained for PBQDS in the two electrolytes were plotted vs. the cycle number, after the 10<sup>th</sup> cycle, in the capacity decrease part (**Figure 3.19**).

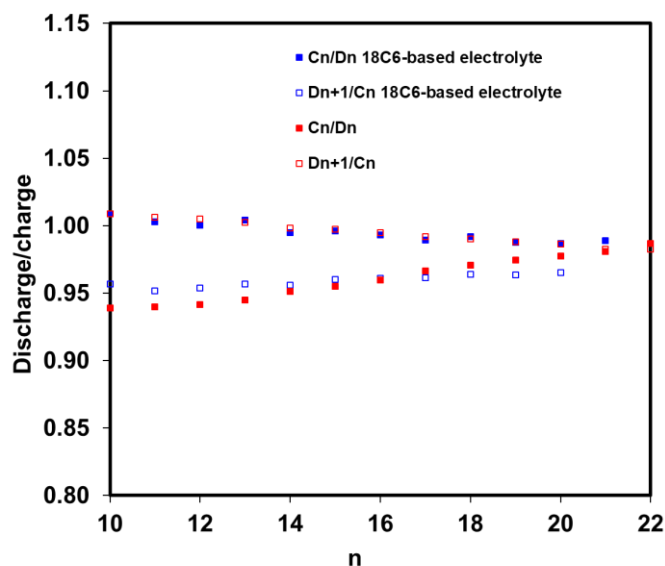


**Figure 3.19.** Comparison plots of the ratio between charge and discharge versus cycles on galvanostatic test on an electrolyte with and without 18-crown-6 ether.

Whereas without additive the ratio  $C_n/D_n$  is close to 0.95, with the addition of 18C6 the ratio  $C_n/D_n$  is close to 1, indicating that the charge is equal to the previous discharge, so no  $Mg^{2+}$  seems to be trapped inside the active material. On the contrary, where  $D_{n+1}/C_n$  is equal to 1 without additive, the presence of 18C6 induces a decrease of this value i.e. 0.95. This capacity delay may be associated with some active material dissolution in its reduced state. To verify this hypothesis, the quantity of  $Mg^{2+}$  inside the electrode after charging was analyzed, the cathode was removed and carefully clean before checking ICP-MS. The magnesium amount is equal to 50 ppm which corresponds to 20 at% (0.2 trapped  $Mg^{2+}$  per quinone) much lower than the one obtained without 18C6. Although the retained capacity after charging is 40 mAh/g in the 30<sup>th</sup> cycle (12% of theoretical capacity), the data from ICP-MS measurement and the charge/discharge ratio indicate that crown ether plays a significant role in the processed. It seems to help to remove  $Mg^{2+}$  with near 3 times lower  $Mg^{2+}$  trapping per quinone unit however the trapping still happens. It could be due to the small quantity of 18C6 using that is not enough for the efficient solvation of  $Mg^{2+}$ , also, 18C6 is a large molecule, some steric entanglement can limit its solvation ability vs.  $Mg^{2+}$  close to the quinone function. The electrolyte was also checked by cyclic voltammetry to evaluate the presence or not of soluble active material in the cell. However, no electrochemical signal was obtained, this can be due to the absence of soluble active compound inside the electrolyte, or as the quantity of active material is extremely small, the concentration of the active material is too low to be detected. Based on the result obtained with ICP-MS test, the presence of crown-ether seems to help to remove  $Mg^{2+}$  during the

charging process, even if some optimization is required, as some  $\text{Mg}^{2+}$  are still trapping. The difference observed in presence of 18-crown-6 can help us to design a suitable electrolyte for this kind of organic material.

### 3.2.7. Forward to calcium batteries

Among multivalent metals, calcium is an attractive element that could be replaced Li in rechargeable batteries thanks to high abundance (5<sup>th</sup> on earth) and close potential ( $E_{\text{Ca}^{2+}/\text{Ca}}^0 = -2.868 \text{ V vs. NHE}$ , 170 mV higher than the couple  $\text{Li}^+/\text{Li}$ ). Given the chemical similarities between magnesium and calcium, the first approach to the calcium-based battery has been based on a similar principle to that developed for magnesium, with the development of ether-based electrolytes which can enable the Ca plating/stripping reversibility and of positive active material adapted to divalent cation. As PBQDS is in its oxidized state, the evaluation of its potentiality in calcium battery can be easily performed by the use of a calcium-based electrolyte i.e. 0.4 M  $\text{Ca}(\text{TFSI})_2$  in sulfolane. To avoid the problem of the metallic calcium interface, an active carbon (AC) electrode was used as counter and reference electrodes, as reported in several publications.<sup>315–317</sup> The large excess of electrolyte used may be considered as a  $\text{Ca}^{2+}$  reservoir.

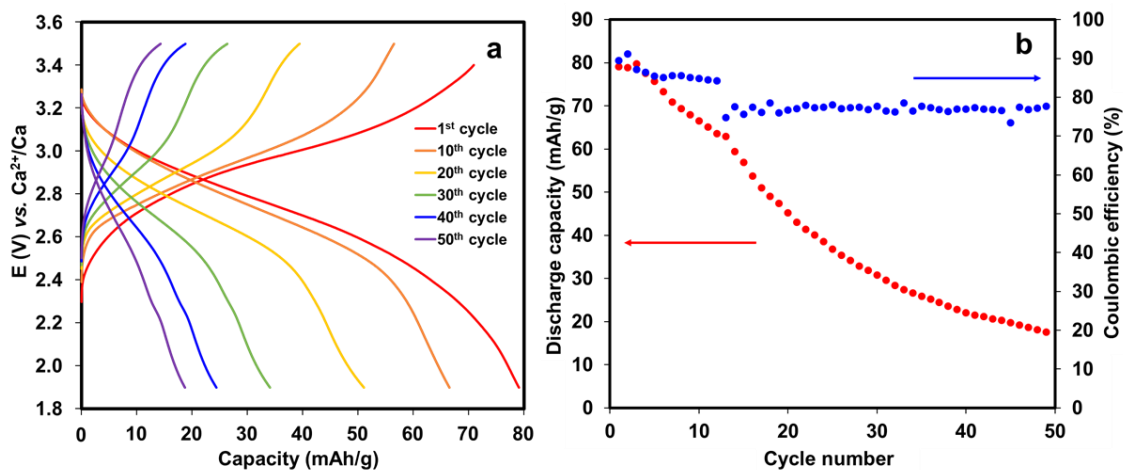


**Figure 3.20.** (a) Charge/discharge profiles in calcium batteries using PBQDS as the positive electrode and AC as counter and reference electrodes, in 0.4 M  $\text{Ca}(\text{TFSI})_2/\text{sulfolane}$  as an electrolyte at C/20 and 40 °C. (b) Discharge capacity and coulombic efficiency of the cell with 3 cycles in C/50 and following cycles in C/20. The potential of the active carbon vs.  $\text{Ca}^{2+}/\text{Ca}$  was determined by using ferrocene/ferrocenium redox couple in sulfolane. The stability of the active carbon potential was evaluated by CV measurements performing during several days as in previous publication.<sup>318,319</sup>



Electrochemical testing was conducted on the galvanostatic test at 40 °C and C/20 to evaluate the shape of the curve and capacity during Ca<sup>2+</sup> insertion/de-insertion processes when PBQDS is applied as positive material. The results are shown in **Figure 3.20** with a potential voltage range of 1.9 V – 3.5 V vs. Ca<sup>2+</sup>/Ca.

Similar to the obtained result on Mg and Li study, the galvanostatic test for Ca batteries shows the same charge/discharge shapes. The capacity for the few first cycles reaches 80 mAh/g at a low C-rate (C/20). This value seems slightly lower than the one obtained in the Mg cell. Moreover, capacity reduces dramatically scan by scan. The capacity is then faded lightly and remains 65 mAh/g after 15 cycles. However, the retained capacity is only 20 mAh/g which is lower than in Mg investigation. The coulombic efficiency increases up to near 90% in a few first cycles before lightly decrease to near 80% after 50 cycles. Although the capacity is still far from the theoretical value and coulombic efficiency is lower than in Li and Mg systems. In the same strategy to prior work, the derivative of potential is derived from Mg and Ca cell at the 4<sup>th</sup> cycle (**Figure 3.21**). The potential shift obtained is directly associated with the shift of the metallic electrode potential; the potential of Mg<sup>2+</sup>/Mg is equal to 500 mV vs. Ca<sup>2+</sup>/Ca. Also, in contrast to Li cell, broad peaks are obtained for the Ca cell which is similar to Mg one with over 200 mV difference between anodic and cathodic peak potential. The electrochemical reaction seems to be very similar between Ca<sup>2+</sup> and Mg<sup>2+</sup>, thus more associated with the divalent character of the ionic species than the size or the charge density.

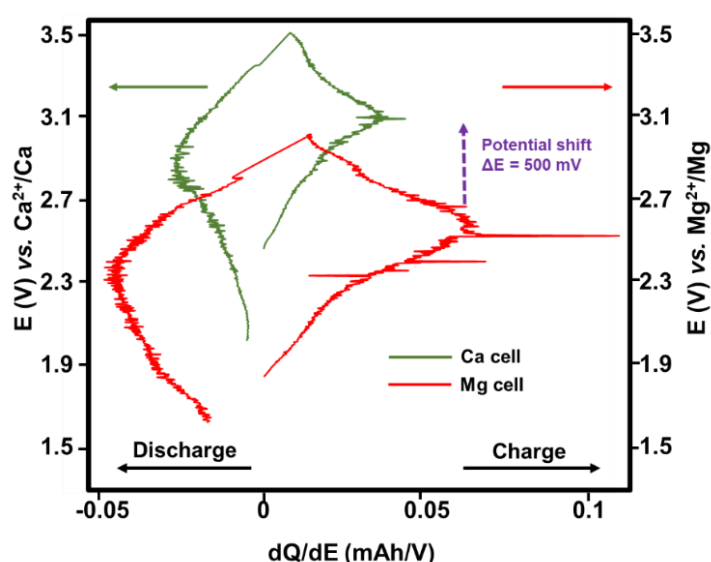


**Figure 3.21.** Superimposition of the potential vs. differential capacity curves (4<sup>th</sup> cycle) for PBQDS in Ca and Mg cells in the sulfolane-based electrolyte.

We performed just a preliminary test, to see if the diffusion limitation observed in the Mg system can be less detrimental using  $\text{Ca}^{2+}$  as a divalent cation, however, the first results obtained seem to indicate near the same limitation, and real work on calcium cell is required.

### **3.3. Conclusion**

In this study, a novel polymer-based on quinone sulfide PBQDS was synthesized in high yield from commercially available starting materials. Electrochemical properties of this polymer have been characterized for both Li and Mg batteries and even in Ca batteries, allowing for comparison of the material performances. PBDQS displays good electrochemical properties in a lithium battery system in sulfolane based electrolyte. Solvent investigation shows a significant role and ethereal solvent such as diglyme, usually applied in Mg battery studies, cannot be used in this case due to the solubility problem. The reduction of the particle size permits to notably improve the capacity obtained, some optimization is required to increase the capacity. For the Mg system, diffusion limitation was observed, which could be limited by the particle size reduction and the use of more solvating solvent however the solubility problem encountered precluded the evaluation of more solvating solvent in this work.

## **Chapter 4:**

# **Organic cathode materials based on salts of 2,5-dihydroxyterephthalic acid**

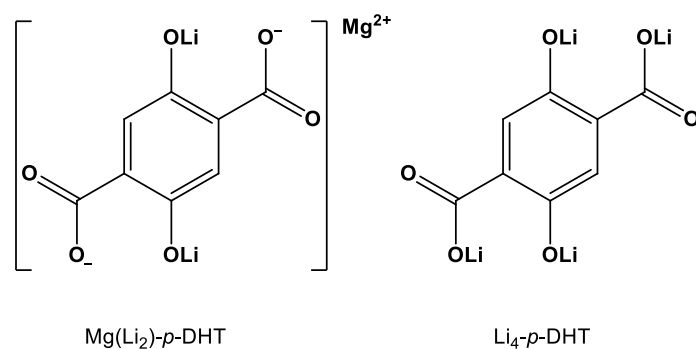
#### 4.1. Overview

Between different approaches to tackling the problem in rechargeable batteries, redox organic salt compounds are applied to improve the insolubility of redox organic materials based electrode in aprotic solutions.<sup>320–323</sup> In 2008, P. Poizot group<sup>324</sup> introduced firstly the conjugated carbonyl dilithium terephthalate as positive material for the Li system, and thanks to this research, a series of enhancements based on the terephthalate salts were implemented and introduced in subsequent years.<sup>325–327</sup>

Organic tetralithium salts of 2,5-dihydroxyterephthalic acid ( $\text{Li}_4\text{C}_8\text{H}_2\text{O}_6$ ) have been investigated as active materials with the morphologies of bulky material, nanoparticles, or nanosheets as positive or negative electrodes in rechargeable LIBs.  $\text{Li}_4\text{C}_8\text{H}_2\text{O}_6/\text{Li}_2\text{C}_8\text{H}_2\text{O}_6$  exhibits a potential at  $\sim 2.6$  V was used as a positive electrode, and  $\text{Li}_6\text{C}_8\text{H}_2\text{O}_6/\text{Li}_4\text{C}_8\text{H}_2\text{O}_6$  at  $\sim 0.8$  V vs.  $\text{Li}^+/\text{Li}$  for a negative one by Chen group in 2013.<sup>328</sup> Nanosheets show the highest discharge capacities of 223 and 145 mAh/g at 0.1 and 5 C rates after 50 cycles respectively using ethylene carbonate (EC) and dimethyl carbonate (DMC) + 1 M  $\text{LiPF}_6$  as an electrolyte.

Dilithium 2,5-dihydroxyterephthalate ( $\text{Li}_2\text{DHTP}$ ) was synthesized and delivers remarkable performances<sup>329</sup> with a high specific capacity of 165 mAh/g over 100 cycles at 30 mA/g with a coulombic efficiency of 98%. Under the high versatility of organic compounds, tetrasodium salt of 2,5-dihydroxyterephthalic acid ( $\text{Na}_4\text{DHTPA}$ ;  $\text{Na}_4\text{C}_8\text{H}_2\text{O}_6$ ), was investigated in sodium cell between 1.6 – 2.8 V vs.  $\text{Na}^+/\text{Na}$  as a positive electrode or between 0.1 – 1.8 V vs.  $\text{Na}^+/\text{Na}$  as a negative one, the two configurations exhibit stable capacities of 180 mAh/g.<sup>330</sup> To manage the potential of the material the magnesium (2,5-dilithium-oxy)-terephthalate ( $\text{Mg}(\text{Li}_2)\text{-}p\text{-DHT}$ ) was prepared by P. Poizot *et al.*<sup>331</sup> The use of  $\text{Mg}^{2+}$  as a spectator ion in the carboxylate group enables to have a shift of 800 mV in potential, whereas the performances in term of capacity and cyclability are the same. Regarding the performance obtained and the well-adapted potential, we decide to investigate this family of material in magnesium battery.

This chapter will then present the electrochemical performance in a similar condition of 3 salts synthesized from 2,5-dihydroxyterephthalic acid:  $\text{Mg}(\text{Li}_2)\text{-}p\text{-DHT}$ ,  $\text{Li}_4\text{-}p\text{-DHT}$ , MOF CPO-27 provided by IMN laboratory in different magnesium-based electrolytes using cyclic voltammetry. Some of the materials will also be investigated in lithium-based electrolyte for the comparison.



**Scheme 4.1.** Structure of Mg(Li<sub>2</sub>)-*p*-DHT, Li<sub>4</sub>-*p*-DHT.

#### 4.2. Galvanostatic test in lithium battery

In the prior study, ethylene carbonate (EC), diethyl carbonate (DEC), and dimethyl carbonate (DMC) were used as solvents. However, the carbonate-based electrolyte can not be used for magnesium battery investigations because it can react with Mg foil and lead to a resistive passivating layer and cause a large polarization effect.<sup>39,141</sup> Therefore, this study would be performed using glyme-based and sulfone-based solvents which seems to be more compatible with metallic Mg foil. That's why the study of the material was first performed in the lithium-based electrolyte.

The procedure for the electrode preparation was described in chapter 5. SuperP® (Timcal) was used as a conductive carbon additive and poly(vinylidene difluoride) (PVdF 5130, Solvay; dissolved in *N*-methyl-2-pyrrolidinone as 12 wt% solution) was selected as a polymeric binder. The electrode composition was set up to be 60/30/10 wt% (active material/C/binder). 1 M LiTFSI in diglyme and 1 M LiTFSI in sulfolane were used as the electrolyte. The galvanostatic cycling tests were performed on a VMP3 potentiostat at C/20 with a potential window from 2.6 to 3.8 V vs. Li<sup>+</sup>/Li.

The electrochemical property of Mg(Li<sub>2</sub>)-*p*-DHT at 25 °C was illustrated in **Figure 4.1**. The practical capacity is over 30 mAh/g after 50 cycles with an initial capacity of near 40 mAh/g which is far from the result obtained using carbonate-based electrolyte with 100 mAh/g.<sup>331</sup> The coulombic efficiency fluctuates at over 80%, this weak coulombic efficiency could be related to the oxidation of electrolyte at high potential during the charge. Concerning the results obtained, glyme + LiTFSI seems to be not relevant as an electrolyte for Mg(Li<sub>2</sub>)-*p*-DHT due to the weak stability of the glyme. For that reason, another choice has been considered which can be suitable for both Li and Mg systems such as a sulfolane-based electrolyte. The properties of

sulfolane as a solvent for electrolyte were presented in chapter 3. We selected this solvent because it presents good electrochemical stability on both the anodic and cathodic sides.<sup>332,333</sup>

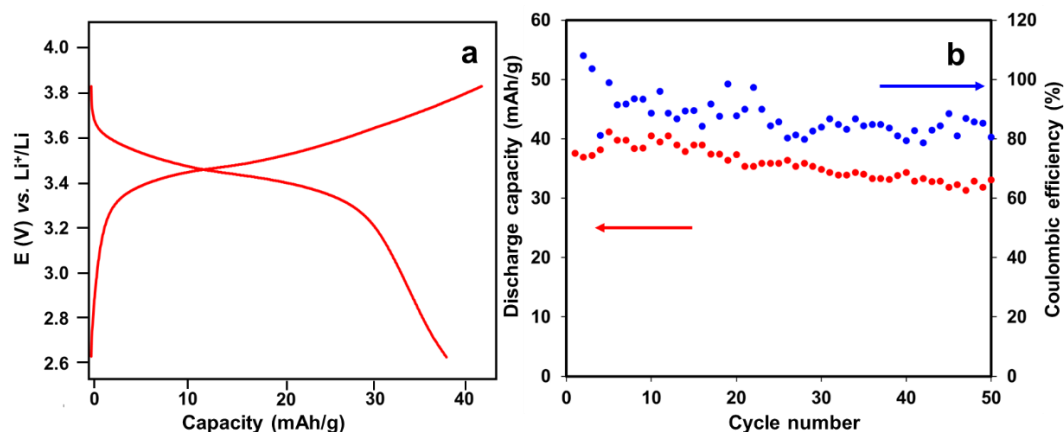


**Figure 4.1.** Electrochemical performance of Mg(Li<sub>2</sub>)-*p*-DHT in diglyme electrolyte at 25 °C: (a) initial cycle voltage profiles at C/20 (b) capacity retention and coulombic efficiency upon 50 cycles at C/20.

As sulfolane exhibits a high viscosity, the electrochemical study was performed at 40 °C to have sufficient ionic conductivity. The initial capacity reaches 70 mAh/g (Figure 4.2), which is much higher than the value obtained in diglyme electrolyte. Upon cycling, a capacity decrease is noticed with a capacity of 50 mAh/g after 30 cycles, with an increase of the coulombic efficiency with the cycle number reaching 95%. Even if the capacity obtained is lower than the one obtained in carbonate-based electrolytes, we selected sulfolane as a solvent for the study of Mg(Li<sub>2</sub>)-*p*-DHT as active material in magnesium battery.

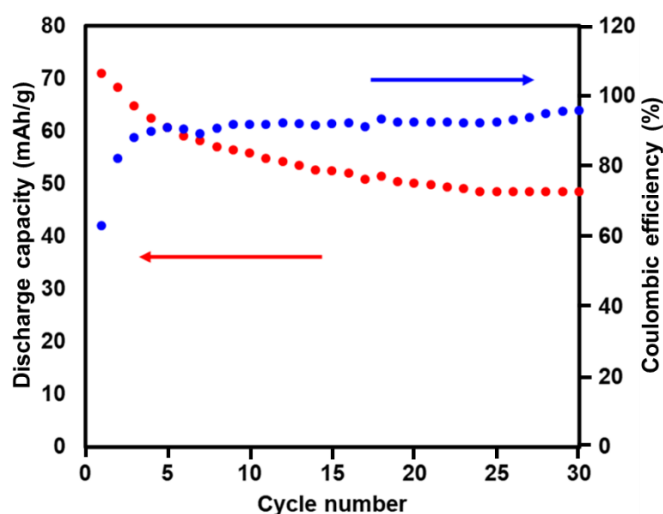


**Figure 4.2.** Galvanostatic cycling results (C/20) of Mg(Li<sub>2</sub>)-*p*-DHT in sulfolane electrolyte at 40 °C.

### 4.3. Electrochemical performance in magnesium system

The sulfolane-based electrolyte was applied to investigate the response of Mg(Li<sub>2</sub>)-*p*-DHT in magnesium cells using cyclic voltammetry in the potential window from 0 to 4 V vs. Mg<sup>2+</sup>/Mg. Due to the insolubility of the material, a cavity microelectrode was used. The response of Mg(Li<sub>2</sub>)-*p*-DHT in sulfolane + 0.4 M Mg(TFSI)<sub>2</sub> is compared to the one in sulfolane + 1 M LiTFSI. The CV curves of the first scan are shown in **Figure 4.3**.

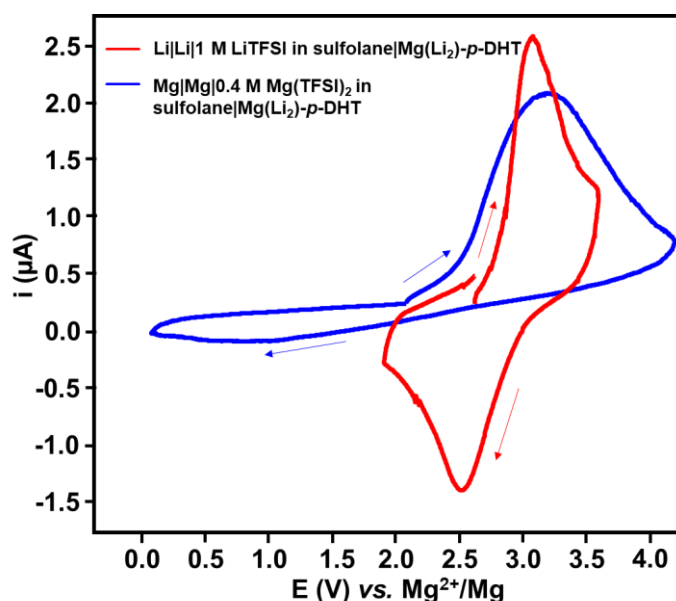


**Figure 4.3.** Cyclic voltammogram of Mg(Li<sub>2</sub>)-*p*-DHT in both 1 M LiTFSI or 0.4 M Mg(TFSI)<sub>2</sub> in sulfolane at 1 mV/s and room temperature.

In lithium electrolyte, a quasi-reversible redox signal is observed at  $E_0 = 3.1$  V vs. Li<sup>+</sup>/Li ( $E_0 = 2.5$  V vs. Mg<sup>2+</sup>/Mg) with  $\Delta E_{\text{peak}} = 500$  mV. Whereas with the use of Mg(TFSI)<sub>2</sub> only an oxidation peak at 3.1 V vs. Mg<sup>2+</sup>/Mg is observed. During the first oxidation of Mg(Li<sub>2</sub>)-*p*-DHT in the quinone form, Li<sup>+</sup> is removed from the structure, that's why, as expected, the oxidation peak potential is obtained at the same value as the one in LiTFSI based electrolyte. However, the oxidation peak is broader and more problematically no reduction of the quinone is observed so no Mg<sup>2+</sup> insertion can be obtained. Unfortunately, the fast kinetic of the intercalation of Li<sup>+</sup> is not reached with Mg<sup>2+</sup> ion. It may be due to the bigger size of [Mg-solvent]<sup>2+</sup> compared to [Li-solvent]<sup>+</sup><sup>334</sup> even if the magnesium ion radius is smaller than the Li-ion radius (0.72 and 0.74 Å, respectively)<sup>335</sup> which can be reinforced by the strong interaction between Mg<sup>2+</sup> and the solvent, associated with the divalent character of Mg<sup>2+</sup>.

To be check that whatever the solvent used, no insertion of Mg<sup>2+</sup> can occur, several solvents were investigated. Indeed, it's well-known that the solvent has a large effect on chemical

reaction kinetic and also electron-transfer reactions (**Figure 4.4**).<sup>336</sup> The electrochemical study of Mg(Li<sub>2</sub>)-*p*-DHT was thus performed also in diglyme and trimethylacetonitrile. The properties of these solvents including acceptor number, donor number, and dielectric constant are presented in **Table 4.1**. The sulfolane presents a higher dielectric constant, favorable for a high ionic species dissociation, and lower DN value (a measurement of the capability to interact with cation) than the other two solvents, so weaker interaction with Mg<sup>2+</sup>. On the opposite, glyme exhibits a much lower dielectric constant but a good affinity with cation, whereas the trimethylacetonitrile has in between properties.

**Table 4.1.** Acceptor number (AN), donor number (DN), and dielectric constant ( $\epsilon$ ) of solvents used in the study of salts of 2,5-dihydroxyterephthalic acid.

Solvent	AN	DN	$\epsilon$
Diglyme	9.9 <sup>337</sup>	18 ± 1 <sup>337</sup>	7.23 (30 °C) <sup>338</sup>
Trimethylacetonitrile	-	Near 16 <sup>339*</sup>	20.2 (30 °C) <sup>340</sup>
Sulfolane	19.2 <sup>341</sup>	14.8 <sup>342</sup>	43.4 (30 °C) <sup>340</sup>

\*The DN of trimethylacetonitrile is not available, but regarding the DN of the different nitrile compounds (butanenitrile, isobutyronitrile, acetonitrile)<sup>339</sup> we may assume a value close to 16.

Trimethylacetonitrile is used instead of acetonitrile due to its reactivity *vs.* metallic electrode associated with the acidic proton presented in the  $\alpha$ -position of the nitrile group. Trimethylacetonitrile presents interesting properties in terms of dielectric constant, DN value, and viscosity and could permit a high salt solubility, high cation solvation ability, and high ionic species mobility.

The mixture of Mg(TFSI)<sub>2</sub> and MgCl<sub>2</sub> as salt was also investigated. Pellion Technologies' early research showed that the addition of MgCl<sub>2</sub> to Mg(TFSI)<sub>2</sub> in ethereal solvents provides electrolytes capable of displaying high Mg plating/stripping coulombic efficiency. The addition of MgCl<sub>2</sub> to the electrolyte enhances Mg plating/stripping reversible by the formation of the binuclear complex, [Mg<sub>2</sub>( $\mu$ -Cl)<sub>2</sub>]<sup>2+</sup>.<sup>343-345</sup> The study of the Yan group also proved that the MgCl<sup>+</sup> monovalent ion is, in presence of chloride salt, the main charge carrier in magnesium rechargeable batteries instead of Mg<sup>2+</sup> with faster kinetic.<sup>174</sup>

In all the electrolytes, as expected, a similar response is obtained in oxidation related to the formation of quinone and the de-insertion of Li<sup>+</sup> with an oxidation peak at 3.1 V *vs.* Mg<sup>2+</sup>/Mg. Whereas no reduction peak is observed in sulfolane based electrolyte, a small broad reduction peak is observed in glyme at a potential from 2.5 to 0.5 V *vs.* Mg<sup>2+</sup>/Mg, the intensity of the



reduction peaks weakly increases in trimethylacetonitrile based electrolyte. However,  $\text{Mg}^{2+}$  insertion is weak. The addition of  $\text{MgCl}_2$  permits to have a weak reduction process with two broad peaks, however, no oxidation peak is obtained during the next cycle. The same behavior is reached in trimethylacetonitrile (**Figure 4.4a**). The weak reduction process and the inefficient oxidation one with the removal of  $\text{Mg}^{2+}$  can be related to the destruction of the crystal structure (mechanical or electrochemical constraints) of the salt in addition to strong chemical bonds between  $\text{Mg}^{2+}$  and the oxygen groups of the quinone limiting the cation mobility (**Figure 4.4b**).

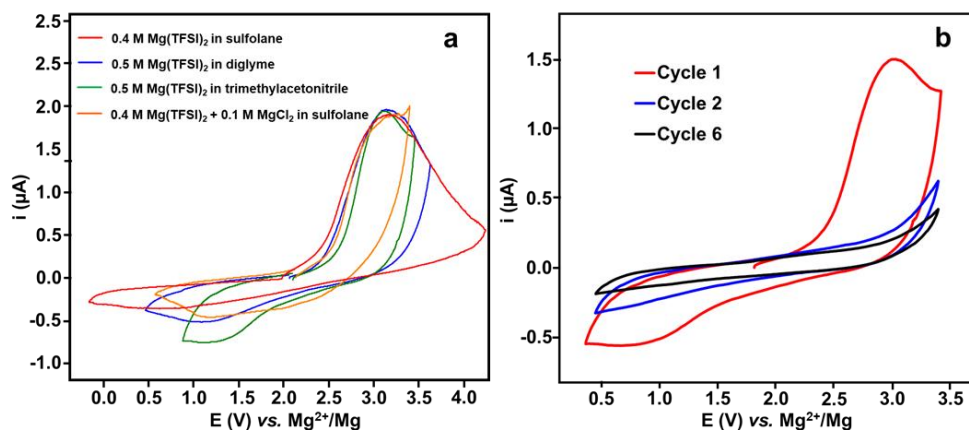


**Figure 4.4.** Cyclic voltammogram of  $\text{Mg}(\text{Li}_2)\text{-}p\text{-DHT}$  (**a**) during the first scan in the different electrolytes at 1 mV/s and (**b**) during several scans in the trimethylacetonitrile-based electrolyte at 1 mV/s at room temperature.

As the irreversibility of the  $\text{Mg}(\text{Li}_2)\text{-}p\text{-DHT}$  redox behavior could be partially related to the high potential of the compound especially using glyme as a solvent, the electrochemical response of  $\text{Li}_4\text{-}p\text{-DHT}$  was also investigated. As discussed at the beginning of this chapter,  $\text{Li}_4\text{-}p\text{-DHT}$  has the same structure as  $\text{Mg}(\text{Li}_2)\text{-}p\text{-DHT}$  with  $\text{Li}^+$  as spectator ion instead of  $\text{Mg}^{2+}$ . The redox responses of  $\text{Li}_4\text{-}p\text{-DHT}$  and  $\text{Mg}(\text{Li}_2)\text{-}p\text{-DHT}$  are compared in **Figure 4.5** in glyme based electrolyte. As expected, regarding the literature, a cathodic shift is observed, with an oxidation peak at 1.5 V vs.  $\text{Mg}^{2+}/\text{Mg}$  for  $\text{Li}_4\text{-}p\text{-DHT}$ , thus 1.32 V lower than the oxidation of  $\text{Mg}(\text{Li}_2)\text{-}p\text{-DHT}$ . The difference in potential is significantly higher than the one observed in the lithium-based electrolyte.<sup>329</sup> The oxidation peak width is very different with a narrow peak for  $\text{Li}_4\text{-}p\text{-DHT}$ . These two elements show that the kinetic of the phenolic function oxidation with the removal of  $\text{Li}^+$  is more favorable in  $\text{Li}_4\text{-}p\text{-DHT}$  than in  $\text{Mg}(\text{Li}_2)\text{-}p\text{-DHT}$  in presence of magnesium salt into the electrolyte. This kinetic difference was not noticed in the lithium-based electrolyte.<sup>329,331</sup> However even for  $\text{Li}_4\text{-}p\text{-DHT}$ , the response in a reduction involving the  $\text{Mg}^{2+}$  insertion is still weak with a broad peak, and no response in both oxidation and reduction is

observed during the second cycle. One reason which could be proposed to explain this behavior is the destruction of the crystal structure of  $\text{Li}_4\text{-}p\text{-DHT}$  when  $\text{Mg}^{2+}$  insertion occurs related to the bigger species intercalated (solvated  $\text{Mg}^{2+}$ ) and/or the divalent character of the species.

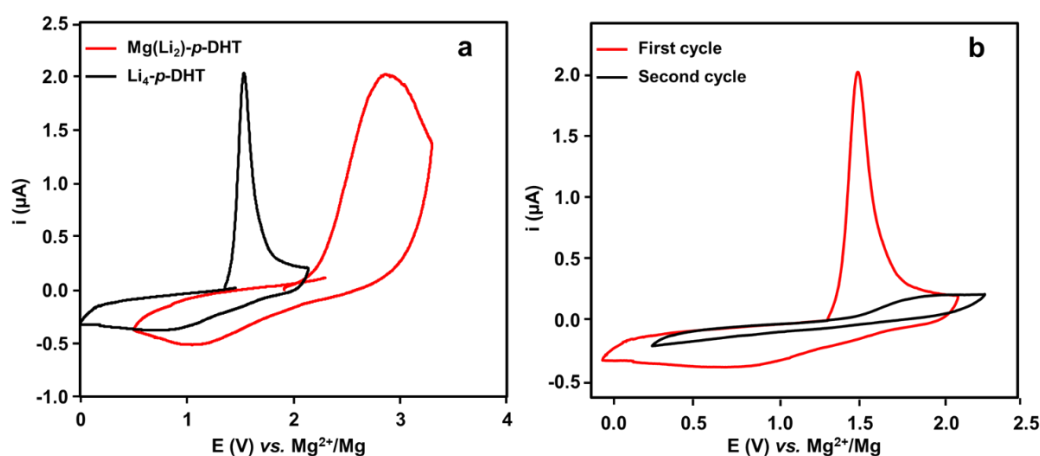
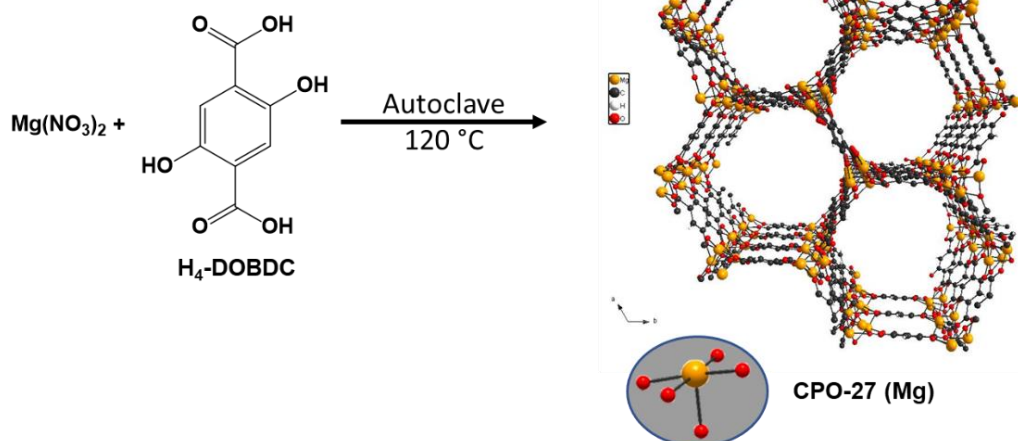


**Figure 4.5.** Cyclic voltammogram of (a)  $\text{Mg}(\text{Li}_2)\text{-}p\text{-DHT}$  and  $\text{Li}_4\text{-}p\text{-DHT}$  study during the first scan and (b)  $\text{Li}_4\text{-}p\text{-DHT}$  study during the first and second scans in the diglyme-based electrolyte at 1 mV/s and room temperature.

In another strategy, the metal-organic framework was applied as positive material for this study. MOF has also emerged as a class of complex organic-inorganic hybrid porous materials consisting of metal ion nodes and organic ligands, known as coordinating polymers.<sup>346–348</sup> Thanks to their high porosity and tunable structure, MOFs have been applied for many purposes including electrochemistry.<sup>349</sup> Although it was used in lithium batteries as sensors or wearable devices, the low electronic conductivity limits their utilization as electrode materials. Some of the modified MOFs were studied as an electrode for supercapacitors ( $\text{Ni}_3(\text{HITP})_2$ <sup>350,351</sup> and  $\text{Ni}/\text{Cu}\text{-HAB}$ ) and for lithium system (CPO-27).<sup>352</sup> CPO-27 (named also MOF-74) was synthesized the 2,5-dihydroxyterephthalic acid ( $\text{H}_4\text{-DOBDC}$ ).<sup>352,353</sup> The  $\text{H}_4\text{-DOBDC}$  is used as a ligand to link the metal clusters to construct an open channel for hexagons.<sup>352</sup> The CPO-27 metal ions are integrated by six O atoms, five of which are from  $\text{H}_4\text{-DOBDC}$  and the last one from the coordinated solvent molecule. For this work, cyclic voltammetry was used to test the electrochemical performance of CPO-27 in Mg electrolyte which was provided by our partner in the IMN laboratory during the postdoc position of Damien Bechu. CPO-27 (Mg) was obtained by the reaction between  $\text{H}_4\text{-DOBDC}$  and magnesium nitrate in an autoclave at 120 °C using MeOH as solvent follow **Scheme 4.2**. The solvent was removed at 180 °C overnight and increased the temperature to 250 °C for 2 hours before using it as an active material.



**Scheme 4.2.** CPO-27 (Mg) preparation from magnesium nitrate and H<sub>4</sub>-DOBDC.

0.5 M Mg(TFSI)<sub>2</sub> in diglyme was prepared and applied as an electrolyte, with Mg foil as counter and the reference electrodes. Active material was mixed with 30 wt% of carbon super P to improve the conductivity of the electrode. The experiment was conducted in the glovebox using a microcavity electrode at room temperature. First, the system was let to run at 1 mV/s as previous tests for terephthalate compounds in the potential window 2.5 – 3.2 V vs. Mg<sup>2+</sup>/Mg.

As seen in **Figure 4.6a**, it could be observed a reversible oxidation/reduction of CPO-27 at around 2.9 V vs. Mg<sup>2+</sup>/Mg. The electrochemical reaction presents several peaks in both oxidation and reduction processes, which can be associated with several oxidation sites. Even if the amount of product introduced in the cavity cannot quantify the current obtained is low compared to the other experiments using the same cavity. The current decreases cycle by cycle and only near 50% of the current density remains after 8 cycles. At 5 mV/s, the redox response is simpler with only one peak in oxidation and reduction, with  $E_{1/2} = 2.8\text{ V vs. Mg}^{2+}/\text{Mg}$  (**Figure 4.6b**). Whatever the scan rate, the shape of the curve is the same and more coherent with a surface response of the active material with a deactivation with time as a redox response of the bulk. The CPO-27 seems to be not adapted as an active material for Mg cell.

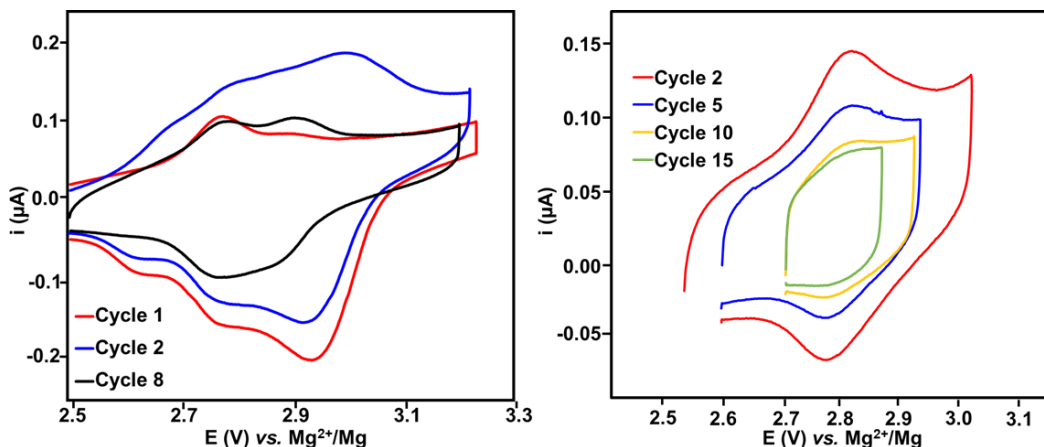


**Figure 4.6.** (a) Cyclic voltammogram of CPO-27 study in 0.5 M  $\text{Mg}(\text{TFSI})_2$  in diglyme as electrolyte and Mg as reference and counter electrodes at room temperature, 1 mV/s in different cycles, and (b) at 5 mV/s in different cycles.

#### 4.4. Conclusion

The reversible of the terephthalate salts is only observed from the study on Li batteries in diglyme and sulfolane-based electrolytes. Although the capacity after 30 cycles is significantly lower than the one obtained in the carbonate-based electrolyte with a capacity of 50 mAh/g in sulfolane based electrolyte with a good coulombic efficiency. However, on Mg battery, no reversibility is obtained with no  $\text{Mg}^{2+}$  insertion whatever the solvent used and even in the presence of  $\text{MgCl}_2$  in the electrolyte. It could be due to the incompatible between the active material and  $\text{Mg}^{2+}$  salt with the destruction of the crystal structure associated with the divalent character, the size of the solvated species, and/or a too strong interaction between oxygen and  $\text{Mg}^{2+}$ .

## **Chapter 5:**

### **Experimental: synthesis and characterizations**

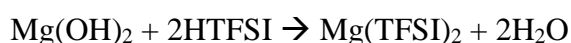
## 5.1. Synthesis

### 5.1.1. Solvent and chemicals preparation

Solvent commercially available was used as received for the synthesis part of the work. On the other hand, the solvent used for electrolyte preparation is distilled and stored under dried condition before using. To reduce the water content to a few ppm, molecular sieves (3 Å) dried at 300 °C for 3 days under vacuum and keep inside the glovebox was used. To achieve the water amount under 2 ppm, the “3 times/week” rule is applied for all of the solvents. Dried molecular sieves were added three times into the solvent. Each time, after two days of reaction, the molecular sieves were released. The dried solvent is then checked by Karl Fischer titration to confirm the quantity of water lower than 10 ppm.

Liquid phenol derivatives and thiophenol are purified by distillation, whereas solid derivatives and  $\pi$ -rich molecules are sublimated and stored under Ar in the glovebox.

Most of the salts using in the electrolytes are commercially available except  $\text{Mg}(\text{TFSI})_2$  which is synthesized by the neutralizing reaction between  $\text{Mg}(\text{OH})_2$  and acid bis(trifluoromethanesulfonyl)imide (HTFSI) at room temperature in aqueous solution:

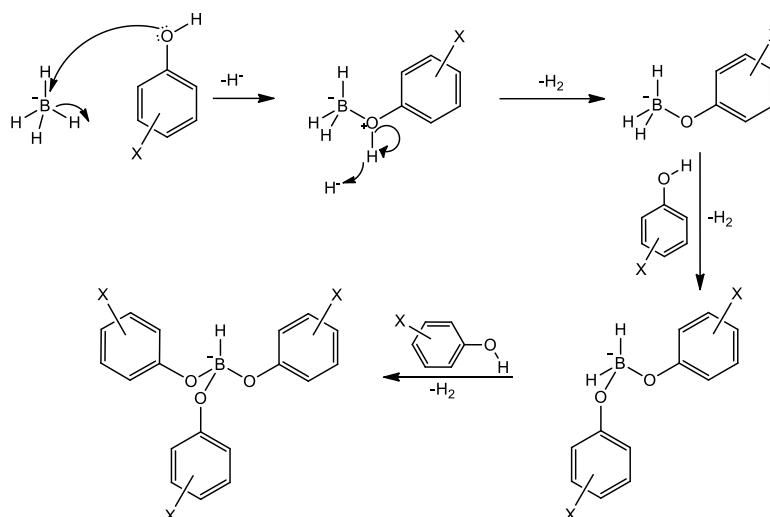


**Scheme 5.1.**  $\text{Mg}(\text{TFSI})_2$  synthesized process.

First, 0.1 M (5.832 g in 1.0 L, 0.10 mol)  $\text{Mg}(\text{OH})_2$  is solubilized in deionized water. The concentrate 80% HTFSI aqueous solution (41.4 mL, 0.21 mol) is added gradually until the pH value reached from 3 to 4. The solution is left to stir overnight before removing water by lyophilization. The crude salt is purified by its dissolution in dichloroethane at 60 °C for 2 days to eliminate HTFSI. Hot filter and clean again with solvent are performed before drying under vacuum at 150 °C for 3 days. The purified product with a high yield of 96% is stored in the glovebox.

### 5.1.2. Borohydride compounds

Several phenol derivatives are used including 2-methoxyphenol, 3-methoxyphenol, 4-methoxyphenol, sesamol, and thiophenol. The reactions between phenol derivatives and  $\text{LiBH}_4$  or  $\text{Mg}(\text{BH}_4)_2$  are performed at room temperature in ethereal solvents: DME, diglyme, PEGDME. The solution is stirred at 500 rpm for 3 hours inside the glovebox. The scheme following show the reaction and mechanism between  $\text{BH}_4^-$  and derivative phenol, several substitution steps depending on the derivatives and its concentration can occur.



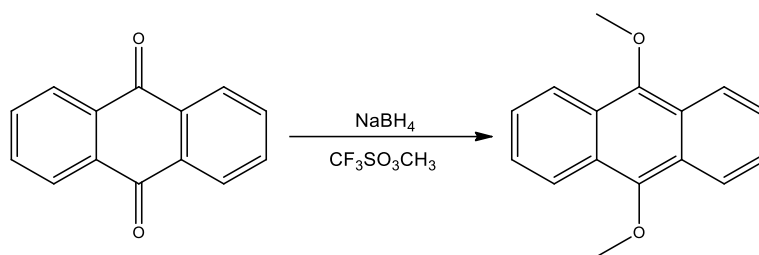
**Scheme 5.2.** The mechanism of derivative phenol and  $\text{BH}_4^-$ .

In the small vials, 2 mL of ethereal solvent is prepared with different  $\text{LiBH}_4$  concentration. Depending on the ratio of phenol derivative/ $\text{BH}_4$  required, several amounts of the phenol derivatives (thiophenol) are added under stirring at room temperature.

The soluble products are characterized by  $^1\text{H-NMR}$ . For some studies, to measure exactly the amount of the different compounds formed during the synthesis in the solvent used (no dilution performed for the analysis), an inner tube containing a reference solution is used. The reference solution is 0.5 M anhydrous tetraethylammonium tetrafluoroborate in  $\text{DMSO-d}_6$ . In NMR study, 0.3 mL of solution in NMR tube containing inner cylinder was prepared in glove box and sealed by parafilm before transferring outside for NMR checking. For the solution used as electrolyte, the reaction is scaled up to 10 mL, filtrated, and dried carefully with molecules sieves before the electrochemical characterization.

### 5.1.3. Alkoxyanthracene

To synthesize 9,10-dimethoxyanthracene (**Scheme 5.3**), 9,10-anthraquinone (1.33 g, 6.37 mmol) is diluted in ethanol (10 mL) and a solution of sodium hydroxide (3.06 g, 76 mmol) in water (20 mL) is added. The mixture is stirred for 15 min at room temperature before the addition of sodium borohydride (0.36 g, 9.58 mmol). After 30 min of stirring, methyl trifluoromethanesulfonate (8.4 mL, 76 mmol) is added and the solution keeps under stirring overnight. The reaction is followed by thin-layer chromatography (TLC) in silica gel using 1% acetone in pentane as eluent solvent. At the end of the reaction, the solution is diluted with water (30 mL) and extracts with dichloromethane (3 x 30 mL). The organic phase is washed consecutively with water (2 x 30 mL). 1.1 g of pure product (72.27% of yield) is obtained.

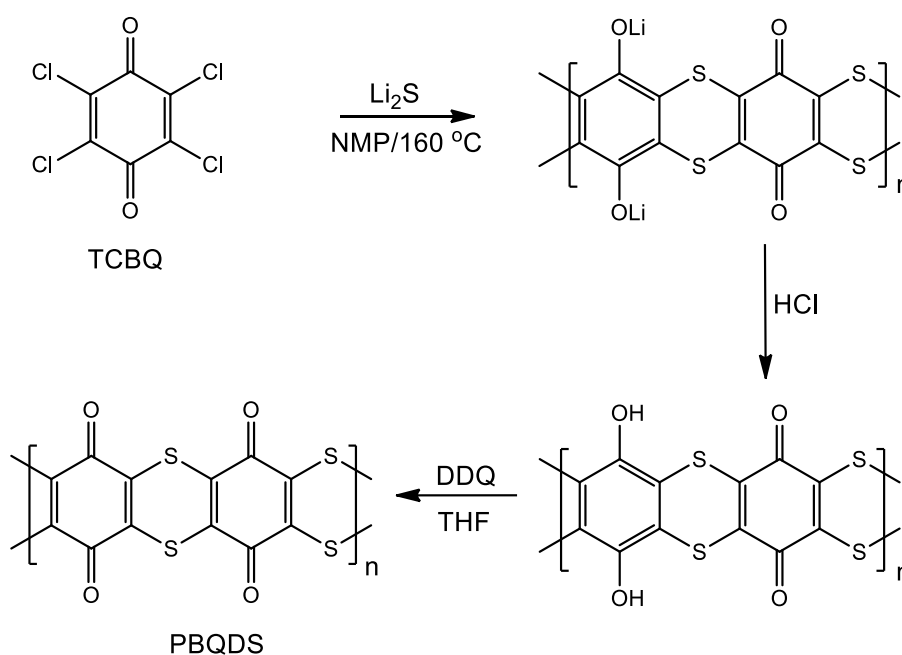


**Scheme 5.3.** 9,10-Dimethoxyanthracene preparation from anthraquinone.

To synthesis 9-methoxyanthracene the same protocol is used with anthrone (0.943 g, 4.85 mmol) instead of 9,10-anthraquinone and obtaining 57.4 mg of pure product (5% of yield). The yield is very weak due to the difficulty in the oxidation step from 9-methoxy-9,10-dihydroanthracene to 9-methoxyanthracene.

#### 5.1.4. Poly(benzonylquinonyldisulfide)

For the synthesis of poly(benzonylquinonyldisulfide) (PBQDS) (Scheme 4), tetrachlorobenzoquinone (TCBQ, 6.150 g, 0.025 mol) is first dissolved in 100 mL *N*-methyl-2-pyrrolidone (NMP) in the glovebox, then anhydrous  $\text{Li}_2\text{S}$  (Sigma-Aldrich 99.98%, 2.875 g, 0.0625 mol) is added into the solution. After 8 hours, the solution is moved out of the glovebox to be heated at 160 °C overnight under stirring in Ar flow. After cooling to room temperature, the mixture is transferred to 400 mL 0.1 M HCl solution for 48 hours to precipitate the product. The precipitate is filtrated with deionized water until the post-filtration waste is colorless.



**Scheme 5.4.** Synthesis of PBQDS from TCBQ.



For purification, the crude product is dissolved in 300 mL 0.1 M LiOH solution. After that, concentrated HCl is added drop by drop into the solution until pH at approximately 1. A large amount of precipitation is formed. The mixture is centrifugated at 5000 rpm for 10 minutes and washed with 0.1 M HCl several times and then washed with 0.1 M HCl in ethanol until the solution is near colorless. The poly(hydroxybenzoylquinonyldisulfide) (PHBQDS) product is dried at 80 °C under vacuum. The black powder is obtained with a high yield of over 95%.

To finish the reaction, the oxidation of the hydroquinone function of PHBQDS to quinone groups needs to be done in the last step. In a procedure, 2.0 g of PHBQDS is homogeneously dispersed in 200 mL anhydrous tetrahydrofuran (THF) in a sonication bath before added an excess of oxidation agent, 4.0 g of 2,3-dichloro-5,6-dicyano-1,4-benzoquinone (DDQ), this reaction occurs at room temperature for 2 days. The mixture is centrifugated at 5000 rpm for 10 minutes and clean with THF until the solution is nearly colorless. PBQDS is dried at 80 °C for 48 hours under vacuum then stored in the Ar glovebox. The final product is obtained with a yield of near 100%.

## **5.2. Characterizations**

### **5.2.1. Spectroscopy**

#### **5.2.1.1. Nuclear magnetic resonance (NMR)**

The NMR spectroscopy is conducted using a Bruker Avance III HD spectrometer for  $^1\text{H}$  at 400.15 MHz. The spectrums are handled with a TopSpin 3.2 program and the chemical shifts ( $\delta$ ) are displayed by parts per million (ppm) unit. In this analysis, the deuterated solvents applied were chloroform- $d_1$  ( $\delta\text{H} = 7.26$  ppm), DMSO- $d_6$  ( $\delta\text{H} = 2.50$  ppm), acetone- $d_6$  ( $\delta\text{H} = 2.04$  ppm), and acetonitrile- $d_3$  ( $\delta\text{H} = 1.94$  ppm). The multiplicity peaks are presented as: s = singlet, d = doublet, t = triplet, m = multiplets.

#### **5.2.1.2. Infrared spectroscopy**

FT-IR measurements are performed with an IR spectrometer (BRUKER, VERTEX 70V). The samples are examined in absorbance from 4000 to 600  $\text{cm}^{-1}$ . The IR spectrums are promoted with 64 accumulations and a resolution of 2  $\text{cm}^{-1}$ . All of the agents, intermediate polymers and polymer products are analyzed in a solid cell with a KBr window and performed under  $\text{N}_2$  flow.

#### **5.2.1.3. Scanning Electron Microscopy (SEM) and elemental mapping with energy-dispersive X-ray spectroscopy (EDX)**

The morphology of the redox polymers is mainly characterized by scanning electronic microscopy (SEM). SEM measurements are carried out using an Ultra 55 (Zeiss) microscope with a voltage of 5 kV and a SE detector. ImageJ is used for post-treatment and analysis of the collected image. All the compounds are deposited on a carbon conductive scotch and analyzed generally without any other preparations. Mapping EDX analysis is performed on the different polymers to identify the elements presented and the homogeneity of the samples on the same instrument with an SDD detector (BRUKER AXS-30 mm<sup>2</sup>).

#### **5.2.1.4. Atomic absorption spectroscopy (AAS)**

Atomic absorption spectroscopy (AAS) measurement is applied to determine the chemical elements using the absorption of optical radiation by free atoms in the gaseous state. AAS is carried out using an AAS PinAAcle 900F PerkinElmer instrument. The product analyzed is dissolved in concentrated HNO<sub>3</sub> before the experiment.

### **5.2.2. Physical properties**

#### **5.2.2.1. Thermogravimetric analysis (TGA)**

The thermogravimetric measurement is a thermal analysis technique in which the sample weight is measured overtime during an isotherm or a temperature ramp. It is carried out using the TGA 1 STARe instrument of METTLER TOLEDO. Data is treated by a STARe software version 12.20. The measurements are performed under air flux at 50 mL/min. The temperature increased from 25 °C up to 1000 °C with a heating rate of 10 ° per minute. 10 – 15 mg of dry samples are put into the TGA sample carrier.

#### **5.2.2.2. Brunauer-Emmett-Teller (BET)**

BET technique is a method to analyze the specific surface area of material based on the physical absorption of gas molecules on a solid surface. In this measurement, the BET instrument using Belsorp-Max (BEL JAPAN) is applied to examine the surface area of the redox polymers synthesized under N<sub>2</sub> liquid after the degassing of the sample at 80 °C under vacuum during one day.

#### **5.2.2.3. Granulometry**

Granulometric analysis methods permit to determine the size distribution of particles in suspension in a solvent. In this thesis, the granulometry instrument MALVERN-Mastersizer 3000 is used to determine the polymer particle sizes dispersed in ethanol under the mechanical ball-milling of the particles.

### 5.2.3. Mechanical milling

The ball-milling technique is used to reduce the particle size of materials. The result of the mechanical process can be affected by many factors including ball and container materials, grinding time and speed, the solvent used, number of ball or temperature, etc. For our polymers, to prevent the contamination of the polymer with conductive species, zirconium oxide was used as container material.

In the aim of the work, different conditions such as time grinding, milling speed (rpm), rest time are applied for pristine PBQDS. The detailed conditions are summarized in **Table 5.1**.

**Table 5.1.** Milling conditions applied for PBQDS.

<b>Grinding speed (rpm)</b>	219	550
<b>Grinding time (minutes)</b>	3, 10, 20, 40, 60, 90	5, 10, 15, 20, 30, 45, 60
<b>Rest time</b>	10' after each milling stint	
<b>Solvent</b>	Ethanol	
<b>Temperature</b>	Room temperature	
<b>Milling container and balls</b>	Zirconium oxide (Zr <sub>2</sub> O) and Ø5 mm balls	
<b>Ratio of balls/material/solvent</b>	1/1/1 by volume	

The particle size of the pristine material and each sample is determined by granulometric and the chemical structure are checked by Raman spectroscopy.

### 5.2.4. Electrochemical characterization

#### 5.2.4.1. Cyclic voltammetry

Cyclic voltammetry (CV) is a potentiodynamic method commonly used in battery research to check the electrolyte voltage window (i.e. potential window in which they are not degraded) but also for a qualitative examination of the electrochemical activity of the active materials. The CV technique is carried out by a VMP3 potentiostat from Biologic. A 3-electrode configuration is used with a platinum electrode (cavity electrode diameter 100 µm for polymer investigation, 2 mm electrode for soluble product study) as a working electrode. The counter and reference electrodes are Mg or Li foil in a protected cell containing electrolyte. Mg electrode was prepared from Mg disk foil (99.9%, 0.25 mm, Goodfellow) after polishing by an abrasive grinding paper from P180 to P2400 until the surface roughness on magnesium metal became completely smooth. The potential of the Mg reference electrode was checked after each experiment by ferrocene/ferrocenium redox couple.

For Cyclic Voltammetry tests performed on the active material, the samples were prepared by mixing 70% active material and 30% carbon black (SuperP®, 99%) in weight. The mixtures were ground with THF two times in the glovebox, after that the solvent was evaporated. Cavity microelectrode offers a good tool to study those compounds which are not soluble in the electrolyte. This method helps to reduce the study time while no battery or cell assembling is needed with only a few hundred nanograms of electroactive materials used. However, the main disadvantage was the non-know quantity of material put inside the cavity, so no quantitative measurement can be performed.

The different solvents used are dried three times using molecular sieves for one week. All of the electrolytes are obtained using the same protocol with two steps. First, 0.5 M Mg(TFSI)<sub>2</sub> in PEGDME or diglyme was prepared and dried with molecules sieves 3 Å until containing water content lower than 2 ppm.

Ferrocene/ferrocenium couple is also used as an internal reference to correct the potential shift of the Mg electrode noticed in some of the solvents used.

#### **5.2.4.2. Galvanostatic Cycling with Potential Limitation**

Batteries cycling is tested by using Galvanostatic Cycling with Potentiostat Limitation (GCPL) (VMP3 potentiostat – Biologic). The voltage variation by time is measured with a constant current density set up. The current rate is designated by the C/x value where x indicates the theoretical number of hour need for the complete reaction. Different currents were applied to test the cell performances at various C-rates, which are specified for each experiment in this manuscript. Cell capacities and thus the current values were calculated, based on the theoretical specific capacity of active material and the amount of active material in each electrode. In this thesis, GCPL tests are operated at different temperatures: 25, 40, and 60 °C depending on the electrolyte used and to determine the impact of temperature on the electrochemical mechanism. Coulombic efficiency was determined as a capacity ratio (n+1) discharge/(n) charge.

#### **5.2.4.3. Galvanostatic Intermittent Titration Technique**

To calculate the thermodynamic potential of a reaction, the device must be relaxed and the potential measured at equilibrium, extending the circuit for a while. A current is applied to the cell in a Galvanostatic Intermittent Titration Technique (GITT) for a defined short time (Closed Circuit Voltage, CCV), accompanied by a long time of open-circuit voltage (OCV). This process is replicated before complete insertion/de-insertion of the cation is achieved. Through

observing the time taken to hit the plateaus in OCV and also the structure of the curve during these times, it is possible to gather information on the kinetics of the electrochemical reactions.

### **5.3. Battery preparation**

#### **5.3.1. Electrolytes preparation**

##### **5.3.1.1. Electrolyte containing hydroborate compound**

The different solvents used are dried using molecular sieves, three times, the complete protocol lasts one week. All of the electrolytes are obtained using the same protocol with two steps. First, 0.5 M Mg(TFSI)<sub>2</sub> in PEGDME or diglyme is prepared and dried with molecules sieves 3 Å until containing water content lower than 2 ppm. The second salt or its compounds, is added and stirred at 500 rpm for 2 hours at room temperature and dried again with molecules sieves for 2 days. In the case of PEGDME, due to its high viscosity, the drying step is performed at 70 °C. The solution is filtrated and used for electrochemical investigation.

##### **5.3.1.2. Electrolyte containing $\pi$ -rich compounds**

To prepare such electrolytes, the electrolyte (0.5 M Mg(TFSI)<sub>2</sub> in diglyme) is prepared with the protocol introduced in the last section. Commercial or synthesized additives are sublimated for purification before being added into the electrolyte. To dissolve all of the additives, the solution is stirred for 30 minutes before using it. Because the quantity of additive is small, these electrolytes are used directly without a second drying process for electrochemical measurements.

#### **5.3.2. CV on microcavity electrode**

The CV on cavity electrode tests performed on the active material, the sample is prepared by mixing 70% active material and 30% carbon black (Super P Conductive, 99%) in weight. The mixture is ground with THF as a solvent in the glovebox two times, the solvent is completely evaporated. A cavity microelectrode with a small hole (**Figure 5.1**) offers a powerful tool for the study of powder compound which is not soluble in the electrolyte. This method helps to reduce the study time while no battery or cell assembling is needed with only a few hundred nanograms of electroactive materials used.<sup>354</sup> It seems the easiest way to investigate the cyclability of battery materials at low cost and on a short-time scale. However, few disadvantages have remained during applying, such as the non-identified quantity of material inside the cavity or difficulty in the insertion task.

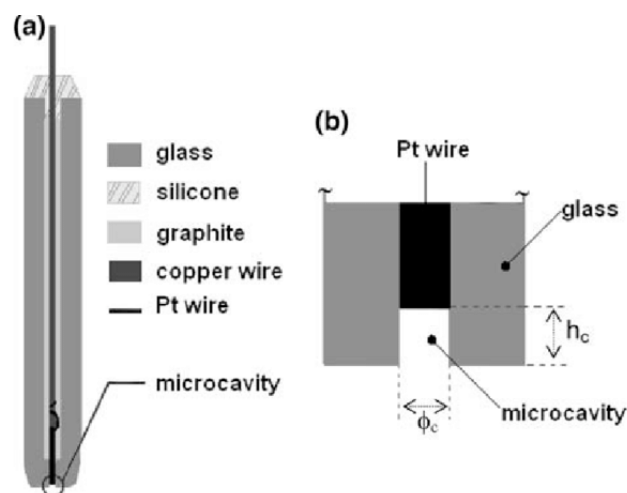


**Figure 5.1.** Cavity microelectrode composition and the zoom of cavity hole.<sup>355</sup>

In our work, a small amount of the active material mixture is placed inside a small vial 2 mL. The cavity microelectrode is then pressed strongly perpendicular to the vial bottom for at least 10 times. After that, the electrochemical measurements are performed. To clean the microelectrode cavity after using, 100 oxidation/reduction cycles of an 0.1 M HClO<sub>4</sub> aqueous solution is performed. Following this step, the electrode is cleaned in pure water, ethanol, and then acetonitrile before drying at 60 °C under vacuum.

### 5.3.3. Ink and cathode preparation

The procedure for the electrode preparation, the active material is mixed with carbon black and polyvinylidene difluoride (PVdF, Solef 5130, Solvay 12 wt.% in NMP Alfa Aesar) as the binder in the ratio 60:30:10. To prepare active material/carbon mixtures, precise amounts of active material and carbon powders are simply ground together in an agate mortar for ~ 15 minutes, with the addition of few drops of cyclohexane (Aldrich, anhydrous, 99.5 %). To finish the ink preparation, the polymeric binder was added into the mixture. An additional volume of NMP was also incorporated to obtain an optimal viscosity of the ink to facilitate the electrode coating. Afterward, the ink is casted onto a current collector in aluminum then dried at 60 °C overnight and kept 1 hour more under vacuum at 80 °C. Later, the electrode is cut at the desired diameter, weighted to collect the mass, and dried again under vacuum at 80 °C for at least 2 hours before stored in the glovebox.

### 5.3.4. Cell assembling

In this thesis, most electrochemical tests are performed using a Swagelok cell. It can be two-electrode or three-electrode type containing a reference electrode as shown in **Figure 5.2**. The

positive electrode disk ( $\text{\O} 8 \text{ mm}$ ) was placed on one of thick stainless steel spacer and covered with one layer of celgard® 3401 - a  $25 \text{ }\mu\text{m}$  thick polypropylene microporous layer (both  $\text{\O} 9 \text{ mm}$  or  $12 \text{ mm}$ ) and Whatman® 1823-070 grade GF/D. Liquid electrolyte is then poured onto the separators, filling all their pores, as well as the pores of the positive electrode. Metallic lithium or magnesium are used as counter electrodes (and reference electrodes for Mg). A disk of Li or Mg ( $\text{\O} 8 \text{ mm}$ ,  $10 \text{ mm}$ ) was punched, placed on the soaked separators, and covered with a thick stainless-steel spacer ( $\text{\O} 9 \text{ mm}$ ,  $12 \text{ mm}$ ). The Mg electrode (Goodfellow) is carefully polished before every use. Several polishing discs are used with several grinding sizes 180, 600, 1200, and 2400.

All the processes are carried out in the glovebox and put in a plastic bag before taking it out. Electrochemical investigations are performed in VMP3 potentiostat – Biologic as discussed in the prior section.

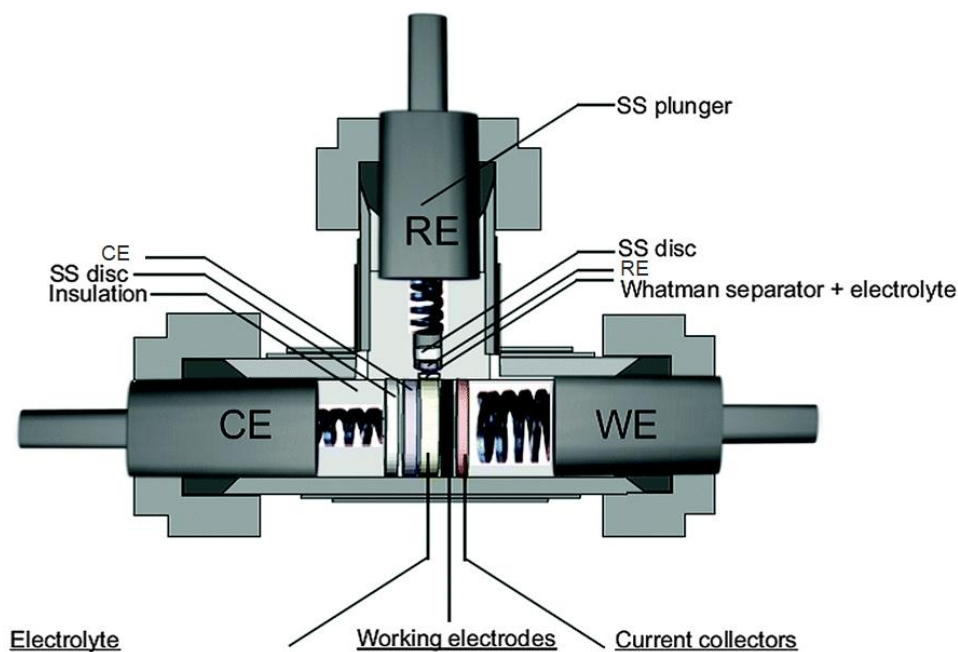


**Figure 5.2.** Three-electrode Swagelok cell and all the components inside.

## **General Conclusion and Perspectives**



The main objectives of this work are to establish a sustainable, efficient magnesium electrolyte and organic-positive-electrode for Magnesium battery. To this end, the work was divided into two main parts, the first one was dedicated to the synthesis and characterisation of borohydride salts and  $\pi$ -rich additives, and the second one to the development of new organic positive electrodes. In the part of electrolyte development, although electrochemical performances are not improved compare to the prior studies using triphenylborohydride as salt and anthracene as  $\pi$ -rich molecule, it gives us the overall point of view in the preparation of borohydride salts containing phenol or thiophenol derivatives.

We were thus able to demonstrate the significant influence of the substituent on phenol derivatives and the use of thiophenol on their reactivity versus  $\text{BH}_4^-$ , with the formation of precipitations or slow kinetics inducing a difficult to control the reaction. The use of substituted phenol did not increase the solubility of the salts obtained, on the contrary, rapid precipitation occurs. Even if obtaining, with the use of thiophenol, borohydride salts which unquestionably increase the reversibility of the Mg plating/stripping, the difficult control of the reaction induces the presence, in the electrolyte, of undesired products preventing the expected results in a complete Mg/Mo<sub>6</sub>S<sub>8</sub> cell.

The evaluation of several  $\pi$ -rich molecules as additive helps us to go deeper into the role and mechanism involved with this family of additives. Crucially, the substitution in positions 9 and 10 of anthracene seems to prevent the formation of a stable magnesocene complex involving as intermediate in the Mg plating/stripping. Thus, the results obtained, even if some efficiency to improve the Mg plating/stripping process can be noticed, are worse than the ones obtained with anthracene. In the other place, the introduction of methyl in the position 2 of anthracene, with the use of 2-(*tert*-butyl)anthracene, permits to obtain the highest coulombic efficiency with a value equal to 80% during a cyclic voltammetry test before at 100 mV/s, however, the performances obtained at low C-rate are worse than the ones obtained with anthracene, which can be associated with some steric hindrance with the use of a bulk substituent. In conclusion, the protons in position 9,10 are primordial for the activity of  $\pi$ -rich molecules as an intermediate in the plating/stripping process. The introduction of functional groups, in order to improve the solubility or the reactivity of this family of additives, can be done but not in these positions. The  $\pi$ -rich molecules are efficient on the Mg plating/stripping process but are not able to depassivate the Mg foil electrode. Thus, these additives cannot be used alone, and a more complex electrolyte formulation has to be developed, for example, the introduction of chloride-based compounds.

In the study of the organic positive electrode, two approaches were investigated. The opportunity of using organic salt in Mg battery was investigated with the study of 2,5-dihydroxyterephthalic acid-based salt including Mg(Li<sub>2</sub>)-*p*-DHT, Li<sub>4</sub>-*p*-DHT, and CPO-27 (Mg). Although those materials are one of the promising compounds as active material in lithium batteries with stable capacity and high coulombic efficiency. There aren't suitable for magnesium one in many solvents used. No insertion of Mg<sup>2+</sup> can be obtained, this can be associated with the incompatible between the active material and Mg<sup>2+</sup> salt with the destruction of the crystal structure associated with the divalent character, the size of the solvated species, and/or a too strong interaction between oxygen and Mg<sup>2+</sup>. Other organic salts have to be designed with a structure that can be adapted to the size (in its solvating form) and the divalent character of Mg<sup>2+</sup>. This investigation is under progress by our partner in IMN Nantes and is part of the ANR, **MA**gnesium batteries with **I**nnovative electrolyte and efficient **O**rganic or **S**ulfur **C**athodes (MAIOSC) project.

The second strategy was to develop a redox polymer that can be used as an organic cathode. The polymer developed in this work, the poly(benzoquinonyldisulfide) (PBQDS), was prepared from green synthesis pathways via a 3 steps reaction from chloranil and lithium sulfide. The synthesized polymer allows obtaining a stable capacity of 140 mAh/g in lithium system. The impact of the particle size on the obtained capacity could clearly be highlighted, and the optimization of the grinding protocol should allow increasing the obtained capacity. In the Mg cell, even if the initial capacities are equivalent, a significant decrease in capacity is observed during cycling; this loss of capacity could be attributed to trapping of the Mg<sup>2+</sup> cation in the polymer structure. Different parameters have been studied to remedy this problem, the presence of crown ether as an additive seems to be the most efficient one. It seems important to counterbalance the oxidized quinone/Mg<sup>2+</sup> interaction by using solvating solvent. However, this strategy was limiting with PBQDS due to the solubility problem, the reduced form of PBQDS is soluble in glyme or in presence of solvating agent. The work carried out shows the difficulties in developing materials adapted to divalent cations, and even if organic materials can allow us to solve the problem of reversibility more easily than inorganic ones, the design of these must be considered, in terms of structure, function, and particle size. The solvent properties of the electrolyte are also a very important aspect, which can be modulated but without compromising the reversibility of the Mg electrode.

To improve the performance obtained in Mg cell, as in the lithium system or even more, the particle size has a main impact, the reduction of it can certainly improve the result obtained.

However, another important aspect it's the solubility problem, to mitigate it, the synthesis of PBQDS can be improved to increase the polymer molecular weight.

The high potential of the PBQDS and its solubility in glyme prevented the use of glyme + triphenylborohydride electrolytes, which present interesting properties vs the Mg plating/stripping whereas it is very important to develop a complete Mg/electrolyte/positive organic system. Nonetheless, it must be acknowledged that a commercial Mg battery cell would take a lot of research and time to achieve because there are still many challenges to be met.

## Reference

1. Klapp, J. *et al.* R. Energy for the Present and Future: A World Energy Overview. in *Towards a Cleaner Planet* 3–34 (Springer Berlin Heidelberg, 2007).
2. Max, M. D. & Johnson, A. H. Energy Overview: Energy Options and Prospects for Natural Gas. in *Exploration and Production of Oceanic Natural Gas Hydrate* 1–55 (Springer International Publishing, 2019).
3. Chen, G. Q. & Wu, X. F. Energy overview for globalized world economy: Source, supply chain and sink. *Renew. Sust. Energ. Rev.* **69**, 735–749 (2017).
4. Global primary energy consumption. <https://ourworldindata.org/grapher/global-primary-energy>.
5. Population Growth by Continent From 2000 to 2018. <https://www.tonymappedit.com/population-growth-by-continent-from-2000-to-2018/>.
6. Diffenbaugh, N. S. & Burke, M. Global warming has increased global economic inequality. *Proc Natl Acad Sci USA* **116**, 9808–9813 (2019).
7. Hughes, T. P. *et al.* Global warming impairs stock–recruitment dynamics of corals. *Nature* **568**, 387–390 (2019).
8. Each Country’s Share of CO<sub>2</sub> Emissions. <https://www.ucsusa.org/resources/each-countrys-share-co2-emissions>.
9. Dyatlov, S. A. *et al.* Prospects for Alternative Energy Sources in Global Energy Sector. *IOP Conf. Ser.: Earth Environ. Sci.* **434**, 012014 (2020).
10. Letcher, T. M. *Future energy: improved, sustainable and clean options for our planet*. (Elsevier, 2008).
11. Adua, L. *Alternative Energy: Political, Economic, and Social Feasibility*, by Christopher A. Simon, Lanham, MD: Rowman. *Rural Sociology* **73**, 684–686 (2008).
12. Goodenough, J. B. Rechargeable batteries: challenges old and new. *J Solid State Electrochem* **16**, 2019–2029 (2012).
13. Goodenough, J. B. & Kim, Y. Challenges for rechargeable batteries. *J. Power Sources* **196**, 6688–6694 (2011).
14. Linden, D. & Reddy, T. B. *Handbook of Batteries*. (McGraw-Hill, 2002).
15. TechNavio. *Global Rechargeable Battery Market 2018-2022*. (2018).
16. Yoo, H. D. *et al.* On the challenge of developing advanced technologies for electrochemical energy storage and conversion. *Materials Today* **17**, 110–121 (2014).
17. Armand, M. & Tarascon, J.-M. Building better batteries. *Nature* **451**, 652–657 (2008).
18. Cheong, J. L. *et al.* A high-performance slurry-coated polysulfide cathode for lithium–sulfur battery. *Nano Energy* **66**, 104114 (2019).

19. Rana, M. *et al.* Review on areal capacities and long-term cycling performances of lithium sulfur battery at high sulfur loading. *Energy Storage Mater.* **18**, 289–310 (2019).
20. Liu, K. *et al.* Stretchable Lithium Metal Anode with Improved Mechanical and Electrochemical Cycling Stability. *Joule* **2**, 1857–1865 (2018).
21. Braga, M. H. *et al.* Alternative strategy for a safe rechargeable battery. *Energy Environ. Sci.* **10**, 331–336 (2017).
22. Choi, J. W. & Aurbach, D. Promise and reality of post-LIBs with high energy densities. *Nat Rev Mater* **1**, 16013 (2016).
23. Shen, X. *et al.* Beyond lithium ion batteries: Higher energy density battery systems based on lithium metal anodes. *Energy Storage Mater.* **12**, 161–175 (2018).
24. Li, F. *et al.* Free-standing Sulfur-Polypyrrole Cathode in Conjunction with Polypyrrole-Coated Separator for Flexible Li-S Batteries. *Energy Storage Mater.* **13**, 312–322 (2018).
25. Placke, T. *et al.* Lithium ion, lithium metal, and alternative rechargeable battery technologies: the odyssey for high energy density. *J Solid State Electrochem* **21**, 1939–1964 (2017).
26. Zeta Potential Analysis of Lithium Ion Battery Electrolytes. <https://www.azom.com/article.aspx?ArticleID=14584>.
27. Yoshio, M. *et al.* *Lithium-ion batteries*. (Springer New York, 2009).
28. Moog, R. Lithium Battery Discussions - Electrode Materials. *Johnson Matthey Technology Review* **60**, 204–208 (2016).
29. Ellis, B. L. *et al.* Positive Electrode Materials for Li-ion and Li-Batteries. *Chem. Mater.* **22**, 691–714 (2010).
30. Schipper, F. *et al.* Study of Cathode Materials for LIBs: Recent Progress and New Challenges. *Inorganics* **5**, 32 (2017).
31. Xin, F. *et al.* Li–Nb–O Coating/Substitution Enhances the Electrochemical Performance of the  $\text{LiNi}_{0.8}\text{Mn}_{0.1}\text{Co}_{0.1}\text{O}_2$  (NMC 811) Cathode. *ACS Appl. Mater. Interfaces* **11**, 34889–34894 (2019).
32. Du, Z. *et al.* Three-dimensional conductive network formed by carbon nanotubes in aqueous processed NMC electrode. *Electrochim. Acta* **270**, 54–61 (2018).
33. Petibon, R. *et al.* The use of ethyl acetate as a sole solvent in highly concentrated electrolyte for LIBs. *Electrochim. Acta* **154**, 287–293 (2015).
34. Croy, J. R. *et al.* Review of the U.S. Department of Energy’s “Deep Dive” Effort to Understand Voltage Fade in Li- and Mn-Rich Cathodes. *Acc. Chem. Res.* **48**, 2813–2821 (2015).

35. Grimaud, A. *et al.* Anionic redox processes for electrochemical devices. *Nature Mater* **15**, 121–126 (2016).
36. Yabuuchi, N. *et al.* High-capacity electrode materials for rechargeable lithium batteries: Li<sub>3</sub>NbO<sub>4</sub>-based system with cation-disordered rocksalt structure. *Proc Natl Acad Sci USA* **112**, 7650–7655 (2015).
37. Zhao, L. *et al.* Significantly stable organic cathode for Li-ion battery based on nanoconfined poly(anthraquinonylsulfide)@MOF-derived microporous carbon. *Electrochim. Acta* **335**, 135681 (2020).
38. Mumyatov, A. V. *et al.* New Naphthalene-Based Polyimide as an Environment-Friendly Organic Cathode Material for Lithium Batteries. *Energy Technol.* **7**, 1801016 (2019).
39. Kim, D.-M. *et al.* Cointercalation of Mg<sup>2+</sup> Ions into Graphite for Magnesium-Ion Batteries. *Chem. Mater.* **30**, 3199–3203 (2018).
40. Chen, X. *et al.* An overview of LIBs for electric vehicles. in *2012 10<sup>th</sup> International Power & Energy Conference (IPEC)* 230–235 (IEEE, 2012).
41. Shukla, A. K. & Kumar, T. P. Materials for next generation lithium batteries. *Current Science* **94**, 314–332 (2008).
42. Li, W. *et al.* Li<sup>+</sup> ion conductivity and diffusion mechanism in  $\alpha$ -Li<sub>3</sub>N and  $\beta$ -Li<sub>3</sub>N. *Energy Environ. Sci.* **3**, 1524 (2010).
43. Gregory, D. H. Lithium nitrides as sustainable energy materials. *Chem. Record* **8**, 229–239 (2008).
44. Pimenta, M. A. *et al.* Ionic conductivity in LiK<sub>0.9</sub>Na<sub>0.1</sub>SO<sub>4</sub> single crystals. *Solid State Communications*, **82**, 755–757 (1992).
45. Lee, H.-Y. & Lee, S.-M. Carbon-coated nano-Si dispersed oxides/graphite composites as anode material for lithium ion batteries. *Electrochem. commun.* **6**, 465–469 (2004).
46. Yoshio, M., Tsumura, T. & Dimov, N. Silicon/graphite composites as an anode material for lithium ion batteries. *J. Power Sources* **163**, 215–218 (2006).
47. Bhatt, M. D. & Lee, J. Y. High capacity conversion anodes in Li-ion batteries: A review. *Int. J. Hydrog. Energy* **44**, 10852–10905 (2019).
48. Besenhard, J. O. & Winter, M. Advances in Battery Technology: Rechargeable Magnesium Batteries and Novel Negative-Electrode Materials for Lithium Ion Batteries. *ChemPhysChem* **5**, 155-159 (2002).
49. Canepa, P. *et al.* Odyssey of Multivalent Cathode Materials: Open Questions and Future Challenges. *Chem. Rev.* **117**, 4287–4341 (2017).

50. Bruce, P. G. *et al.* Li–O<sub>2</sub> and Li–S batteries with high energy storage. *Nature Mater* **11**, 19–29 (2012).
51. Manthiram, A. *et al.* Rechargeable Lithium–Sulfur Batteries. *Chem. Rev.* **114**, 11751–11787 (2014).
52. Read, J. A. *et al.* Dual-graphite chemistry enabled by a high voltage electrolyte. *Energy Environ. Sci.* **7**, 617–620 (2014).
53. Yabuuchi, N. *et al.* Research Development on Sodium-Ion Batteries. *Chem. Rev.* **114**, 11636–11682 (2014).
54. Ponrouch, A. *et al.* Towards a calcium-based rechargeable battery. *Nature Mater* **15**, 169–172 (2016).
55. Aurbach, D. *et al.* Nonaqueous magnesium electrochemistry and its application in secondary batteries. *Chem. Record* **3**, 61–73 (2003).
56. Klein, F. *et al.* Conversion reactions for sodium-ion batteries. *Phys. Chem. Chem. Phys.* **15**, 15876 (2013).
57. Hu, Y.-S. Batteries: Getting solid. *Nat Energy* **1**, 16042 (2016).
58. Weber, A. Z. *et al.* Redox flow batteries: a review. *J Appl Electrochem* **41**, 1137–1164 (2011).
59. World Battery Production. <https://energycentral.com/c/ec/world-battery-production>.
60. Bucur, C. B. *et al.* Why Grignard’s Century Old Nobel Prize Should Spark Your Curiosity. in *Rechargeable Batteries* 611–635 (Springer International Publishing, 2015).
61. Selis, S. M. *et al.* A High-Rate, High-Energy Thermal Battery System. *J. Electrochem. Soc.* **111**, 6 (1964).
62. Aurbach, D. *et al.* The Electrochemical Behavior of Calcium Electrodes in a Few Organic Electrolytes. *J. Electrochem. Soc.* **138**, 3536–3545 (1991).
63. Staniewicz, R. J. A Study of the Calcium-Thionyl Chloride Electrochemical System. *J. Electrochem. Soc.* **127**, 782–789 (1980).
64. Meitav, A. & Peled, E. SEI (SEI) electrode-V. the formation and properties of the SEI on calcium in thionyl chloride solutions. *Electrochim. Acta* **33**, 1111–1121 (1988).
65. Rong, Z. *et al.* Materials Design Rules for Multivalent Ion Mobility in Intercalation Structures. *Chem. Mater.* **27**, 6016–6021 (2015).
66. Ponrouch, A. *et al.* Assessing Si-based anodes for Ca-ion batteries: Electrochemical decalciation of CaSi<sub>2</sub>. *Electrochem. commun.* **66**, 75–78 (2016).
67. Wang, D. *et al.* Plating and stripping calcium in an organic electrolyte. *Nature Mater* **17**, 16–20 (2018).



68. Shyamsunder, A. *et al.* Reversible Calcium Plating and Stripping at Room Temperature Using a Borate Salt. *ACS Energy Lett.* **4**, 2271–2276 (2019).
69. See, K. A. *et al.* A High Capacity Calcium Primary Cell Based on the Ca-S System. *Adv. Energy Mater.* **3**, 1056–1061 (2013).
70. Elia, G. A. *et al.* An Overview and Future Perspectives of Aluminum Batteries. *Adv. Mater.* **28**, 7564–7579 (2016).
71. Das, S. K. *et al.* Aluminium-ion batteries: developments and challenges. *J. Mater. Chem. A* **5**, 6347–6367 (2017).
72. Jayaprakash, N. *et al.* The rechargeable aluminum-ion battery. *Chem. Commun.* **47**, 12610 (2011).
73. Reed, L. D. & Menke, E. The Roles of V<sub>2</sub>O<sub>5</sub> and Stainless Steel in Rechargeable Al–Ion Batteries. *J. Electrochem. Soc.* **160**, A915–A917 (2013).
74. Lin, M.-C. *et al.* An ultrafast rechargeable aluminium-ion battery. *Nature* **520**, 324–328 (2015).
75. Elia, G. A. *et al.* An Aluminum/Graphite Battery with Ultra-High Rate Capability. *Batteries & Supercaps* batt.201800114 (2018).
76. Bitenc, J. *et al.* Anthraquinone-Based Polymer as Cathode in Rechargeable Magnesium Batteries. *ChemSusChem* **8**, 4128–4132 (2015).
77. Kim, D. J. *et al.* Rechargeable aluminium organic batteries. *Nat Energy* **4**, 51–59 (2019).
78. Mordike, B. L. & Ebert, T. Magnesium Properties – applications – potential. *Mater. Sci. Eng. A* **9**, 37–45 (2001).
79. Fichtner, M. Motivation for a Magnesium Battery. in *Magnesium Battery* 1–16 (Royal Society of Chemistry, 2020).
80. Muldoon, J. *et al.* Quest for Nonaqueous Multivalent Secondary Batteries: Magnesium and Beyond. *Chem. Rev.* **114**, 11683–11720 (2014).
81. Kim, H. *et al.* Metallic anodes for next generation secondary batteries. *Chem. Soc. Rev.* **42**, 9011 (2013).
82. Yoo, H. D. *et al.* Mg rechargeable batteries: an on-going challenge. *Energy Environ. Sci.* **6**, 2265 (2013).
83. Davidson, R. *et al.* Formation of Magnesium Dendrites during Electrodeposition. *ACS Energy Lett.* **4**, 375–376 (2019).
84. Balbuena, P. B. & Wang, Y. *Lithium-Ion Batteries - Solid-electrolyte Interphase*. (Imperial College Press, 2004).

85. Aurbach, D. *et al.* A short review on the comparison between Li battery systems and rechargeable magnesium battery technology. *J. Power Sources* **97–98**, 28–32 (2001).
86. Nist-Lund, C. A. *et al.* Improving halide-containing magnesium-ion electrolyte performance via sterically hindered alkoxide ligands. *J. Power Sources* **362**, 308–314 (2017).
87. Nelson, E. G. *et al.* A magnesium tetraphenylaluminate battery electrolyte exhibits a wide electrochemical potential window and reduces stainless steel corrosion. *J. Mater. Chem. A* **2**, 18194–18198 (2014).
88. Carter, T. J. *et al.* Boron Clusters as Highly Stable Magnesium-Battery Electrolytes. *Angew. Chem. Int. Ed.* **53**, 3173–3177 (2014).
89. Saha, P. *et al.* Rechargeable magnesium battery: Current status and key challenges for the future. *Progress in Materials Science* **66**, 1–86 (2014).
90. Crowe, A. J. *et al.* Kinetics of Magnesium Deposition and Stripping from Non-Aqueous Electrolytes. *J. Phys. Chem. C* **121**, 20613–20620 (2017).
91. Gregory, T. D. *et al.* Nonaqueous Electrochemistry of Magnesium. *J. Electrochem. Soc.* **137**, 6 (1990).
92. Liebenow, C. *et al.* The electrodeposition of magnesium using solutions of organomagnesium halides, amidomagnesium halides and magnesium organoborates. *Electrochem. commun.* **2**, 641–645 (2000).
93. Yu, X. & Manthiram, A. Performance Enhancement and Mechanistic Studies of Magnesium–Sulfur Cells with an Advanced Cathode Structure. *ACS Energy Lett.* **1**, 431–437 (2016).
94. Zhao-Karger, Z. *et al.* Performance Improvement of Magnesium Sulfur Batteries with Modified Non-Nucleophilic Electrolytes. *Adv. Energy Mater.* **5**, 1401155 (2015).
95. Kim, H. S. *et al.* Structure and compatibility of a magnesium electrolyte with a sulphur cathode. *Nat Commun* **2**, 427 (2011).
96. Zhao-Karger, Z. *et al.* Bisamide based non-nucleophilic electrolytes for rechargeable magnesium batteries. *RSC Adv.* **3**, 16330 (2013).
97. Liao, C. *et al.* The unexpected discovery of the  $\text{Mg}(\text{HMDS})_2/\text{MgCl}_2$  complex as a magnesium electrolyte for rechargeable magnesium batteries. *J. Mater. Chem. A* **3**, 6082–6087 (2015).
98. Merrill, L. C. & Schaefer, J. L. Conditioning-Free Electrolytes for Magnesium Batteries Using Sufone–Ether Mixtures with Increased Thermal Stability. *Chem. Mater.* **30**, 3971–3974 (2018).

99. Merrill, L. C. & Schaefer, J. L. Electrochemical Properties and Speciation in Mg(HMDS)<sub>2</sub>-Based Electrolytes for Magnesium Batteries as a Function of Ethereal Solvent Type and Temperature. *Langmuir* **33**, 9426–9433 (2017).
100. Mandai, T. *et al.* A key concept of utilization of both non-Grignard magnesium chloride and imide salts for rechargeable Mg battery electrolyte. *J. Mater. Chem. A*, 3152–3156 (2017).
101. Wang, F. *et al.* A novel electrolyte system without a Grignard reagent for rechargeable magnesium batteries. *Chem. Commun.* **48**, 10763 (2012).
102. Liao, C. *et al.* Highly soluble alkoxide magnesium salts for rechargeable magnesium batteries. *J. Mater. Chem. A* **2**, 581–584 (2014).
103. Kim, I.-T. *et al.* Effects of alkoxide addition on the electrochemical deposition and dissolution in triglyme-based solution dissolving magnesium bis(trifluoromethanesulfonyl)amide. *J. Power Sources* **278**, 340–343 (2015).
104. Xu, K. Nonaqueous Liquid Electrolytes for Lithium-Based Rechargeable Batteries. *ChemInform* **35**, (2004).
105. Pan, B. *et al.* Exploring Reliable Organic Cathode Materials for High-Performance Mg-Ion Batteries. (2016).
106. Viestfrid, Yu. *et al.* Microelectrode studies of reversible Mg deposition in THF solutions containing complexes of alkylaluminum chlorides and dialkylmagnesium. *J. Electroanal. Chem* **576**, 183–195 (2005).
107. Doe, R. E. *et al.* Novel, electrolyte solutions comprising fully inorganic salts with high anodic stability for rechargeable magnesium batteries. *Chem. Commun.* **50**, 243–245 (2014).
108. Liu, T. *et al.* A facile approach using MgCl<sub>2</sub> to formulate high performance Mg<sup>2+</sup> electrolytes for rechargeable Mg batteries. *J. Mater. Chem. A* **2**, 3430 (2014).
109. Luo, J. *et al.* Tertiary Mg/MgCl<sub>2</sub>/AlCl<sub>3</sub> Inorganic Mg<sup>2+</sup> Electrolytes with Unprecedented Electrochemical Performance for Reversible Mg Deposition. *ACS Energy Letters* 1197–1202 (2017).
110. Barile, C. J. *et al.* Electrolytic Conditioning of a Magnesium Aluminum Chloride Complex for Reversible Magnesium Deposition. *J. Phys. Chem. C* **118**, 27623–27630 (2014).
111. Barile, C. J. *et al.* Exploring Salt and Solvent Effects in Chloride-Based Electrolytes for Magnesium Electrodeposition and Dissolution. *J. Phys. Chem. C* **119**, 13524–13534 (2015).

112. Keyzer, E. N. *et al.* Mg(PF<sub>6</sub>)<sub>2</sub>-Based Electrolyte Systems: Understanding Electrolyte–Electrode Interactions for the Development of Mg-Ion Batteries. *J. Am. Chem. Soc.* **138**, 8682–8685 (2016).
113. Lu, Z. *et al.* On the electrochemical behavior of magnesium electrodes in polar aprotic electrolyte solutions. *J. Electroanal. Chem* **466**, 203–217 (1999).
114. Shterenberg, I. *et al.* Hexafluorophosphate-Based Solutions for Mg Batteries and the Importance of Chlorides. *Langmuir* **33**, 9472–9478 (2017).
115. Dong, H. *et al.* Directing Mg-Storage Chemistry in Organic Polymers toward High-Energy Mg Batteries. *Joule* **3**, 782–793 (2019).
116. Mohtadi, R. *et al.* Magnesium Borohydride: From Hydrogen Storage to Magnesium Battery. *Angew. Chem.* **124**, 9918–9921 (2012).
117. Tutusaus, O. *et al.* An Efficient Halogen-Free Electrolyte for Use in Rechargeable Magnesium Batteries. *Angew. Chem. Int. Ed.* 7900–7904 (2015).
118. Zhang, Z. *et al.* Novel Design Concepts of Efficient Mg-Ion Electrolytes toward High-Performance Magnesium-Selenium and Magnesium-Sulfur Batteries. *Adv. Energy Mater.* **7**, 1602055 (2017).
119. Shterenberg, I. *et al.* The challenge of developing rechargeable magnesium batteries. *MRS Bull.* **39**, 453–460 (2014).
120. Ha, S.-Y. *et al.* Magnesium(II) Bis(trifluoromethane sulfonyl)imide-Based Electrolytes with Wide Electrochemical Windows for Rechargeable Magnesium Batteries. *ACS Appl. Mater. Interfaces* **6**, 4063–4073 (2014).
121. Hebié, S. *et al.* Electrolyte Based on Easily Synthesized, Low Cost Triphenolate–Borohydride Salt for High Performance Mg(TFSI)<sub>2</sub>-Glyme Rechargeable Magnesium Batteries. *ACS Appl. Mater. Interfaces* 28377–28385 (2017).
122. Hebié, S. *et al.* Magnesium Anthracene System-Based Electrolyte as a Promoter of High Electrochemical Performance Rechargeable Magnesium Batteries. *ACS Appl. Mater. Interfaces* **10**, 5527–5533 (2018).
123. Singh, N. *et al.* Achieving High Cycling Rates via In Situ Generation of Active Nanocomposite Metal Anodes. *ACS Appl. Energy Mater.* **1**, 4651–4661 (2018).
124. Arthur, T. S. *et al.* Interfacial Insight from Operando XAS/TEM for Magnesium Metal Deposition with Borohydride Electrolytes. *Chem. Mater.* **29**, 7183–7188 (2017).
125. Nakayama, Y. *et al.* Zinc Blende Magnesium Sulfide in Rechargeable Magnesium-Sulfur Batteries. *Chem. Mater.* **30**, 6318–6324 (2018).

126. Ma, Z. *et al.* Mg Cathode Materials and Electrolytes for Rechargeable Mg Batteries: A Review. *Batteries & Supercaps* **2**, 115–127 (2019).
127. Cheek, G. T. *et al.* Studies on the Electrodeposition of Magnesium in Ionic Liquids. *J. Electrochem. Soc.* **155**, D91 (2008).
128. Yoshimoto, N. *et al.* Mixed electrolyte consisting of ethylmagnesiumbromide with ionic liquid for rechargeable magnesium electrode. *J. Power Sources* **195**, 2096–2098 (2010).
129. Terada, S. *et al.* Thermal and Electrochemical Stability of Tetraglyme–Magnesium Bis(trifluoromethanesulfonyl)amide Complex: Electric Field Effect of Divalent Cation on Solvate Stability. *J. Phys. Chem. C* **120**, 1353–1365 (2016).
130. Girish, G. & Munichandraiah, N. Reversibility of Mg/Mg<sup>2+</sup> couple in a gel polymer electrolyte. *Electrochim. Acta* **44**, 2663–2666 (1999).
131. Bakker, A. *et al.* Contact ion pair formation and ether oxygen coordination on the polymer electrolytes M[N(CF<sub>3</sub>SO<sub>2</sub>)<sub>2</sub>]<sub>2</sub>PEO<sub>n</sub> for M = Mg, Ca, Sr and Ba. *Polymer* 4371–4378 (1995).
132. Ramalingaiah, S. *et al.* Conductivity and discharge characteristic studies of novel polymer electrolyte based on PEO complexed with Mg(NO<sub>3</sub>)<sub>2</sub> salt. *Mater. Lett* **29**, 285–289 (1996).
133. Polu, A. R. & Kumar, R. Preparation and characterization of pva based solid polymer electrolytes for electrochemical cell applications. *Chin J Polym Sci* **31**, 641–648 (2013).
134. Ab Aziz, A. & Tominaga, Y. Magnesium ion-conductive poly(ethylenecarbonate) electrolytes. *Ionics* **24**, 3475–3481 (2018).
135. Ponmani, S. & Prabhu, M. R. Development and study of solid polymer electrolytes based on PVdF-HFP/PVAc:Mg(ClO<sub>4</sub>)<sub>2</sub> for Mg ion batteries. *J Mater Sci: Mater Electron* **29**, 15086–15096 (2018).
136. Shanmuga Priya, S. *et al.* Study of biopolymer I-carrageenan with magnesium perchlorate. *Ionics* **24**, 3861–3875 (2018).
137. Park, B. & Schaefer, J. L. Review-Polymer Electrolytes for Magnesium Batteries: Forging Away from Analogs of Lithium Polymer Electrolytes and Towards the Rechargeable Magnesium Metal Polymer Battery. *J. Electrochem. Soc.* **167**, 070545 (2020).
138. Liang, Y. *et al.* Rechargeable Mg Batteries with Graphene-like MoS<sub>2</sub> Cathode and Ultrasmall Mg Nanoparticle Anode. *Adv. Mater.* 640–643 (2011).
139. Li, W. *et al.* Metallic Magnesium Nano/Mesoscale Structures: Their Shape-Controlled Preparation and Mg/Air Battery Applications. *Angew. Chem. Int. Ed.* 6009–6012 (2006).
140. Peng, B. *et al.* Magnesium nanostructures for energy storage and conversion. *J. Mater. Chem.* **19**, 2877 (2009).

141. Son, S.-B. *et al.* An artificial interphase enables reversible magnesium chemistry in carbonate electrolytes. *Nature Chemistry* 532–539 (2018).
142. Dahn, J. R. Phase diagram of  $\text{Li}_x\text{C}_6$ . *Phys. Rev. B* **44**, 9170–9177 (1991).
143. Novak, P. *et al.* Magnesium insertion electrodes for rechargeable nonaqueous batteries - a competitive alternative to lithium? *Electrochim. Acta* 351–367 (1999).
144. Cohn, A. P. *et al.* Durable potassium ion battery electrodes from high-rate cointercalation into graphitic carbons. *J. Mater. Chem. A* **4**, 14954–14959 (2016).
145. Er, D. *et al.* Defective Graphene and Graphene Allotropes as High-Capacity Anode Materials for Mg Ion Batteries. *ACS Energy Lett.* **1**, 638–645 (2016).
146. Pontiroli, D. *et al.* Ionic conductivity in the Mg intercalated fullerene polymer  $\text{Mg}_2\text{C}_{60}$ . *Carbon* **51**, 143–147 (2013).
147. Margadonna, S. *et al.*  $\text{Li}_4\text{C}_{60}$ : A Polymeric Fulleride with a Two-Dimensional Architecture and Mixed Interfullerene Bonding Motifs. *J. Am. Chem. Soc.* 15032–15033 (2004).
148. Jache, B. & Adelhelm, P. Use of Graphite as a Highly Reversible Electrode with Superior Cycle Life for Sodium-Ion Batteries by Making Use of Co-Intercalation Phenomena. *Angew. Chem.* 10333–10337 (2014).
149. Schoderböck, P. & Boehm, H. P. Observations of staging in the electrochemical intercalation of lithium into graphite from dimethyl sulfoxide solutions. *Synthetic Metals* **44**, 239–246 (1991).
150. Kim, H. *et al.* Sodium intercalation chemistry in graphite. *Energy Environ. Sci.* **8**, 2963–2969 (2015).
151. Kawaguchi, M. & Kurasaki, A. Intercalation of magnesium into a graphite-like layered material of composition  $\text{BC}_2\text{N}$ . *Chem. Commun.* **48**, 6897 (2012).
152. Chen, C. *et al.* Layered  $\text{Na}_2\text{Ti}_3\text{O}_7/\text{MgNaTi}_3\text{O}_7/\text{Mg}_{0.5}\text{NaTi}_3\text{O}_7$  Nanoribbons as High-Performance Anode of Rechargeable Mg-Ion Batteries. *ACS Energy Lett.* **1**, 1165–1172 (2016).
153. Wu, N. *et al.* Improving the Electrochemical Performance of the  $\text{Li}_4\text{Ti}_5\text{O}_{12}$  Electrode in a Rechargeable Magnesium Battery by Lithium-Magnesium Co-Intercalation. *Angew. Chem. Int. Ed.* **54**, 5757–5761 (2015).
154. Obrovac, M. N. Si-alloy negative electrodes for LIBs. *Current Opinion in Electrochemistry* **9**, 8–17 (2018).
155. Murgia, F. *et al.* Electrochemical Mg alloying properties along the  $\text{Sb}_{1-x}\text{Bi}_x$  solid solution. *Electrochim. Acta* **259**, 276–283 (2018).

156. Arthur, T. S. *et al.* Electrodeposited Bi, Sb and Bi<sub>1-x</sub>Sb<sub>x</sub> alloys as anodes for Mg-ion batteries. *Electrochem. commun.* **16**, 103–106 (2012).
157. Ellis, L. D. *et al.* In Situ XRD Study of Silicon, Lead and Bismuth Negative Electrodes in Nonaqueous Sodium Cells. *J. Electrochem. Soc.* **161**, A416–A421 (2014).
158. Murgia, F. *et al.* Insight into the electrochemical behavior of micrometric Bi and Mg<sub>3</sub>Bi<sub>2</sub> as high-performance negative electrodes for Mg batteries. *J. Mater. Chem. A* **3**, 16478–16485 (2015).
159. Singh, N. *et al.* A high energy-density tin anode for rechargeable magnesium-ion batteries. *Chem. Commun.* **49**, 149–151 (2013).
160. Zhao, M. *et al.* Tin-based nanomaterials for electrochemical energy storage. *RSC Adv.* **6**, 95449–95468 (2016).
161. Gabaudan, V. *et al.* Electrochemical Alloying of Lead in Potassium-Ion Batteries. *ACS Omega* **3**, 12195–12200 (2018).
162. Periyapperuma, K. *et al.* The Reversible Magnesiumation of Pb. *Electrochim. Acta* **165**, 162–165 (2015).
163. Murgia, F. *et al.* First investigation of indium-based electrode in Mg battery. *Electrochem. commun.* **60**, 56–59 (2015).
164. Zhang, Q. *et al.* High Energy Density Electrode Materials for Rechargeable Magnesium Batteries. *ECS Transactions* **66**, 171–181 (2015).
165. Zhao, T. *et al.* TiC<sub>2</sub>: a new two-dimensional sheet beyond MXenes. *Nanoscale* **8**, 233–242 (2016).
166. Zeng, J. *et al.* Li<sub>3</sub>VO<sub>4</sub>: an insertion anode material for magnesium ion batteries with high specific capacity. *Electrochim. Acta* **247**, 265–270 (2017).
167. Novák, P. *et al.* Magnesium insertion batteries - an alternative to lithium? *J. Power Sources* **54**, 479–482 (1995).
168. Levi, E. *et al.* On the Way to Rechargeable Mg Batteries: The Challenge of New Cathode Materials. *Chem. Mater.* **22**, 860–868 (2010).
169. Bruce, P. G. *et al.* Nanomaterials for Rechargeable Lithium Batteries. *Angew. Chem. Int. Ed.* **47**, 2930–2946 (2008).
170. Obrovac, M. N. *et al.* The Electrochemical Displacement Reaction of Lithium with Metal Oxides. *J. Electrochem. Soc.* **148**, A576 (2001).
171. Whittingham, M. S. Electrical Energy Storage and Intercalation Chemistry. *Science* **192**, 1126–1127 (1976).

172. Yoo, H. D. *et al.* Fast kinetics of magnesium monochloride cations in interlayer-expanded titanium disulfide for magnesium rechargeable batteries. *Nat Commun* **8**, 339 (2017).
173. Shuai, J. *et al.* Density functional theory study of Li, Na, and Mg intercalation and diffusion in MoS<sub>2</sub> with controlled interlayer spacing. *Mater. Res. Express* **3**, 064001 (2016).
174. Li, Z. *et al.* Fast kinetics of multivalent intercalation chemistry enabled by solvated magnesium-ions into self-established metallic layered materials. *Nat Commun* **9**, 5115 (2018).
175. Liang, Y. *et al.* Interlayer-Expanded Molybdenum Disulfide Nanocomposites for Electrochemical Magnesium Storage. *Nano Lett.* **15**, 2194–2202 (2015).
176. Aurbach, D. *et al.* Prototype systems for rechargeable magnesium batteries. *Nature* **407**, 724–727 (2000).
177. Zhang, R. & Ling, C. Status and challenge of Mg battery cathode. *MRS energy sustain.* **3**, E1 (2016).
178. Li, Z. *et al.* Morphology-dependent electrochemical performance of VS<sub>4</sub> for rechargeable magnesium battery and its magnesiation/demagnesiation mechanism. *J. Power Sources* **451**, 227815 (2020).
179. Yuan, C. *et al.* Investigation of the intercalation of polyvalent cations (Mg<sup>2+</sup>, Zn<sup>2+</sup>) into  $\lambda$ -MnO<sub>2</sub> for rechargeable aqueous battery. *Electrochim. Acta* 404–412 (2014).
180. Rasul, S. *et al.* M. High capacity positive electrodes for secondary Mg-ion batteries. *Electrochim. Acta* **82**, 243–249 (2012).
181. Zhang, M. *et al.* Communication—Investigation of Anatase-TiO<sub>2</sub> as an Efficient Electrode Material for Magnesium-Ion Batteries. *J. Electrochem. Soc.* **163**, A2368–A2370 (2016).
182. Amatucci, G. G. *et al.* Investigation of Yttrium and Polyvalent Ion Intercalation into Nanocrystalline Vanadium Oxide. *J. Electrochem. Soc.* **148**, A940 (2001).
183. Doe, R. E. *et al.* Layered materials with improved magnesium intercalation for rechargeable magnesium ion cells, *US Patent. US9401528B2*, (2016).
184. Sa, N. *et al.* Is alpha-V<sub>2</sub>O<sub>5</sub> a cathode material for Mg insertion batteries? *J. Power Sources* **323**, 44–50 (2016).
185. Mao, M. *et al.* A critical review of cathodes for rechargeable Mg batteries. *Chem. Soc. Rev.* **47**, 8804–8841 (2018).
186. Duffort, V., Sun, X. & Nazar, L. F. Screening for positive electrodes for magnesium batteries: a protocol for studies at elevated temperatures. *Chem. Commun.* **52**, 12458–12461 (2016).



187. Xiong, F. *et al.* Magnesium storage performance and mechanism of CuS cathode. *Nano Energy* **47**, 210–216 (2018).
188. Chung, J.-S. & Sohn, H.-J. Electrochemical behaviors of CuS as a cathode material for lithium secondary batteries. *Journal of Power Sources* **108**, 226–231 (2002).
189. Yue, J.-L. *et al.* Cu<sub>2</sub>Se with facile synthesis as a cathode material for rechargeable sodium batteries. *Chem. Commun.* **49**, 5868 (2013).
190. Tashiro, Y. *et al.* Copper Selenide as a New Cathode Material based on Displacement Reaction for Rechargeable Magnesium Batteries. *Electrochim. Acta* **210**, 655–661 (2016).
191. Wang, L. *et al.* Sponge-Like Porous Manganese(II,III) Oxide as a Highly Efficient Cathode Material for Rechargeable Magnesium Ion Batteries. *Chem. Mater.* **28**, 6459–6470 (2016).
192. Okamoto, S. *et al.* Intercalation and Push-Out Process with Spinel-to-Rocksalt Transition on Mg Insertion into Spinel Oxides in Magnesium Batteries. *Adv. Sci.* 1500072 (2015).
193. Jain, A. *et al.* Commentary: The Materials Project: A materials genome approach to accelerating materials innovation. *APL Materials* **1**, 011002 (2013).
194. Hannah, D. C. *et al.* On the Balance of Intercalation and Conversion Reactions in Battery Cathodes. *Adv. Energy Mater.* **8**, 1800379 (2018).
195. Zainol, N. H. *et al.* Synthesis and characterization of Ti-doped MgMn<sub>2</sub>O<sub>4</sub> cathode material for magnesium ion batteries. *Ionics* **25**, 133–139 (2019).
196. Lopes, P. P. *et al.* Real-Time Monitoring of Cation Dissolution/Deintercalation Kinetics from Transition-Metal Oxides in Organic Environments. *J. Phys. Chem. Lett.* **9**, 4935–4940 (2018).
197. Liu, M. *et al.* Spinel compounds as multivalent battery cathodes: a systematic evaluation based on ab initio calculations. *Energy Environ. Sci.* **8**, 964–974 (2015).
198. Song, Z. *et al.* Anthraquinone based polymer as high-performance cathode material for rechargeable lithium batteries. *Chem. Commun.* 448–450 (2009).
199. Genorio, B. *et al.* Electroactive Organic Molecules Immobilized onto Solid Nanoparticles as a Cathode Material for LIBs. *Angew. Chem. Int.* **122**, 7380–7382 (2010).
200. Senoh, H. *et al.* A two-compartment cell for using soluble benzoquinone derivatives as active materials in lithium secondary batteries. *Electrochim. Acta* **56**, 10145–10150 (2011).
201. Lv, D. *et al.* A Scientific Study of Current Collectors for Mg Batteries in Mg(AlCl<sub>2</sub>EtBu)<sub>2</sub>/THF Electrolyte. *J. Electrochem. Soc.* **160**, A351–A355 (2013).

202. Tang, M. *et al.* Carbonyl polymeric electrode materials for metal-ion batteries. *Chin Chem Lett* **29**, 232–244 (2018).
203. Abraham, I. *et al.* Recent advances in 1,4-benzoquinone chemistry. *J. Braz. Chem. Soc.* **22**, 385–421 (2011).
204. Wang, Y. *et al.* Recent Advances in Direct Functionalization of Quinones: Recent Advances in Direct Functionalization of Quinones. *Eur. J. Org. Chem.* **2019**, 2179–2201 (2019).
205. Bitenc, J. *et al.* Quinone Based Materials as Renewable High Energy Density Cathode Materials for Rechargeable Magnesium Batteries. *Materials* **13**, 506 (2020).
206. Sano, H. *et al.* Mg<sup>2+</sup> Storage in Organic Positive-electrode Active Material Based on 2,5-Dimethoxy-1,4-benzoquinone. *Chem. Lett.* **41**, 1594–1596 (2012).
207. Senoh, H. *et al.* Sulfone-Based Electrolyte Solutions for Rechargeable Magnesium Batteries Using 2,5-Dimethoxy-1,4-benzoquinone Positive Electrode. *J. Electrochem. Soc.* **161**, A1315–A1320 (2014).
208. Tian, J. *et al.* High-Capacity Mg–Organic Batteries Based on Nanostructured Rhodizonate Salts Activated by Mg–Li Dual-Salt Electrolyte. *ACS Nano* **12**, 3424–3435 (2018).
209. Kim, H. S. *et al.* Structure and compatibility of a magnesium electrolyte with a sulphur cathode. *Nat Commun* **2**, 427 (2011).
210. Bitenc, J. *et al.* Anthraquinone-Based Polymer as Cathode in Rechargeable Magnesium Batteries. *ChemSusChem* **8**, 4128–4132 (2015).
211. Vizintin, A. *et al.* Probing electrochemical reactions in organic cathode materials via in operando infrared spectroscopy. *Nat Commun* **9**, 661 (2018).
212. Pan, B. *et al.* Polyanthraquinone-Based Organic Cathode for High-Performance Rechargeable Magnesium-Ion Batteries. *Adv. Energy Mater.* **6**, 2–4 (2016).
213. Song, Z. *et al.* Polyanthraquinone as a Reliable Organic Electrode for Stable and Fast Lithium Storage. *Angew. Chem. Int. Ed.* **54**, 13947–13951 (2015).
214. Cui, L. *et al.* Salt-controlled dissolution in pigment cathode for high-capacity and long-life magnesium organic batteries. *Nano Energy* **65**, 103902 (2019).
215. Zhuang, Y. *et al.* Polyimides containing aliphatic/alicyclic segments in the main chains. *Progress in Polymer Science* **92**, 35–88 (2019).
216. Bančič, T. *et al.* Electrochemical performance and redox mechanism of naphthalene-hydrazine diimide polymer as a cathode in magnesium battery. *J. Power Sources* **395**, 25–30 (2018).

217. Zhou, L. *et al.* Interlayer-Spacing-Regulated VOPO<sub>4</sub> Nanosheets with Fast Kinetics for High-Capacity and Durable Rechargeable Magnesium Batteries. *Adv. Mater.* **30**, 1801984 (2018).
218. Xie, J. *et al.* Transition-Metal-Free Magnesium-Based Batteries Activated by Anionic Insertion into Fluorinated Graphene Nanosheets. *Adv. Funct. Mater.* **25**, 6519–6526 (2015).
219. Meng, Y. *et al.* Competition between insertion of Li<sup>+</sup> and Mg<sup>2+</sup>: An example of TiO<sub>2</sub>-β nanowires for Mg rechargeable batteries and Li<sup>+</sup>/Mg<sup>2+</sup> hybrid-ion batteries. *J. Power Sources* **346**, 134–142 (2017).
220. Zhang, R. *et al.* A conceptual magnesium battery with ultrahigh rate capability. *Chem. Commun.* **51**, 1487–1490 (2015).
221. Fan, X. *et al.* A Universal Organic Cathode for Ultrafast Lithium and Multivalent Metal Batteries. *Angew. Chem. Int. Ed.* **57**, 7146–7150 (2018).
222. Qiang, C. *et al.* PTMA/Graphene as a Novel Cathode Material for Rechargeable Magnesium Batteries. **5** (2013).
223. NuLi, Y. *et al.* A new class of cathode materials for rechargeable magnesium batteries: Organosulfur compounds based on sulfur–sulfur bonds. *Electrochem. commun.* **9**, 1913–1917 (2007).
224. Bitenc, J. *et al.* Poly(hydroquinoyl-benzoquinonyl sulfide) as an active material in Mg and Li organic batteries. *Electrochem. commun.* **69**, 1–5 (2016).
225. Song, Z. *et al.* Poly(benzoquinonyl sulfide) as a High-Energy Organic Cathode for Rechargeable Li and Na Batteries. *Adv. Sci.* **2**, 1500124 (2015).
226. Kumar, G. *et al.* Polyaniline as an electrode material for magnesium reserve battery. *Synthetic Metals* **80**, 279–282 (1996).
227. Sano, H. *et al.* Mg<sup>2+</sup> Storage in Organic Positive-electrode Active Material Based on 2,5-Dimethoxy-1,4-benzoquinone. *Chem. Lett.* **41**, 1594–1596 (2012).
228. Pan, B. *et al.* Polyanthraquinone-Based Organic Cathode for High-Performance Rechargeable Magnesium-Ion Batteries. *Adv. Energy Mater.* 1600140 (2016).
229. Bitenc, J. *et al.* Poly(hydroquinoyl-benzoquinonyl sulfide) as an active material in Mg and Li organic batteries. *Electrochem. commun.* **69**, 1–5 (2016).
230. Rodríguez-Pérez, I. A. *et al.* Mg-Ion Battery Electrode: An Organic Solid’s Herringbone Structure Squeezed upon Mg-Ion Insertion. *J. Am. Chem. Soc.* **139**, 13031–13037 (2017).
231. Wagner, R. *et al.* Counterintuitive Role of Magnesium Salts as Effective Electrolyte Additives for High Voltage LIBs. *Adv. Mater. Interfaces* **3**, 1600096 (2016).

232. Höche, D. *et al.* Performance boost for primary magnesium cells using iron complexing agents as electrolyte additives. *Sci Rep* **8**, 7578 (2018).
233. S Song, J. *et al.* Mapping the Challenges of Magnesium Battery. *J. Phys. Chem. Lett.* **7**, 1736–1749 (2016).
234. Lu, Z. *et al.* On the electrochemical behavior of magnesium electrodes in polar aprotic electrolyte solutions. *J. Electroanal. Chem* **466**, 203–217 (1999).
235. Li, W. *et al.* Synthesis, Crystal Structure, and Electrochemical Properties of a Simple Magnesium Electrolyte for Magnesium/Sulfur Batteries. *Angew. Chem.* **128**, 6516–6520 (2016).
236. Gao, T. *et al.* Reversible  $S^0/MgS_x$  Redox Chemistry in a  $MgTFSI_2/MgCl_2/DME$  Electrolyte for Rechargeable Mg/S Batteries. *Angew. Chem.* **129**, 13711–13715 (2017).
237. Osawa, E. & Musso, H. Application of Molecular Mechanics Calculations to Organic Chemistry. in *Topics in Stereochemistry* 117–195 (John Wiley & Sons, 1982).
238. Zhao-Karger, Z. *et al.* A new class of non-corrosive, highly efficient electrolytes for rechargeable magnesium batteries. *J. Mater. Chem. A* 10815–10820 (2017).
239. Tutusaus, O. & Mohtadi, R. Paving the Way towards Highly Stable and Practical Electrolytes for Rechargeable Magnesium Batteries. *ChemElectroChem* **2**, 51–57 (2015).
240. Attias, R. *et al.* Anode-Electrolyte Interfaces in Secondary Magnesium Batteries. *Joule* **3**, 27–52 (2019).
241. Deivanayagam, R. *et al.* Progress in development of electrolytes for magnesium batteries. *Energy Storage Mater.* **21**, 136–153 (2019).
242. Lee, B. *et al.* Strategic combination of Grignard reagents and allyl-functionalized ionic liquids as an advanced electrolyte for rechargeable magnesium batteries. *J. Mater. Chem. A* **6**, 3126–3133 (2018).
243. Cuan, J. *et al.* Borohydride-Scaffolded Li/Na/Mg Fast Ionic Conductors for Promising Solid-State Electrolytes. *Adv. Mater.* 1803533 (2018).
244. Zaidi, S. A. A. *et al.* Transition metal complexes of potassium dihydridobis-, hydridotris- and tetrakis-(thiophenyl)borate anions. *Transition Met Chem* **15**, 231–235 (1990).
245. Bukowski, W. The Effect of Diglyme on the Kinetics of Chromium(III) Ethanoate-Catalyzed Reactions of Carboxylic Acids with Epichlorohydrin. *Org. Process Res. Dev.* **6**, 10–14 (2002).
246. Tang, S. & Zhao, H. Glymes as versatile solvents for chemical reactions and processes: from the laboratory to industry. *RSC Adv.* **4**, 11251 (2014).

247. Shao, Y. *et al.* Coordination Chemistry in magnesium battery electrolytes: how ligands affect their performance. *Sci Rep* **3**, 3130 (2013).
248. Ngo, H. P. K. Reversibility of Mg Deposition/Dissolution in Electrolyte Solution for Rechargeable Magnesium Batteries. (2016).
249. Golub, I. E. *et al.* The interplay of proton accepting and hydride donor abilities in the mechanism of step-wise boron hydrides alcoholysis. *Inorganica Chimica Acta* **456**, 113–119 (2017).
250. Tuerxun, F. *et al.* High concentration magnesium borohydride/tetraglyme electrolyte for rechargeable magnesium batteries. *J. Power Sources* **276**, 255–261 (2015).
251. Perrin, D. D., Dempsey, B. & Serjeant, E. P. *pKa Prediction for Organic Acids and Bases*. (Chapman & Hall, 1981).
252. Borsari, M. *et al.* Electrochemical Behavior of Diphenyl Disulfide and Thiophenol on Glassy Carbon and Gold Electrodes in Aprotic Media. *Electroanalysis* **15**, 1192–1197 (2003).
253. Karaman, R. Effects of substitution on the effective molarity (EM) for five membered ring-closure reactions – A computational approach. *J. Mol. Struct* **939**, 69–74 (2010).
254. Osawa, E. & Musso, H. Molecular Mechanics Calculations in Organic Chemistry: Examples of the Usefulness of this Simple Non-Quantum Mechanical Model. *Angew. Chem. Int.* 1–12 (1983).
255. Zhang, D. *et al.* Studies on capacity fade of LIBs. *J. Power Sources* **91**, 122–129 (2000).
256. Markovsky, B. *et al.* The basic electroanalytical behavior of practical graphite–lithium intercalation electrodes. *Electrochim. Acta* **43**, 2287–2304 (1998).
257. Saha, P. *et al.* A rapid solid-state synthesis of electrochemically active Chevrel phases ( $\text{Mo}_6\text{T}_8$ ; T = S, Se) for rechargeable magnesium batteries. *Nano Res.* **10**, 4415–4435 (2017).
258. Woo, S.-G. *et al.* Copper incorporated  $\text{Cu}_x\text{Mo}_6\text{S}_8$  ( $x \geq 1$ ) Chevrel-phase cathode materials synthesized by chemical intercalation process for rechargeable magnesium batteries. *RSC Adv.* **4**, 59048–59055 (2014).
259. Murgia, F. *et al.* Express and low-cost microwave synthesis of the ternary Chevrel phase  $\text{Cu}_2\text{Mo}_6\text{S}_8$  for application in rechargeable magnesium batteries. *J. Solid State Chem.* **242**, 151–154 (2016).
260. Ling, C. & Suto, K. Thermodynamic Origin of Irreversible Magnesium Trapping in Chevrel Phase  $\text{Mo}_6\text{S}_8$ : Importance of Magnesium and Vacancy Ordering. *Chem. Mater.* **29**, 3731–3739 (2017).

261. Fedorov, I. A. *et al.* Electronic structure and chemical bond in naphthalene and anthracene. *Phys. Chem. Chem. Phys.* **13**, 5679 (2011).
262. Nicholson, R. S. Theory and Application of Cyclic Voltammetry for Measurement of Electrode Reaction Kinetics. *Analytical Chemistry* 1351–1356 (1965).
263. Espinoza, E. M. *et al.* Practical Aspects of Cyclic Voltammetry: How to Estimate Reduction Potentials When Irreversibility Prevails. *J. Electrochem. Soc.* **166**, H3175–H3187 (2019).
264. Ponrouch, A. *et al.* Multivalent rechargeable batteries. *Energy Storage Materials* **20**, 253–262 (2019).
265. Mori, T. *et al.* Anti-site mixing governs the electrochemical performances of olivine-type MgMnSiO<sub>4</sub> cathodes for rechargeable magnesium batteries. *Phys. Chem. Chem. Phys.* **18**, 13524–13529 (2016).
266. Yang, S. *et al.* First-Principles Study of Zigzag MoS<sub>2</sub> Nanoribbon as a Promising Cathode Material for Rechargeable Mg Batteries. *J. Phys. Chem. C* **116**, 1307–1312 (2012).
267. Levi, E. *et al.* On the Way to Rechargeable Mg Batteries: The Challenge of New Cathode Materials. *Chem. Mater.* **22**, 860–868 (2010).
268. Liu, Y. *et al.* Sandwich-structured graphene-like MoS<sub>2</sub>/C microspheres for rechargeable Mg batteries. *J. Mater. Chem. A* **1**, 5822 (2013).
269. Zhang, R. & Ling, C. Unveil the Chemistry of Olivine FePO<sub>4</sub> as Magnesium Battery Cathode. *ACS Appl. Mater. Interfaces* **8**, 18018–18026 (2016).
270. Yin, J. *et al.* Magnesium-ion battery-relevant electrochemistry of MgMn<sub>2</sub>O<sub>4</sub>: crystallite size effects and the notable role of electrolyte water content. *Chem. Commun.* **53**, 3665–3668 (2017).
271. Murgia, F. *et al.* Express and low-cost microwave synthesis of the ternary Chevrel phase Cu<sub>2</sub>Mo<sub>6</sub>S<sub>8</sub> for application in rechargeable magnesium batteries. *J. Solid State Chem.* **242**, 151–154 (2016).
272. Koketsu, T. *et al.* Reversible magnesium and aluminium ions insertion in cation-deficient anatase TiO<sub>2</sub>. *Nature Mater* **16**, 1142–1148 (2017).
273. Shea, J. J. & Luo, C. Organic Electrode Materials for Metal Ion Batteries. *ACS Applied Materials & Interfaces* (2020).
274. Liang, Y. *et al.* Organic electrode materials for rechargeable lithium batteries. *Adv. Energy Mater.* **2**, 742–769 (2012).
275. Muench, S. *et al.* Polymer-Based Organic Batteries. *Chemical Reviews* **116**, 9438–9484 (2016).

276. Pan, B. *et al.* 2,5-dimethoxy-1,4-benzoquinone (DMBQ) as organic cathode for rechargeable magnesium-ion batteries. *J. Electrochem. Soc* **163**, A580–A583 (2016).
277. Rodríguez-Pérez, I. A. *et al.* Mg-Ion Battery Electrode: An Organic Solid's Herringbone Structure Squeezed upon Mg-Ion Insertion. *J. Am. Chem. Soc.* **139**, 13031–13037 (2017).
278. Gomez, I. *et al.* D. Poly(anthraquinonylsulfides): High Capacity Redox Polymers for Energy Storage. *ACS Macro Lett.* **7**, 419–424 (2018).
279. Qiang, C. *et al.* PTMA/Graphene as a Novel Cathode Material for Rechargeable Magnesium Batteries. *Acta Physico-Chimica Sinica* **29**, 2295–2299 (2013).
280. Attias, R. *et al.* Solvent Effects on the Reversible Intercalation of Magnesium-Ions into V<sub>2</sub>O<sub>5</sub> Electrodes. *ChemElectroChem* **5**, 3514–3524 (2018).
281. Deivanayagam, R. *et al.* Progress in development of electrolytes for magnesium batteries. *Energy Storage Mater.* **21**, 136–153 (2019).
282. Bitenc, J. *et al.* Effect of salts on the electrochemical performance of Mg metal–organic battery. *J. Power Sources* **430**, 90–94 (2019).
283. Lu, D. *et al.* Magnesium ion based organic secondary batteries. *J. Mater. Chem. A* **6**, 17297–17302 (2018).
284. Bitenc, J. *et al.* Anthraquinone-Based Polymer as Cathode in Rechargeable Magnesium Batteries. *ChemSusChem* **8**, 4128–4132 (2015).
285. Song, Z. *et al.* Anthraquinone based polymer as high-performance cathode material for rechargeable lithium batteries. *Chem Commun* 448–450 (2009).
286. Delacourt, C. *et al.* One-Step Low-Temperature Route for the Preparation of Electrochemically Active LiMnPO<sub>4</sub> Powders. *Chem. Mater.* **16**, 93–99 (2004).
287. Lee, W. *et al.* Electrochemical Properties of Poly(Anthraquinonyl Sulfide)/Graphene Sheets Composites as Electrode Materials for Electrochemical Capacitors. *Nanomaterials* **4**, 599–611 (2014).
288. Li, S. *et al.* An improved method for synthesis of lithium difluoro(oxalato)borate and effects of sulfolane on the electrochemical performances of LIBs. *Electrochim. Acta* **91**, 282–292 (2013).
289. Li, S. *et al.* Composition analysis of the SEI film on carbon electrode of Li-ion battery based on lithium difluoro(oxalate)borate and sulfolane. *J. Power Sources* **217**, 503–508 (2012).
290. Sa, N. *et al.* Concentration dependent electrochemical properties and structural analysis of a simple magnesium electrolyte: magnesium bis(trifluoromethane sulfonyl)imide in diglyme. *RSC Adv.* **6**, 113663–113670 (2016).

291. Merrill, L. C. & Schaefer, J. L. Conditioning-Free Electrolytes for Magnesium Batteries Using Sufone–Ether Mixtures with Increased Thermal Stability. *Chem. Mater.* **30**, 3971–3974 (2018).
292. Li, S. *et al.* Effect of sulfolane on the performance of lithium bis(oxalato)borate-based electrolytes for advanced lithium ion batteries. *Electrochimica Acta* **65**, 221–227 (2012).
293. Mao, L. *et al.* Electrochemical performance of electrolytes based upon lithium bis(oxalate)borate and sulfolane/alkyl sulfite mixtures for high temperature lithium-ion batteries. *Electrochim. Acta* **79**, 197–201 (2012).
294. Xing, L. *et al.* Electrode/Electrolyte Interface in Sulfolane-Based Electrolytes for Li Ion Batteries: A Molecular Dynamics Simulation Study. *J. Phys. Chem. C* **116**, 23871–23881 (2012).
295. Geoffroy, I. *et al.* Electrolytic characteristics of ethylene carbonate–diglyme-based electrolytes for lithium batteries. *Electrochim. Acta* **45**, 2019–2027 (2000).
296. Baskin, A. & Prendergast, D. Exploration of the Detailed Conditions for Reductive Stability of Mg(TFSI)<sub>2</sub> in Diglyme: Implications for Multivalent Electrolytes. *J. Phys. Chem. C* **120**, 3583–3594 (2016).
297. Xia, J. & Dahn, J. R. Improving sulfolane-based electrolyte for high voltage Li-ion cells with electrolyte additives. *J. Power Sources* **324**, 704–711 (2016).
298. Benítez, A. *et al.* Lithium sulfur battery exploiting material design and electrolyte chemistry: 3D graphene framework and diglyme solution. *J. Power Sources* **397**, 102–112 (2018).
299. Hofmann, A. *et al.* Mixtures of Ionic Liquid and Sulfolane as Electrolytes for LIBs. *Electrochim. Acta* **147**, 704–711 (2014).
300. Fujii, K. *et al.* Structural Study on Magnesium Ion Solvation in Diglyme-Based Electrolytes: IR Spectroscopy and DFT Calculations. *J. Phys. Chem. B* **122**, 8712–8717 (2018).
301. Picard, T. & Sergent, N. Tetraglyme - Ca(TFSI)<sub>2</sub>, a non-monotonic liquid electrolyte. (2020).
302. Gao, J. *et al.* Effects of Liquid Electrolytes on the Charge–Discharge Performance of Rechargeable Lithium/Sulfur Batteries: Electrochemical and in-Situ X-ray Absorption Spectroscopic Studies. *J. Phys. Chem. C* **115**, 25132–25137 (2011).
303. Allcorn, E. *et al.* Lithium diffusivity in antimony-based intermetallic and FeSb–TiC composite anodes as measured by GITT. *Phys. Chem. Chem. Phys.* **17**, 28837–28843 (2015).



304. Deiss, E. Spurious chemical diffusion coefficients of  $\text{Li}^+$  in electrode materials evaluated with GITT. *Electrochim. Acta* **50**, 2927–2932 (2005).
305. Dees, D. W. *et al.* Analysis of the Galvanostatic Intermittent Titration Technique (GITT) as applied to a Li-ion porous electrode. *J. Power Sources* **189**, 263–268 (2009).
306. Li, Z. *et al.* Electrochemical Kinetics of the  $\text{Li}[\text{Li}_{0.23}\text{Co}_{0.3}\text{Mn}_{0.47}]\text{O}_2$  Cathode Material Studied by GITT and EIS. *J. Phys. Chem. C* **114**, 22751–22757 (2010).
307. Ba, Z. *et al.* Benzoquinone-Based Polyimide Derivatives as High-Capacity and Stable Organic Cathodes for LIBs. *ACS Appl. Mater. Interfaces* **12**, 807–817 (2020).
308. Yin, J. *et al.* Synthetic control of manganese birnessite: Impact of crystallite size on Li, Na, and Mg based electrochemistry. *Inorganica Chim. Acta* **453**, 230–237 (2016).
309. Yabuuchi, N. *et al.* Research Development on Sodium-Ion Batteries. *Chem. Rev.* **114**, 11636–11682 (2014).
310. Wang, H. *et al.* Electrolytes Enriched by Crown Ethers for Lithium Metal Batteries. *Adv. Funct. Mater.* 2002578 (2020).
311. Zhang, S. Suppressing Li Dendrites via Electrolyte Engineering by Crown Ethers for Lithium Metal Batteries. *Nano-Micro Lett.* **12**, 158 (2020).
312. Zhang, H. & Lerner, M. M. Preparation of Graphite Intercalation Compounds Containing Crown Ethers. *Inorg. Chem.* **55**, 8281–8284 (2016).
313. Christy, F. A. & Shrivastav, P. S. Conductometric Studies on Cation-Crown Ether Complexes: A Review. *Crit. Rev. Anal. Chem* **41**, 236–269 (2011).
314. Sagane, F. *et al.* The Effect of Cyclic Ethers on Mg Plating/Stripping Reaction in Ionic Liquid Electrolytes. *J. Electrochem. Soc.* **166**, A5054–A5058 (2019).
315. Stettner, T. *et al.* Ionic Liquid-Based Electrolytes for Calcium-Based Energy Storage Systems. *J. Electrochem. Soc.* **167**, 100544 (2020).
316. Verrelli, R. *et al.* Steps Towards the Use of  $\text{TiS}_2$  Electrodes in Ca Batteries. *J. Electrochem. Soc.* **167**, 070532 (2020).
317. Arroyo-de Dompablo, M. E. *et al.* Achievements, Challenges, and Prospects of Calcium Batteries. *Chem. Rev.* **120**, 6331–6357 (2020).
318. Kawakubo, M. *et al.* High capacity carbon anode for dry polymer LIBs. *J. Power Sources* **225**, 187–191 (2013).
319. Zhang, L. Direct electrochemistry of cytochrome c at ordered macroporous active carbon electrode. *Biosensors and Bioelectronics* **23**, 1610–1615 (2008).
320. Atsbeha Kahsay, B. *et al.* Maleamic Acid as an Organic Anode Material in LIBs. *Polymers* **12**, 1109 (2020).

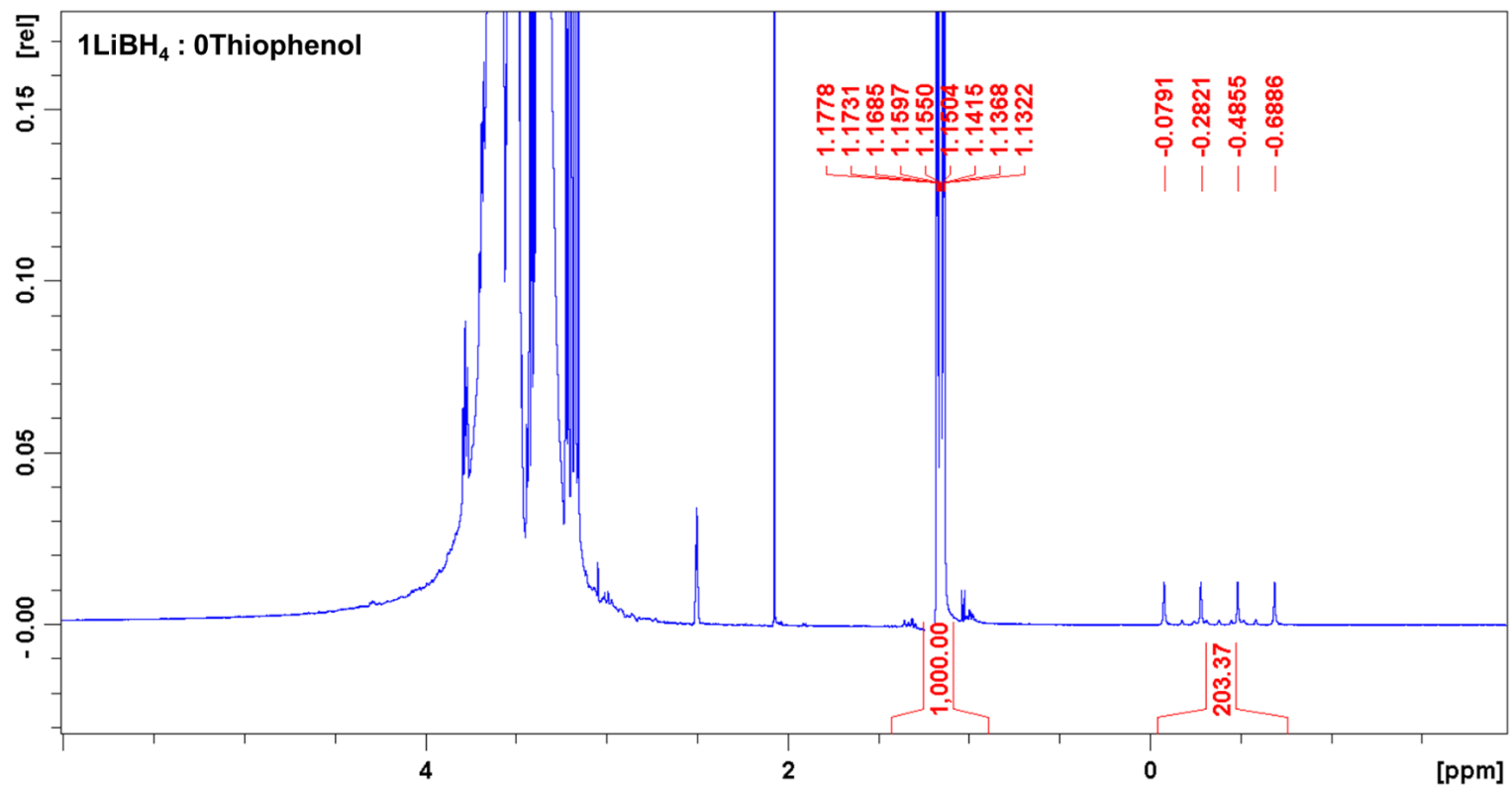
321. Liang, Y. *et al.* Organic Electrode Materials for Rechargeable Lithium Batteries. *Adv. Energy Mater.* **2**, 742–769 (2012).
322. Xu, Y. *et al.* Organic materials for rechargeable sodium-ion batteries. *Materials Today* **21**, 60–78 (2018).
323. Lu, Y. & Chen, J. Prospects of organic electrode materials for practical lithium batteries. *Nat. Rev. Chem.* **4**, 127–142 (2020).
324. Armand, M. *et al.* Conjugated dicarboxylate anodes for LIBs. *Nature Mater.* **8**, 120–125 (2009).
325. Renault, S. *et al.* A green Li–organic battery working as a fuel cell in case of emergency. *Energy Environ. Sci.* **6**, 2124 (2013).
326. Zhao, Q. *et al.* Nanostructured organic electrode materials grown on graphene with covalent-bond interaction for high-rate and ultra-long-life LIBs. *Nano Res.* **10**, 4245–4255 (2017).
327. Quarez, É. *et al.* From partial to complete neutralization of 2,5-dihydroxyterephthalic acid in the Li–Na system: crystal chemistry and electrochemical behavior of  $\text{Na}_2\text{Li}_2\text{C}_8\text{H}_2\text{O}_6$  vs. Li. *CrystEngComm* **22**, 1653–1663 (2020).
328. Wang, S. *et al.* Organic  $\text{Li}_4\text{C}_8\text{H}_2\text{O}_6$  Nanosheets for LIBs. *Nano Lett.* **13**, 4404–4409 (2013).
329. Deng, Q. *et al.* The electrochemical behaviors of  $\text{Li}_2\text{C}_8\text{H}_4\text{O}_6$  and its corresponding organic acid  $\text{C}_8\text{H}_6\text{O}_6$  as anodes for LIBs. *J. Electroanal. Chem* **761**, 74–79 (2016).
330. Wang, S. All Organic Sodium-Ion Batteries with  $\text{Na}_4\text{C}_8\text{H}_2\text{O}_6$ . *Angew. Chem.* 6002–6006 (2014).
331. Jouhara, A. *et al.* Raising the redox potential in carboxyphenolate-based positive organic materials via cation substitution. *Nat Commun* **9**, 4401 (2018).
332. Poland & Kurc, B. Sulfolane with  $\text{LiPF}_6$ ,  $\text{LiNTf}_2$  and LiBOB - as a non-Flammable Electrolyte Working in a Li-ion battery with a  $\text{LiNiO}_2$  Cathode. *Int. J. Electrochem. Sci.* 5938–5955 (2018).
333. Nakanishi, A. *et al.* Sulfolane-Based Highly Concentrated Electrolytes of Lithium Bis(trifluoromethanesulfonyl)amide: Ionic Transport, Li-Ion Coordination, and Li–S Battery Performance. *J. Phys. Chem. C* **123**, 14229–14238 (2019).
334. Huang, J. *et al.* Recent Progress of Rechargeable Batteries Using Mild Aqueous Electrolytes. *Small Methods* **3**, 1800272 (2019).
335. Levi, M. D. *et al.* Kinetic and Thermodynamic Studies of  $\text{Mg}^{2+}$  and  $\text{Li}^+$  Ion Insertion into the  $\text{Mo}_6\text{S}_8$  Chevrel Phase. *ChemInform* **35**, (2004).

336. Reichardt, C. & Ebel, H. F. *Solvents and solvent effects in organic chemistry*. (VCH Verlagsgesellschaft, 1988).
337. Lutz, L. *et al.* High Capacity Na–O<sub>2</sub> Batteries: Key Parameters for Solution-Mediated Discharge. *J. Phys. Chem. C* **120**, 20068–20076 (2016).
338. Hoshi, K. *et al.* Purification of Perovskite Quantum Dots Using Low-Dielectric-Constant Washing Solvent “Diglyme” for Highly Efficient Light-Emitting Devices. *ACS Appl. Mater. Interfaces* **10**, 24607–24612 (2018).
339. Gutmann, V. Empirical parameters for donor and acceptor properties of solvents. *Electrochim. Acta* 661–670 (1976).
340. Bornstein, L. Group IV Physical Chemistry 6. in *Physical Chemistry* 40–78 (Springer, 2009).
341. Gutmann, V. *The donor-acceptor approach to molecular interactions*. (Plenum Press, 1978).
342. Domańska, U. *et al.* Solubility of Sulfolane in Selected Organic Solvents. *J. Chem. Eng. Data* **41**, 261–265 (1996).
343. Keyzer, E. N. *et al.* Mg(PF<sub>6</sub>)<sub>2</sub> -Based Electrolyte Systems: Understanding Electrolyte–Electrode Interactions for the Development of Mg-Ion Batteries. *J. Am. Chem. Soc.* **138**, 8682–8685 (2016).
344. Lu, Z. *et al.* On the electrochemical behavior of magnesium electrodes in polar aprotic electrolyte solutions. *J. Electroanal. Chem* **466**, 203–217 (1999).
345. Shterenberg, I. *et al.* Hexafluorophosphate-Based Solutions for Mg Batteries and the Importance of Chlorides. *Langmuir* **33**, 9472–9478 (2017).
346. Zhao, R. *et al.* Metal-Organic Frameworks for Batteries. *Joule* **2**, 2235–2259 (2018).
347. Shi, W. *et al.* Metal-organic framework-derived structures for next-generation rechargeable batteries. *Funct. Mater. Lett.* **11**, 1830006 (2018).
348. He, Y. *et al.* The potential of electrolyte filled MOF membranes as ionic sieves in rechargeable batteries. *Energy Environ. Sci.* **12**, 2327–2344 (2019).
349. Walton, I. M. *et al.* The role of atropisomers on the photo-reactivity and fatigue of diarylethene-based metal–organic frameworks. *New J. Chem.* **40**, 101–106 (2016).
350. Sheberla, D. *et al.* Conductive MOF electrodes for stable supercapacitors with high areal capacitance. *Nature Mater* **16**, 220–224 (2017).
351. Vlad, A. & Balducci, A. Porous materials get energized. *Nature Mater* **16**, 161–162 (2017).

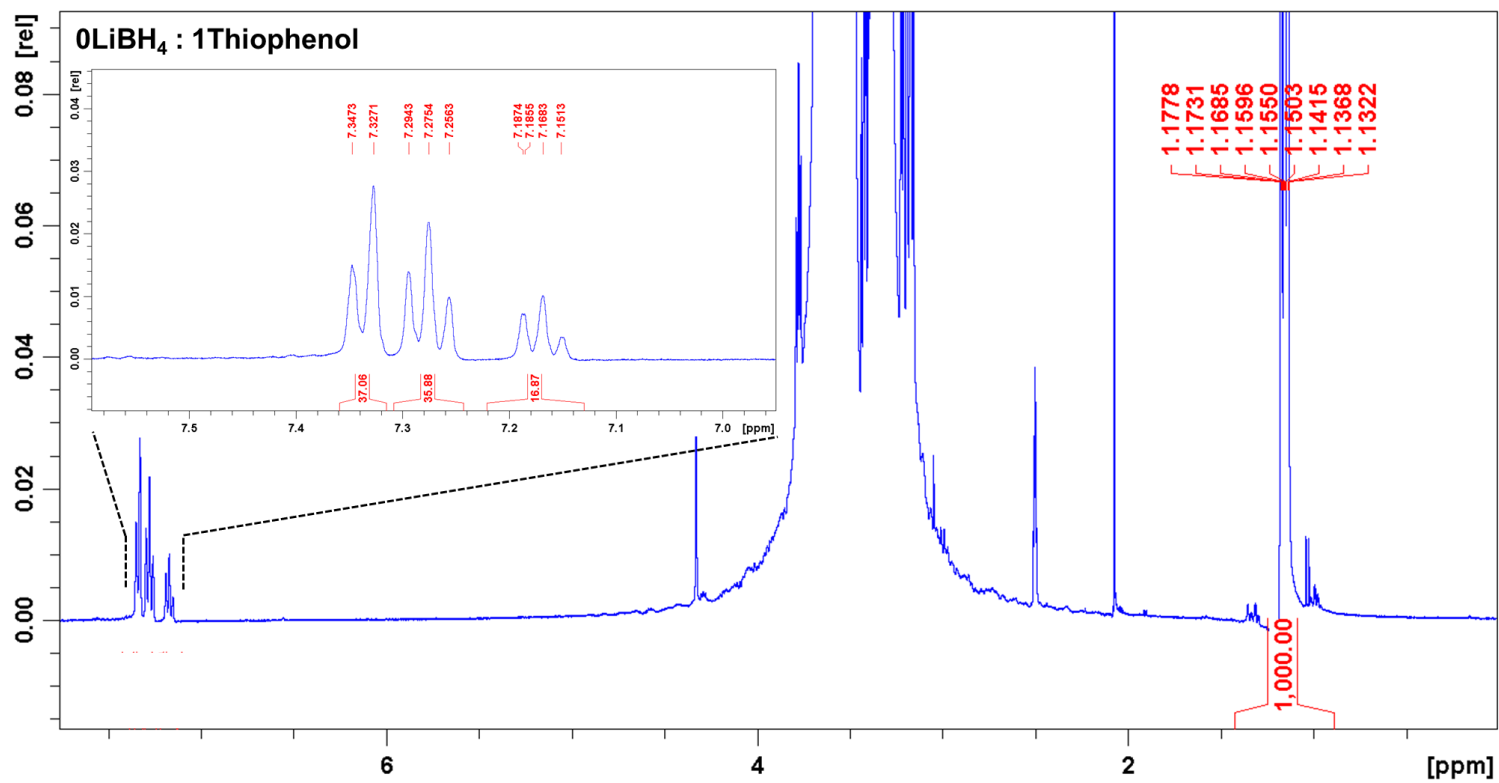
352. Zhou, D. *et al.* Self-supported multicomponent CPO-27 MOF nanoarrays as high-performance anode for lithium storage. *Nano Energy* **57**, 711–717 (2019).
353. Zhang, H. *et al.* MOF-derived nanohybrids for electrocatalysis and energy storage: current status and perspectives. *Chem. Commun.* **54**, 5268–5288 (2018).
354. Bouazza, S. *et al.* Cations Insertion in Molybdenum Cluster Compounds: Electronic Structure and Electrochemical Study Using Cavity Microelectrode. *J Clust Sci* **20**, 133–143 (2009).
355. Cachet-Vivier, C. *et al.* Development of cavity microelectrode devices and their uses in various research fields. *J. Electroanal. Chem* **688**, 12–19 (2013).

# **Annex**

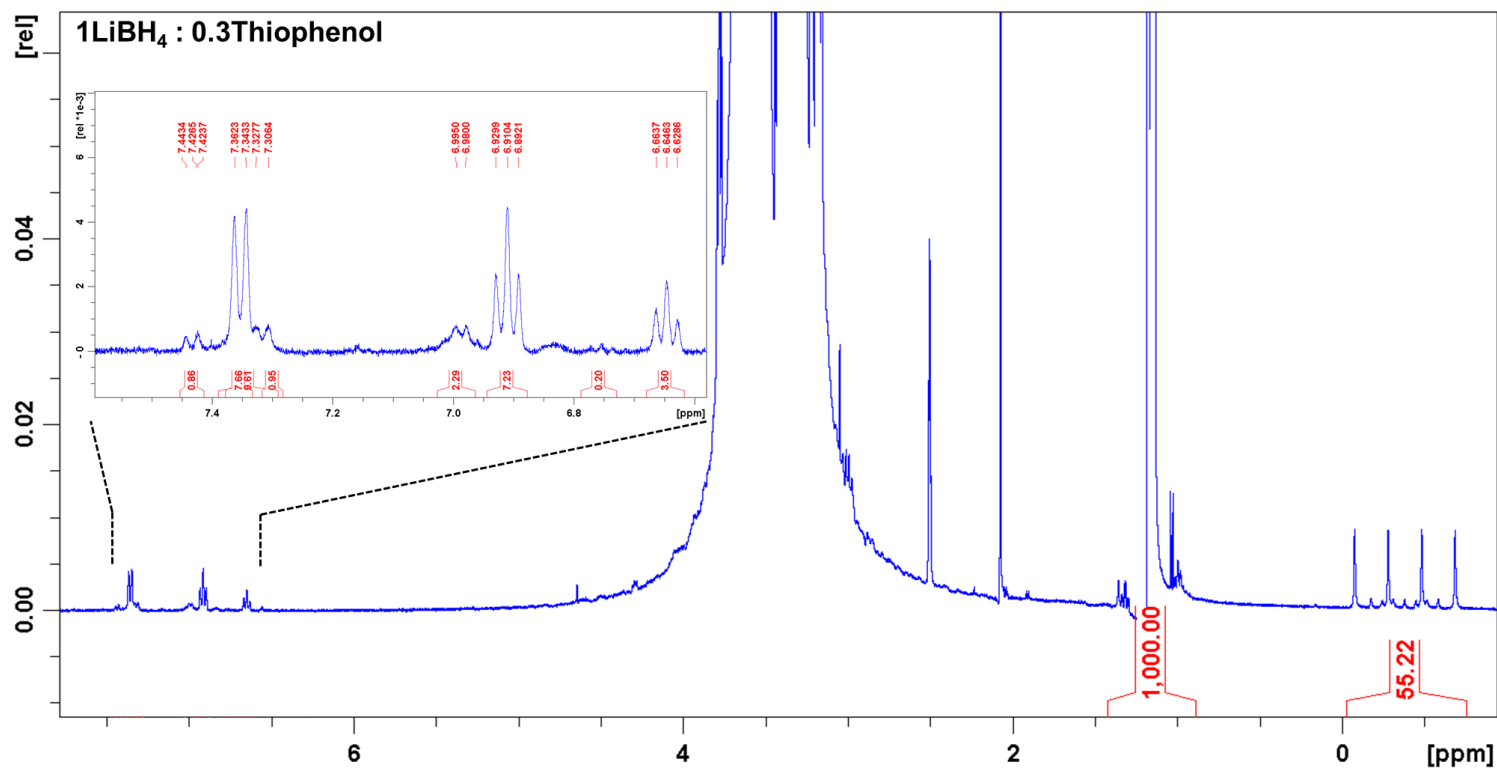
**Annex 1.**  $^1\text{H}$ -NMR spectra of 0.033 M  $\text{LiBH}_4$  in diglyme using insect tube as a reference.



Annex 2.  $^1\text{H-NMR}$  spectra of 0.033 M thiophenol in diglyme using insect tube as a reference.

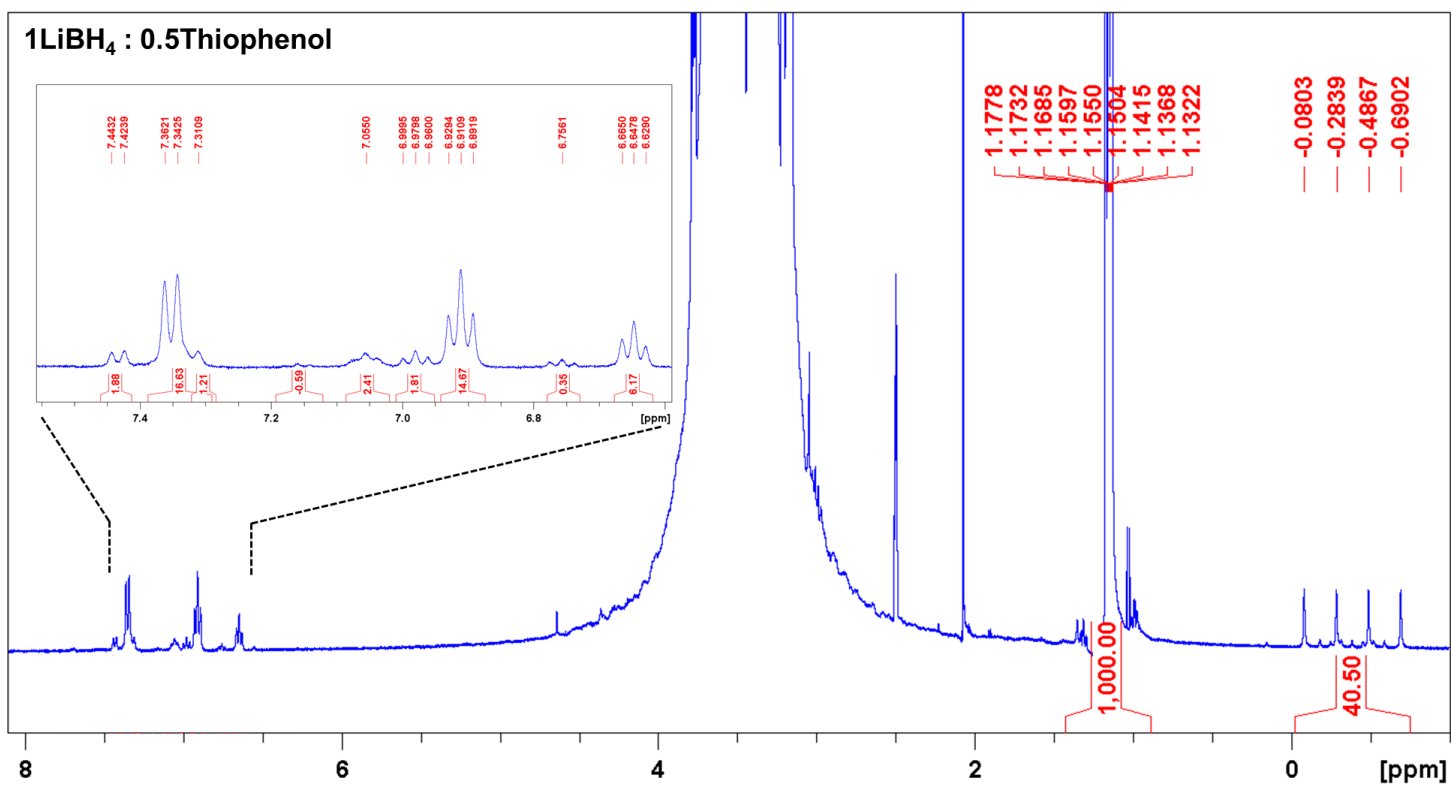


**Annex 3.**  $^1\text{H-NMR}$  spectra of 0.033 M  $\text{LiBH}_4$  and thiophenol (with  $\text{LiBH}_4$ :thiophenol = 1:0.3) in diglyme using insect tube as a reference.

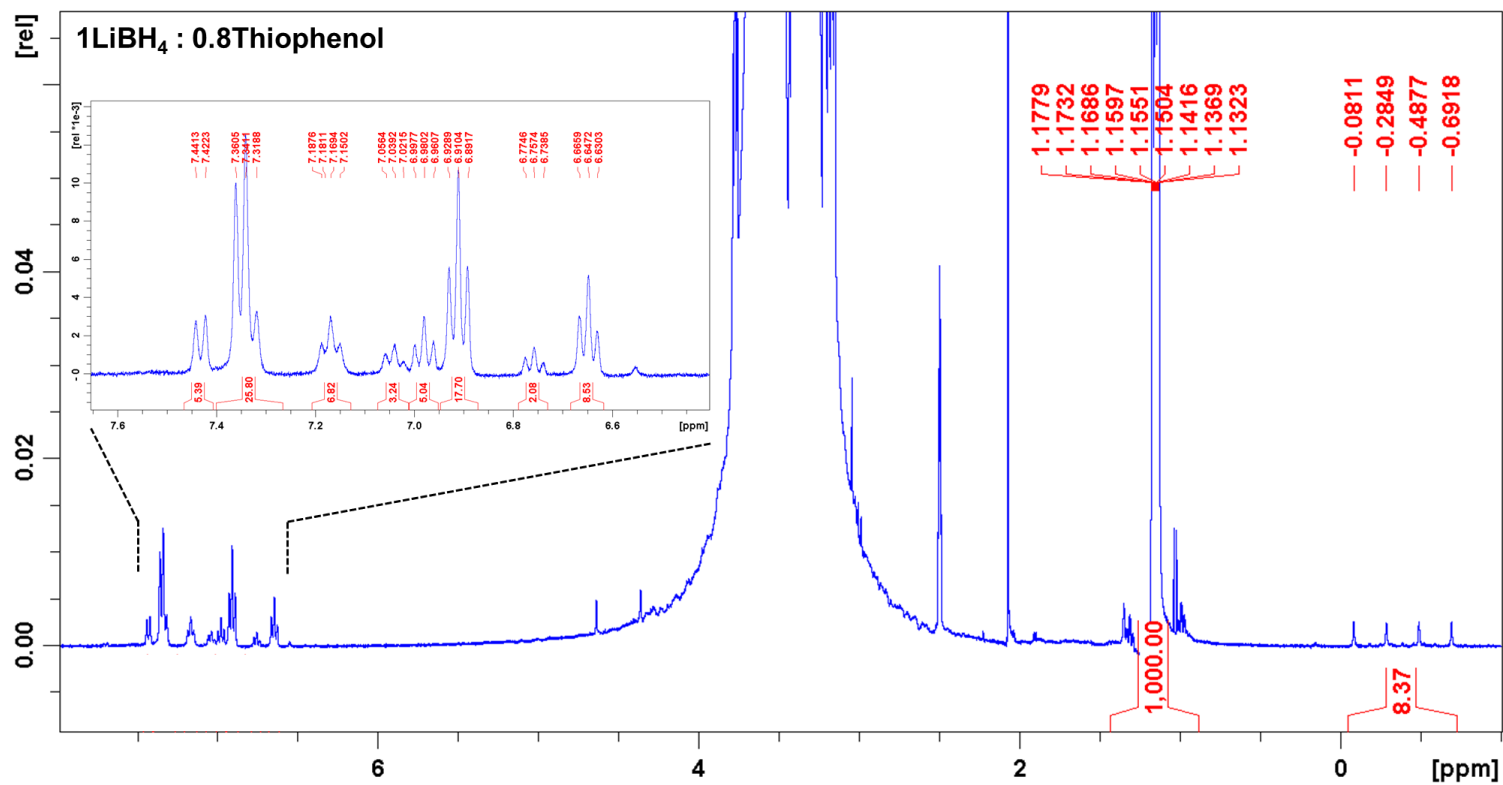




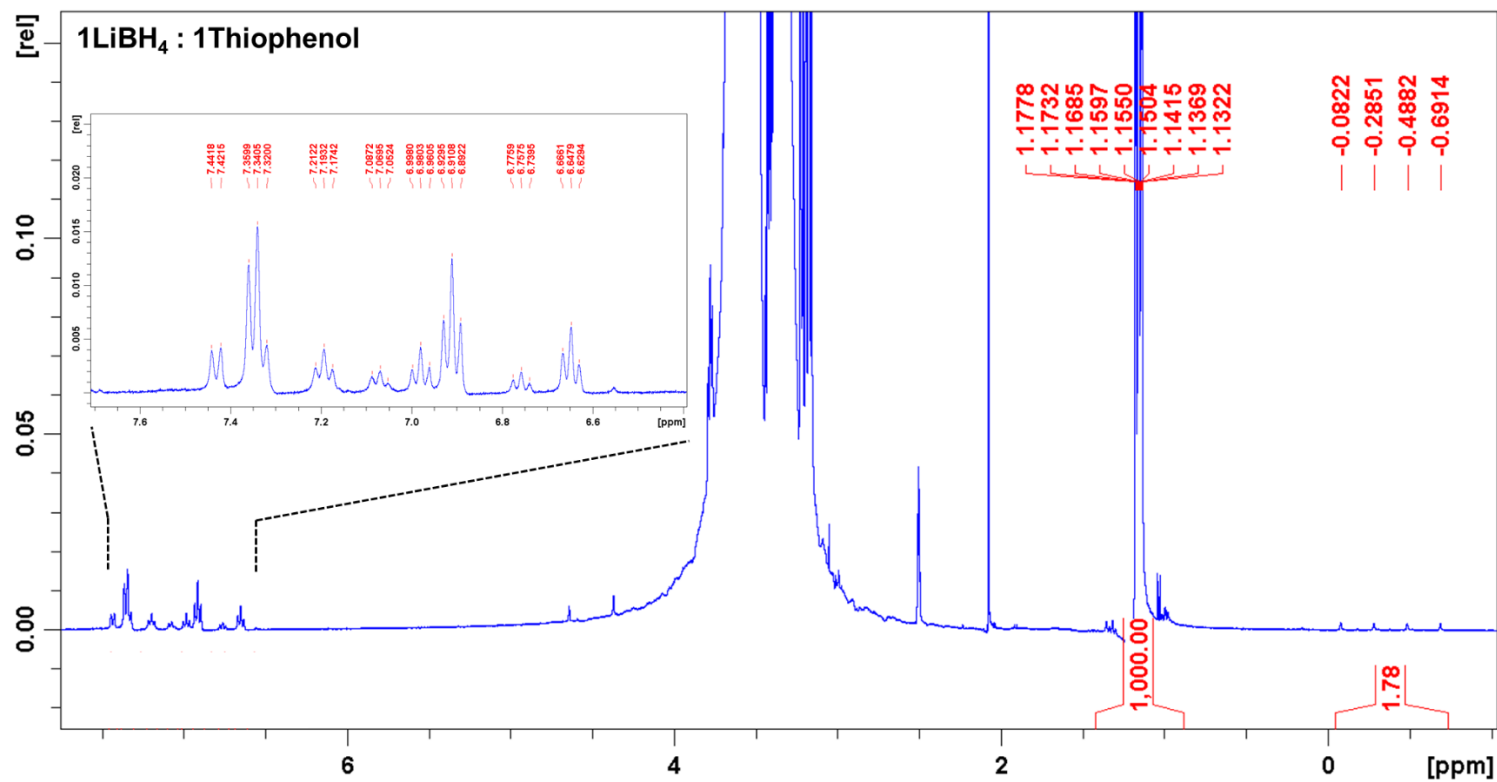
**Annex 4.**  $^1\text{H-NMR}$  spectra of 0.033 M  $\text{LiBH}_4$  and thiophenol (with  $\text{LiBH}_4$ :thiophenol = 1:0.5) in diglyme using insect tube as a reference.



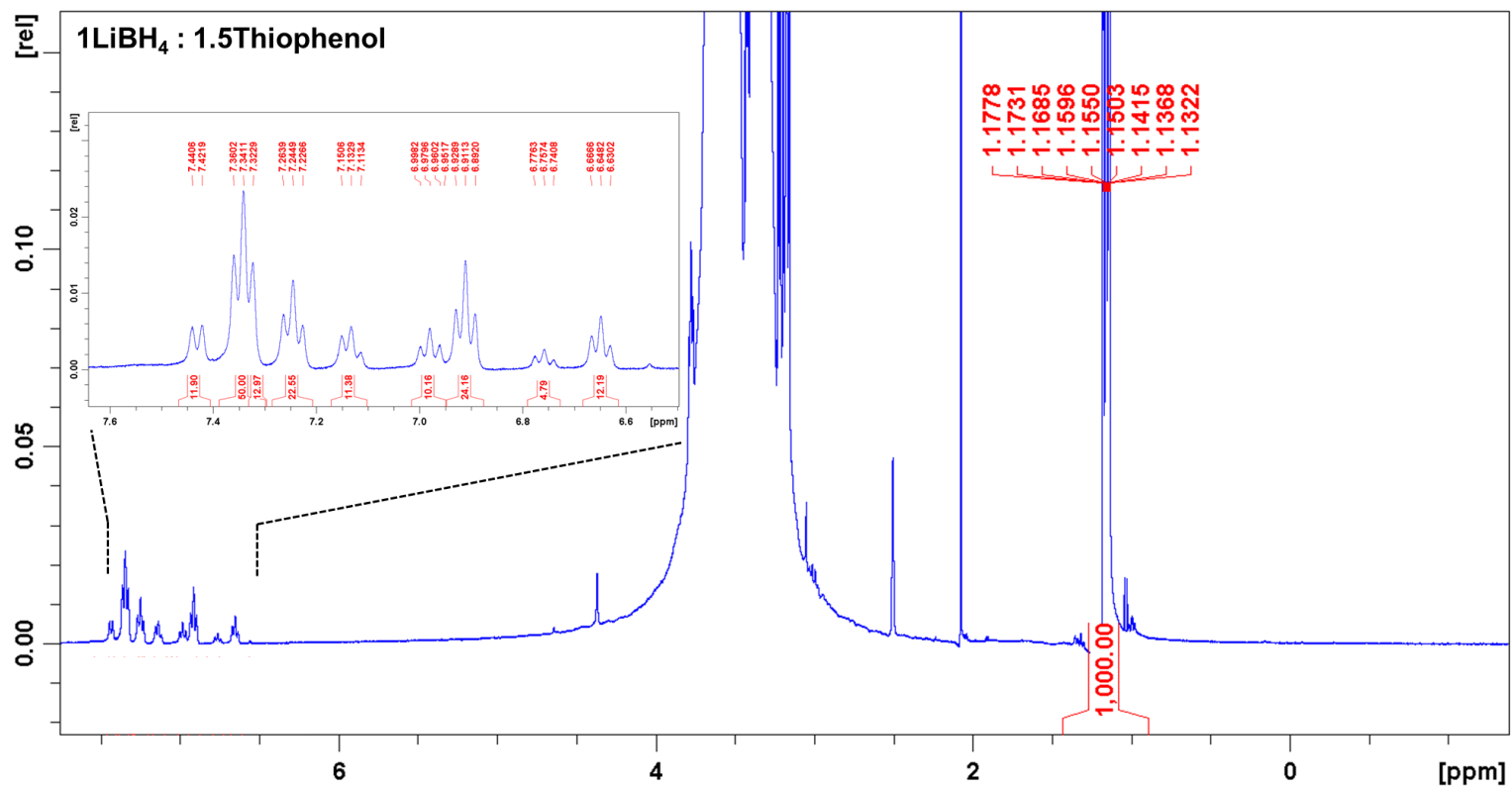
**Annex 5.**  $^1\text{H-NMR}$  spectra of 0.033 M  $\text{LiBH}_4$  and thiophenol (with  $\text{LiBH}_4$ :thiophenol = 1:0.8) in diglyme using insect tube as a reference.



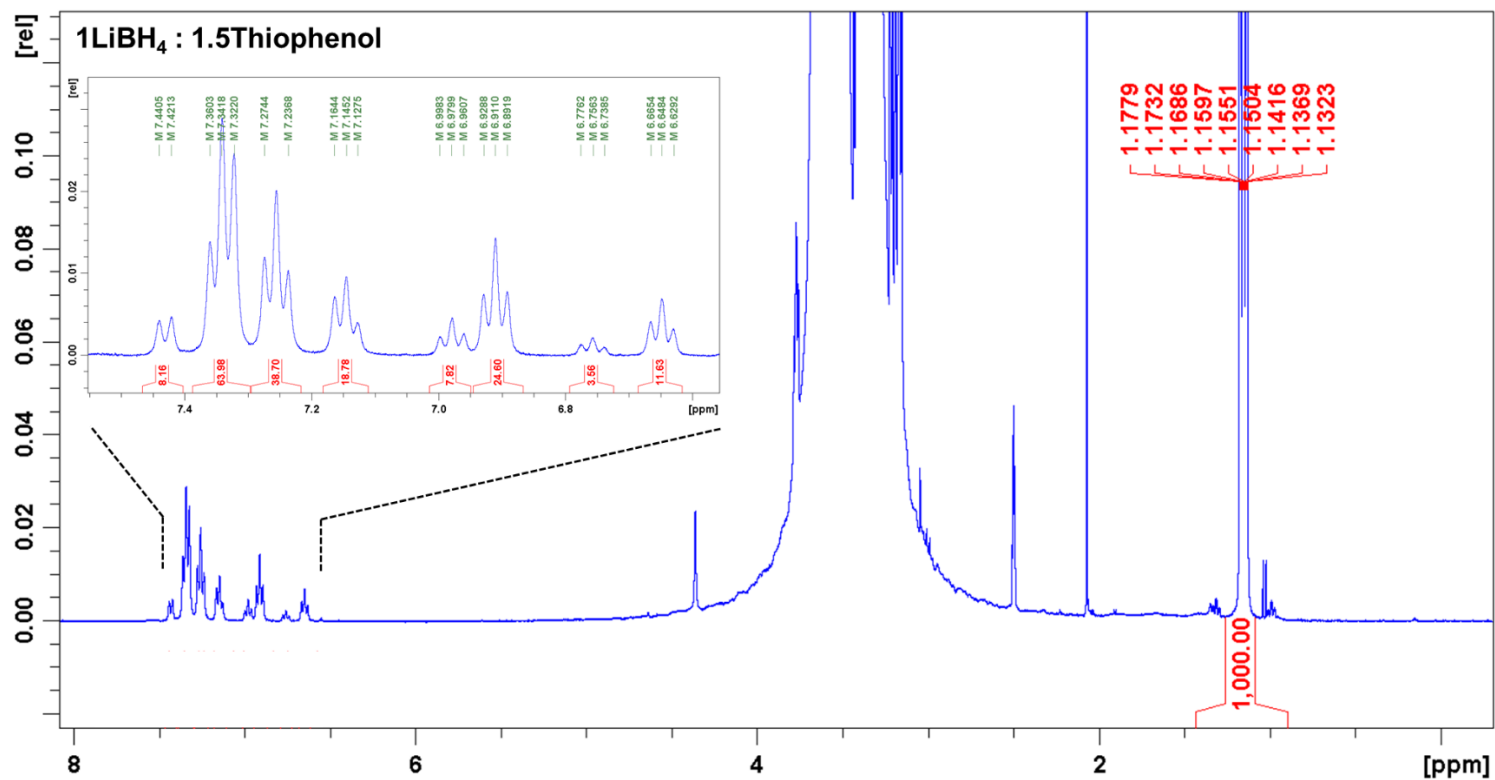
**Annex 6.**  $^1\text{H-NMR}$  spectra of 0.033 M  $\text{LiBH}_4$  and thiophenol (with  $\text{LiBH}_4$ :thiophenol = 1:1) in diglyme using insect tube as a reference.



**Annex 7.**  $^1\text{H-NMR}$  spectra of 0.033 M  $\text{LiBH}_4$  and thiophenol (with  $\text{LiBH}_4$ :thiophenol = 1:1.5) in diglyme using insect tube as a reference.



**Annex 8.**  $^1\text{H-NMR}$  spectra of 0.033 M  $\text{LiBH}_4$  and thiophenol (with  $\text{LiBH}_4$ :thiophenol = 1:2) in diglyme using insect tube as a reference.



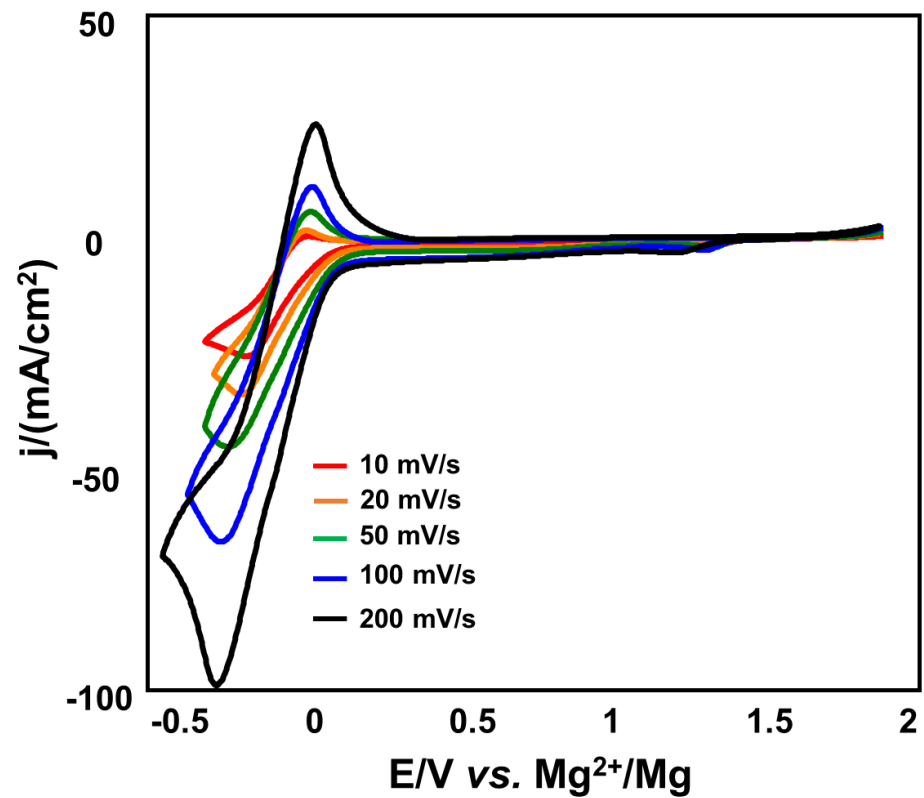
**Annex 9.**  $^1\text{H-NMR}$  integration of 0.033 M  $\text{LiBH}_4$  and thiophenol in different ratio of  $\text{LiBH}_4$ :thiophenol using insect tube as a reference.

Chemical shift (ppm)		1.17	7.34	7.28	7.17	7.35	6.91	6.65	7.43	6.98	6.76	-0.38		
Ratio ( $\text{BH}_4$ /thiophenol)	Chemical and Concentration (M)		CH <sub>3</sub> -(ref)	H <sub>α1</sub>	H <sub>β1</sub>	H <sub>γ1</sub>	H <sub>α2</sub>	H <sub>β2</sub>	H <sub>γ2</sub>	H <sub>α3</sub>	H <sub>β3</sub>	H <sub>γ3</sub>	H( $\text{BH}_4$ )	H aromatic
	LiBH <sub>4</sub>	Thiophenol												
0/1		0.0333	1000.00	37.00	36.00	17.00	0.00	0.00	0.00	0.00	0.00	0.00	0.00	92.00
1/0	0.0333		1000.00	0.00	0.00	0.00	0.00	0.00	0.00	0.00	0.00	0.00	80.00	0.00
1/0.3	0.0333	0.0100	1000.00	1.95	1.95	1.00	7.66	7.23	3.50	0.86	0.86	0.50	55.20	25.00
1/0.5	0.0333	0.0167	1000.00	2.40	2.40	1.20	14.20	14.67	6.17	1.88	1.81	0.90	40.50	40.00
1/0.8	0.0333	0.0267	1000.00	7.30	6.82	3.27	18.20	17.70	8.53	5.39	5.04	2.08	8.37	74.00
1/1.0	0.0333	0.0333	1000.00	9.80	8.90	4.60	21.20	20.80	10.50	8.11	7.60	3.31	1.78	98.00
1/1.5	0.0333	0.0500	1000.00	24.00	22.60	11.40	26.00	24.20	12.20	11.90	10.20	4.80	0.00	154.00
1.2.0	0.0333	0.0667	1000.00	40.00	38.70	18.80	24.00	24.60	11.60	8.20	7.80	3.60	0.00	181.00

**Annex 10.** Integration of proton signals for solution containing 0.033 M LiBH<sub>4</sub> and thiophenol in different ratio of LiBH<sub>4</sub>:thiophenol = 1:1 using insect tube as a reference by different time investigation

Time (hour)	Proton [C <sub>6</sub> H <sub>5</sub> SBH <sub>3</sub> <sup>-</sup> ]	Proton [(C <sub>6</sub> H <sub>5</sub> S) <sub>2</sub> BH <sub>2</sub> <sup>-</sup> ]	Proton [BH <sub>4</sub> <sup>-</sup> ]	DMSO-d <sub>6</sub> (ref)
2	264.20	125.00	79.70	100.00
24	312.60	122.80	37.60	100.00
72	316.10	119.80	19.42	100.00
216	292.85	133.00	17.00	100.00
504	166.40	202.50	13.90	100.00
840	132.70	304.40	0.00	100.00
1512	89.20	259.80	0.00	100.00

**Annex 11.** Cyclic voltammetry on Pt electrode of diglyme solution containing 0.5 M Mg(TFSI)<sub>2</sub> and 0.04 M 9,10-dimethylantracene





## Abstract

The objectives of this thesis are, on the one hand, to develop new electrolytes by the design of new non-hazardous magnesium salts or by the use of aromatic additives such as anthracene and, on the other hand, to synthesize an organic polymer with redox properties suitable for its use as a positive electrode in magnesium batteries. The first methodology was the synthesis of several magnesium salts obtained by the reaction of substituted phenol or thiophenol with the tetrahydroborate anion. The best results were obtained with the salt obtained by the reaction of thiophenol and tetrahydroborate. The impact of this new salt on the improvement of the Mg/electrolyte interface was characterized by chronoamperometry and impedance spectroscopy measurements. In addition, the performance of full cell Mg/Mo<sub>6</sub>S<sub>8</sub> was evaluated, a capacity of 75 mAh/g was obtained after 20 cycles, with a weak polarization of the Mg electrode. The second methodology several  $\pi$ -rich compounds were used. The best promising molecule is the 2-(*tert*-butyl)anthracene with an improvement in the Mg plating/stripping process reversibility. The second part of this thesis will present the electrochemical performance of organic material using as positive electrode for both lithium and magnesium batteries. Poly(benzoquinonyldisulfide) (PBQDS) was synthesized with very high yield in a green and easy way. After the particle size reduction using ball milling technique, the discharge capacity reaches a stable value of 140 mAh/g at C/20 in sulfolane based electrolyte. In Mg cell, even if similar capacity is obtained in the first cycles, a large capacity fading is observed associated with the trapping of Mg<sup>2+</sup> in the active material, due to strong oxygen/Mg<sup>2+</sup> interaction. The use of solvation additive (crown ether) in the electrolyte mitigates partially this behaviour, given some interesting leads of improvement.

## Résumé

Les objectifs de cette thèse sont d'une part, de développer de nouveaux électrolytes par la conception de nouveaux sels de magnésium non dangereux ou par l'utilisation d'additifs aromatiques comme l'anthracène et d'autre part de synthétiser un polymère organique ayant des propriétés redox adaptées à son utilisation comme électrode positive dans des batteries au Magnésium.

La première méthodologie a été la synthèse de plusieurs sels de magnésium obtenus par la réaction de phénol substitués ou de thiophénol avec l'anion tétrahydroborate. Les meilleurs résultats ont été obtenus avec le sel obtenu par réaction du thiophénol et du tétrahydroborate. L'impact de ce nouveau sel sur l'amélioration de l'interface Mg/électrolyte a été caractérisé par des électrochimie. En outre, les performances de la cellule complète Mg/Mo<sub>6</sub>S<sub>8</sub> ont été évaluées, et une capacité de 75 mAh/g a été obtenue après 20 cycles, avec une faible polarisation de l'électrode de Mg. La deuxième méthodologie a consisté à étudier l'effet d'additifs aromatiques sur le processus de dépôt/dissolution du Mg, et ainsi permettre d'approfondir notre compréhension du mécanisme assisté sous-jacent. La deuxième partie de cette thèse présente les performances électrochimiques de matériaux organiques utilisés comme électrode positive pour les batteries au lithium et au magnésium. Le polybenzoquinonedisulfure (PBQDS) a été synthétisé avec un rendement très élevé de façon écologique et facile. Les performances obtenues en cellule Li sont intéressantes, alors qu'en cellule Mg, une perte de capacité importante est obtenue associée au piégeage des ions Mg<sup>2+</sup> au sein de l'électrode, due à une forte interaction oxygène/Mg<sup>2+</sup>. L'utilisation d'un additif solvatant, un éther couronne, dans l'électrolyte atténue partiellement ce comportement, proposant ainsi des pistes d'amélioration intéressantes.

